University of the Witwatersrand

School of Geography, Archaeology and Environmental Science

A Southern Hemisphere Tropical Cyclone Climatology: Analysis of Variability Under a Changing Climate

Dissertation submitted to the Faculty of Science in fulfilment of the requirements for the degree Master of Science

Micheal Teron Pillay

801813

15 August 2019

Declaration

I hereby declare that this dissertation is my own unaided and original work except where acknowledged. It is being submitted for the Degree of MSc to the University of the Witwatersrand, Johannesburg. I have not submitted this work before for any degree or examination at any other University.

______________________ 15/08/2019

Micheal Pillay Date

Abstract

Tropical cyclones are becoming more intense and the locations at which they form and attain their lifetime maximum intensities are migrating poleward, exposing more regions to tropical cyclone impacts. This study investigated a new climatology for Southern Hemisphere tropical cyclones, aimed to update and re-examine the previous tropical cyclone climatology from the canonical works of Gray (1968, 1979). The optimal and minimum ranges of thermodynamic and dynamic climate variables during tropical cyclogenesis were determined, to define the conditions at which the majority of Southern Hemisphere tropical cyclones are generated. The change over time of tropical cyclone activity and the magnitude of the climate drivers at the 1000and 850mb levels was also examined. The sea surface temperatures of 27.5-28.5°C is observed as the optimal range at which a majority of storms undergo genesis. However, the lowest observed magnitude at which genesis was possible is 24°C. This challenges the 26.5°C threshold for genesis in the Southern Hemisphere. Based on factor analysis weightings and multivariate regression, sea surface temperature, air temperature and relative humidity also account for a relatively large amount of variability in the formation process of tropical cyclones, compared to the other climate variables examined. Over 1980-2016, an increase for Southern Hemisphere tropical cyclone maximum intensity of 2.4 $m.s^{-1}$ per decade is observed. Of the climate drivers measured at the point of genesis; omega, meridional shear, sea surface temperature and solar flux display statistically significant correlations with tropical cyclone intensity. Sea surface temperature, air temperature, solar flux and vertical shear at the point of genesis for Southern Hemisphere tropical cyclones, demonstrate statistically significant increases in magnitude, while omega and relative humidity indicate a decreasing trend. The increase in thermodynamic variables and their relationship to storm intensity infers that a warming climate is capable of influencing tropical cyclone intensity. The El Niño Southern Oscillation, Indian Ocean Dipole, Southern Annular Mode and volcanic eruption events indicated a statistically significant relationship to metrics of tropical cyclone activity, mainly intensity and longitude of storm genesis. The tropical cyclone climatology established here by providing an up to date seasonality and background of Southern Hemisphere tropical cyclone activity, can assist impact and risk assessment studies in areas potentially vulnerable to tropical cyclone impacts within the Southern Hemisphere.

Acknowledgments

I must thank my supervisor Dr Jennifer Fitchett. Her support and guidance were of the utmost importance in the completion of my project. The editing and reading done by my supervisor aided the efficient completion of my project. I am also grateful for the ideas and clarity Dr Fitchett provided throughout the project and for her patience and time. The opportunity she provided by helping me attend the South African Society of Geographers (SSAG) 2018 conference allowed me to and acquire new and interesting knowledge from various Geographers across South Africa.

I must thank my family for their support and understanding throughout the duration of my project. I must especially thank by brother, Christopher for writing the code that allowed me to extract the data used in my project. Also, the time taken from his busy schedule as a fellow student, to help me proof-read and check my referencing is greatly appreciated. I give thanks to my mother Desanne, as she helped in the proof-reading and always made time to hear about my research. I must also thank my fellow students who gave me ideas, and advice and also helped with reading through my research.

The National Research Foundation (NRF), must also be acknowledged for providing the financial support for this MSc through the NRF Freestanding, Innovation and Scarce Skills Development Fund from 2018 to 2019. Thanks also goes to the University of the Witwatersrand for their financial support through the PMA award.

List of Figures

List of Tables

List of Acronyms, Abbreviations and Statistical Terms

BoM: Australian Bureau of Meteorology

EA: East Australia

ENSO: El Nino Southern Oscillation

IBTrACS: International Best Track Archive for Climate Stewardship

IOD: Indian Ocean Dipole

IPCC: Intergovernmental Panel on Climate Change

ITCZ: Inter-Tropical Convergence Zone

LMI: Lifetime Maximum Intensity

MEI: ENSO Multivariate Index

MJO: Madden-Julian Oscillation

NCEP-NCAR: National Centers for Environmental Protection/University Corporation for Atmospheric Research

NH: Northern Hemisphere

Niño 3.4: Niño Index

NOAA: National Oceanic and Atmospheric Administration

OISST V2: Optimal Interpolation Sea Surface Temperature Version 2

PDO: Pacific Decadal Oscillation

SAM/AAO: Southern Annular Mode/Antarctic Oscillation

SD: Standard Deviation

SH: Southern Hemisphere

SIO: South Indian Ocean

SOI: Southern Oscillation Index

SP: South Pacific

SST: Sea Surface Temperature

TC: Tropical Cyclone

WA: West Australia

WMO: World Meteorological Organization

°C.yr^{-1}: Degree Celsius change in temperature per year.

°C: Degree Celsius.

°E,W,N,S: Degrees of bearing.

hPa: hector Pascals.

m.s^{-1}: meters per second.

mb: millibar indicating pressure.

pascal.s^{-1}: pascals per second, indicating the displacement of pressure and change in pressure following air movement.

TC's.yr^{-1}: Tropical Cyclones per year.

W.m^{-2}: Watts per meter squared, indicating solar energy input over an area.

yr^{-1}: per year.

A: Alpha coefficient representing wind shear for v-wind and u-wind components.

ω: Omega variable, representing vertical velocity in the atmosphere via pressure change following movement of air parcels.

$\bar{x}$: Average.

Statistical Terms

ANOVA: Analysis of Variance.

MANOVA: Multivariate Analysis of Variance.

n: total number of observations or sample size.

p: The p-value denotes the statistical significance of a regression or correlation outcome. The p-value is measured from 0 to 1, but any observation with a value smaller than an alpha of 0.05 is considered to have a high probability of occurring.

r: Pearson Correlation Coefficient – the value between -1 and 1, which provides the strength of the linear relationship between two variables. The values closer to +1 (-1) indicate a strong positive (negative) relationship between the two factors. The values closer to 0 indicate a weak correlation.

R^2: The Coefficient of Determination, which is a value between 0 and 1, that represents the amount of variance for a dependent variable (response) that is explained by the independent variable within a regression model. Values closer to 1 indicate that the independent variables explain more of the variability.

1. Introduction

1. Introduction: Background of Tropical Cyclones

Tropical cyclones are large non-frontal storm systems which range from 100 to around 1,000km in diameter and predominantly form in the northern and southern hemispheric tropical ocean basins, over the tropical latitudes between 5-20° N/S of the equator (L. Zhang *et al*., 2017). They are dynamic and destructive storm systems generated and influenced by complex thermodynamic and dynamic interactions between the ocean and atmosphere (Walsh *et al*., 2016). The thermodynamic elements include but are not limited to sea surface and air temperature, moisture and convection (Klotzbach *et al*., 2017; Bhaskaran *et al*., 2018). The dynamic elements refer to the vertical wind shear and low-level convergence present in the environment (Gray, 1998; Nolan & McGauley, 2012). Tropical cyclones are characterised by a low-pressure center, surrounded by clockwise (in the Southern Hemisphere; anticlockwise in the Northern Hemisphere) rotating bands of clouds and intense winds (Bhatia *et al*., 2019). Over the period 1980-2009 an average of 32 tropical storms/cyclones occurred annually at a global scale, with an interannual range of 16-66 storms (Doocy *et al*., 2013; Temmerman *et al*., 2013; Klotzbach *et al*., 2018).

The process of tropical cyclogenesis, intensification and dissipation varies for every storm, as each one is unique (Bhaskaran *et al*., 2018). However, tropical cyclogenesis typically begins with a tropical disturbance, which is an organised convective system up to 600 km large and persists for longer than 24 hours and is sometimes characterised synoptically by a perturbation in the usually parallel wind or pressure fields (McTaggart-Cowan *et al*., 2013; Klotzbach *et al*., 2017; Bhaskaran *et al*., 2018). As the convection related to this disturbance deepens and the pressure drops, a weak vortex develops as air rushes in to replace the rising air (Bhaskaran *et al*., 2018). Clouds form as warm moist air condenses and latent heat is released adding energy to the storms. If sea surface temperatures are large enough and there is high moisture available, deep convection and evaporative heating will progress and the tropical cyclone may then develop, with strong surface air convergence which is then transported up the vortex and ejected at the top outflow through upper air divergence (Klotzbach *et al*., 2017). As the system intensifies, the vortex (low pressure eye) becomes more defined and the large cloud bands rotate around it faster and the tropical cyclone will continue intensifying until it attains the maximum intensity that the environment can support i.e. its potential intensity (Sebastian & Behera, 2015). The system will dissipate once ocean heat and moisture cannot support it or it makes landfall, where it cannot be sustained by the warm ocean and moisture (Emanuel *et al*., 2004).

There has been increasing concern that anthropogenic climate change is responsible for driving changes in tropical cyclone activity via increased global mean temperatures, and that these changes will only be exacerbated or continue into the future (Kossin *et al*. 2014; Yoshida *et al*., 2017). The increased prevalence of extreme tropical cyclones (category 4-5 on the Saffir-Simpson scale which classifies storm intensity based on windspeed) has led to increased destruction of infrastructure and mortality, especially in the Southern Hemisphere where the majority of developing countries are located (Li *et al*., 2017; Klotzbach *et al*., 2018). The economic damages from these storms are also concentrated in these developing regions (Doocy *et al*., 2013; Cinco *et al*., 2016). Intense tropical cyclones are associated with higher levels of precipitation, winds and storm surges, which contribute to their increased destructiveness (Doocy *et al*., 2013; Khouakhi *et al*., 2017). Over a 30-year period (1980-2009) 466 million people were affected, with 20.1 million made homeless and over 400,000 deceased (Doocy *et al*., 2013; Klotzbach *et al*., 2018). The developing countries in the South

Indian and South Pacific regions are especially vulnerable, as the tropical cyclone related impacts experienced by the landmasses around these basins are compounded by the lack of early warning systems and knowledge to predict or understand tropical cyclones (Li *et al*., 2017). The future projections and current observations of increased intense storms heightens the necessity to develop meaningful and accurate understandings of tropical cyclone activity, the mechanisms behind it and the changes that a warming climate may instigate (Walsh *et al*., 2016).

1.1. Rationale

Research in the Southern Hemisphere, specifically for the South Indian Ocean which experiences the largest number of tropical cyclone events relative to the Australian and South Pacific regions, has predominantly focused on the western region of the South Indian Ocean (Fitchett, 2018). Furthermore, the global climatology and requirements of tropical cyclone genesis was developed by Gray (1968, 1979), however, the foundations of these studies were based on low-resolution data and for the Southern Hemisphere (Watterson *et al*, 1995; Kossin *et al*., 2007, 2013). Specifically, the records on tropical cyclone genesis location and wind speed were not as reliable as they are after 1970-1980 (Webster *et al*., 2005; Diamond *et al*., 2012; McTaggart-Cowan *et al*., 2013; Magee *et al*., 2016). In addition, reexaminations of Gray's (1968, 1979) seasonal genesis indices indicate that only observations for the Northern Hemisphere (North Atlantic, North and Central Pacific) tropical cyclone activity can be replicated reliably enough to agree with observational data (Watterson *et al*., 1995; Kossin *et al*., 2007). In addition, when constructing the genesis indices Gray (1968) drew on multiple and incomplete data sources. In addition, the definitions used by Gray (1968) to delineate the different basins for the Southern

Hemisphere, by combining the northeast Australian coast and South Pacific were not climatologically accurate; it is considered better practice to examine the whole Southern Hemisphere, not individual basins (Schreck *et al*., 2014). Therefore, creating a new tropical cyclone climatology, by examining the locations and intensity (based off homogenous wind speed data) is required for the whole Southern Hemisphere. Such investigations have already been done for the North Atlantic (Camara *et al*., 2010; Kossin *et al*., 2013) and for the North Pacific (Colbert *et al*., 2015). Meanwhile, recent studies examining the Southern Hemisphere have only investigated sea surface temperature at the point of genesis (Defforge & Merlis, 2017a), the trends in central pressure of South Indian and Pacific Ocean tropical cyclones (Kuleshov *et al*., 2010) and the relationship between ENSO and Southern Hemisphere tropical cyclone activity (Kuleshov *et al*., 2009; Dowdy *et al*., 2012).

One of the significant reasons for this study lies in the issue of data quality. Limitations exist within studies based on historical data compiled through various observation systems, including irregular ship logs, aircraft records and low-resolution satellites prior to 1980 (Landsea et al., 2006; Osuri *et al*., 2012; Kossin *et al*., 2013; Fitchett & Grab, 2014). Additional caveats in the data prior to 1980 include the use of various methods used to adjust and calculate wind speed, which has affected the consistency of northern and Southern Hemisphere tropical cyclone intensity data (Befort *et al*., 2016). From the mid-1970s geostationary satellite coverage became common around the world with the release of GOES-1, GMS-1 and Meteosat (Velden *et al*., 2006; Ramsay *et al*. 2012). As a result, there are now datasets available, which overcome these shortfalls in capturing and assimilating data by combing multiple best track data sources into one database, namely, the NOAA IBTrACS used in this study (Knapp *et al*., 2010; Kossin *et al*., 2007; Fitchett & Grab, 2014;

Barcikowska *et al*., 2017). Furthermore, the IBTrACS is endorsed officially by the World Meteorological Organization (Fitchett, 2018), and a recent investigation (Song *et al*., 2018) confirms a statistically significant and accurate representation of tropical cyclone intensity from 1981-2016. Since this study is focusing on the tropical cyclones from 1980-2016, the use of the IBTrACS data can be applied with good confidence regarding trends in intensity over the study period. Similarly, the optimum interpolation sea surface temperature version 2 (OISST v2) dataset used in this study to describe sea surface temperature, is the best spatial (0.25°x0.25°) and temporal (daily) resolution dataset, which covers the 1981-2016 period. Therefore, this study on tropical cyclone climatology will be based on accurate and precise datasets, which is a factor usually not inherent in many studies using tropical cyclone data prior to 1970/1980 (Befort *et al*., 2016; Rai *et al*., 2019). Using the OISST v2 dataset provides over 30 years of sea surface temperature data, which will allow an accurate climatology of tropical cyclone genesis and intensification sea surface temperatures to be derived for the Southern Hemisphere. Such studies with similar data accuracy and precision have not to date been performed at the hemispheric or 30-year time scale.

Despite the in-depth understanding of trends in global and regional tropical cyclone frequency and intensity, there is a deficiency of studies examining tropical cyclone activity and climatology in the Southern Hemisphere, compared to the number of detailed studies related to northern hemispheric basins, namely, the North Atlantic and Pacific (Camara *et al*., 2010; Mei *et al*., 2015; Burns *et al*., 2016; Patricola & Wehner, 2018; Yoshida *et al*., 2017; Song *et al*., 2018). Specifically, the majority of climate change-tropical cyclone studies have focused on the Northern Hemisphere or on global trends in storm activity (Gleixner *et al*., 2014; Daloz & Camargo, 2018). The deficit of studies dealing with the Southern Hemisphere is problematic, as the active tropical cyclone zones in the Southern Hemisphere are unique compared to the Northern Hemisphere, since the South Indian and South Pacific are not separated by continental landmasses as is the case in the north Pacific and Atlantic, there is greater solar input in the Southern Hemisphere and the Northern Hemisphere basins have relatively greater heat capacity (Maue, 2009; Lee *et al*., 2015; Gastineau *et al*., 2018). Furthermore, the activity and variability of all tropical cyclones in the Southern Hemisphere are influenced by multiple ocean and atmospheric forcers or teleconnections, including but not limited to ENSO, QBO, IOD, Madden-Julian Oscillation (MJO), Pacific Decadal Oscillation (PDO), sunspots and solar energy fluxes and the interactions between these climatic forcers across spatial bounds of the Southern Hemisphere ocean basins (Ramsay *et al*., 2012; Mao *et al*., 2013; Wieners *et al*., 2016). For example, the IOD affects the South Indian and south east Pacific Ocean temperatures and atmospheric Walker Circulation, but there exists no investigation on how this multi-basin variability impacts the general activity of southern hemispheric tropical cyclones, or if any teleconnections between them and other climatic modes of variability influence tropical cyclones (Markle *et al*., 2015; Wieners *et al*., 2016; Gleixner et al., 2014). Consequently, teleconnections are observed between the northern Pacific and Atlantic basins, which exhibit an ENSO modulation on the tropical cyclone activity across the two basins (Clem *et al*., 2016; Sobel *et al*., 2016; Patricola & Wehner, 2018). Therefore, the spatial and climatic conditions of the southern hemispheric basins which have no physical barriers separating them, indicate a high possibility of demonstrating integrated teleconnections between climatic modes of variability, climatic oscillations and tropical cyclone activity.

Another avenue that requires attention is the specific conditions under which tropical cyclones form, intensify and then dissipate. Until recently, it was believed that tropical cyclone genesis and intensification is initiated under specific conditions, specifically, that they require sea surface temperatures of 26.5° C or above (Gray, 1979; McBride, 1995; Henderson-Sellers, 1998; Mavume *et al*., 2009). However, Defforge and Merlis (2017b) argued that increases in sea surface temperature alone do not reconcile the changes in genesis location and storm intensity, as it is not the only factor governing tropical cyclone activity. This is supported by analyses on five basins of tropical cyclone occurrence, which indicates that there are variable sea surface temperature thresholds for tropical cyclone genesis in each basin (McTaggart-Cowan *et al*., 2015; Defforge & Merlis, 2017b). Instead, it is the climatological backgrounds of each basin, which includes sea surface temperature, baroclinicity and convective stability which determines the formation potential of tropical cyclones (McTaggart-Cowan *et al*., 2015; Mawren & Reason, 2017; Wang & Moon, 2017). Furthermore, a statistically significant variation of over 1°C has been observed between the various basins under tropical cyclone genesis, which implies that sea surface temperature is not as deterministic to genesis as previously thought (Defforge & Merlis, 2017a). This variation in the observed sea surface temperature at genesis was concealed by averaging out the genesis sea surface temperatures across the globe, which provided the benchmark 26.5-27°C threshold. Gray's (1968) index for tropical cyclone genesis followed by multiple authors and utilised in model-based studies is therefore brought into question, as clearly the conditions for genesis and intensification vary between north and southern basins (Watterson *et al*., 1995; Camargo & Wing, 2016; Defforge & Merlis, 2017a). The specific nature of this variation requires investigation to determine the Southern Hemisphere tropical cyclone formation requirements.

The data caveats related to tropical cyclone location accuracy and the overestimation of storm intensity prior to 1980, have made it difficult to investigate the time it takes for a tropical cyclone to attain lifetime maximum intensity (Walsh *et al*., 2015; Lin *et al*., 2017). There is also difficulty for model-based simulations to capture the drivers and environmental variables which are responsible for rapid or extreme cases of intensification (Lin *et al*., 2017). This study will, therefore, attempt to investigate the time taken to attain maximum intensity and the location at which Southern Hemisphere tropical cyclones reach this maximum intensity. This could prove important to model-based studies and increase the understanding of tropical cyclone intensification, and the state of environment at this point, as well as allow an understanding of the dynamics of the intensification process, specifically regarding its response to sea surface temperature (Emanuel, 2000).

This study applies a hemispheric approach to studying trends in tropical cyclone activity, which is a well-tested methodology for examining tropical cyclone activity at a large scale, while maintaining a climatologically sound boundary (Kuleshov *et al*., 2010; Dowdy *et al*., 2012; Ramsay *et al*., 2012). It also allows for comparison with the existing hemispheric-based studies (e.g. Kuleshov *et al*., 2010; Diamond *et al*., 2015a). The issues related to changes in global and regional frequency and intensity of tropical cyclones in a warming environment have been thoroughly addressed in numerous studies (Webster *et al*., 2005; Holland & Bruyere, 2014; Kossin *et al*., 2014). The approach favoured in these studies includes hemispheric-based analysis which examines tropical cyclone activity across the Northern or Southern hemispheres separately, in order to interrogate and determine the causes behind changing activity across a large spatial scale (Daloz & Camargo, 2018). Hemispheric analysis allows a holistic perspective on tropical cyclone investigations compared to global or single-basin studies, as they account for the variable climatological factors in each hemisphere and offer relatively increased detail on tropical cyclone behaviour as they allow for the multiple interactions of the ocean-atmospheric system to be captured (Maue, 2009; Gleixner *et al.*, 2014). Hemispheric studies additionally allow more robust trend analysis, by providing a more accurate representation of modulating factors of tropical cyclone activity (Daloz & Camargo, 2018). An example is the effects of large spatial modulators (which impact the ocean-atmospheric system across multiple basins), including but not limited to ENSO, SAM and the PDO which can be derived relatively accurately at a hemispheric scale of analysis (Walsh *et al.*, 2016; Daloz & Camargo, 2018). Overall, this study may have far-reaching implications regarding the conditions that actually initiate tropical cyclone genesis and intensification, specifically on how the findings could change the current application of northern hemispheric based observations normally applied to tropical cyclone climatology in the Southern Hemisphere, and therefore warrants investigation (Defforge & Merlis, 2017a).

1.2. Aims and Objectives

The primary aim of the study is to explore and provide a detailed synoptic climatology of tropical cyclones in the Southern Hemisphere and determine the influences of climate change and synoptic/large-scale environmental variables on tropical cyclone variability and trends. This aim will be achieved through the following objectives:

1) Determine the dynamics and climatology of Southern Hemisphere tropical cyclones from 1980- present including:

    a) annual number of storms in each ocean basin

b) latitude and longitude of each tropical cyclone genesis event

c) density in tropical cyclone genesis and intensification events

d) duration of tropical cyclones and maximum intensity attained across their lifetime.

2) Assess sea surface temperature, to interrogate minimum and optimal sea surface temperature required for formation and intensification of tropical cyclones in the Southern Hemisphere.

3) Assess mean, minimum and optimal surface pressure, air temperature, relative humidity zonal, meridional and vertical wind shear and the omega/vertical velocity associated with each of these genesis events to determine the synoptic requirements of formation of these Southern Hemisphere storms.

4) Assess the roles of ENSO and other mechanisms or modes of variability including but not limited to the IOD, MJO, PDO, AAO (SAM), solar energy flux and volcanic activity regarding tropical cyclone activity across the three major ocean basins regions (South Indian and Pacific Ocean Australian) of the Southern Hemisphere.

1.3. Outline of Major Chapters

1.3.1 Literature Review

The literature review aims to provide the current understanding of tropical cyclone genesis and the drivers/mechanisms influencing tropical cyclone activity. The literature review examines the global scale trends in tropical cyclones activity, followed by the Southern Hemisphere tropical cyclone activity and trends for each basin. An overview of the earliest known and present research on tropical cyclone genesis (also referred to as storm genesis) along with a specific description of the major large-scale environmental variables known to influence tropical cyclone genesis is presented. Related to this, the debate on sea surface temperature thresholds required for the formation of tropical cyclones is explored. The changes in tropical cyclone activity over time and under climate change, along with the recent hemispheric studies and trends in tropical cyclone activity and the drivers and mechanisms responsible for the observed changes are presented. Model based studies will also be included regarding their projections and contributions to the understanding of tropical cyclone activity. A brief summary for the modes of variability known to modulate Southern Hemisphere tropical cyclone activity and the known teleconnections between the Southern Hemisphere basins is also offered. The research and physical processes between the northern and Southern Hemispheres will provide the disparities between these regions and how the manifestation of these differences is impacting tropical cyclone activity in the two hemispheres.

1.3.2 Study Site

This chapter will provide the sectors delineating the Southern Hemisphere ocean basins. A background of the climate, ocean currents and the tropical cyclone activity for each Southern Hemisphere ocean basin will be outlined. In addition, historical and projected sea surface temperature and evaporation for the Southern Hemisphere will be presented to frame the present and future energy patterns over the Southern Hemisphere ocean basins. A brief assessment of the vulnerability based on population density and the areas of tropical cyclone activity in the Southern Hemisphere will highlight the regions at risk in the Southern Hemisphere.

1.3.3 Methods and Data

This section will detail the data selection, acquisition for both the tropical cyclone track data and climate data for the drivers at the point of genesis. The data sources, processing and verification processes will also be outlined. The statistical analysis and methods used to interrogate and extract information, correlations and measures of statistical significance for the tropical cyclone data and climate data will also be provided.

1.3.4 Results

The results chapter will cover the outputs of the statistical analyses. The sections will cover the mean activity of Southern Hemisphere tropical cyclones, presented per basin and at a hemisphere-scale. The minimum and optimal magnitudes for each climate variable at the point of genesis is presented alongside genesis flow charts, indicating each climate driver/variable at the point of genesis and their factor weights. The change in tropical cyclone activity and the climate variables/drivers at the point of genesis over the study period of 1980-2016 indicates the shifting trends in storm activity and the genesis drivers. Lastly the results of the multivariate regressions for tropical cyclone activity and modes of variability and volcanic eruptions are provided to indicate the observed influences and degree of statistical significance for each mode and forcer.

1.3.4 Discussion

The discussion will focus on the main findings, with all non-statistically significant trends excluded. Firstly, the mean, minimum and optimal magnitudes of the climate variables at the point of tropical cyclone genesis will discussed in relation to the existing magnitudes recorded for in the literature, with a focus on the differences and similarities to Gray's

(1968, 1979) seasonal genesis index. The new genesis factors will be compared to those in the Northern Hemisphere, then the possible reason for the differences will be outlined. The implications of findings related to the sea surface temperatures required for genesis will be discussed in relation to the sea surface temperature threshold debate. Following this, the statistically significant observed trends of change in tropical cyclone activity and the drivers at the point of genesis will be examined in relation to the existing trends of change, and how this differs from the trends recorded for the Northern Hemisphere tropical cyclones. Then statistically significant correlations between tropical cyclone activity at the point of genesis and intensification, the drivers at the point of genesis and the modes of variability will be compared to existing findings. A critical evaluation on the use of modes of variability will examine the use and efficacy of using these modes to explain tropical cyclone variability. Then the implications of this study and its relevance to future studies and applications will be outlined and lastly the limitations faced in this study will be discussed.

2. Literature Review

2. Introduction: Tropical Cyclones

Research on tropical cyclones has adopted increasingly dynamic approaches, which do not solely focus on the number of storms or their intensity, but on the dynamics and mechanisms which modulate these aspects of tropical cyclone activity (Emmanuel, 1986; Li *et al*., 2013; Kossin *et al*., 2014; Burns *et al*., 2016; Defforge & Merlis, 2017; Scoccimaro *et al*., 2017). At a global scale, tropical cyclone frequency is decreasing, while the numbers of intense storms (category 3-5) are increasing in occurrence and intensity as the environmental energy available to them increases as a result of global warming (Kossin *et al*., 2014). Conflating this increased intensity, the locations at which tropical cyclone maximum intensity and storm genesis occur are migrating poleward (Daloz & Camargo, 2018). These changes are not within the range of natural variability and imply a climate change forcing on tropical cyclone activity (Altman *et al*., 2018). These intense storms migrating poleward in both hemispheres pose new risks to regions located at higher latitudes and have little experience dealing with the occurrence and landfalls of tropical cyclones and their accompanying rainfall and destructive winds (Doocy *et al*., 2013; Altman *et al*., 2018; Schultz *et al*., 2018). In addition to climate change, modes of variability (ENSO, IOD, MJO, SAM and PDO) drive or instigate changes in tropical cyclone activity from intra-seasonal to decadal scales (Camargo *et al*., 2009). One of the obstacles in tropical cyclone research, is the assumptions that the conditions for tropical cyclone behaviour are uniformitarian (Defforge & Merlis, 2017a). While studies recognise that each ocean basin and the tropical cyclones occurring within them, behave different from one another, with their own specific climate drivers and modes of variability, the Southern Hemisphere remains under represented in the literature regarding drivers of formation and basin-hemispheric scale tropical cyclone climatologies (Malan *et al*., 2013; Walsh *et al*., 2016; Defforge & Merlis, 2017a, b). There is an inequality in the amount of tropical cyclone research between the northern and Southern Hemisphere, with a comparatively greater amount of work covering the Northern Hemisphere (Figure 2.2). In addition, much of the recent research on the tropical cyclone climatology in the Southern Hemisphere (Kuleshov *et al*., 2010; Dare & McBride, 2011; Diamond *et al*., 2015a, b; Tory & Dare, 2015; Defforge & Merlis, 2017a, b) and research specifically on the conditions they form under, have been based on the indices created by Gray (1968, 1979), which have demonstrated inherent bias toward Northern Hemisphere tropical cyclone activity and climate data (Watterson *et al*., 1995). In addition, the conditions proposed by Gray (1968, 1979) have been labelled as necessary, but not sufficient, as it is accepted that the variables used in the existing genesis indices do not account for all the factors allowing or preventing a tropical cyclone forming (Klotzbach *et al*., 2017). This complexity warrants investigation, to determine whether other climate drivers/variables influence the genesis environment. In addition, existing genesis indices which apply the same index to predict or describe the seasons of tropical cyclone occurrence across the southern and Northern Hemisphere, typically present problems in accurately reproducing the tropical cyclone potential activity and seasonality for the Southern Hemisphere (Tippett *et al*., 2011), or they do not replicate decreases in tropical cyclone frequency observed in climate models and recent observational trends (Camargo *et al*., 2014; Walsh *et al*., 2016). In light of the current changes in tropical cyclone activity taking place under a warming climate, specifically, the increased number of high intensity storms migrating and forming further poleward in the Southern Hemisphere (Kossin *et al*., 2014; Klotzbach *et al*., 2017; Fitchett, 2018) and a deficit in Southern Hemisphere studies on tropical cyclones (Figure 2.2), a complete examination of the drivers relating to the phases of tropical cyclone formation and intensification is required for the Southern Hemisphere to increase understanding on the dynamics of Southern Hemisphere tropical cyclone activity.

This literature review consists of five main sections. The first section will examine the global trends in tropical cyclone activity, specifically focusing on storm frequency, intensity and location. Within this section the state of the current trends relating to tropical cyclone activity will be highlighted, for the South Indian Ocean, the Australian region (west and east coastal regions), and the South Pacific Ocean. The second section will examine the existing thermodynamic and dynamic meteorological and synoptic conditions required for tropical cyclone genesis. The section will then expand on the requirements of tropical cyclone formation with an emphasis on sea surface temperature thresholds and requirements for storm genesis. Section three examines the Climate change and the effects of a warming climatic system on tropical cyclone activity and the poleward migration of tropical cyclone activity and the mechanisms behind this. Additionally, the applications and merits to observational and model-based tropical cyclone studies is included. The fourth section examines the external influences on tropical cyclone activity by outlining the influence of modes of variability on tropical cyclone activity. The fifth section will outline the existing Southern Hemisphere studies and present the data caveats that are inherent in studies prior to the 1980 satellite era.

2.1. Tropical Cyclone Trends

2.1.1 Global Conditions

The established trends regarding tropical cyclone activity found by observational and model-based studies under climate change, indicate that the globally, tropical cyclone frequency is decreasing (Gleixner *et al*., 2014; Kossin *et al*., 2014; Klotzbach & Landsea, 2015). Meanwhile the number of intense tropical cyclones (category 4-5) is increasing across all the active tropical cyclone regions (Kuleshov *et al*., 2010; Knutson *et al*., 2010; Yoshida *et al*., 2017; Bhatia *et al*., 2019). Regarding the global average frequency, a near doubling in the occurrence of category 4-5 tropical cyclones was observed from 1975 and leading up to 2004 (Webster *et al*., 2005). Specifically, the trend in storm intensity is still found to be increasing globally at a decadal rate of 1 $m.s^{-1}$ (Holland & Bruyere, 2014). The more recent study supporting these findings used the latest track data, which has increased accuracy and homogeneity to examine tropical cyclone activity from 1982-2009 (Kossin *et al*., 2014). The increase of intensity for the strongest storms within each basin has been observed across all basins with tropical cyclone activity (Kossin *et al*., 2014). The strongest magnitude of increase in storm intensity with an 8 $m.s^{-1}$ increase in intensity per decade is recorded for the north Atlantic tropical cyclones (Kossin *et al*., 2014). The overall observations for tropical cyclone frequency and intensity at a global or hemispheric scale are presented in Table 2.1. Some studies (Holland & Bruyere, 2014; Klotzbach & Landsea, 2015) posit that the increasing trend in storm intensity will likely not exceed a 40-50% increase of intensity for category 4-5 tropical cyclones, as it will not be possible for the environment to support such storms. As it stands Klotzbach and Landsea (2015) reported that the percentage increase in category 4 and 5 storms across the southern and Northern Hemispheres is lower over the 1990-2014 period than previously reported (cf. Webster *et al*., 2005).

Table 2.1 Summary table of literature on tropical cyclones categorised by intensity and trends in frequency over time.

Author	**Frequency**	**Lifetime Maximum Intensity**		**Migration**
		Category 1-3	Category 4-5	
Webster *et al*. (2005)	NH: No Change SH: Decreasing	Global Decrease	Global Increase (25%)	-
Oouchi *et al*. (2006)	-	-	NH Increase (+3.3 $m.s^{-1}$) SH Increase (+7.3 $m.s^{-1}$)	
Elsner *et al*. (2008)	Decreasing	Decreasing	Increasing: 0.15 $m.s^{-1}.yr^{-1}$	-
Bender *et al*. (2010)	Global Decrease	Global Decrease (7%)	Global Increase (11%)	-
Emanuel (2010)	Global Decrease (SH=17.5%)	-	-	-
Kuleshov *et al*. (2010)	SH: Increase in high intensity storms	Decrease	Increase	-
Murakami *et al*., (2012a)	Global Decrease (13-25%)	Decrease	Increase (1-7%)	Northward shift (Cat-5 storms)
Emmanuel (2013)	Global Increase	Global Increase	Global Increase	-
Kossin *et al*. (2013, 2014)	Global Decrease	Global Decrease	Global Increase (+1 $m.s^{-1}$ per decade) but lower Mean LMI	NH & SH: Poleward (53 & 62 km^{-1} per decade)
Gleixner *et al*. (2014)	NH Decrease: (6%) SH Decrease: (22%)	NH: Increase SH: Decrease	NH: Increase SH Increase	-
Holland and Bruyere (2014)	Global Annual Count: Neutral	Global Decrease	Global Increase (25-30 %)	-
Klotzbach and Landsea (2015)	Global Decrease	Global Decrease	Global Increase (40%)	-
Daloz and Camargo (2018)	Globally Decreasing	Global Decrease	Global Increase	NH & SH: Poleward ½ ° per decade
Yoshida *et al*. (2017)	Global Decrease (33%)	Global Decrease	Global LMI increase (9%)	-
Fitchett (2018)	SH: Increase (Category 5 Storms)	-	SH Increase	Poleward (27, 28 and 29°C SST isotherms and TC's)
Bacmeister *et al*. (2018); Bhatia *et al*. (2019)	Global Decrease	Global Decrease	Global Increase	Poleward
Wehner *et al*. (2018): model	Global decrease	Global Decrease	Global Decrease	-

Anthropogenic climate warming indices demonstrate the global warming trend has the potential to cause a 25-30% increase in category 4 and 5 tropical cyclones (Holland & Bruyere, 2014), while climate models project a 33% decrease in the global number of tropical cyclones by 2099 under the current warming regime (Yoshida *et al*., 2017). Relating to severe tropical cyclones, it is projected that their frequency will increase within a range of 10-40% by the 3rd quarter of the 21st century, with the Northern Hemisphere basins accounting for a majority of this increase (Emanuel, 2013). Using power dissipation as an indicator of storm intensity, Emanuel (2013) also projected a 40% increase of storms that are category 3 and higher. This increasing trend of storm intensity with sea surface warming is observed to be especially higher in magnitude for the Pacific and Indian Oceans (Yoshida *et al*., 2017). However, model-based projections related to storm intensity should be viewed with caution, as much of the physical parameters relating to air-sea interactions remain unresolved and all the mechanisms which influence intensity are not yet well-known or understood (Tippett *et al*., 2011; Soloviev *et al*., 2014).

2.1.2 Tropical Cyclone Activity and Trends for the Southern Hemisphere

2.1.2.1 South Indian Ocean

In the South Indian Ocean, the frequency of storms is decreasing, while the intensity trends of South Indian Ocean storms indicates an increase in the occurrence of category 4 to 5 storms, following the global trend (Webster *et al*., 2005; Mavume *et al*., 2009). The number of high intensity tropical cyclones with central pressures below 950mb in the South Indian Ocean is observed to be increasing at a rate of +0.15 $TCs.yr^{-1}$ (Kuleshov *et al*., 2010). In a recent study, Fitchett (2018) reported an increased occurrence in category 5 storms since 1989 in the South Indian Ocean, with their observed occurrences taking place at increasingly poleward latitudes. The tropical cyclone season initiates in November and persists until April, while the interannual variation of tropical cyclone activity ranges from 5-15 tropical cyclones, with an annual mean of 9-12.5 tropical cyclones per year (Mavume *et al*., 2009; Fitchett & Grab, 2014). These tropical cyclones tend to occur towards the east and north of the basin in November and April, however, genesis activity shifts further south during February and March (Mavume *et al*., 2009). In the South Indian Ocean, while genesis is observed across the entire region, the location where the highest number of tropical cyclones undergo genesis is found within 5-15°S; 60-130°E (Kuleshov *et al*., 2009; Mavume *et al*., 2009; Malan *et al*., 2013; Burns *et al*., 2016). Between the African coast and 60°E tropical cyclone genesis displays a tendency to take place south of and between 10-25°S (Kuleshov *et al*., 2009; Mavume *et al*., 2009). These regions of formation are characterised by warmer sea surface temperatures during the tropical cyclone season and coincide with the approximate location of the Intertropical Convergence Zone (ITCZ) over the Indian Ocean (Mavume *et al*., 2009; Chen *et al*., 2019). The tropical cyclones predominantly impact the island regions of Madagascar, La Reunion, Mauritius and the coastline of Mozambique, located off the southern African east coast (Malan *et al*., 2013).

2.1.2.2 Australian Region

The frequency of tropical cyclones in the Australian region (105-165°E), which includes both the east and west coastal regions of the continent, indicates that the overall number of tropical cyclones is decreasing, while the average number of intense tropical cyclones display an increase over time (Hassim & Walsh, 2008; Dowdy *et al*., 2012). In the west Australian region, a decreasing trend of -0.017 TCs.yr^{-1} is observed, with a decreasing rate of -0.038 TCs.yr^{-1} in the eastern Australian region (Kuleshov *et al*., 2010). Related to the sub-regions of Australia, it is also noted that the west and eastern regions of the Australian continent indicate substantial contrasts regarding duration and number of these intense storms, which indicate a decrease in frequency over the eastern region, but a low amplitude decreasing trend in the western region (Hassim & Walsh, 2008). The typical season of tropical cyclone occurrence begins in November and ends in April, with a peak in activity during March (Hassim & Walsh, 2008; Haig *et al*., 2014). In the most complete climatological studies of the Australian region to date from 1979 (McBride & Keenan, 1982; Diamond *et al*., 2012, 2015a, 2015b), the tropical cyclone season extended from November to May, with a peak in activity during January. The Australian east coast region is observed as the most active region of tropical cyclone activity compared to the western sector (Hall *et al*., 2001). However, higher intensity storms are recorded over the western region compared to the eastern sector (Hall *et al*., 2001; Hassim & Walsh, 2008). Similar to the rest of the Southern Hemisphere tropical cyclones, the most common genesis locations for the Australian tropical cyclones were found to coincide with the ITCZ location (Hall *et al*., 2001). The preferred locations of genesis are reported to exist around the Australian coastline at 120°, 135° and 150°E and 5-15°S (Dare & Davidson, 2004). Around 13 tropical cyclones occur each season with approximately 50% of these occurring in the western region with a range of 6-20 tropical cyclones per season (Kuleshov *et al*., 2009; Mavume *et al*., 2009). Tropical cyclones in the Australian region persist for a mean of 4-7.5 days, with western storms experiencing longer durations up to five days (Dare & Davidson, 2004; Hassim & Walsh, 2008). The tropical cyclones formed in the Australian region primarily impact the west and eastern coastlines of the Australian continent (Hassim & Walsh, 2008). However, the storms formed in this broad region, additionally track over and make landfall within the Gulf of

Carpentaria and the southern regions of Papua New Guinea and the Indonesian Archipelago (Hassim & Walsh, 2008; Mulyana *et al*., 2018).

2.1.2.3 South Pacific

The severe tropical cyclones (category 4-5) in the south west Pacific Ocean have displayed an increased occurrence in the South Pacific from 1982-2006 (Webster *et al*, 2005; Kuleshov *et al*., 2008). Specifically, an increase in intensity observed through increased storms with a central pressure smaller than 945mb has been found for the South Pacific tropical cyclones, however, the increase was no longer statistically significant (Kuleshov *et al*., 2008). The frequency of South Pacific storms is decreasing at a rate of 0.096 TC's.yr^{-1} (Kuleshov *et al*., 2010). The range of tropical cyclone occurrence is 10.4 TCs.yr^{-1}, but 13.03 TC's from 1981-2010 (Diamond *et al*., 2013). The tropical cyclone season extends from November to April, with a peak in activity during February and the genesis location of the South Pacific tropical cyclones situated around 13.3°S; 168°E (Hassim & Walsh, 2008; Diamond *et al*., 2013). The main regions impacted by South Pacific tropical cyclones include the multitude of small island nations within the South Pacific, namely, Tonga, New Zealand and regions of eastern Australia (Ramsay *et al*., 2008; Callaghan & Power, 2011). The duration of South Pacific tropical cyclones is highly variable but relatively short, with lifetimes of 25 hours to 23 days (Terry & Gienko, 2010). Studies examining tropical cyclone dynamics in the South Pacific Ocean report that only the long-term trend in mean sea level pressure presented as a statistically significant factor for the South Pacific, with the tropical cyclone frequency displaying a non-significant decreasing trend (Kuleshov *et al*., 2010; Terry & Gienko, 2010). However, Nott (2011) reported that the long-term trends may not be stochastic, and that underlying patterns of activity could be present in the South Pacific basin. Subsequently, it was found that intensity has increased at a rate of 2.5 $m.s^{-1}$ per decade (Kossin *et al*., 2014).

2.1.2.4 General Trends: Southern Hemisphere Basins

In climate models, significant variances exist between the outputs for southern and northern hemispheric tropical cyclones, regarding the possible extent and magnitude of changes in intensity and frequency (Gleixner *et al*., 2014). Consequently, tropical cyclone activity is projected to decrease by 6% in the Northern Hemisphere, while a greater decrease of 22% is projected for the Southern Hemisphere by 2100 (Mao *et al*., 2013; Gleixner *et al*., 2014). Presently, according to model-based and historical studies, the largest decreases in frequency and corresponding increases in intensity are observed in the Indian, north west and south west Pacific Oceans (Kossin *et al*., 2014; Daloz & Camargo, 2018, 2018; Sun *et al*., 2017). The difference between the trends (Table 2.2) in northern (specifically the North Atlantic Ocean) and southern hemispheric tropical cyclone frequency is attributed to ocean-atmospheric changes, for example, the weakening of the tropical Walker Circulation and increased sea surface temperatures under a warming climate (Walsh *et al*., 2016). However, no observational studies have attempted to reconcile these trends for the entire Southern Hemisphere or determine whether they differ from northern hemispheric or basin-scale trends (Webster *et al*., 2005; Gleixner *et al*., 2014; Holland & Bruyere, 2014).

Table 2.2 Summary of literature capturing trends of change in tropical cyclone activity: Tropical cyclone frequency, intensity and category 4-5 incidence for Southern Hemisphere basins (SIO, Australian Region and the SP) and global observations.

Author	South Indian Ocean	Australian Region	South Pacific Ocean	Global
		Tropical Cyclone Frequency		
Kuleshov *et al*. (2010) Trend per 26-year period	+0.8 TCs	-1.2 TCs	-2.8 TCs	-2 TCs
Diamond *et al*. (2013)	5-15 per year	-	6 per year	-
Yoshida *et al*. (2017)	Projected Decrease (-44%)	Decrease (-44%) Included in SIO (west of 135°E)	Decrease (-40%)	Decrease
Hassim and Walsh (2008)	-	Decreasing	-	-
		Tropical Cyclone Intensity		
Oouchi et al. (2006); Harper *et al*. (2008)	Increasing (14.1%)	Increasing	Weak signal (stationary)	-
Bacmeister et al. (2018)	-	-	-	Increasing
Elsner *et al*. (2008) 75-99th percentile	0.28-0.69$ms^{-1}.yr^{-1}$	-	-0.04-0.46$ms^{-1}.yr^{-1}$	0.15 $m.s^{-1}.yr^{-1}$
Kuleshov et al. (2010)	+0.15 $TCs.yr^{1}$(+28%)	**+18% (per 26 years)	**+2% (per 26 years)	+0.14 $TCs.yr^{-1}$ at +17 % (per 26 years)
Kossin *et al*. (2014)	+1.7 $m.s^{-1}$ per decade	Part of SIO extent	+2.5 $m.s^{-1}$ per decade	+1 $m.s^{-1}$ per decade
Holland and Bruyere, (2014); Klotzbach and Landsea (2015)	-	-	-	Currently 40% increase
Sobel *et al*. (2016)	-	-	-	Mean of 0.2 $m.s^{-1}$/year
Parker *et al*. (2018) model	-	Increase (-11mb pressure and +5-10% wind speeds)	-	-
		Number/Frequency of Category 4-5 storms		
Webster *et al*. (2005)	Increasing (34%)	Omitted	Increasing (28%)	-
Hassim and Walsh (2008)	-	Increasing (12% for WA and 23% for EA)	-	-
Knutson *et al*. (2010)	Increasing	Increasing	Increasing	Increasing
Kuleshov *et al*. (2010)	Increasing	Increasing	Increasing	Increasing
Weinkle *et al*. (2012)	-	-	-	21 TCs per 1°C Increase
Wu and Zhao (2012)	-	-	-	43% Increase
Done *et al*. (2015)	-	-	-	NA only (19% Increase)
Walsh *et al*. (2016)	Increasing	Increasing	Increasing	Increasing
Fitchett (2018)	Increasing no. of Category 5 storms	-	-	-

2.2. Requirements for Tropical Cyclone Formation

Tropical cyclones refer to any cyclonically rotating large scale (synoptic) storm system which originates in the tropical regions of the oceans (Bhaskaran *et al*., 2018). Such storms are usually warm core systems as they are driven by the heat energy from the ocean (Tory & Dare, 2015). The development of these tropical features is influenced by dynamic and thermodynamic climate variables, which interact with each other and depending on the interactions, lead to either conducive or non-conducive conditions for cyclogenesis (Juracic & Raymond, 2016; Klotzbach *et al*., 2017). In order for tropical cyclones to undergo successful storm genesis and attain tropical cyclone intensity, they require the alignment of specific large-scale environmental variables, which were set out in the seasonal genesis index by Gray (1968, 1979) and have been used in multiple studies to forecast and project seasonal tropical cyclone activity (Camargo *et al*., 2007; Li *et al*., 2013; Camp *et al*., 2019). This section will examine these required variables and explain their significance in tropical cyclone investigations. The thermodynamic variables: sea surface temperature and relative humidity and dynamic variables: vertical velocity, and wind shear will be explained. Sea surface temperature will be discussed in a subsection, as it incorporates the latest debates and reviews regarding the relevance of sea surface temperature in the role of tropical cyclone genesis.

2.2.1 Seasonal Genesis Index: Climate Variables/Drivers

There are six known critical drivers which play a role in promoting the conducive conditions required for tropical cyclone storm formation as outlined by existing genesis studies (Gray, 1979; Klotzbach *et al*., 2017). The specific conditions which are set out in Gray (1968, 1979) and have been cited in multiple subsequent studies (cf. Emanuel, 2003; Camargo *et al*., 2009; Diamond *et al*., 2013; Li *et al*., 2013; Malan *et al*., 2013; Bhaskaran *et al*., 2018) are:

1) A minimum sea surface temperature ≥ 26.5°C (to provide adequate thermal energy) with a deep thermocline extending down ≥ 60m.

2) High moisture levels in the low and mid-troposphere, i.e. adequate relative humidity around the 700mb atmospheric level.

3) Conditionally unstable atmosphere that supports deep convection (whereby saturated air will be allowed to ascend).

4) A large magnitude of relative vorticity (fluid rotation) in the lower troposphere,

5) Low vertical shear in the horizontal wind fields; differences in wind speed between different atmospheric levels must be below 15 $m.s^{-1}$.

6) The location of genesis must be >5°N/S away from the equator in both hemispheres, in order for Coriolis force (resultant force created by the planets rotation) to have an influence on the angular momentum of the rotating tropical cyclone system.

[Gray, 1979; Klotzbach *et al*., 2017]

Prior to cyclogenesis, an atmospheric disturbance (trough of low pressure) must be present in conjunction with warm sea surface temperatures and high moisture content (Emanuel, 2003; Diamond *et al*., 2013). Most of these factors as outlined by Gray (1968, 1979) are actually present persistently across most of the tropical regions of the ocean (Bhaskaran *et al*., 2018). Specifically, throughout the summer period, sea surface temperatures greater than 26.5°C and the presence of a conditionally unstable atmosphere, are present in the tropical regions of the ocean (Tory & Frank, 2010). However, tropical cyclones do not always form, regardless of the presence of these conducive conditions, therefore, the determining factors which promote storm genesis are likely the degree of magnitude and variation in the nature of these climate drivers (Tory & Frank, 2010; Vecchi *et al*., 2014; Klotzbach *et al*., 2017). Some consistent factors include disturbances, which are clearly observed for the majority of tropical cyclone events (Riehl, 1948; Bhaskaran *et al*., 2018). These disturbances are characterised as large-scale waves (easterly and westerly waves) that possess horizontal shear, which initiates a rotation flow that develops the wave into a cyclonic system reminiscent of a mature tropical cyclones motion (Emanuel, 2003; Tory & Frank, 2010).

2.2.1.1 Moisture

Aside from sea surface temperature, the moisture content of the atmosphere may be one of the most important factors in storm genesis and intensification (Tory & Dare, 2015; Wu *et al*., 2015). Tropical cyclones attain their energy from the latent heat released from condensation, which is part of the positive feedback inherent between the atmosphere and the ocean during tropical cyclone formation (Tory & Dare, 2015; Scoccimarro *et al*., 2017). It was found that even when vertical wind shear was at a higher and therefore detrimental level for initiating storm genesis, the high relative humidity overshadowed this factor and allowed the initiation of storm genesis, indicating a greater weighting of influence on the formation stage (Li *et al*., 2013). Subsequently, only the combined effect of sea surface temperature, vorticity and vertical shear were able to instigate genesis minimum during the boreal summer, i.e. during the season of maximum tropical cyclone activity (Li *et al*., 2013). High relative humidity allows for the deep moist convection which allows the spiral cloud bands of tropical cyclones to form (Emmanuel, 2003; Tory & Dare, 2015; Bhaskaran *et al*., 2018). Aside from aiding the formation and sustaining a tropical cyclone, the atmospheric moisture content or relative humidity has been observed to promote rapid development and intensification of tropical cyclones (Camargo *et al*., 2009; Li *et al*., 2013; Klotzbach *et al*., 2017). Apart from influencing the formation, Ying and Zhang (2012) report that the intensity of some tropical cyclones is inhibited by excess moisture, which causes increased convection in the storms outer cloud bands, increases the storm size, and as a result weakens the intensity. Low moisture, however, can cause the storm to contract in size, which favours higher intensification (Ying & Zhang, 2012). The presence of dry air advecting into the storm environment has indicated a small influence on tropical cyclone formation potential provided the low moisture air was present over 270 km away from the storm (Wu *et al*., 2015). However, when the dry air intrudes into an area closer to the storm extent, specifically the core, then the intensity of the tropical cyclone is greatly decreased, as upward motion and deep moist convection is negatively impacted (Braun *et al*., 2012). Wu *et al*. (2015) confirmed that high levels of moisture in the boundary layer do contribute moisture to the tropical cyclones core and in turn promote intensification, provided the wet air intrusion is located within the rear quadrant of the tropical cyclone. These observations indicate that relative humidity is not just necessary in terms of the levels present in the environment, but the location of the moisture plays a role as well.

2.2.1.2 Vorticity

Vorticity refers to the spin of the fluid. A positive vorticity indicates a cyclonic spin in the Northern Hemisphere, while a negative vorticity indicates a cyclonic spin in the Southern Hemisphere (Yu *et al*., 2016). The large-scale horizontal surface wind shear which is translated into cyclonic shear (relative vorticity) is required for the surface convergence strongly associated with the initiation of vertical motion (Tory & Frank, 2010; Klotzbach *et al*., 2017; Daloz & Camargo, 2018). Studies indicate that increased rates of storm genesis occur when these conditions of strong low-level vorticity are present in the environment (Yu *et al*., 2016; Huangfu *et al*., 2018). Indeed, the majority of storms indicate upper-level anticyclonic vorticity and low-level cyclonic vorticity, (Emanuel, 2003; Pezza & Simmonds, 2005; Yu *et al*., 2016; Song *et al*., 2018). It was determined by Tippett *et al*. (2011), that once low-level vorticity increases, so does the probability of genesis, however, the other variables of formation will limit the rate of this effect once vorticity becomes large enough, so that genesis will not increase even if vorticity continues to increase (Li *et al*., 2013). An increase in storm intensity has also been statistically linked to relative vorticity at 850mb in a model-based study by Murakami *et al*. (2012a).

2.2.1.3 Vertical Wind Shear

Wind shear is the change in wind speed with a change in location or height (Robe & Emanuel, 2001). The exact maximum threshold of vertical shear required to facilitate genesis is not well understood, as the range varies arbitrarily from storm to storm during the point of genesis and across a tropical cyclone's lifetime (Tory & Frank, 2010). However, the general rule observed, is that low vertical wind shear of horizontal wind flows encourages tropical cyclone formation (Emanuel, 2003). Increased magnitudes of shear have been observed to decrease tropical cyclone intensity and formation potential with the ability to completely break down the genesis or vortex formation of a tropical cyclone (Nolan & McGauley, 2012; Bhaskaran *et al*., 2018). Tropical cyclones have been observed to develop (dissipate) when the vertical shear is small (large) over the center of developing storms and upper tropospheric flow displays strong (weak) anticyclonic shear (Klotzbach *et al*., 2017). It is established that strong vertical shear inhibits cyclogenesis and that low shear values as close to zero as possible are linked to greater storm intensification and formation potential (Gray, 1968; Emanuel, 2003). Yu *et al*. (2016) determined that vertical shear impacts formation potential differently depending on location, when vertical shear was observed as a better predictor of genesis in the North West Pacific Ocean, compared to the South China Sea. This indicates that vertical shear, while inherently a necessary driver for genesis, may influence the formation of tropical cyclones differently, depending on the location (Yu *et al*., 2016). Compared to the Northern Hemisphere genesis events, where a shear value of 12-15 $m.s^{-1}$ is recorded as the optimal levels of shear required for storm genesis (Vecchi & Soden, 2007; Chen *et al*., 2018), the optimal shear values observed for the Southern Hemisphere genesis events ranges from a much lower magnitude of shear of 1-4 $m.s^{-1}$ (Nolan & Rappin, 2008). Notably, Chen *et al*. (2018) recently found that when low-level mean flow (wind flow) was orientated to the left (right) of the vertical shear then tropical cyclone intensification (storm size) was favoured. Notably, shear is also the main factor which is the most problematic to model in storm intensity projections, and as a result creates the most uncertainty in projections of storm intensity (Emanuel *et al*., 2004).

2.2.2 Sea surface temperature

Sea surface temperature is another critical driver of tropical cyclone formation (Gray, 1968; Malan *et al*., 2013; Defforge & Merlis, 2017a). Emanuel (1986, 1988) determined that sea surface temperature dictated the intensity of a tropical cyclone, with the highest maximum potential intensity (highest storm intensity the environment can support) increasing with sea surface temperature. Multiple studies have since reported and supported this significant feedback between the sea surface temperature and its influence on tropical cyclone intensity (Halliwell *et al*., 2015; Strazzo *et al*., 2015; Wing *et al*., 2015; J.A. Zhang *et al*., 2017; Zhou *et al*., 2017). Sea surface temperature additionally influences the moisture and heat fluxes in the storm formation environment (Tory & Dare, 2015). A tropical cyclone forms under conditions of sustained heating of the ocean, which drives the increase in atmospheric moisture content and subsequent latent heat release (Bhaskaran *et al*., 2018). This latent heat release must be larger than the heat lost through evaporation, for deep convection (the turbulent mixing mechanism which displaces warm moist air upwards through the troposphere) to be initiated and sustained (Tory & Dare, 2015; Wing *et al*., 2015).

Table 2.3 Summary of literature: The varying sea surface temperature thresholds reported as a requirement at the point of genesis. The time period over which the research was done, the general magnitude reported as a threshold and the northern and Southern Hemisphere sea surface temperature thresholds as reported.

Minimum SST required for storm genesis	Time Period	Averaged for all Oceans	Northern Hemisphere	Southern Hemisphere
Palmen (1948)	-	26-27°C	-	-
Fisher (1958)	1954-1955	-	26.1°C (NA)	
Gray (1968)	1870-1968 (Approximate)	26.5°C	-	-
Wendland (1977)	1962-1971	-	26.8°C (NA)	-
Rodgers *et al*. (2000)	1997 (One-year analysis)	>26°C	-	-
Mavume *et al*. (2009)	1980-2007	-	-	28-29°C (SWIO)
Dare and McBride (2011)	1981-2008	25.5°C		
Malan *et al*. (2013)	1948-2007	26-27°C		
Defforge (2016)	1982-2014	26.4°C	25.7°C (NA) 27°C (WP)	

2.2.2.1 Surface Fluxes

Sea surface temperature is not the only important influencer of storm intensity (Kunkel *et al*., 2013). The air and sea interact close to the surface, with large amounts of heat and energy exchanges taking place via the sea surface temperature, convection and surface winds (Michaud, 2012; Vecchi *et al*., 2014). Under high wind conditions during hurricanes/tropical cyclone occurrence, the energy transfer from the air to sea via sea spray and evaporation reaches over 100000 W.m^{-2}, which is a great loss of heat from the sea to the atmosphere (Michaud, 2012). With reference to the above, the tropical cyclone intensity is related to, or can be viewed as a product of the exchange of energy between the ocean and atmosphere (Kunkel *et al*., 2013). Air temperature of the troposphere is also observed as an important driver in storm formation and intensification (Emanuel, 2013; Tory & Dare, 2015; Rai *et al*., 2019). Furthermore, the potential intensity of tropical cyclones is reported to increase by only 0.4 m.s^{-1} for every 1°C increase in sea surface temperature and does not account for the increasing trend observed for intensity (Emanuel, 2013). It is stated that the fluxes or exchange of heat between the ocean and atmosphere influences the processes which provides tropical cyclones with their energy (J.A. Zhang *et al*., 2017). Lin *et al*. (2009) reported that the air-sea interaction involving enthalpy flux (the exchange and interactions of the total heat content contained within the ocean and atmospheric systems at a point in time) or heat and moisture exchanges were the drivers for the rapid and extreme intensification of Tropical Cyclone Nargis in 2008. It was noted that ocean heat content was the core element in intensification, as the energy required for the intensification originates there, and it is especially important in assisting storm intensification for category 3-5 storms (Lin *et al*., 2009). This is echoed in findings by Fitchett (2018), where the high intensity category 5 tropical cyclones required a higher magnitude of sea surface temperature in order to intensify into a severe storm. In addition, the intensification of tropical cyclones in the south west Indian Ocean was attributed to greater barrier layer thickness, which is the difference between the mixed layer (vertical region of uniform temperature and salinity) and isothermal layer (uniform temperature) depths, while the formation of tropical cyclones was linked to ocean temperature (Mawren & Reason, 2017). As indicated above, sea surface temperature indicates great influence on the formation and intensification of a tropical cyclone, however, the vertical heat content of the ocean and thermal energy related to the atmosphere cannot be disregarded (Burns *et al*., 2016).

In another examination of the air-sea interaction with intense tropical cyclones, Mcphaden *et al*. (2009) noted that the ocean loses at least 2-3°C of heat to the atmosphere via turbulent mixing. In addition, the air temperature near the surface tends to mirror the magnitude of the ocean temperature, yet it does so at a temperature which is a few degrees lower than the ocean (Mcphaden *et al*., 2009; Vecchi *et al*., 2014). When sea surface temperature is lower by 0.2-0.4K, a decrease of intensity by 7mb is observed to take place provided the sea surface temperature decrease occurs within close proximity to the tropical cyclone center (Rai *et al*., 2019). These interactions of the tropical cyclone with the heat content of the air and sea demonstrates an inherent negative feedback, where strong surface divergence and mixing takes place at the base of the storm and leads to a decrease in sea surface temperature as enthalpy is lost to the environment (Scoccimaro *et al*., 2017; Bhaskaran *et al*., 2018). Recently, the air-sea flux mechanism has become less effective at cooling the ocean via heat exchanges, which in turn has created a surplus of heat in the ocean and contributed to increased sea surface temperatures (Zhang *et al*., 2018). While the air-sea interaction theory, including the fluxes between the ocean and air, have been studied broadly (Emanuel, 1986; Lin *et al*., 2009; Mcphaden *et al*., 2009; Evans & Waters, 2012; L. Zhang *et al*., 2017; Zhang *et al*., 2018), the direct relationship between air temperature across the troposphere in relation to storm frequency, genesis and intensification has not previously been explored in depth, particularly within the Southern Hemisphere basins.

2.2.3 Thresholds of sea surface temperature

The reason the 26.5°C requirement was put forward for storm formation, is that the optimal convection appears to initiate at this temperature, which in turn promotes the deep moist convection required for storm formation (Tory & Dare, 2015). The 26.5°C threshold originates from the observation that the above deep convection will rarely occur at temperatures lower than this. The threshold range required for deep convection falls within a range of 26-27°C as reported by Johnson and Xie (2010), while Evans and Webster (2014) reported that the mean global threshold for deep convection is approximately 27°C. The large amounts of energy required for storm genesis, comes from high sea surface temperatures, which drive the surface fluxes of heat and moisture and promote self-sustaining circulations i.e. a mature tropical cyclone (McTaggart-Cowan *et al*., 2015). The saturated air rises and cools, eventually condensing and forming the spiral rain bands characteristic of tropical cyclones (Wu *et al*., 2015; Bhaskaran *et al*., 2018). Latent heat is released as the evaporated moisture within the rising air condenses into clouds, which provides further energy for a tropical cyclone (Scoccimaro *et al*., 2017).

2.2.3.1 The 26.5°C Threshold for Tropical Cyclone Genesis

A threshold is defined as the point at which an occurrence will start, or a change in any arbitrary process will take place (Tory & Dare, 2015). However, sea surface temperature thresholds for tropical cyclone formation may become meaningless in a changing climate (Johnson & Xie, 2010). The results attained by modelling studies examining the current global warming trends (Knutson *et al*., 2010; Evans & Waters, 2012; Walsh *et al*., 2016; Hsu *et al*., 2018) do not reveal the changes expected in tropical cyclone activity and genesis; the projections do not capture a uniform change in tropical cyclone activity with a warming climate across the different ocean basins. If a threshold sea surface temperature was relevant to storm formation, it would not only be predictable and consistent across multiple basins, but storms would be unable to form at temperatures below this threshold (Table 2.3), which is contrary to observations where storm genesis takes place at magnitudes lower than 26.5°C (Mavume *et al*., 2009; Tory & Dare, 2015; Defforge & Merlis, 2017a). It is further stated that the main uncertainty inherent in projecting tropical cyclone activity is attributed to the trends in sea surface temperature within the warming climate (Yoshida *et al*., 2017). Therefore, it is best to adopt the notion that as the ocean warms and sea surface temperatures increase within the tropical cyclone formation zones, then so will the threshold or alternatively, the range of temperatures at which tropical cyclones have the greatest probability of undergoing genesis (Knutson *et al*., 2010; Evans & Waters, 2012; Walsh *et al*., 2016; Defforge & Merlis 2017). However, the sea surface temperatures observed at the point of genesis indicate little change in magnitude. This is based on Dare & McBride's (2011) examination of storms from 1981-2008, which indicated that only small changes have occurred in the sea surface temperatures at the point of genesis (+ 0.20°C).

The 26°C sea surface temperature threshold (See Table 2.3 for different SST thresholds) was first posited by Palmen (1948), based on visual distributions of tropical cyclone formation zones. Gray (1968) later adopted the threshold but as 26.5°C, in his seminal paper on tropical cyclone climatology, which was based on the 26.5°C isotherm that existed over the regions of tropical cyclone genesis at the time. However, Gray (1968) based this threshold predominantly on the Northern Hemisphere storm population (Watterson *et al*., 1995; McTaggart-Cowan *et al*., 2015). Dare and McBride (2011) qualitatively assessed the sea surface temperature threshold by analysing over 2000 storms from 1981-2008, and observed that globally, 98.3% of genesis events take place at a sea surface temperature above 25.5°C. It was also found that for a tropical cyclone to form, it had to encounter sea surface temperatures of 25.5°C, at least once over the last 48-hours, even if sea surface temperature was recorded as higher or lower after six hours (Dare & McBride, 2011). Fitchett (2018) reports that the occurrence of category 5 tropical cyclones is increasing alongside the observed poleward shift in the 29°C isotherms. In the south west Indian Ocean, the majority of tropical cyclones forming at a sea surface temperature of 28-29°C occurred during January to March, while lower temperatures at the point of genesis are recorded for tropical cyclones which occurred from November to December (Mavume *et al*., 2009). Examining the upper end of sea surface temperature thresholds, the reason posited for no storm occurrences above 32°C is that these high temperatures rarely occur during most storm formation events to begin with (Defforge & Merlis, 2017b). Alternatively, an upper limiting threshold is posited to exist, whereby tropical cyclone formation and intensification potential may decrease under a continuously increasing sea surface temperature trend (Holland & Bruyere, 2014). Underlying the assumption for the existence of a threshold, is the observation that tropical cyclones source the entirety of its energy from the conditional instability of the atmosphere and the subsequent deep convection incited on by sea surface temperatures above 26°C (Palmen, 1948; Emanuel, 2003; Dare & McBride, 2011; Tory & Dare, 2015).

2.2.3.2 Reexaminations of the Threshold

Based on the sizeable influence which has been attributed to sea surface temperature thresholds and their role in tropical cyclone genesis, multiple studies re-examined the issue (McTaggart-Cowan *et al*., 2015; Tory & Dare, 2015; Defforge & Merlis, 2017a, b). Dare and McBride (2011) observed the majority of tropical cyclone formation events from 1980-2008, occurring at a sea surface temperatures above 25.5°C. Building on this, Tory and Dare (2015) provided updated findings which indicate that storms forming below the 25.5°C and 26.5°C thresholds do so, not by attaining all of their energy via deep convection promoted by optimal sea surface temperatures, but from baroclinic instability. This supports research by McTaggart-Cowen (2013, 2015) that observed, 16% of the tropical cyclones developing via a baroclinic mechanism, instead of deep convection. Specifically, tropical cyclones which form at a lower threshold sea surface temperature (<26.5°C) have been observed to do so in the presence of a baroclinic environment over the region of genesis (McTaggart-Cowan, 2015; Bhaskaran *et al*., 2018). Approximately five percent of tropical cyclones have been demonstrated to form at sea surface temperatures 4-5°C cooler than the 26.5°C threshold, but it was argued that this does not discount the reliability of the 26.5°C threshold as a majority of storms did occur at this temperature (cf. Korty *et al*., 2012; Tory & Dare, 2015; McTaggart-Cowan, 2015). However, since a small number of storms are found to form below the 26.5°C threshold, there has been doubt relating to the data accuracy when capturing these storm tracks and climate data (Dare & McBride, 2011). Therefore, there has been continued support of the 26.5°C threshold, provided the storm gestation period or the time it takes to develop at a temperature above 26.5°C is in the region of 24 hours (Tory & Dare, 2015). McTaggart-Cowan *et al*. (2015) reinvestigated Gray's (1968) sea surface temperature threshold of tropical cyclone genesis by assessing the probability of genesis events under different sea surface temperatures and atmospheric states and confirmed that the 26.5°C threshold is still applicable to the majority of tropical cyclone genesis events. Although, these genesis events that occurred at sea surface temperatures below 26.5°C, were not explained fully by sea surface temperature, and therefore indicates that it is not always the main modulator of storm genesis (McTaggart-Cowan *et al*., 2015; Tory & Dare, 2015; Defforge & Merlis, 2017a). The quantitative proof that tropical cyclone genesis does not necessarily require an absolute threshold temperature for genesis also highlights that sea surface temperature may not be the core driver during genesis events (Johnson & Xie, 2010; Defforge & Merlis, 2017a). The specific environment in which the storms with low sea surface temperatures form, tend to have large values of vertical wind shear and low-level atmospheric equilibrium conditions, which promotes rising air parcel buoyancy in the storm, so they maintain their height (McTaggart-Cowan *et al*., 2006, 2015). These cold sea surface temperature genesis events are rarely observed in the Pacific basins, but were well represented in the North Atlantic, while these events for the Southern Hemisphere basins were not addressed in detail (McTaggart-Cowan *et al*., 2015).

While recognising the previous works on the sea surface temperature threshold, Defforge and Merlis (2017a) argued that sea surface temperature increases do not fully reconcile the changes in genesis location and storm intensity, as it is not the only factor governing tropical cyclone activity. Instead, it is the climatological backgrounds of each basin, which includes the influencing mechanisms of genesis, specifically, sea surface temperature, baroclinicity and convective stability (McTaggart-Cowan *et al*., 2015; Mawren & Reason, 2017; Wang & Moon, 2017). Across the northern and Southern Hemisphere, variable sea surface temperature thresholds for tropical cyclone genesis are observed in each basin (Defforge & Merlis, 2017a, b). In the northern Atlantic basin, the lowest sea surface temperatures at the point of genesis are recorded, while the highest genesis sea surface temperatures are recorded in the western Pacific region (Defforge & Merlis, 2017a). Overall, only 5% of all the storms from 1982-2014 underwent genesis at sea surface temperatures lower than 25.7°C in the North Atlantic, while in the west Pacific it was 27°C and at the global scale, the coolest genesis sea surface temperature was 26.4°C (Defforge & Merlis, 2017a). Importantly, the sea surface at genesis appears to be determined and influenced by a basin's background environmental sea surface temperature, i.e. basins with higher mean sea surface temperatures and heat uptake, such as the Pacific, will demonstrate genesis sea surface temperatures greater than a basin with lower mean sea surface temperatures (Mavume *et al*., 2009; Dare & McBride, 2011; Defforge & Merlis, 2017a).

Furthermore, Defforge and Merlis (2017a, b) report a high variability in the range of genesis sea surface temperatures across basins and therefore no preference for warmer sea surface temperatures at the point of genesis, which brings into question the use of a threshold, especially in a changing climate, where variability is increasing. While the 26.6-27°C isotherms and thresholds are observed by the above studies as the temperature range under which the majority of tropical cyclones should form, a statistically significant variation of over 1°C is observed between the various basins under tropical cyclone genesis, which implies that the sea surface temperature threshold is not as deterministic to genesis as previously thought (McTaggart-Cowan *et al*., 2015; Tory & Dare, 2015; Defforge & Merlis, 2017a, b). Additionally, when examining the estimated pre-historical thresholds, as done in the paleo-study by Korty *et al*. (2012), it was observed that during the last glacial maximum, tropical cyclone genesis events took place around the same locations of the 24°C isotherm (Korty *et al*., 2012). Therefore, it has been observed that the threshold of formation shifts to colder magnitudes under a colder climate, but as the climate warms the isotherms that locations of genesis normally follow, may be increasing in conjunction with the increasing temperatures, which supports the argument by Defforge and Merlis (2017a). This provides further evidence that specific sea surface temperature thresholds may not explicitly be required for storm genesis to occur, especially in a perturbed climate state such as the present warming trend (Sobel *et al*., 2016; Walsh *et al*., 2016). This may alter the existing hemispheric and basin-scale tropical cyclone climatology, including the climate factors (specifically sea surface temperature) involved in tropical cyclone genesis and intensification and therefore, warrants investigation (Defforge & Merlis, 2017a).

It is apparent that the basins of the Southern Hemisphere are rarely addressed or critically evaluated in terms of their climatologies related to sea surface temperature, as the above studies do not examine the South Indian Ocean, Australian region and South Pacific as explicitly in their discussions, compared to the Northern Hemisphere basins. This is compounded by the lower percentage of research outputs for Southern Hemisphere basins (Figure 2.2). Based on this, closer examination and evaluation of tropical cyclogenesis in relation to sea surface temperature is warranted.

2.3. Tropical Cyclone Activity and Climate Change

Climate change has become a widely debated topic in regard to tropical cyclone activity and Walsh *et al*. (2016) has stated that a climate theory for tropical cyclones and their genesis remains elusive. Tropical cyclones are relatively rare events compared to meteorological events, with around 60-80 occurring per year globally, which makes it difficult to discern whether changes in activity are being instigated by climate change forcing, or are a presentation of natural variability (Camargo, 2013; Klotzbach & Landsea, 2015; Sobel *et al*., 2016; Defforge & Merlis, 2017b; Wehner *et al*., 2018). However, the manner and extent which changing patterns of temperature and variability modulate present and future tropical cyclone activity (frequency and intensity) are significant questions in the research of how tropical cyclones may be changing over time in a warming climate (Korty *et al*., 2008; Sriver, 2013; Bhatia *et al*., 2019). This section will discuss both observational and model-based studies and their findings related to climate change and how tropical cyclone activity is being impacted.

2.3.1 Changing Patterns of Frequency and Intensity

The oceans are a major climate heat sink for the Earth's energy, and anthropogenically driven warming trends from the surface to the abyssal depths have been observed for the ocean in the recent decades (Durack *et al*., 2018). Future trends in tropical cyclone activity based on the warming scenarios by the Intergovernmental Panel on Climate Change (IPCC) indicates that tropical cyclone frequency will decrease globally by 13-25%, as the average temperatures increase, while storm intensity will increase (Emanuel, 2005; Knutson *et al*., 2010; Murakami *et al*., 2012b; IPCC, 2014). Webster *et al*. (2005) assessed observational data and also determined that the high intensity storms (category 4-5) have increased in occurrence by almost twice the amount compared to the 1970's. A decrease in frequency (cyclone days) by a rate of 40% from 1995-2003 was also observed (Webster *et al*., 2005). In assessing the results of Webster *et al*. (2005), it was found that over the period 1990-2014, the frequency of category 4-5 storms demonstrates a small non-significant downward trend (Klotzbach & Landsea, 2015). This disparity between the observations of the studies was attributed to data heterogeneity and different collection methods used post-1980, hence the overestimation in the numbers of intense storms reported by studies examining intensity trends with data from that period (Landsea *et al*., 2006; Kossin *et al*., 2013; Klotzbach & Landsea, 2015). To alleviate this problem, some studies (Holland & Bruyere, 2014; Strazzo *et al*., 2015) applied different approaches to quantify the effect of climate change on tropical cyclone activity. Using an anthropogenic climate index to assess whether tropical cyclone activity is actually related to anthropogenic warming, Holland and Bruyere (2014) confirmed that category 4-5 tropical cyclones have displayed an increase of 25-30% (7.9 $m.s^{-1}$) for every 1°C of warming, while the category 1 and 2 tropical cyclones display a decrease in numbers over time (Holland & Bruyere, 2014). The authors state that this trend is observed globally, however, they also introduce the assumption that a saturation level exists, and past a certain amount of continued warming, there will be no further increase in the intensity of tropical cyclones (Holland & Bruyere, 2014; Strazzo *et al*., 2015; Muthige *et al*., 2018). Apart from observational studies which have reported progressive changes in the trends of lifetime maximum intensity, there has also been statistically significant increases in variability related to the trends of lifetime maximum intensity across the majority of ocean basins (Song *et al*., 2018). In addition, the increasing trend for sea surface temperatures does not yet demonstrate an influence on storm days/duration (Wang *et al*., 2010).

2.3.2 Model-Based Assessments

A use of climate models helps to simulate the influence that long-term environmental change can have on tropical cyclone activity, which is an alternative to using observational data to extrapolate potential impacts (Walsh *et al.*, 2016). The summer–season sea surface values display a definitive increasing trend for all basins (Klotzbach & Landsea, 2015; Defforge & Merlis, 2017b; Bhatia *et al.*, 2018). It has also been recorded that the warming trends of sea surface temperature are attributed to anthropogenic origins (Defforge & Merlis, 2017b). In agreement with observations, climate models project that the higher the potential warming, the greater the degree of decrease in tropical cyclone number per year with 72.5 $TCs.yr^{-1}$ at a 1.5°C warming and 67.5 $TCs.yr^{-1}$ with a 2.0°C warming scenario (Wehner *et al.*, 2018). The first study to model category 4-5 tropical cyclones over a multi-decadal scale, notes that category 5 storms will shift equatorward in the west North Pacific (Murakami *et al.*, 2012a, b). This is supported by additional projections, which indicate an increase in category 5 tropical cyclone duration and track length (Wehner *et al.*, 2018). High resolution models which may be computationally expensive to run, are better at capturing the dynamics of high intensity storms and therefore provide more accurate projections regarding the activity of intense storms, which low resolution models struggle to accomplish (Murakami *et al.*, 2012a; J.A. Zhang *et al.*, 2017). The future tropical cyclone activity for 2069-2100 with a 21°C climate scenario, is expected to decrease by 6% in the Northern Hemisphere with a larger 22% reduction for the Southern Hemisphere storms frequency, with the bulk of decreased storm occurrences projected for the South Indian Ocean (Gleixner *et al.*, 2014). A weakened Walker Circulation over the Southern Hemisphere tropics is posited as a possible mechanism inducing the projected decrease in frequency, while the strengthened vertical wind shear is reported as the instigator of the decreased frequency in the South Pacific (Gleixner *et al*., 2014). Overall, some model-based and observational studies determine that the decrease in tropical cyclone frequency is due to a deficit in saturation, which occurs as temperatures increase but relative humidity remains at a relatively constant level, which in turn acts as a limiting factor for formation as only an increase in moisture would increase frequency (Emanuel, 2010; Camargo *et al*., 2014; Sobel *et al*., 2016; L. Zhang *et al*., 2017). However, moisture is relatively constant within the Earth's hydrological budget, and higher temperatures cannot produce more moisture, as the air can only hold a certain amount before it reaches saturation (Tyson & Preston-Whyte, 2000). This decrease in low intensity storms, however, means there is more stored energy in the ocean-atmosphere system, which will promote and sustain high intensity storms when they do form as observed (Elsner *et al*., 2008; Kang & Elsner, 2016).

Potential genesis and intensification indices are used as tools to assess the effects of global warming or environmental changes on tropical cyclone activity, as an alternative to only using sea surface temperature or other climate variables in isolation (Camargo *et al*., 2014). Potential intensity, which is the maximum intensity the ocean-atmosphere system can support, is related to sea surface and the general temperatures or heat content present in the environment (Elsner *et al*., 2008; Sobel *et al*., 2016) and has been used in previous model-based studies (Camargo *et al*., 2014; Wing *et al*., 2015; Sobel *et al*., 2016; J.A. Zhang *et al*., 2017) as a substitute for sea surface temperature. Based on this premise, air temperature was incorporated by both Vecchi *et al*. (2013) and Kossin *et al*. (2015) to assess the role of upper atmospheric temperature in influencing the potential tropical cyclone intensity which the environment could support. It was observed that the increasing temperatures in the tropical tropopause layer and therefore the changing air temperatures are positively influencing the potential intensity of the environment, i.e. the environment is able to support more intense storms (Vecchi *et al*., 2013). However, Kossin *et al*. (2015) report no statistically significant trends for global potential intensity, indicating that potential intensity is not increasing. This does not refute an increasing trend of storm intensity, just that the poleward migration of tropical cyclone activity may be offsetting the observed potential intensity trends as storm activity moves toward environments with lower inherent potential intensities resulting from the cooler sea surface temperatures present in the regions poleward of the normal formation zones (Kossin *et al*., 2015; Sobel *et al*., 2016).

Genesis indices are based on the factors known to influence tropical cyclone formation and are used to simulate the possible seasonal tropical cyclone occurrence (Camargo *et al*., 2014). However, there are large inconsistencies, reported to exceed 50% at the regional scale regarding the output of these genesis indices, when attempting to determine the potential frequency of tropical cyclone events (Menkes *et al*., 2012). The use of genesis indices to project the environments potential ability to support genesis is also limited by the historical data and climate variables used to construct the index, as all the climate variables and influences over tropical cyclone genesis are usually not known or incorporated within these indices (Menkes *et al*., 2012; Li *et al*., 2013; Camargo *et al*., 2014). While the ability to simulate and explain tropical cyclone intensity through potential intensity indices and models is well understood, there remains difficulty in constructing an accurate and reliable index or theory of tropical cyclone genesis (Walsh *et al*., 2016). In general model-based investigations, can be taken as reliable when high resolution data and proper downscaling techniques (see Walsh *et al*., 2016) are applied. However, the use of low-resolution and low-cost models along with the diverse array of model physics and representations of the large-scale environmental variables integrated in climate models, results in inconsistent projections and are not well suited to providing reliable simulations (Murakami *et al*., 2012a, 2016; Walsh *et al*., 2016).

2.3.3 Poleward Migration of Tropical Cyclone Genesis and Intensity

Under the warming climate regime (from 1982-2012), the locations at which tropical cyclones undergo genesis and attain maximum intensity, are migrating toward poleward latitudes at a rate of 0.5-1° per decade, as documented in Kossin *et al*. (2014) and supported in multiple reassessments (Daloz & Camargo, 2017; Tennille & Ellis, 2017). The tropical cyclone activity observed in the South Indian, South Pacific and west North Pacific Oceans, indicates statistically significant rates of poleward migration, and this poses threats to the highly populated Island and developing regions that are vulnerable to poleward occurring storms (Kossin *et al*., 2014,2016). Specifically, the Northern Hemisphere tropical cyclone activity is migrating poleward by 53km per decade, while the rate for the Southern Hemisphere is greater, with a rate of 62km per decade (Kossin *et al*., 2014). Individually, the highest rate of migration in tropical cyclone intensification and genesis regions is recorded over the South Pacific (Daloz & Camargo, 2017).

The poleward migration of the tropical cyclone activity is of importance, as the mechanisms and forcers driving it, are linked to the climate system (Tennille & Ellis, 2017). The poleward migration of tropical cyclone activity is driven by the expansion of the tropical regions and the widening of the Hadley cell, which is one of the mechanisms promoting the movement of warmer tropical conditions towards the poles (Kossin *et al*., 2014; Walsh *et al*., 2016).

Therefore, the conducive conditions for tropical cyclone formation and intensification, are being observed over latitudes further poleward of the usual formation zones, which in turn is promoting the incidence of genesis and intensification over these poleward regions (Kossin *et al*., 2014; Tennille & Ellis, 2017). The Hadley and tropical belt expansion observed since 1979, for the Northern Hemisphere is driven in part, by the sea surface temperature variability linked to the PDO, which has been implicated in encouraging the expansion of the tropical belts in the Northern Hemisphere (Allen *et al*., 2014). Alternative forcing mechanisms include the anthropogenic warming resulting from emission activities, which has increased sea surface temperatures and contributed to the poleward migration of the 27-28°C sea surface temperature isotherms (Lucas *et al*., 2014; Walsh *et al*., 2016). Furthermore, a poleward migration of the 28°C and 29°C isotherms are observed over the South Indian Ocean, which has coincided with an increased number of category 5 storms occurring further poleward (Fitchett, 2018). Radiative forcing is another possible contributor to the poleward expansion of the tropics, which is compounding the sea surface temperature increase (Sobel *et al*., 2016). The ITCZ position, which is found over regions with high convective activity, usually coincides with the majority of tropical cyclone genesis regions and is also shifting poleward as it follows the increased sea surface temperatures, moisture and convective activity (Chen *et al*., 2019). Indeed, the parameters of each known required climate variable for tropical cyclone genesis, from sea surface temperature, vorticity, relative humidity and shear as described by Gray (1968, 1979) are found within the ITCZ (Mavume *et al*., 2009; Chen *et al*., 2019).

2.4 Variability and Teleconnections

2.4.1 Influence of Modes of Variability

Within the confines of average tropical cyclone frequency and intensity, there exists substantial natural variability (Walsh *et al*., 2016). This variability is instigated by the modulative nature which the different modes of variability have on the ocean atmospheric system, that is then translated into impacting tropical cyclone activity at varying timescales ranging from seasonal to decadal (Mao *et al*., 2013; Burns *et al*., 2016; Patricola & Wehner, 2018). This section will give a brief outline of the modes of variability that are most prominent in the Southern Hemisphere basins (Figure 2.1): ENSO, IOD, SAM, MJO, PDO and solar flux (as a proxy for the influence of solar energy input), and how each one has been observed to modulate storm activity. These modes of variability also provide a window into the interactions and linkages between the Southern Hemisphere basins (Liu & Chan, 2012). For instance, the Pacific Ocean is the largest basin and understandably has a great influence over the global climate through its heat storage capacity and teleconnections, specifically inherent modes of variability such as ENSO and the PDO which manifest within this basin (Dowdy *et al*., 2012). In the South Indian Ocean, there are four modes of variability (ENSO, IOD, MJO and the SAM) and the teleconnections between them, which are known to influence the ocean atmospheric system in the Southern Hemisphere and in turn the tropical cyclone activity to varying degrees (Camargo *et al*., 2009; Kuleshov *et al*., 2009; Matyas, 2015; Clem *et al*., 2016). An implication of the modes related to sea surface temperature, is that the variation of sea surface temperature across the spatial domain has so far indicated a much larger modulating effect on tropical cyclone activity than the increasing trend in temperature driven by climate warming (Wang *et al*., 2010; Mao *et al*., 2013). These modes are able to impact ocean heat content greatly over a small geographical area, which in turn forces changes in air-sea heat exchange, moisture fluxes and resultant atmospheric circulations such as the Walker Circulation and wind flows (Girishkumar *et al*., 2015; Cai *et al*., 2018a).

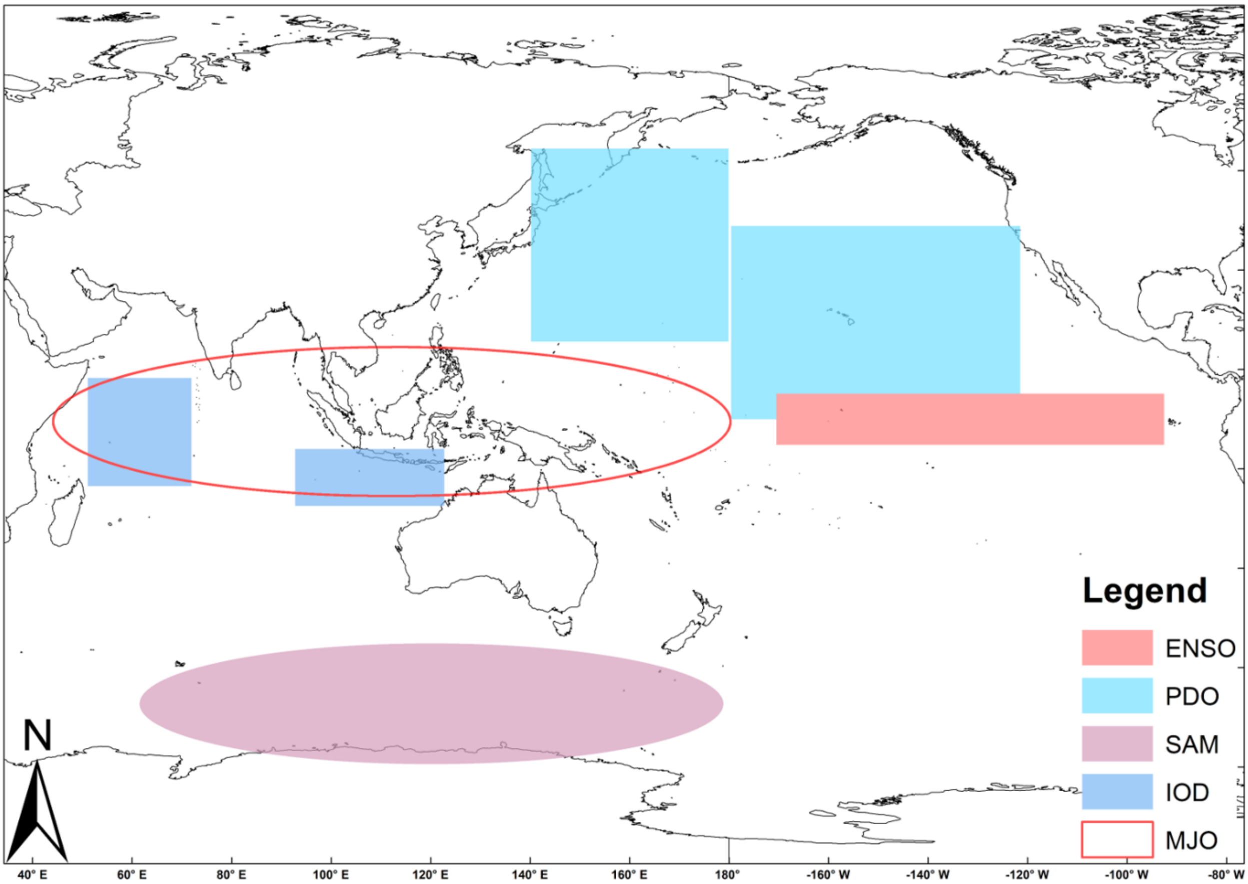

Figure 2.1 Modes of variability which modulate Southern Hemisphere climate and tropical cyclone activity. Specifically, the PDO, SAM, MJO,IOD and ENSO. Purple band around 60°S represents the extent of influence of the SAM on the zonal winds over this region. The shaded ENSO region encapsulates the area which the Niño Indices are calculated from, but its actual influence is much greater in range.

2.4.1.1 El Niño Southern Oscillation

The ENSO is characterised by the large-scale ocean-atmospheric interaction based over the central east Pacific, which is known to modulate sea surface temperature, pressure and circulation patterns across the globe (Mao *et al*., 2013; Burns *et al*., 2016; Patricola &

Wehner, 2018; Song *et al*., 2018). During a warm ENSO event (El Niño), sea surface temperatures in the East Pacific Ocean increase, with the opposite true during a cold ENSO (La Niña) event (Timmermann *et al*., 2018). The ENSO mode persists for approximately a year and occurs in a cycle of three to seven years, with the sea surface temperatures increasing or decreasing by 1-3°C relative to the average temperature during an active phase (Kim *et al*., 2017). ENSO exhibits a significant effect on tropical cyclone activity in all basins, however, the nature of this influence is usually differentiated by the geographic location of the storm occurrence (Menkes *et al*., 2012; Mao *et al*., 2013; Astier *et al*., 2015). In the South Indian Ocean, ENSO has demonstrated influence over the location of genesis and motion of the tropical cyclones across their lifetime via its modulation on the large-scale environmental variables such as sea surface temperature, relative humidity and vorticity (Kuleshov *et al*., 2009; Ash & Matyas, 2012; Ramsay *et al*., 2012; Mao *et al*., 2013). For example, as a result of geographical shift in relative humidity and vorticity during a La Niña, the Southern Hemisphere tropical cyclone formation zones over the South Indian Ocean and South Pacific Ocean shift away from the equator, while tropical cyclone genesis increases over the eastern regions of the basins and reduces over the western regions (Kuleshov *et al*., 2009). In the South Pacific, the incidence of a warm (cold) ENSO event is associated with increased (decreased) tropical cyclone frequency, while in the South Indian Ocean, frequency decreases during intense warm ENSO events (Astier *et al*., 2015). In the Australian region, whereby tropical cyclone frequency is lower (higher) during warm (cold) ENSO phases (Callaghan & Power, 2011; Diamond *et al*., 2013,2015a). It is also observed that tropical cyclone frequency increases relatively more in the eastern (western) Australian region during a warm (cold) ENSO phase (Diamond *et al*., 2013; Diamond & Renwick, 2015). In the South Pacific, there is an eastward shift in tropical cyclone activity during warm ENSO phases, hence tropical cyclones are found to form further away from the Australian east coast (Camargo *et al*., 2010; Diamond *et al*., 2013). These effects are significant, as there are implications in a warming world, whereby, the ENSO phenomena are projected to intensify, as recently observed and will most likely impact tropical cyclone activity to a greater extent (Timmermann et al., 2018; Liu, 2019). This could impose a permanent warm ENSO modulation on the climate system and tropical cyclone activity, thereby increasing activity and landfalls in regions prone to such activity under a warm ENSO (Sun *et al*., 2017; Timmermann *et al*., 2018). Such an observation is already recorded in the South China Sea (see Liu & Chan, 2018). Over the Indo-Pacific region, warm ENSO events shift the tropical cyclone activity towards the equator, which results in longer lifespans, which are up to three days longer than during cold ENSO events (Wang *et al*., 2010). In a global study on the impacts of variability, ENSO shared 70% of the explained variability of tropical cyclone activity with the north Atlantic oscillation and was specifically noted to influence tropical cyclone activity of high energy storms, i.e. storms that reached category 3 and above (Frank & Young, 2007).

2.4.1.2 Indian Ocean Dipole and South Indian Ocean Dipole

The IOD and South Indian Ocean Dipole (SIOD) are the Indian Ocean equivalents of ENSO, characterised by changes in sea surface temperatures between the western and eastern regions of the Indian Ocean basin, which influence the ocean currents and pressure anomalies across the basin (Ash & Matyas, 2012; Ramsay *et al*., 2012). In a positive (negative) IOD phase the western (eastern) region has a higher sea surface temperature than the eastern region (Saha & Wasimi, 2013). There are significant correlations with the positive and negative IOD phases and the incidence of increased tropical cyclone occurrence over the west and east Australian regions (Saha & Wasimi, 2013). Tropical cyclone frequency is additionally observed to be highly modulated by what is known as the transverse Indian Ocean dipole, which is characterised by sea surface temperature anomalies across a southwest-northeast diagonal spatial extent of the South Indian Ocean (Ramsay *et al*., 2017). This transverse dipole has a 46% greater skill in explaining the Indian Ocean tropical cyclone frequency per year than the ENSO modes (Ramsay *et al*., 2017). In the South Indian Ocean, an occurrence of a positive IOD phase has also been found to influence tropical cyclone intensity, via changes in the ocean barrier layer thickness (i.e. by increasing the thermocline depth), however, the impact is variable, as some positive years do not coincide with increased frequency and intensity (Burns *et al*., 2016). Overall, tropical cyclone occurrence is strongly related to the IOD specifically when it occurs in August to October, prior to the tropical cyclone season in the South Indian Ocean (Saha & Wasimi, 2013).

2.4.1.3 Madden-Julian Oscillation

The MJO is the dominant mode of intra-seasonal variability within the tropics with a period of 30 to 60 days (Kim *et al*., 2012). The MJO modulates the deep convection over the tropical regions, which develops in the Indian Ocean and propagates eastwards (Bessafi & Wheeler, 2006). Due to the nature of the MJO, it innately has an influence over convective phenomena in the tropics, specifically tropical cyclones (Kim *et al*., 2012; Mao *et al*., 2013). Tropical cyclones have a 2.6 times higher probability of occurring during an active MJO phase than during an inactive one (Bessafi & Wheeler, 2006; Mao *et al*., 2013). Over the Indian Ocean, the MJO demonstrates a larger influence on storm genesis compared to when ENSO events are taking place (Ramsay *et al*., 2012; Tsuboi *et al*., 2016). The MJO has additional influence over the drivers of tropical cyclone genesis including, relative humidity, vertical shear, and vorticity, however, the exact mechanism by which MJO influences storm activity remains unknown (Camargo, 2009; Tsuboi *et al*., 2016). Though, Hall (2001) found that low-level vorticity is influenced by the MJO, which in turn forces changes in tropical cyclone formation (Camargo *et al*., 2009, 2010). In the Pacific, however, the tropical cyclone activity is influenced more strongly by ENSO, than the MJO (Tsuboi *et al*., 2016; Diamond *et al*., 2013).

2.4.1.4 Southern Annular Mode

The SAM (also known as the Antarctic Oscillation) is the dominant mode of variability for the mid-high latitudes and extratropical regions of the Southern Hemisphere (Diamond & Renwick, 2015). This mode is characterised by the north-south (dipole) displacement of the wind and pressure belts of the South Indian and Antarctic regions (Matyas, 2015). During a positive SAM, regions of low-pressure shift over Antarctica, which initiates a poleward shift of the westerly winds and the mid-latitude sub-tropical Jetstream (Diamond & Renwick, 2015). This causes the presence of stronger zonal (east to west) winds over the active zones (15-30°S) of tropical cyclone activity (Mao *et al*., 2013; Diamond & Renwick, 2015; Matyas, 2015). In the South Indian Ocean (Mozambique Channel), it is reported that a northward (southward) shift in the location of tropical cyclone genesis coincides with a negative (positive) SAM (Matyas, 2015). In addition, Mao *et al*. (2013) reported a positive correlation between the SAM/AAO and tropical cyclone activity in the South Indian Ocean. During a positive SAM in the Australian region, sea surface temperatures are favourably modulated, which increases tropical cyclone genesis and frequency in this region (Mao *et al*., 2013). This is especially observed in strong positive phases of the SAM/AAO, which promotes increased storm genesis over the northwestern coast of Australia (Mao *et al*., 2013). Relative humidity is also increased to an extent that provides conducive moisture conditions which promote tropical cyclone genesis (Mao *et al*., 2013). Specific patterns found in the Australian and South Pacific regions during positive SAM events are increases in tropical cyclone frequency over the sub-tropical regions of the ocean, as the storms track further poleward, while tropical cyclone frequency increases in general during a negative phase of the SAM (Diamond & Renwick, 2015). The positive (negative) SAM is also related to the cold (warm) ENSO phases, which influence the mid-latitude circulation anomalies and incidentally, highlight the teleconnection between these modes and the different regions of the ocean in which they manifest (Fogt *et al*., 2011; Clem *et al*., 2016).

2.4.1.5 Pacific Decadal Oscillation

The Pacific decadal mode is characterised by climate variability at a decadal time scale and is the predominant mode of variability in the Pacific Ocean, but with a larger modulative capacity over the North Pacific (Wang *et al*., 2015). During a warm PDO phase, the sea surface temperatures increase near the equator, while the cold PDO phase is characterised by cooler temperatures over the equatorial/tropical regions (Wang *et al*., 2015; Vishnu *et al*., 2018). These phases usually span cycles of 20 to 30 years (Vishnu *et al*., 2018). The PDO has been shown to instigate variability in tropical cyclone tracks at a decadal scale (Wang *et al*., 2015). During a positive PDO phase in the Southern Hemisphere, there is an increase in storm activity equatorward of 20°S, characterised by an increase in the number of tropical cyclone occurrences and storm days, while there is decreasing activity observed poleward of this (Wang *et al*., 2010). The PDO-ENSO coupling effect is observed to drive the fluctuations in global storm days, which indicates their teleconnections and scale of modulations on tropical cyclone activity (Wang *et al*., 2010; Girishkumar *et al*., 2015). Though, there are decreases of total storm days per year observed in the South Pacific and an increase of storm days over the northwestern region of Australia, which are driven by the ENSO-PDO modulation (Hassim & Walsh, 2008; Wang *et al*., 2010).

2.4.1.6 Solar Flux and Volcanic Activity

Solar flux is an external influencer of the climate as it is related to the sun's incoming energy, while volcanic activity is an internal influencer of the Earth's climate (Evan, 2012; Khodri *et al*., 2017; Li *et al*., 2018). Solar flux and volcanic activity both relate to the energy balance and are therefore linked intrinsically to the temperature and circulation patterns across the planet (Xue *et al*., 2012; Pausata & Camargo, 2019). Solar flux is the concentrated measure of sunlight radiation being experienced over a region (Li *et al*., 2018). Usually, the sunspot number, total solar irradiance or sea surface temperatures in the tropics have been used to quantify the impact that the incoming solar energy has on the climate system (Li *et al*., 2017,2018). It has however, been observed that tropical cyclone activity at a global scale shares a stronger relationship with solar flux, than the abovementioned variables as stated in Li *et al*. (2018), while it is also noted that larger magnitudes of solar flux (driven by increased geomagnetic activities) promotes higher tropical cyclone intensity. Apart from Li *et al*. (2017, 2018), there are few other investigations on tropical cyclones which include solar flux, as it has only recently been indicated as a reliable metric to determine solar influence of tropical cyclone activity. Volcanic activity has been associated with large-scale influences on the climate system, and as a result also demonstrates the potential to modulate tropical cyclone activity (Guevara-Marua *et al*., 2015). Following a major volcanic eruption over the tropical regions, the ejection of material into the atmosphere instigates a cooling effect over the planet, but specifically over the area of the eruption (Evan *et al*., 2012). This cooling effect has been observed to influence the location of the ITCZ, which tends to shift poleward away from the hemisphere where the eruption occurred (Chen *et al*., 2019; Pausata & Camargo, 2019). As a result, the tropical cyclone activity also tends to follow the ITCZ, with more storms occurring in the Southern Hemisphere if the ITCZ shifts southward from the equator as consequence of a volcanic eruption in the Northern Hemisphere and conversely so if the eruption occurs in the Southern Hemisphere (Pausata & Camargo, 2019).

2.4.1.7 Evaluation of Variability

The ENSO and PDO modes account for a large percentage of influence on tropical cyclone activity (Wang *et al*., 2010; Fogt *et al*., 2011), with ENSO and IOD found as major contributors to the Southern Hemisphere variability (Ash & Matyas, 2012; Diamond *et al*., 2013). However, the variability in the annual number of approximately 80 tropical cyclones per year still lacks a comprehensive explanation by the modes of variability at a global and hemispheric scale, with many years indicating unexplained storm activity, which cannot be reconciled by natural modes of variability or the large-scale environmental drivers related to tropical cyclone activity (Wang *et al*., 2010; Knutson *et al*., 2010; Walsh *et al*., 2016). This difficulty in accounting for the complete variability in tropical cyclone activity has brought into question whether the variability is a product of natural variation or is being forced by climate change (Frank & Young, 2007; Song *et al*., 2018). Indeed, relative humidity and vorticity are found to be responsible for South China Sea tropical cyclone variability (Yu *et al*., 2016), while the variability of upper ocean heat content plays a role in influencing tropical cyclone intensity, however, there may be many more influencing factors that are currently unknown (Mawren & Reason, 2017; Scoccimaro *et al*., 2017). At the principal level the modes of variability are manifested through changes in the large-scale environment, including but not limited to sea surface temperature, pressure and wind flows, and a change in the climate state is therefore in turn altering these variables and therefore the modes of variability (Zhan *et al*., 2017a, b; Cai *et al*., 2018a; Song *et al*., 2018). However, the argument that tropical cyclones modulate the climate also exists, which indicates that tropical cyclones are not just being influenced by the environment, they similarly play a role in influencing it (Mei *et al*., 2013; Sriver, 2013).

2.5 Southern Hemisphere Studies

The existing studies examining the Southern Hemisphere, predominantly focus on tropical cyclone trend analysis regarding storm intensity, frequency and the variables influencing these aspects (Leroy & Wheeler, 2008; Kuleshov *et al*., 2010; Gleixner *et al*., 2014). The physical mechanisms and variability influencing Southern Hemisphere tropical cyclone storm tracks i.e. the translation of tropical cyclones across the ocean were examined by Ash and Matyas (2012) and Ramsay *et al*. (2012). Some of the foremost studies which investigated Southern Hemisphere storms, examined the impacts of ENSO on tropical cyclone activity (Kuleshov *et al*., 2008, 2009). In another Southern Hemisphere study, using an updated reanalysis dataset, Kuleshov *et al*. (2010) observed that intense storm occurrences with central pressures below 945hPa have increased in the Southern Hemisphere from 10% in 1980 to 30% in 2000, which supports the consensus that intense storms are increasing in the southern and Northern Hemisphere (Webster *et al*., 2005; Klotzbach & Landsea, 2015). Model-based studies which examined extreme tropical cyclones in the Southern Hemisphere, also project that future increases in intensity are highly likely (Chang, 2017; Yoshida *et al*.,2017; L. Zhang *et al*., 2017). Chang (2017) goes further to state that the South Atlantic may also be affected by an increased number of intense extratropical cyclones, which is abnormal considering the South Atlantic has only one storm which has been recorded within this region (Chang, 2017).

The global findings surrounding tropical cyclone trends and variability across the ocean basins, indicate a progressive poleward shift of tropical cyclone tracks, location of maximum intensity and genesis locations over time (Burns *et al*., 2016; Daloz & Camargo, 2018; L. Zhang *et al*., 2017). Increases of global sea surface temperature and the expansion and migration of the tropical belt with the Hadley cell is also shifting the sea surface isotherms poleward in both hemispheres, and this is likely affecting tropical cyclones by shifting the locations at which they undergo genesis and attain maximum intensity poleward of the normal formation zones, which are usually located 5-20° north and south of the equator (Kossin *et al*., 2014; Zhan & Wang, 2017; Daloz & Camargo, 2018). In addition, tropical cyclones are becoming larger and slower at a global scale, as the climate warms (Sun *et al*., 2017). As a result of the warming oceans, increased low level convergence and buoyancy are promoted, which in turn are posited to support larger tropical cyclones and by extension greater intensities (Hill & Lackman, 2009; Sun *et al*., 2017). A decrease of 10% in tropical cyclone movement is reported globally, with the largest decrease of 22% observed over Australia (Kossin, 2018). The consequence of slower and larger storms is that they deposit large amounts of rain and cause sustained winds over one region for longer, which increases the damage and mortality rates associated with such storms (Sun *et al*., 2017; Kossin, 2018; Schenkel *et al*., 2018). Many studies have investigated this poleward shift and increased frequency of intense storms and have subsequently derived an updated climatology for extreme tropical cyclones in the northern hemispheric basins, thus determining the effects of a changing climate on tropical cyclone activity in those regions (Oouchi *et al*., 2006; Sobel *et al*., 2016; Tennille & Ellis, 2017; Zhan & Wang, 2017). However, recent studies (Sun *et al*., 2017; Kossin, 2018; Schenkel *et al*., 2018; Pugatch *et al*., 2019), continue to observe new changes in tropical cyclone activity and their impacts resulting from a warming climate. However, within the context of climate change, Southern Hemisphere studies have only examined the effects of the shifting sea surface temperature isotherms on tropical cyclone location of genesis and maximum intensity at a regional scale, therefore the effects of the poleward shift and increased sea surface temperatures for the whole Southern Hemisphere tropical cyclone climatology are not well understood (Fitchett & Grab, 2014; Li *et al*., 2017; Ma & Williams, 2017).

2.5.1 Disparities Between the North and South Hemispheres

The Northern and Southern Hemisphere have distinct differences, including the size of surrounding landmasses, ocean area, and modes of variability which dictate the ocean-atmospheric circulatory states for each basin (J.A. Zhang *et al*., 2017; Patricola & Wehner, 2018). These major differences between the Northern and Southern hemisphere influences the climate system and therefore the respective tropical cyclone activity (Gleixner *et al*., 2014; Defforge & Merlis, 2017b). Oouchi *et al*. (2006) found that the intensity of tropical cyclones increased by 7.3 $m.s^{-1}$ in the Northern Hemisphere, while it increased by 3.3 $m.s^{-1}$ in the Southern Hemisphere. Similarly, studies observed that tropical cyclone occurrence and intensity vary between the different ocean basins (Klotzbach & Landsea, 2015; Defforge & Merlis, 2017b). The sea surface temperature is also observed to vary between each basin, which also contributes to the contrasting and variable trends in tropical cyclone activity (Klotzbach & Landsea, 2015; Defforge & Merlis, 2017b). With reference to Webster *et al*. (2005) mentioned in Section 2.3.1, Klotzbach and Landsea (2015) examined an additional decade of tropical cyclone intensity trends for all the basins and reported the absence of a significant trend for increasing storm intensity in the Southern Hemisphere. This change is attributed to observational heterogeneity existing in the track records from the pre-1980 satellite period, which caused an overestimation in the number of intense tropical cyclones (Klotzbach & Landsea, 2015). Similar findings are reported for the South Indian, Pacific and Australian region, where no significant trend is observed in the frequency and proportion of intense tropical cyclones, with data quality being cited as the potential cause (Kuleshov *et al*., 2010). Meanwhile, the North Atlantic Basin projections of tropical cyclone activity had the highest skill based on Gray's (1968) climatology, as much of the data sources for this region were complete and spanned a longer time range (Klotzbach *et al*., 2017). With the larger amount of observational data existing for Northern Hemisphere tropical cyclones coupled with the larger number of models used to project hurricane activity, the skill at successfully predicting Northern Hemisphere, specifically north Atlantic and Pacific tropical cyclones is comparatively greater (Emanuel, 2005; Camargo, 2013; Vecchi *et al*., 2014; Klotzbach *et al*., 2017). This is superior to the Southern Hemisphere data, which only has reliable data from geostationary satellites post-1980 for the South Indian basin, which accounts for the majority of Southern Hemisphere storms (Landsea *et al*., 2006; Kuleshov *et al*., 2008, 2010; Mao *et al*., 2013; Defforge & Merlis, 2017b). Further variance is observed between the migration of tropical cyclone main development areas and locations of maximum intensity, which display a larger poleward shift in the Southern Hemisphere, compared to the Northern Hemisphere (Kossin et al., 2014; L. Zhang *et al*., 2017). The warming trends and concentration of greenhouse gases are not uniformly distributed across the Earth either, therefore creating increased variation between climatological processes in the southern and Northern Hemisphere (Gleixner *et al*., 2014; Lucas *et al*., 2014; Korty *et al*., 2014; Sun *et al*., 2017).

The Southern Hemisphere as a whole is underrepresented in the literature (Figure 2.2), as most climate change-tropical cyclone studies have focused on the Northern Hemisphere or on global trends (Gleixner *et al*., 2014; Daloz & Camargo 2018). The graphs (Figure 2.2) both indicate that more research related to tropical cyclone activity exists for the Northern Hemisphere basins. Studies which investigate the global trends and dynamics of tropical cyclone activity usually focus on Northern Hemisphere basins, based on the availability of reliable reanalysis and observational datasets for these regions (Done *et al*., 2015; Eichler & Gottschalck, 2013; McTaggart-Cowan, 2015). Specifically, the seminal papers by Gray (1968), which based the 26.5°C sea surface requirement for storm genesis was more relevant to the Northern Hemisphere tropical cyclones; the data on Southern Hemisphere tropical cyclones was highly irregular and inaccurate during the time these tropical cyclone genesis climatologies and thresholds of sea surface temperature were compiled (Watterson *et al*, 1995; Landsea *et al*., 2006; Klotzbach & Landsea, 2015). One of the first instances that the Southern Hemisphere basins and tropical cyclones were included in a meaningful manner, was when Dare and McBride (2011) investigated a new sea surface temperature threshold. However, the sea surface thresholds provided here were still not basin specific, and instead focused on the global average. This is problematic, as Defforge and Merlis (2017a, b) report that the sea surface temperature and other drivers of tropical cyclone genesis differ significantly between basins. For example, the sea surface temperatures at which genesis is most likely to occur, tends to be on the colder spectrum of ocean temperatures for the North Atlantic, but on the warmer spectrum for the South Indian and South Pacific Oceans (Leroy & Wheeler, 2008; Defforge & Merlis, 2017a). However, the studies (Dare & McBride, 2011; tory & Dare, 2015; Defforge & Merlis, 2017a) which reassessed the genesis sea surface temperatures, chose to remove or discount the occurrence of storm genesis events with sea surface temperatures that were too low or did not occur often, and maintained the existence of a threshold temperature. The deficit of studies dealing with the Southern Hemisphere is problematic, due to the South Indian and Pacific basins having some of the most active regions of tropical cyclone activity in the Southern Hemisphere (Kuleshov *et al*., 2008, 2010). In addition, as mentioned by Kossin *et al*. (2014), the largest magnitude of poleward shift is observed in the Southern Hemisphere (see section 2.3.3 & Table 2.1), which is accounted for by the migration of tropical cyclones related to the South Indian and Pacific Ocean basins (Daloz & Camargo, 2018).

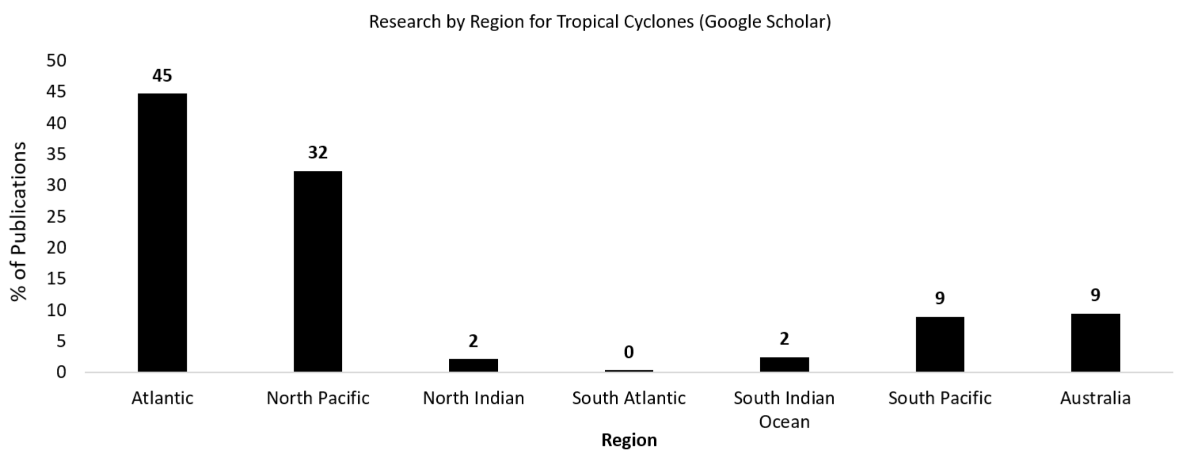

Figure 2.2 Research output for northern and Southern Hemisphere tropical cyclone activity. (top: Compiled from Google Scholar) Indicates the percentage of research papers published from 1920-2019 on tropical cyclone activity in the respective basins.

The active tropical cyclone zones in the Southern Hemisphere are unique compared to the Northern Hemisphere, since the South Indian and South Pacific Oceans are not separated by continental landmasses as is the case in the North Pacific and Atlantic (Maue, 2009). Hence the activity and variability of all tropical cyclones in the Southern Hemisphere can be influenced by ocean and atmospheric forcers or teleconnections, including but not limited to ENSO, MJO, QBO, IOD, PDO, sunspots and solar energy fluxes and the interactions between these climatic forcers across spatial bounds of the Southern Hemisphere ocean basins (Kuleshov *et al*., 2009; Sobel *et al*., 2016; Wieners *et al*., 2016; Li *et al*., 2018). For example, the IOD phases affect the South Indian and south east Pacific Ocean temperatures and the atmospheric Walker Circulation (Markle *et al*., 2015; Wieners *et al*., 2016; Gleixner *et al*., 2014). The presence of teleconnections between basins and the interaction between multiple modes of variability are reported for the Southern Hemisphere (Fogt *et al*., 2011; Ash & Matyas, 2012; Eichler & Gottschalck, 2013; Walsh *et al*., 2016; Cai *et al*., 2018b; Timmerman *et al*., 2018). For instance, ENSO and IOD or ENSO and SAM, have demonstrated a combined influence on the climate system and the resultant tropical cyclone activity across the Southern Hemisphere, when these modes coincide (Eichler & Gottschalk, 2013; Diamond *et al*., 2015a, b; Cai *et al*., 2018a). Teleconnections are also observed between the northern Pacific and Atlantic basins, which exhibit an ENSO modulation on the tropical cyclone activity across the two basins, despite the existence of the land barrier between them (Sobel *et al*., 2016; Patricola & Wehner, 2018).

2.5.2 Pre-1980s Data Limitations

Limitations exist in the majority of the tropical cyclone studies based on observational and historical data, which was compiled through irregular ship logs, aircraft records and low-resolution satellites prior to 1980 and resulted in data heterogeneity (Landsea *et al*., 2006). Two of the major implications of this include a lack of reliable data post 1979/1980, specifically for the Southern Hemisphere and an overestimation of storm intensity (Kuleshov *et al*., 2010; Kossin *et al*., 2013; Fitchett & Grab, 2014). This data heterogeneity has been well studied and is attributed to different approaches of analysis, collection and quality of the tropical cyclone track and wind speed data prior to the 1980's, after which breakpoint analysis indicates a statistically significant change in the proportion of intense tropical cyclones (Kuleshov *et al*., 2010). There is consensus that trend analysis alone may not suffice in providing an accurate state of tropical cyclone trends and activity, specifically regarding the occurrence of extreme tropical cyclones under climate change, as intensity is overestimated by the pre-1980 track data (Landsea *et al*., 2006; Kuleshov *et al*., 2010; Fitchett & Grab, 2014; Klotzbach & Landsea, 2015). In another review on tropical cyclone data quality, Magee *et al*. (2016) reported that observational and historic data from the pre-1980 satellite era regarding tropical cyclone occurrence, genesis and landfall locations do not display statistically significant differences to the pre-satellite era (1945-1969), which infers that intensity data is the main issue present in pre-satellite era records.

2.6 Synthesis

Globally, tropical cyclone intensity is increasing, while frequency is decreasing. The storm locations of genesis, maximum intensity, landfall location and even the isotherms that previously influences the formation of tropical cyclones are shifting poleward globally (Daloz & Camargo, 2018). Recently tropical cyclones have also increased in size and demonstrated a slowdown of their track speed (Kossin, 2018). Combined, this indicates that storms are becoming more dangerous and pose a threat to regions which have not previously experienced tropical cyclone activity. A detailed climatology for tropical cyclones in the Southern Hemisphere would benefit the understanding of their formation, aid in early warning systems and provide a future trajectory for tropical cyclone genesis, intensification, track motion and intensity downgrade over storm lifetime under a changing climate. The use of the 26.5°C sea surface temperature threshold has persisted since its introduction, however, recent reexaminations (Dare & McBride, 2011; McTaggart-Cowen *et al*., 2015; Tory & Dare, 2015; Defforge & Merlis, 2017) have brought its use into question. Therefore, an investigation of this threshold for Southern Hemisphere tropical cyclones may provide new outlooks on the sea surface temperatures required for storm genesis. Average storm lifetime and duration of a tropical cyclone at maximum lifetime intensity for the hemisphere will also be valuable, as models have projected that storm lifetimes should increase with a warmer climate (Korty *et al*., 2017). However, with regard to the time taken by tropical cyclones to attain their lifetime maximum intensity, there is no evidence to date suggesting that a study has addressed this issue in the Southern Hemisphere using observational data, and an investigation into this has been recommended (Walsh *et al*., 2015; Lin *et al*., 2017). While some of these aspects have been examined, this paper will take a holistic approach to determine the interplay between these factors of tropical cyclone activity for the Southern Hemisphere, while updating and revising the past southern hemispheric studies temporal and spatial interrogations, as many of them have either used heterogenous datasets with pre-1980 track data or have not examined the recent decade due to time of publishing (Kuleshov *et al*., 2008). Additionally, many studies using models or reanalysis datasets, provide varying results, specifically regarding trends of intensity in extreme tropical cyclones (Schreck *et al*., 2014; Chang, 2017). Meanwhile, studies covering modes of variability have observed teleconnections between basins and interactions between modes of variability. Modes of variability are demonstrated to account for much of the variance inherent in tropical cyclone activity, however, they do not explain all the variability observed (Camargo, 2013; Walsh *et al*., 2016; Cai *et al*., 2018a, b).

3. Study Site

3. Introduction: Study Region

The study regions (Figure 3.1, Table 3.1) encompass the ocean areas within the Southern Hemisphere from the equator to the poles. The Southern Hemisphere study site is determined by examining the tropical cyclone events for each of the Southern Hemisphere basins (excluding the South Atlantic). The study sites are based on the tropical cyclone formation zones over the 1980-2016 period, with any region in the Southern Hemisphere that has experienced a tropical cyclone genesis event included within the study area. However, the extents of the modes of variability (e.g. SAM or IOD), which may not manifest over the formation zones, but are inherent to the Southern Hemisphere climatology are also included in the study area (Figure 2.1). The 135°E meridian is found to be a natural climatological divide separating the South Pacific from the South Indian Ocean, resulting from differences in mean ocean temperatures and landmass influences (Kuleshov *et al.*, 2010; Diamond *et al.*, 2015). However, for the purposes of this study, the 100-165°E delineation of the Australian region (adapted from Hassim & Walsh, 2008; Kuleshov *et al.*, 2008) is used. This chapter will provide an outline of the spatial extent for each basin within the Southern Hemisphere, the climatological background and their associated modes of variability.

3.1 Location and Background

3.1.1 South Indian Ocean

The South Indian Ocean study region for the purposes of this paper have been set as 0-35°S and 30-100°E. This incorporates the two main tropical cyclone development regions located around 50-80°E and 80-100°E (Mavume et al., 2009). The latitudinal extent regarding analysis of the South Indian Ocean and the other Southern Hemisphere basins is set at 0-35°S as this encompasses the tropical cyclone formation zones of each basin (5-25°S) and the poleward locations where extratropical transitions (25-35°S) usually occur (Diamond et al., 2012). The South Indian Ocean is bounded by southern Africa at its western extent, with the Madagascan, La Reunion and Mauritian Islands located at approximately 19°S 46°E, 21°S 55°E and 20°S 57°E respectively at their center. These are the main regions which experience landfall events from South Indian Ocean generated tropical cyclones (Mavume et al., 2009). Additionally, the norther coastlines of Australia have similarly experienced tropical cyclone landfall events between 1980-2016 (Figure 3.1). The South Indian Ocean and the Pacific Ocean are connected by the Indonesian seas (via the Indonesian Throughflow) above the Australian continent (Diamond et al., 2015).

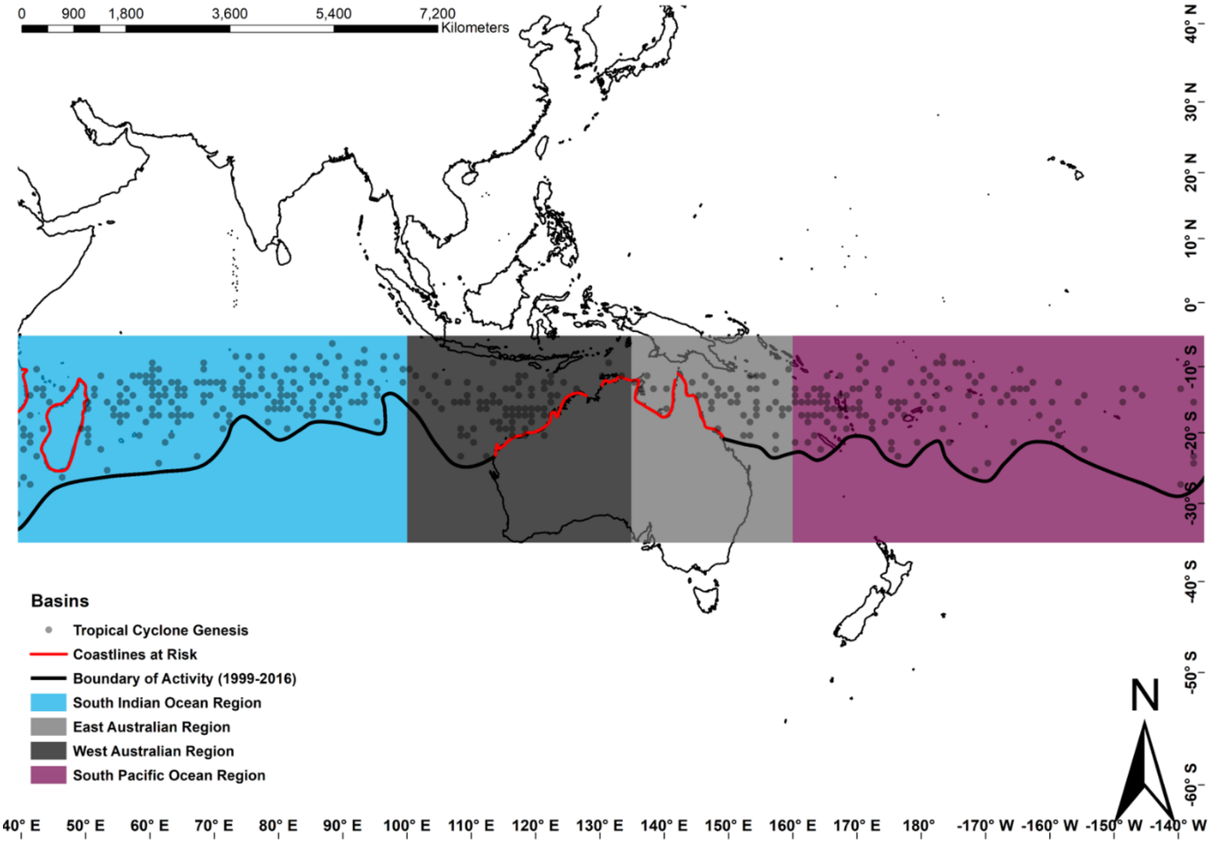

Figure 3.1 Study site map. Southern hemisphere basins, with tropical cyclone events from 1980-2016. The black line indicates the poleward boundary over which no storm genesis event has been recorded to date. The red lines indicate the coastline regions at risk to current tropical cyclone activity and landfalls. The shaded zones represent the boundaries of each Southern Hemisphere basin (SIO, WA, EA and SP).

The Indian Ocean displays a consistent warming trend over the past decades (Roxy *et al.*, 2014, 2015; Zhang *et al.*, 2018). Specifically, the South Indian Ocean has indicated a greater sea surface temperature increase over the last few decades than any other ocean basin (Roxy *et al.*, 2014; Swapna *et al.*, 2014; Durack *et al.*, 2018; Zhang *et al.*, 2018). This ocean basin is characterised by high sea surface temperatures up to 28°C, with mean sea surface temperatures decreasing below 27°C south of 10-15°S (Rao *et al.*, 2012; Roxy *et al.*, 2015). The warmest region within this basin is the Indian Ocean Warm Pool, which is an area over the tropical Indian Ocean with ocean temperatures above 28°C (Rao *et al.*, 2012). Over the last 100 years, the Indian Ocean Warm Pool has warmed by 0.7°C, while the western South Indian Ocean region warmed by 1.2°C (Roxy *et al*., 2014; Durack *et al*., 2018). The South Indian Ocean experiences maximum observed sea surface temperatures during the summer months with a peak in April, with the minimum sea surface temperatures observed during the August to September months (Rao *et al*., 2012; Durack *et al*., 2018). The sea surface temperature tends to be warmer during tropical cyclone genesis events over the western formation region (50-75°E) than over the eastern (75-90°E) formation zone (Mavume *et al*., 2009). Geographically, the South Indian Ocean is bounded by the Asian continent, which prevents heat transfer northwards, while the sector over the south east Asian archipelago (i.e. maritime continent) is characterised by a strong Walker Circulation, which impacts the regularity of the tropical easterlies over the South Indian Ocean (Schott *et al*., 2009; Zhang *et al*.,2018). During IOD and ENSO events this Walker Circulation and surface temperatures over the South Indian Ocean are altered, with resultant impacts on the climate and weather over the landmasses and the South Indian Ocean tropical cyclone activity (Kuleshov *et al*., 2009; Mavume *et al*., 2009; Ash & Matyas, 2012).

3.1.2 Australian Region

The Australian region, not specifically being an ocean is part of the South Indian and South Pacific on its western and eastern regions respectively, but for this study's purpose the west and east regions will be examined as independent tropical cyclone formation regions following previous tropical cyclone studies of the Australian region (Hassim & Walsh, 2008; Diamond *et al*., 2015). The Australian region experiences marked differences in tropical cyclone activity on its western region compared to its eastern region (Hassim & Walsh, 2008; Haig *et al*., 2014). This east-west difference has been used to frame investigations into the climatology and tropical cyclone activity of the respective regions (Hassim & Walsh, 2008; Diamond *et al*., 2015). Therefore, within this study the zone of Australian tropical cyclone activity is further divided into the West Australian region, which is defined as 100-135°E and the East Australian region defined as 135-160°E based on the delineation set out in Diamond *et al*. (2015) and the IBTrACS based classification of storm basin location which also divides the tropical cyclone zones into West and East Australia (Knapp *et al*., 2010).

A warming trend in the maritime environment around the northern region of Australia is observed, with the fastest warming in the western and eastern regions of the ocean around Australia (Diamond *et al*., 2015b). Off the Australian west coast is the Leeuwin current, which is the eastern boundary current, responsible for transporting large amounts of heat from the west Australian coast, poleward, however, it is weakening over time, which will allow heat content to accumulate off the west coast of Australia (Ridgeway & Godfrey, 2015). Records of oxygen isotope analysis on stalagmites has indicated that compared to the last 1500 years, tropical cyclone activity has been at its lowest over the Australian region (Haig *et al*., 2014). Increased sea surface temperatures over East and West Australia linked to La Niña events have been linked to a favourable environment for tropical cyclone genesis (Kuleshov *et al*., 2009).

3.1.3 South Pacific Ocean

The South Pacific Ocean is defined as the region from 0-35°S and 160°E-120°W and is bounded by the Australian continent to the west, with multiple small islands (e.g. French Polynesia, Fiji, New Caledonia and the Cook Islands) in the southeastern regions of the ocean (Diamond *et al*., 2012). Annually, tropical cyclone activity and variability in the South Pacific Basin, demonstrates the strongest response to the El Niño (La Niña) phase, with an increased number of tropical cyclones forming east (west) of 170°E as a result of ENSO-related changes in sea surface temperature, vertical wind shear and increased convective activity (Dowdy *et al*., 2012; Diamond *et al*., 2013). The genesis locations or main development regions for the South Pacific are found in the western region of the basin at approximately 5-15°S and 160-180°E and over the South Pacific Tropical Convergence Zone (Diamond *et al*., 2015). Overall, the main tropical cyclone development zones are located over regions where temperatures are the warmest, which in this case is observed across 5-25°S and 50-180°E in the Southern Hemisphere (Jourdain *et al*., 2011; Ramsay *et al*., 2018).

The South Pacific Ocean has a well-defined diagonal convergence zone termed the South Pacific Convergence Zone, which extends toward the southeast from the warm pool in the western Pacific at 140°E close to the equator (van der Wiel *et al*., 2016). The importance of this convergence zone is that the majority of the South Pacific rainfall and major convective activity takes place here, while moisture availability, air and sea surface temperatures have a large influence over this convection zone (van der Wiel *et al*., 2016). The increased convection and convergence associated with the convergence zone presents favourable conditions for tropical cyclones, however, the convergence zone is impacted by zonal disparities of sea surface temperature, hence why the ENSO impacts the locations of tropical cyclone genesis during a warm phase (van der Wiel *et al*., 2016). The South Pacific Ocean also displays an increase of its sea surface temperatures over time (Jourdain *et al*., 2011). However, the Pacific Ocean heat content is strongly linked to the PDO whereby decades of negative (positive) PDO phases consisting of up to 25 years can cause warmer (cooler) than normal oceans around the South Pacific region (Linsley *et al*., 2015). Additionally, extreme cooling tends have been known to encourage weaker convergence and convection over the South Pacific Convergence Zone, resulting in decreased tropical cyclone activity (van der Wiel *et al*., 2016).

3.2 Climatology and Mean Conditions 1980-2016

3.2.1 Basin Interactions

The Southern Hemisphere basins are unique compared to the Northern Hemisphere basins, as they are not entirely separated from each other by landmasses, they experience a larger magnitude of solar input and have smaller basins and therefore, less water mass and heat capacity than Northern Hemisphere basins (Halperin *et al*., 2013; Befort *et al*., 2016; Song *et al*., 2018). Sea surface temperature is a major factor regarding ocean characteristics, as it is a central element in driving convection, evaporation and precipitation over the basin and the surrounding coastlines (Rao *et al*., 2012). Specifically, the South Indian Ocean warming influences the Pacific via ocean atmosphere interactions, by intensifying the east to west zonal winds (Walker Circulation/ Bjerknes feedback) which enhances La Niña conditions (Luo *et al*., 2012). Recently the MJO, has been found to greatly influence the sea level of the tropical Indian Ocean by barotropic processes (i.e. involving the entire water column) over the tropical Indian Ocean, which in turn is responsible for large exchanges of water mass between the Pacific and Indian Ocean (Rohith *et al*., 2019). The Indonesian throughflow is another physical aspect of the Southern Hemisphere oceans which is responsible for moving large amounts of heat energy from the Pacific into the South Indian Ocean (Zhang *et al*., 2018).

Table 3.1 Locations of latitude and longitude indicating the extent of each basin/region, the zones where tropical cyclones have been recorded to form and the modes of variability associated with these basins.

	South Indian Ocean	Australian Region	South Pacific Ocean
Extent	30-100E°	110-160E°	160-120°W
Tropical cyclone Formation Zones	50-80E° and 80-100E°	120E° (WA) 160E° (EA)	160E-180E° (Mainly over South Pacific Convergence Zone).
Modes of Variability	IOD, MJO, SAM	IOD, MJO, SAM	ENSO, MJO, SAM, PDO

3.2.2 Climate Trends and Ocean Currents

The climate projections and historical mean sea surface temperature output from the Coupled Model Intercomparison Project (CMIP5), indicates the distribution of ocean heat content and the position of sea surface temperature isotherms for the ocean basins across the 1956-2005 period (Figure 3.2). The basin warm pools and the regions that have higher rates of evaporation are visible over the tropical regions of the Southern Hemisphere ocean basins (Figure 3.2: panel a). The regions poleward of 30°N/S display lower sea surface temperatures and evaporation, while the projected climate scenario (Figure 3.2: panel c) indicates that the Southern Hemisphere tropical regions and the locations of the tropical cyclone formation zones will experience a warming trend and an increase in evaporation according to the Regional Concentration Pathways (RCP2.6 scenario) based on a warming of 2.6°C by 2055. The greatest deviation from the mean sea surface temperatures is observed over the equatorial Pacific (Figure 3.2: Panel b), while the projected variance of sea surface temperatures and evaporation is expected to increase comparatively more for poleward regions in both hemispheres (Figure 3.2: Panel d). These CMIP5 outputs indicate that the sea surface temperature and evaporation rate over the Southern Hemisphere basins will experience a sustained increase into the future, specifically over the tropical and poleward regions.

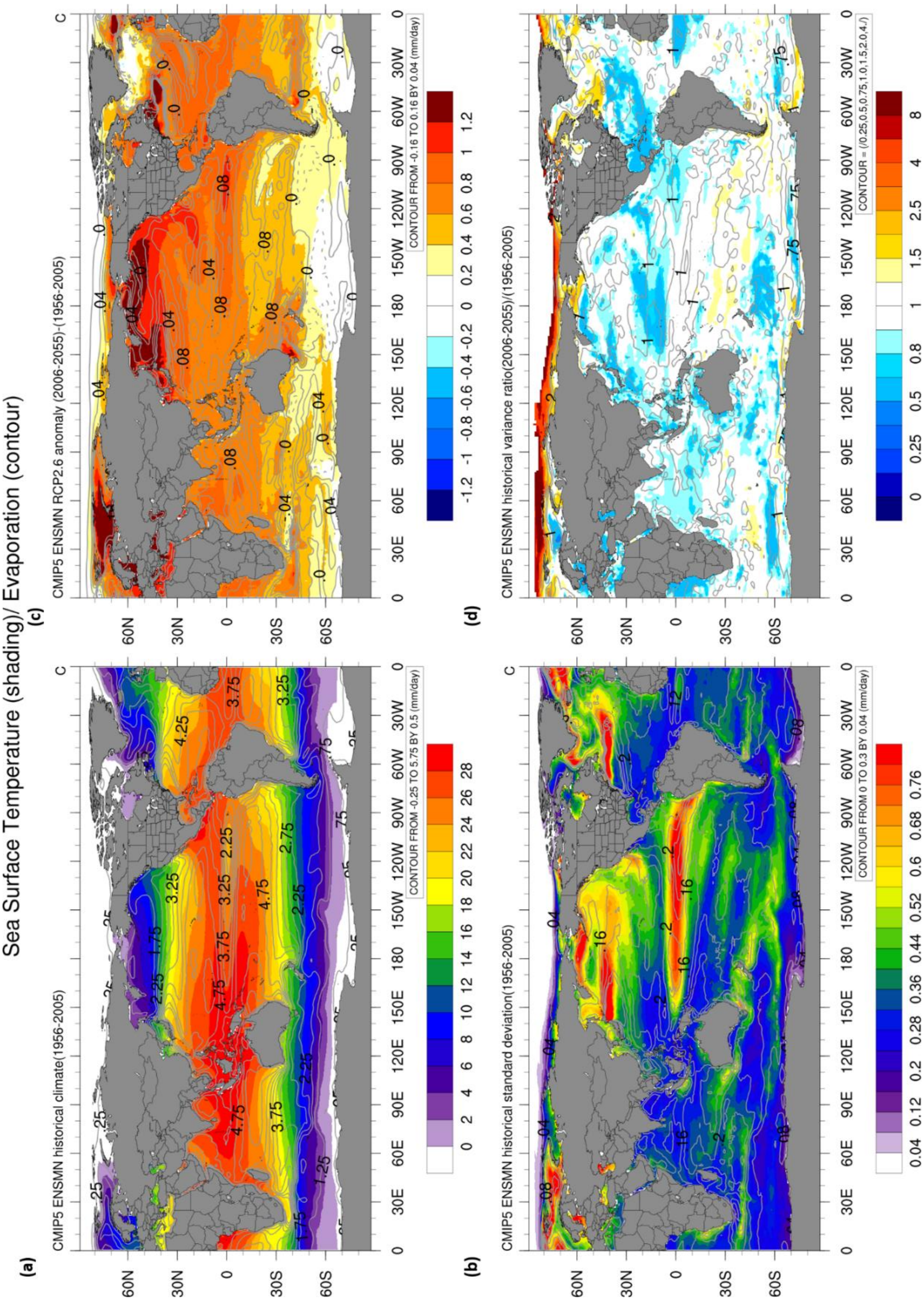

Figure 3.2 Sea surface temperature and Evaporation. Historical (1956-2005) and Projected (2006-2055) mean distribution from the CMIP 5 Model output. Outputs created using the CMIP 5 online plotting tools from NOAA ESRL Physical Science Division. Sea surface temperature and evaporation represented by shading and contours respectively (1956-2005). (a) Historical mean (1965-2005) and (b) standard deviation of sea surface temperature and evaporation. (c) Projected change (2006-2055) and (d) variance ration between historical and projected sea surface temperature and evaporation.

The ocean currents are important within climatological studies, as they are responsible for ocean mixing and energy transfer, while also influencing storm tracks in the mid-latitudes (Seager & Simpson, 2016; Yang *et al*., 2016). Specifically, western boundary currents in the Southern Hemisphere, such as the Agulhus Current for the South Indian Ocean and the east Australian Current in the South Pacific are responsible for transporting large amounts of heat poleward, via movements of warm subtropical water (Seager & Simpson, 2016). The eastern boundaries of the ocean basins do not have an equivalently strong current (Yang *et al*., 2016). Under a changing climate, with increased sea surface temperatures in the sub-tropics, more heat energy is being moved poleward, however, it is also observed that the currents themselves are shifting poleward (Yang *et al*., 2016). While the Agulhas Current is expanding instead of intensifying, the Australian western boundary current is increasing in intensity, thereby moving warmer equatorial water up to 350 km poleward compared to 60 years ago (Seager & Simpson, 2016). This has implications for the climate and the ocean temperatures, which will cause higher sea surface temperatures to be dispersed poleward, thereby warming the cooler regions of the basins and instigating changes in their climatology (Seager & Simpson, 2016; Yang *et al*., 2016). This agrees with the CMIP 5 projections (Figure 3.2). Specifically, the regions with the 28-29°C sea surface temperature isotherms indicate that by 2055, these regions will have migrated poleward. Incidentally, this migration of warmer sea surface temperature poleward is already being observed (Zhan & Wang, 2017a; Altman *et al*., 2018; Fitchett, 2018).

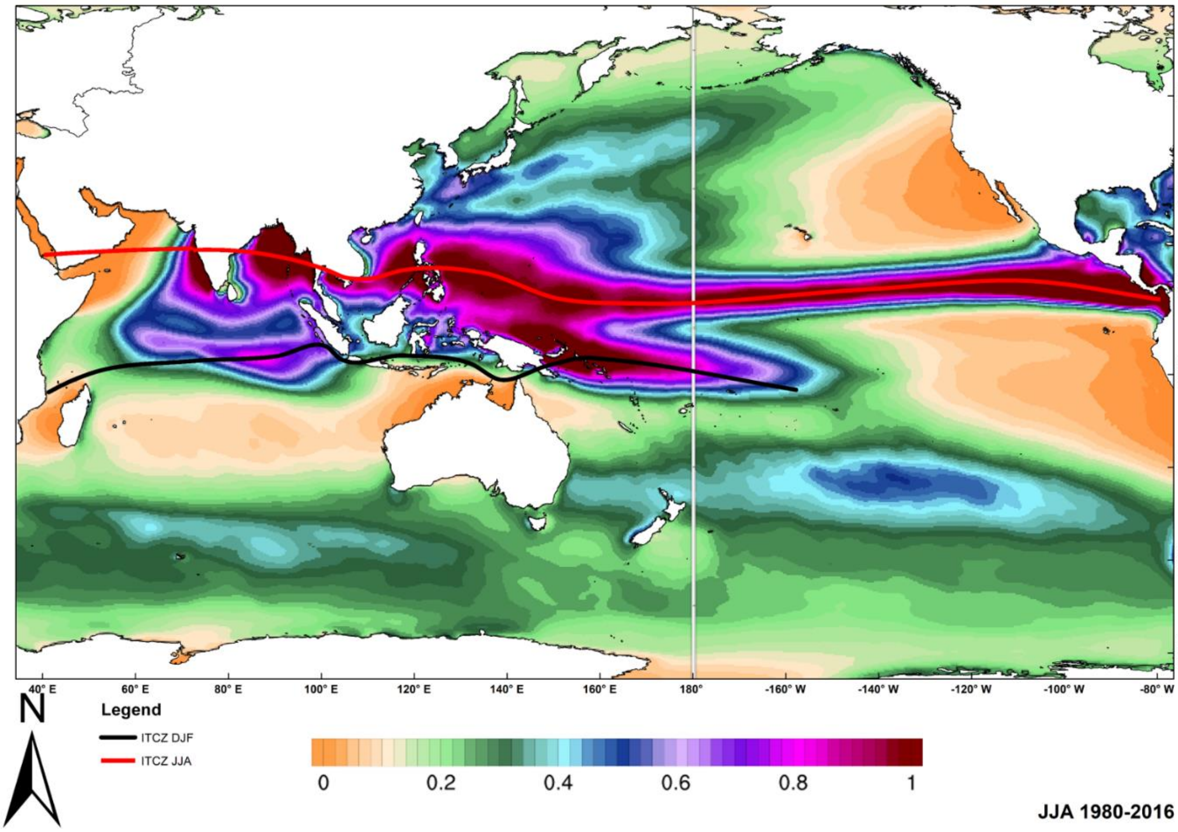

Figure 3.3 Mean precipitation over the tropical regions delineating the Inter Tropical Convergence Zone (ITCZ). The winter season (JJA) from 1980-2016 when tropical cyclones rarely occur.

The migration of the ITCZ is reflected in Figure 3.3 and Figure 3.4, where the ITCZ, marked by increased precipitative activity shifts southward from the equator during the December-February season. The diagonal convergence zones in the South Pacific are also evident over the eastern regions off Australia's east coast. During the winter months in the Southern Hemisphere, the ITCZ is shown to migrate equatorward, therefore shifting the high precipitation zones with it, with the additional observation of no tropical cyclone activity occurring in the Southern Hemisphere during the June to August months when the ITCZ has shifted northward and away from the Southern Hemisphere oceans (Chen *et al*., 2019).

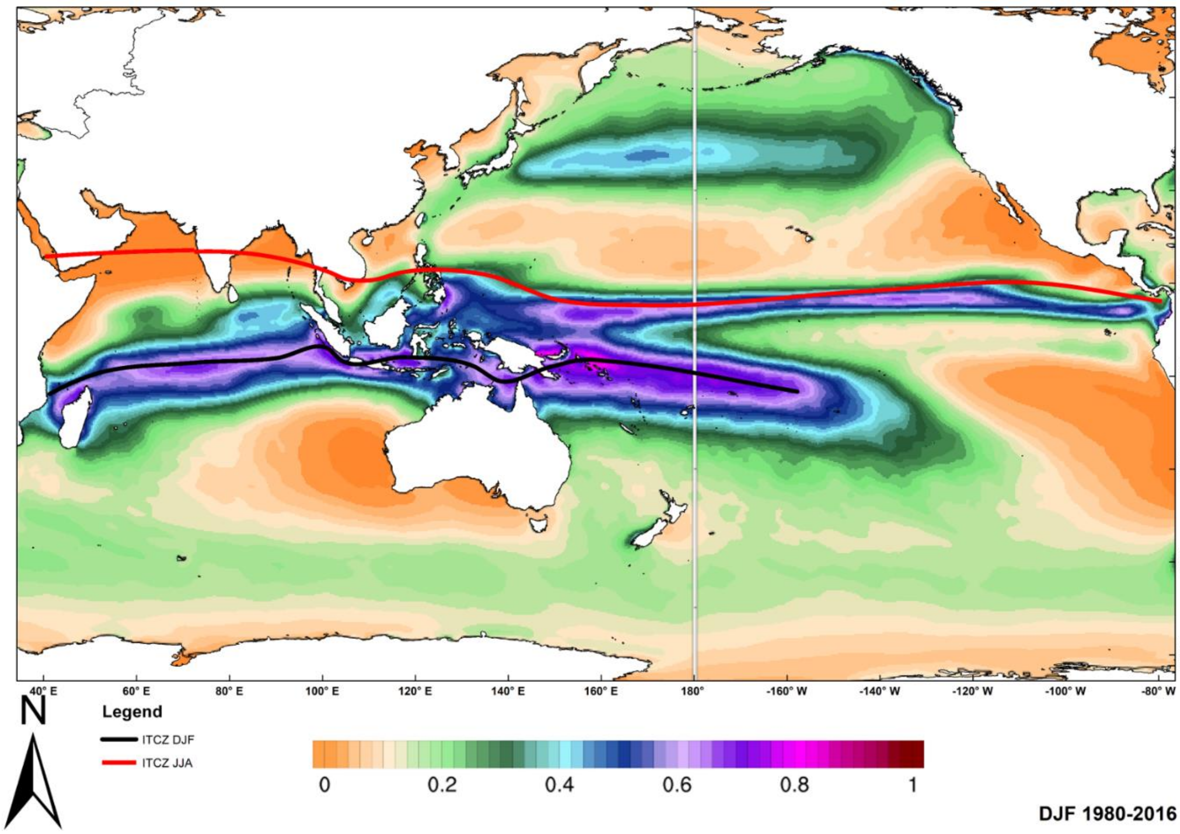

Figure 3.4 Mean precipitation over the tropical regions delineating the Inter Tropical Convergence Zone (ITCZ). Mean precipitation and position of the ITCZ compared between the early tropical cyclone season (DJF).

3.2.2.1 Outline of Variability

There are multiple modes of variability (Figure 2.1) which influence tropical cyclone activity across the Southern Hemisphere. In the South Indian Ocean, the IOD is present, while the ENSO and PDO modes are the major drivers of interannual and decadal variability in the Pacific Ocean respectively (Ash & Matyas, 2012; Diamond *et al*., 2013) The MJO propagates across the equatorial tropical zones of the Southern Hemisphere, while the SAM is located over the more poleward regions at 60°S, but has no landmass blocking its influence on the Southern Hemisphere basins (Camargo *et al*., 2009; Diamond *et al*., 2015a). Regardless of their location theses modes impact the majority of the Southern Hemisphere tropical cyclone basins via their impacts on the ocean atmospheric system and teleconnections (Cai *et al*., 2018a; Magee & Verdon-Kidd, 2018).

3.2.2.2 Vulnerability

The Southern Hemisphere basins are bounded by two major continents, the maritime continent and multiple small island nations. These landmasses consist of developed and developing nations and all of them are potentially exposed to future tropical cyclone landfall events (Temmerman *et al*., 2013; Cinco *et al*., 2016). Particularly with the future warming projected in the Southern Hemisphere (Figure 3.2), coupled with the observations of a poleward shift in tropical cyclone activity (Kossin *et al*., 2014), the regions poleward of 35°S, could also be at risk, as the conditions required for tropical cyclone formation such as increased sea surface temperatures and convective environments (represented by increased evaporation potential) shift further poleward and threaten more areas (Daloz & Camargo, 2018). The population density maps below indicate that much of the coastlines except for Australia have a high population density. These coastlines indicate that large populations of people are therefore at risk within the Southern Hemisphere. The implications of a tropical cyclone impact and the subsequent damage is related to reduced economic growth as a result of damage to key infrastructure, which further increases poverty (Fussell *et al*., 2017). There is also the prevalence of diseases which follow tropical cyclone landfalls, especially in underdeveloped nations (Fussell *et al*., 2017). Apart from tropical cyclones impacting landmasses, the Southern Hemisphere has important and often used shipping lanes from the southern African region to Asia and Australia (Klotzbach *et al*., 2018). Based on the population density map (Figure 3.5) and the study site map (Figure 3.1) indicating the areas which have been at risk from tropical cyclone landfalls over the 1980-2016 period, there a number of regions which present a potentially increased vulnerability to tropical cyclone landfall events. The Madagascan coastlines, the southern east African regions of Mozambique and the islands in the maritime content, i.e. the Indonesian archipelago, demonstrate overlap of high population density and risk from tropical cyclone landfalls.

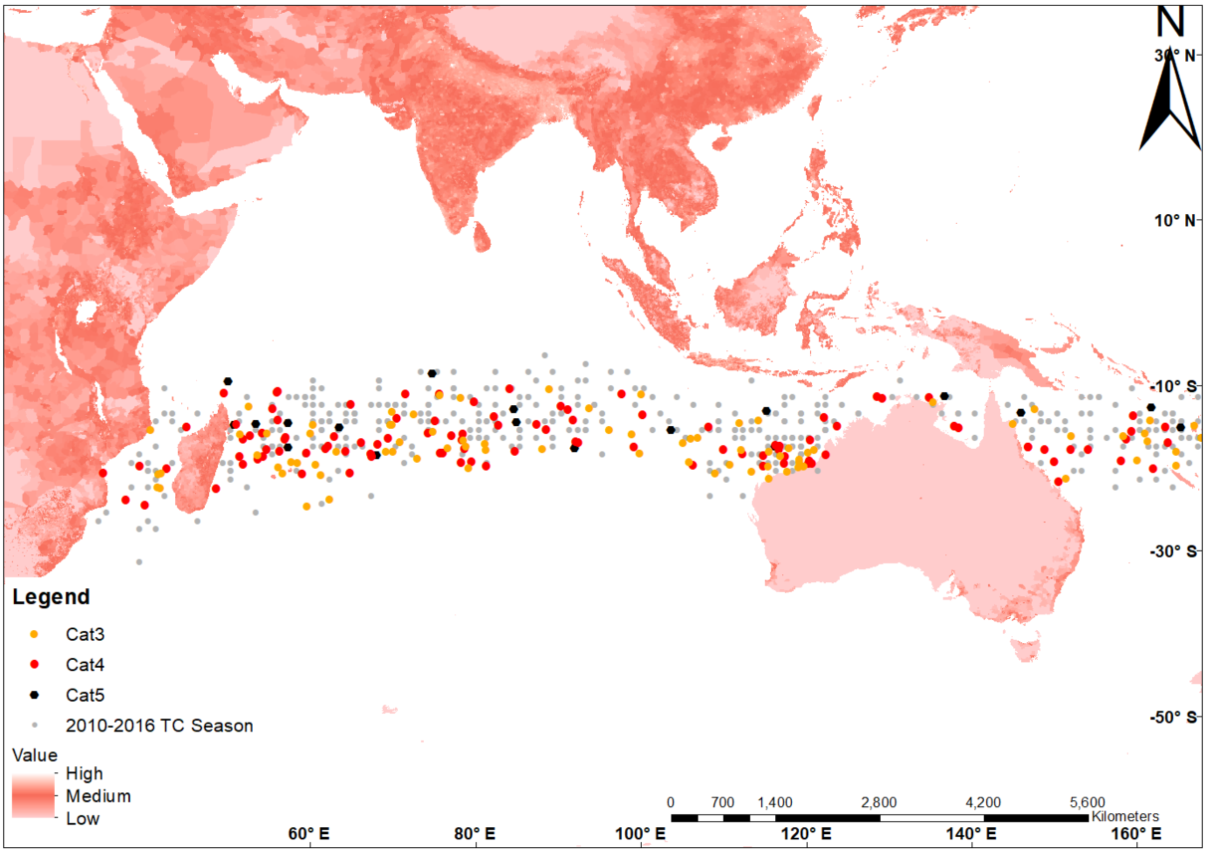

Figure 3.5 Population Density with the dark red indicating 10000 per km^2. Tropical cyclone activity for the latest 6 year period is shown, alongside all category 3,4 and 5 storms from 1980-2016.

4. Data and Methodology

4. Introduction: Data and Methodology

The overall aim of this study is to construct an updated tropical cyclone climatology for the Southern Hemisphere ocean basins, update and re-evaluate the existing Southern Hemisphere studies related to tropical cyclone activity and variability, and investigate trends of change in tropical cyclone activity and the climate variables associated with storm genesis (cf. Kuleshov *et al*., 2008,2009,2010; Ash & Matyas, 2012; Ramsay *et al*., 2012; Dowdy *et al*., 2012; Tory & Dare, 2015; Defforge & Merlis, 2017a). The methodology provides the procedures undertaken to acquire, process, verify and analyse the data. The data were grouped into three sub-categories; 1) tropical cyclone data, 2) climatic data and 3) indices for climatic modes of variability. The three categories of data were acquired, processed and then joined into a single database. This combined database was then used to perform the data analysis, which entailed the examination of relationships between the three data categories and determining the degree of influence the climatic drivers and modes of variability had on the tropical cyclone activity of the Southern Hemisphere. The overall use of statistical analysis and the quantitative approach applied within this study, are adapted from existing tropical cyclone studies (Jobson, 2012; Fitchett & Grab, 2014; Ramsay *et al*., 2017; Rai *et al*., 2019).

4.1 Data Acquisition

When constructing a climatology which describes long-term trends and change in the ocean and atmospheric system, a minimum of 30 years of meteorological data is required (WMO, 2017). This is necessary to capture trends and variability related to the variables being investigated, as well as monitoring effects of long-time scale changes such as environmental warming signals (Emanuel, 2005; Timmermann et al., 2018). Therefore, to determine the nature, change and influence of the climate drivers related to tropical cyclone activity, along with the possible forcing of a warming ocean-atmospheric system, the diagnostic data on tropical cyclone activity over time were examined in relation to the large-scale environmental/climate variables corresponding to each storm event. These climate variables were selected based on Gray's (1968, 1979) existing indices for tropical cyclone genesis, as these climate variables are known influencers or drivers of tropical cyclone genesis, and have been applied and verified in multiple observational studies (Dare & McBride, 2011; Malan *et al*., 2013; Tory & Dare, 2015; Defforge & Merlis, 2017b) and model-based studies (Emanuel, 2010; Evans & Waters, 2012; Camargo, 2013; Wu *et al*., 2015; Rai *et al*., 2019). Therefore, the application of these climate variables to establish the parameters of a tropical cyclone genesis climatology for the Southern Hemisphere was required, however, additional climate variables/drivers have also been included to explore new influencing factors for tropical cyclone genesis.

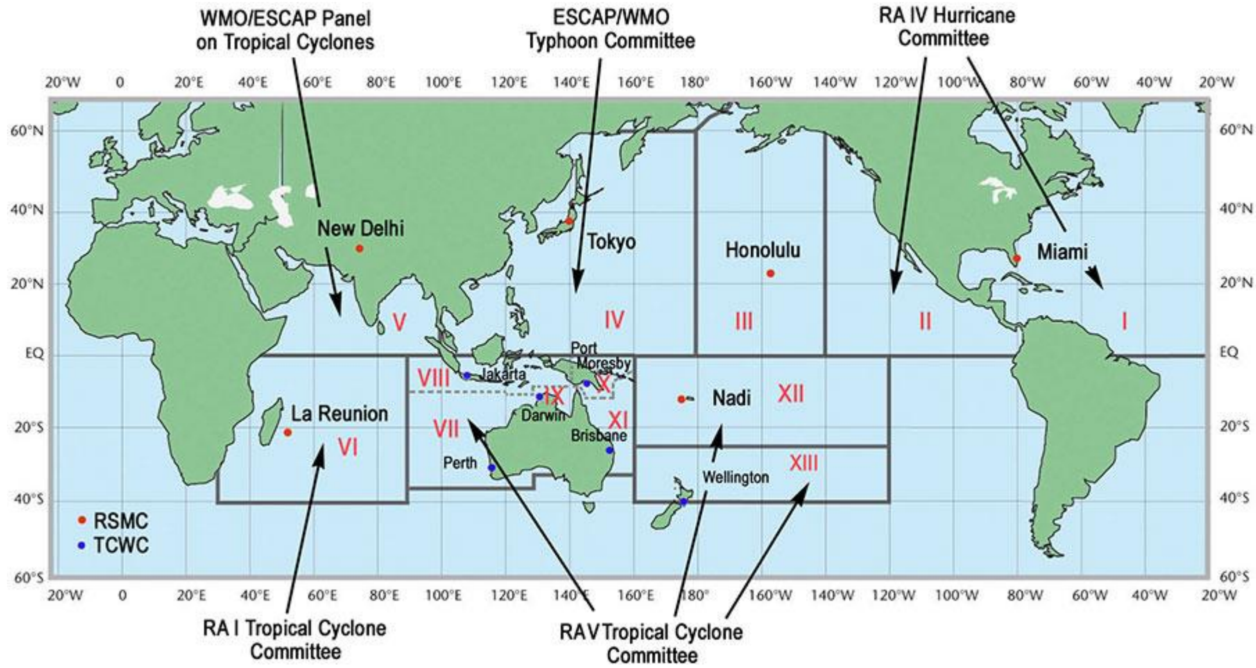

Figure 4.1 Map of data centers capturing tropical cyclone data and their spatial coverage. (Source: WMO Tropical Cyclone Programme - www.wmo.int/pages/prog/www/tcp/Advisories-RSMCs.html).

4.1.1 Tropical Cyclone Data

The majority of tropical cyclone studies make use of best track data compiled from multiple data centers worldwide (Figure 4.1) with emphasis placed on creating and using data products with the best possible reliability (Knapp *et al*., 2010; Diamond *et al*., 2012; Osuri *et al*., 2012; Magee *et al*., 2016). In this study the tropical cyclone dataset used was the International best track archive for climate stewardship (IBTrACS), provided by the National Oceanic and Atmospheric Association (NOAA) from https://www.ncdc.noaa.gov/ibtracs/ (Knapp *et al*., 2010; Magee *et al*., 2016). The IBTrACS dataset provides comparatively reliable tropical cyclone data for all the basins and includes the data from the geostationary satellite era (1980-present), which is available for the ocean basins examined in this study: the South Indian, West Australian, East Australian and South Pacific Ocean regions (Schreck *et al*., 2014; Magee *et al*., 2016). The tropical cyclone data captured, includes the date, latitude, longitude, wind speed and central pressure of the storm across its lifetime: from development as a tropical storm, to tropical cyclone genesis, lifetime maximum intensity and dissipation, while the pressure and wind speed used to calculate storm intensity are provided at intervals of six hours (Knapp *et al*., 2010; Magee *et al*., 2016). Once a storm or tropical disturbance develops and attains tropical storm intensity, the wind speeds of the system will have reached 34-63 knots or 55-101 km.hr^{-1} (Jiang, 2012). Genesis of the tropical cyclone is the point at which the tropical storm cloud bands rotate at a wind speed of 64 knots (119 km.hr^{-1}) or above (Webster *et al*., 2005). Lifetime maximum intensity is the stage when the tropical cyclone attains its highest wind speed and lowest central pressure, and this metric was used to determine the category (Category 1-5, see Table 4.1 for Saffir Simpson scale of intensity) to classify the storm intensity (Knapp, 2010; Song *et al*., 2018). Dissipation is the point at which the storm starts experiencing a decrease in its wind speed until it weakens significantly, the organised spiral cloud bands disperse, and the storm system does not re-intensify (Sebastian & Behera, 2015).

Table 4.1 Saffir Simpson scale of tropical cyclone (TC) wind speeds in km/h, central pressure and related categories of intensity. Source: https://www.nhc.noaa.gov/aboutsshws.php.

Km.hr^{-1}	Central Pressure	Category
118-153	960-979	Category 1
154-177	945-959	Category 2
178-209	930-944	Major TC Category 3
210-249	905-929	Major TC Category 4
>250	<905	Major TC Category 5

4.1.2 Tropical Cyclone Data Extraction and Compilation

The date, location (latitude and longitude), wind speed and central pressure were extracted for each tropical cyclone (attaining a 10-min sustained wind speed >119 km.hr^{-1}). In addition to the Saffir-Simpson scale, a majority of authors along with the NOAA IBTrACS recognise and classify the 64 Knot/119 km.hr^{-1} wind speed threshold as the point at which a tropical storm transitions to a tropical cyclone (Ramsay *et al*., 2012; Mao *et al*., 2013; Schreck *et al*., 2014; Magee *et al*., 2016; Bhaskaran *et al*., 2018). Any system classified as a tropical cyclone occurring within the seasons of 1980-2016 were extracted (2017-2019 data were not in final release at the time of extraction). This timespan was chosen, as it provides a period of more than 30 years and was created using homogenous and accurate satellite data and therefore does not have the biases usually inherent in tropical cyclone intensity data from pre-1980 periods (Landsea *et al*., 2006; Magee *et al*., 2016).

The tropical cyclone data was captured in an excel data table, to construct a storm database on which statistical analysis could be performed easily. The lifetime (L1) of the entire storm (from tropical storm phase to dissipation) was calculated by:

$$L1 = Date\ of\ Dissipation - Date\ of\ Storm\ Formation$$

The duration (L2) of the tropical cyclone (time spent above 119 km.hr^{-1}) was calculated by:

$$L2 = Date\ of\ Dissipation - Date\ of\ Genesis$$

The tropical cyclones were sorted into their season of occurrence. Generally, the Southern Hemisphere has a tropical cyclone season from November to March, therefore the storms were sorted by grouping the storms from the preceding year of the season (e.g. 1980: November-December) with storms from the sequential year of the season e.g. 1981: January-March (Mavume *et al*., 2009). Therefore, a season is defined by a two-year combination (Kuleshov *et al*., 2008), with seasons in this study spanning from 1980/81-2015/16. The category of the storms was based on the wind speeds (as outlined in the Saffir-Simpson scale: Table 4.1). Wind speed data were extracted at the main phases of the systems life cycle (from the IBTrACS database), namely the tropical storm stage, the genesis stage and the time at which a storm attained its lifetime maximum intensity. The wind speed data, provided in knots, was converted to meters per second ($m.s^{-1}$).

4.1.3 Climate Data Sources

The climate data used in this study was extracted from the National Center of Environmental Predictions NCEP-DOE reanalysis II dataset collection (Saha *et al*., 2010). This dataset improves on the previous NCEP Reanalysis I model output, with data availability from 1979 to present at varying gridded spatial resolutions (detailed in Section 4.2.4) and provided at a four times daily temporal resolution from http://www.cpc.ncep.noaa.gov/products/wesley/reanalysis2/kana/reanl2-1.htm. The climate variables that were extracted, consisted of relative humidity, air temperature, omega, v-wind, u-wind, geopotential height, solar flux and sea level pressure. All the climate variables were extracted at two atmospheric levels: 1) the 1,000mb level and 2) the 850mb level. Generally, the mechanisms or environmental variables driving tropical cyclone activity are examined at the lower troposphere and surface and the mid to upper levels of the troposphere, which allows for a multi-level (upper and lower) representation of the storm environment and climate interactions (Gray, 1968; Tory & Dare, 2015; Defforge & Merlis, 2017a). In addition, between the near surface (1,000mb) and the mid 850mb levels, variations in both temperature and moisture are observed to influence the genesis environment (Parodi & Emanuel, 2009; Sahany *et al*., 2012). However, at higher levels (500mb), only moisture fluxes play the dominant role in modulating the genesis environment (Sahany *et al*., 2012). Gray (1968), also stated that the surface and lower atmosphere fluxes in temperature and moisture have a larger effect on the genesis conditions than the higher atmospheric levels. According to the data quality review, there are no caveats for any of the data extracted from the NCEP Reanalysis II (Kanamitsu *et al*., 2002). The sea surface temperature data was extracted from a separate NOAA dataset known as the OISST v2, found within https://www.esrl.noaa.gov/psd/data/gridded/data.noaa.oisst.v2.highres.html. The climate modes of variability were acquired as indices describing the phase of each mode over a monthly average for each year (1980-2016). The Niño 3.4 index was attained from http://www.esrl.noaa.gov/psd/gcos_wgsp/Timeseries/Nino34/. The DMI, SOI and Niño 3.4 indices were acquired from https://www.esrl.noaa.gov/ psd/gcos_wgsp/Timeseries/. The multivariate ENSO index or MEI, which is another index used to study ENSO, was acquired from https://www.esrl.noaa.gov/psd/enso/mei/table.html. The data for the stages and magnitudes of the MJO index was acquired from the Australian Bureau of Meteorology in http://www.bom.gov.au/climate/mjo/graphics/ rmm.74toRealtime. txt. The compiled index describing the PDO was acquired from http://research.jisao.washington.edu/pdo/ PDO.latest.txt. The SAM/Antarctic Oscillation (AAO) was adopted from the Marshal reanalysis https://legacy.bas.ac.uk/ met/gjma/sam.html (Marshal, 2003). Volcanic eruption data were acquired from https:// www.ngdc.noaa.gov/nndc/struts/form?t=102557&s=50&d=50.

4.1.4 Climate Data Selection

The OISST v2 dataset contains the highest spatial (0.25°x0.25°) and temporal (daily mean) resolution from the 1980s to the present, and has been applied widely in the latest tropical cyclone studies related to sea surface temperature (Reynolds *et al*., 2007; Xu *et al*., 2016; Defforge & Merlis, 2017a, b; Fitchett, 2018). This dataset only provides surface magnitudes of temperature, with no depth element, however, Mawren and Reason (2017) determined that sea surface temperature performs nominally as a proxy for the ocean thermocline layer depth (depth that the observed sea surface temperature extends to). The remaining reanalysis datasets (air temperature, relative humidity, omega, v-wind and u-wind, geopotential height, solar flux and sea level pressure) have a spatial resolution of 2.5°x2.5° with a global grid coverage of 90°N-90°S;0°E-360°E (Kanamitsu *et al*., 2002).

The motivation for including the climate variables and drivers, specifically, sea surface temperature, is that each basin has demonstrated a unique threshold of sea surface temperature and climatology, which is related to the mean magnitude of the other climate variables known to influence tropical cyclone formation (Defforge & Merlis, 2017a). Since tropical cyclone genesis does not necessarily require the 26.5°C threshold to be present and the other variables mentioned have not demonstrated specific magnitudes which best promote tropical cyclone formation in different basins, specifically the Southern Hemisphere (Emanuel, 2013; Defforge & Merlis, 2017a; Klotzbach *et al*., 2017), it is therefore acceptable to explore a new southern hemispheric tropical cyclone climatology, with a focus on the climate variables related to tropical cyclone genesis. The majority of these climate variables have already demonstrated an influence over tropical cyclone genesis and activity (Nolan & McGauley, 2012; Wang *et al*., 2015; Klotzbach *et al*., 2017). Therefore, regarding these known influencers of tropical cyclone formation, what remains to be investigated is the magnitude of these climate variables, and which drivers at the point of genesis demonstrate the greatest favourability and influence on Southern Hemisphere tropical cyclone genesis (Li *et al*., 2013; Tory & Dare, 2015).

The OISST v2 and relative humidity datasets were chosen as sea surface temperature and atmospheric moisture content are widely recognised drivers of tropical cyclone genesis (Gray, 1968, Dare & McBride, 2011; Wu *et al*., 2015; Klotzbach *et al*., 2017). This has been based on the premise that tropical cyclones are heat engines and are sustained on heat energy and moisture (Tory & Dare, 2015; Scoccimaro *et al*., 2017). Related to this, air temperature was included as recent studies indicate that tropospheric temperatures play an important role in the genesis and intensification process of the tropical cyclone lifecycle, as well as providing a sustaining environment to the storm (Mcphaden *et al*., 2009; Dare & McBride, 2011; Vecchi *et al*., 2013). Therefore, while not a required element in the existing genesis indices (outlined in Section 2.3.1), air temperature was considered as a necessary driver to explaining a part of the tropical cyclone climatology, as it is related to sea surface temperature (via air-sea interactions) and influences relative humidity and convective activity, as higher air temperatures promote higher moisture content (Hill & Lackmann, 2009; Jiang, 2012). Investigations have similarly stated that solar flux is the preferential metric when attempting to define the impact of solar energy input on tropical cyclone activity (Korty *et al*., 2012b; Li *et al*., 2017, 2018). The Southern Hemisphere also tends to receive more solar radiation than the Northern Hemisphere (Korty *et al*., 2012a). Solar flux is therefore included in this study to determine whether this metric of solar activity has an impact or modulation on Southern Hemisphere tropical cyclone activity.

The v-wind and u-wind vector components were applied within this study, to derive zonal and meridional wind shear respectively. The widely used vertical wind shear metric was derived from the u-wind and v-wind components (Gray, 1968; Nolan & McGauley, 2012). Vertical velocity or buoyancy, which is the upward motion in the atmosphere and vertical wind shear are recognised as core elements in the formation environment of a tropical cyclone and have often been used in climatological and tropical cyclone studies (Gray, 1968; Tory & Franks, 2010; Dare & McBride, 2011). Usually vorticity data is used to assess the vertical and relative motion of the environment, along with the convergence present during tropical cyclone formation (Gray, 1968; Yu *et al*., 2016). This study has instead used omega as a representation of large-scale upward motion in the atmosphere and surface convergence/divergence during the point of genesis.

Omega (ω) is a representation of the large-scale environmental vertical velocity. By using the change in pressure to calculate omega (ω), the horizontal divergence and resultant large-scale upward motion of air can be determined and can be used to estimate vertical motion in the atmosphere (Pike, 1985; Hastenrath & Greischar, 2001; Kiranmayi & Maloni, 2011). In this case the omega is presented in pascal seconds (pascals/s^{-1}) which delineates dynamic viscosity of the atmosphere. Viscosity decreases with pressure and height, therefore the velocity at the surface is approximately zero (Franklin *et al*., 1996). To simplify, when the omega (ω) rate is negative (positive), the atmosphere is being expanded (compressed), resulting in horizontal convergence (divergence), increased (decreased) vertical velocity and buoyancy (Figure 4.2). The NCEP-DOE reanalysis provides omega data in pascal seconds, which should therefore increase in magnitude (negatively) as height increases and pressure decreases, which will indicate the large-scale magnitude of upward motion in the atmosphere (Song *et al*., 2018, 2019). Omega has been used previously as a large-scale environmental predictor of stability, with negative (positive) values taken as an unstable (stable) atmosphere (Song *et al*., 2019). By extracting omega values for the longitude and latitude delineating the location of the tropical cyclone, an accurate picture of the vertical motion relating to the cyclone environment can be discerned (Pike, 1985; Franklin *et al*., 1996).

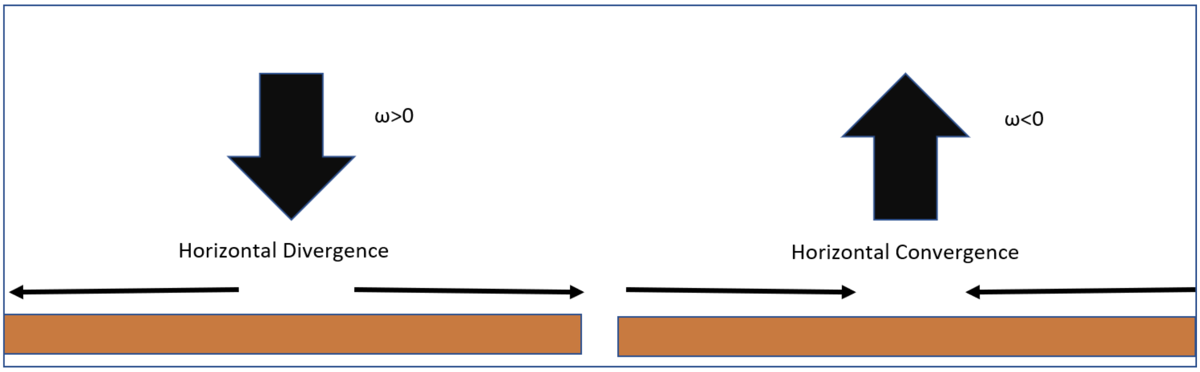

Figure 4.2 Illustration of vertical velocity/omega (ω) with surface horizontal divergences under a positive omega and horizontal convergence under a negative omega. During a negative omega the vertical velocity is upward indicating buoyancy of the atmosphere (after Wallace & Hobbs, 2006).

U-wind components represent the zonal winds (westerly and easterly winds), while v-wind components represent the meridional winds (northerly and southerly winds) and are provided in $m.s^{-1}$ with the direction. These wind components have been used instead of raw wind speed data, as they allow the different components such as direction of the horizontal wind shear to be examined (Vecchi & Soden, 2007; Osuri *et al*., 2012). Using v-wind and u-wind from two different height levels, allows for the resultant environmental wind speed and wind shear to be computed for the meridional and zonal components of the wind (Vecchi & Soden, 2007). Related to this, geopotential height is required to give information on the heights (Equation 1) of the pressure surfaces at the 1,000mb and 850mb levels (Li *et al*., 2010; Bratton & Womeldorf, 2011). In addition to using geopotential height to derive wind shear, the variable was used to discern how these heights changed with different tropical cyclone events, as the geopotential height can be used as a measure of the convective potential of the storm system and environment and has been reported to influence tropical cyclone activity (Vecchi & Soden, 2007; Li *et al*., 2010; Matyas, 2015). Sea level pressure was selected to provide data on the pressure variability at the surface of the ocean, as this acts as a pressure indicator for the lower atmosphere environment, since the central pressure for the tropical cyclone only provides the lowest pressure present within the eye of the storm (Nguyen & Molinari, 2015). The pressure variable has been important in determining the effectiveness of convergence at the surface, as the air converges and rises, the pressure drops at the surface (Parodi & Emanuel, 2009). Additionally, tropical cyclone intensity is a function of minimum sea-level pressure, with the highest intensities occurring at the lowest sea level pressures (Atkinson & Holiday, 1977; Yamada *et al*., 2017).

The climate modes of variability and the timing and magnitude of volcanic eruptions (using the volcanic explosivity index) served as indicators to assess how climatic variability and forcers may modulate tropical cyclone activity. The influence that modes of variability have on tropical cyclone activity across all the Southern Hemisphere basins has previously been explored (Bessafi & Wheeler, 2006; Ramsay *et al*., 2012; Mao *et al*., 2013; Fitchett & Grab, 2014; Diamond & Renwick, 2015; Wang *et al*., 2015; Walsh *et al*., 2016; Patricola & Wehner, 2018). These modes influence the ocean-atmospheric system via altering sea surface temperatures, pressure patterns and wind field intensities at predictable and relatively constant cycles ranging from timescales of intra-seasonal with the MJO, interannual with the DMI, SAM and ENSO and decadal with the PDO (Allen *et al*., 2014; Diamond *et al*., 2015a; Clem *et al*., 2016; Cai *et al*., 2018a, b). Volcanic eruptions are more random in the timing of their occurrence, however, they can instigate large effects on the Earth's energy budget via changes in the atmospheric reflectance and scattering ability of the incoming solar radiation (Korty *et al*., 2012; Pausata & Camargo, 2019). The modes of variability are included in this study, as they are known to influence the climate variables used in this study (Kuleshov *et al*., 2009). Therefore, in the interest of creating a thorough and encompassing climatology for Southern Hemisphere tropical cyclones, the modes need to be assessed to determine if there are any relationships or teleconnections between the modes and tropical cyclone activity (Kuleshov *et al*., 2009; 2010).

4.1.5 Data limitations

The IBTrACS record is compiled from multiple sources to ensure the best possible accuracy (Schreck *et al*., 2014). However, there are no means to discern whether or not the recorded 6-hourly locations of the storm are entirely precise (Knapp *et al*., 2010, 2011). This introduces possible errors when extracting the climate data based on each storm's location, as the data may be extracted for a location at which the storm was not precisely located. This will have continuous effects on the climate data extracted which is based on these locations and dates that are related to tropical cyclone genesis and intensification. It should also be noted that omega is a large-scale environmental variable averaged over a large area, while a tropical cyclone spans a smaller area in comparison and is characterised by localised conditions (Kiranmayi & Maloni, 2011; Song *et al*., 2019). This could impact the results, as the recorded omega representing the overall environmental upward motion, may not align with the localised upward motion present over the tropical cyclone region of formation.

4.2 Climate Data Extraction and Processing

All the climate data was extracted using the Network common data form (netcdf) module software and libraries provided by Unidata in https://www.unidata.ucar.edu/software/netcdf/. A python script was compiled to extract the data from the netcdf files based on location and time (Knapp *et al*., 2011; Yablonsky *et al*., 2015). The climate data was extracted for each individual storm based on the storm latitude, longitude and the calendar date. This allowed for accurate and precise extraction of climate data values related to each tropical cyclone event (Walsh *et al*., 2013; Wehner *et al*., 2014). Specifically, the climate data was first extracted for each location and date at which a storm underwent genesis, then for the location and date at which the tropical cyclone reached lifetime maximum intensity (Ren *et al*., 2014).

4.2.1 Wind Component Calculations

Wind shear refers to the difference between wind speed and direction between two height levels. In this case wind shear was calculated between the 1,000mb and 850mb levels for v-wind and u-wind as adapted from (Vecchi & Soden, 2007; Na *et al*., 2018). The zonal and meridional components of wind shear were calculated using equation 2 adapted from equation 1 (Sen *et al*., 2012). Equation 3 demonstrates the calculation for vertical wind shear across two different heights.

(Equation 1)

$$v_2 = v_1 \cdot \left(\frac{z_2}{z_1}\right)^{\alpha}$$

(Na *et al*., 2018)

(Equation 2) Equation 1 was converted into the log version to accommodate solving for α co-efficient for u-wind (zonal) and v-wind (meridional): (Xu *et al*., 2014).

$$\alpha = \log_{\left(\frac{v_2}{v_1}\right)} \frac{z_2}{z_1}$$

(Equation3)

$$Vertical\ Wind\ Shear\ =\ \sqrt{(u850mb - u1000mb)^2 + (v850mb - v1000mb)^2}$$

V_1 = is v-wind velocity (in $m.s^{-1}$) at 1,000mb

V_2 = is v-wind velocity at 850mb

Z_1 = geopotential height reference heights of the wind fields 1,000mb

Z_2 = geopotential height reference heights of the wind fields 850mb

α = The wind shear is the exponent

(Xu *et al.*, 2014)

V_1 and V_2 were substituted by U_1 (u-wind at 1,000mb) and U_2 (u-wind at 850mb) when computing the u-wind shear component (Bratton & Womeldorf, 2011). Regarding the wind shear exponent α, the larger the magnitude of the exponent α, the greater the vertical gradient of the wind speed and the subsequent wind shear (Xu *et al.*, 2014). Lower values of α favour tropical cyclone genesis (Nolan & Rappin, 2008). The vertical wind shear commonly used in the majority of studies examining shear at the point of genesis uses the least squares fitting method, which is reported to have the highest accuracy in its vertical shear output (Xu *et al.*, 2014).

The mean environmental horizontal wind speed was derived from the u-wind and v-wind data by the use of the following equation which denotes the Pythagorean theorem:

$$ws = \sqrt{(V^2 + U^2)}$$

Where *ws* is environmental wind speed (m.s^{-1}), *V* is the v-wind component and *U* is the u-wind component. This method of calculating the mean horizontal wind speed was adapted from (Quirino & Gopalakrishnan, 2016).

4.3. Methodology

4.3.1 Data Processing

Exploratory data analysis was performed on the completed database (Diamond *et al.*, 2012). Data verification was performed on each climate variable to ensure that the data were accurately extracted by the netcdf software. This involved choosing a random sample (n=50; 10%) of storms and cross referencing the extracted values of each climate variable to the manually extracted values (using the same location and date). The manual data verification was performed using the NOAA ESRL online analysis tool available from https://www.esrl.noaa.gov/psd/cgi-bin/data/getpage.pl. Once the data were verified the outliers for each metric of tropical cyclone activity (location, wind speed and pressure during the stages of genesis and lifetime maximum intensity) and the climate variables at the point of genesis were individually assessed and verified to ensure they did not result from errors in data extraction. Tropical cyclones with no pressure data or location data (resulting from no data found in the IBTrACS) were removed. Climate variables, specifically sea level pressure, v-wind and u-wind, and air temperature required conversion to simplified units. Sea level pressure was converted from pascals to millibars, the v-wind and u-wind components were computed into a single wind shear component α and vertical wind shear (Section 4.3.1). Air temperature was converted from kelvin to degrees Celsius.

4.3.2 Initial Data Analysis

The analysis was performed separately on storms from each of the four regions:

1) South Indian Ocean,

2) West Australian region,

3) East Australian region and

4) the South Pacific Ocean.

Analysis was also carried out at a hemispheric scale, which included all the tropical cyclones from the four basins (Schreck *et al*., 2014). This pattern of analysis was adhered to throughout the data analysis, including the analysis of the climate variables recorded during the storm genesis and lifetime maximum intensity phases. Firstly, the annual average (1980-2016) was computed for each metric of tropical cyclone activity and climate variable at the point of genesis, for each basin and the hemisphere. Any calculation related to the hemisphere included all the Southern Hemisphere tropical cyclone occurrences regardless of their basin. The initial data analysis consisted of descriptive statistics and five number summaries to explore and determine the spread, variability and mean conditions related to tropical cyclone activity and the climate data (Mavume *et al*., 2009; Huangfu *et al*., 2018). Therefore, the mean, max, min, standard deviation and the first standard deviation i.e. the range of values within 1 standard deviation of the mean, were calculated for latitude, longitude, wind speed and central pressure at the point of tropical cyclone genesis and lifetime maximum intensity (Huangfu *et al*., 2018). Additionally, the duration for the entire tropical cyclone lifetime and time spent at the highest intensity was computed in this manner. The storm frequency and category (Category 1-5) were also summarised into tables displaying the counts per year and percentage per category. The mean, minimum, maximum and standard deviations were also calculated for all the tropical cyclone metrics and climate variables in their raw data form (all the storms) before finding the average magnitudes or values per year.

4.3.3 Data Analysis

4.3.3.1 Mean Conditions

The mean conditions at the point of genesis were established using the descriptive statistics analysis outlined in Section 4.2.2. By establishing mean conditions of each basin, a climatology based on the 1980-2016 data is possible, as it creates a baseline of the tropical cyclone activity and the climate variables at the time of tropical cyclone formation (Zhan & Wang, 2017). Mean metrics of storm activity and climate variable statistics at the point of genesis and lifetime maximum intensity, along with the min and max values were used to present the average, and outlier conditions inherent to each basin and the hemisphere. This was aided by creating genesis and intensity hotspot maps to indicate where the most storms form and reach their maximum intensity respectively. The kernel density method in ArcMap GIS software (using the spatial analyst tool) as applied by Haikun *et al*. (2009) and Zhong *et al*. (2018), was used with a search area of 10 decimal degrees to calculate the density regions of tropical cyclone genesis and intensification. The search radius was determined using the following equation:

$$Search\ Radius = 0.9 * min\left((SD)\sqrt{\frac{1}{ln(2)}} \times\ D_m \right) \times n^{-2}$$

(Silverman, 2018; Haikun *et al*., 2009)

Where *SD* is standard distance (calculated with the standard distance tool), D_m is median distance (derived from mean distance between centers for all points), n is the number of storms, while min basically denotes that the smallest value between points (i.e. locations tropical cyclones underwent genesis and intensification) will be used.

The mean time period and season of formation was examined by separating the storms by yearly and monthly occurrence, for all storms of the Southern Hemisphere and by basin. This allowed for a full hemispheric and basin-scale seasonality of tropical cyclone formation and occurrence to be defined. Examining the mean conditions of the climate variables, allowed for the central tendency, maximum and minimum of each variable to be defined, and also provided the variability within each climate variable at the point of genesis. The standard deviation and the variability of each variable (calculated using 1 standard deviation from the mean), along with five number summary plots were used to display overall variability and distribution in the tropical cyclone activity and climate variables at the time of genesis, between the Southern Hemisphere basins. Relating to lifetime maximum intensity, an examination of the time taken for a tropical cyclone to attain its maximum intensity was done, as adapted from Emanuel (2000) and suggested in Walsh *et al*. (2015). This has been an important question in tropical cyclone climatology, usually hard to determine as a result of low-resolution spatial location and wind speed data (Walsh *et al*., 2015). In determining the time taken to attain peak intensity, an estimation of how many storms can reach peak intensity before making landfall will provide a possible explanation into the intensification trends and dynamics of current tropical cyclones (Walsh *et al*., 2015).

4.3.3.2 Using Peak Occurrence and Percentiles to Establish Climatology

The use of histograms were applied to determine the nature of the climate variables also labelled climate drivers of tropical cyclone genesis (sea surface temperature, relative humidity, air temperature, omega, v-wind shear, u-wind shear, sea level pressure and solar flux) at both 1,000mb and 850mb (Elsner *et al*., 2008; Nolan & McGauley, 2012). Using histograms allowed for the distribution of the climate data per storm to be allocated into a percentile bin. The bins that had the majority of storms occurring at that interval were then used as the peak or optimal interval. Examining the peak/optimal bin or interval for each climate variable at which the most tropical cyclone occurred, allowed for the establishment of a current climatology denoting Southern Hemisphere tropical cyclone formation conditions. Adapting the histogram method used in Elsner *et al*. (2008) and Nolan & McGauley (2012), in some cases a maximum of 2-3 of the bins with the highest tropical cyclone occurrence were used, provided, the intervals were numerically closer to each other and allowed for an overall higher percentage of storms at those magnitudes of the climate variables. Therefore, intervals with storm counts of approximately 80 and above were used to output a range for each variable. Providing an interval for more than one peak column also allowed for a more accurate representation of the climate drivers at the point of genesis, as this method captured the majority of storms falling within 1 standard deviation of the mean, and prevented any loss of data which may have been a product of natural variability (Elsner *et al*., 2008; Camargo *et al*., 2010). This was also required, since some interval bins were so small, they were duplicated after normalization. The five number summaries or boxplots of each climate variable were used to compare the distribution and variability between the climate drivers of each basin compared to the overall Southern Hemisphere distribution (Li *et al*., 2016; Patricola & Wehner, 2018).

4.3.3.3 Factor Analysis

To determine the contribution of each climate variable towards tropical cyclone genesis, factor analysis was performed. The factor analysis (as performed by Frank & Young, 2007) allowed for the explanation of the variability related to the climate variables at the point of genesis. The climate variables were selected and a varimax rotation was applied on the first two factors in order to remove intermediate weightings, and instead attain the strongest and weakest coefficient weightings (Gutzler *et al*., 2013). These weightings were derived for two scenarios (i.e. two factor analyses were run). Namely, 1) Factor analysis for all climate drivers at the point of genesis related to the tropical cyclones that occurred over 1980-2016 in the Southern Hemisphere, and 2) Factor analysis was applied only to the climate data from which the optimal peak intervals for each climate variable were derived; the data points from the intervals of sea surface temperature, relative humidity, wind shear etc. at which the most storms underwent successful genesis. The optimal magnitudes for each climate variable (peak intervals/percentiles) observed during genesis and the factor analysis weightings were combined and used to construct genesis flow charts to display the majority conditions at which tropical cyclone genesis took place and the average minimum conditions at which storms could undergo genesis.

4.3.3.4 Trend Analysis

The trend analysis was performed to assess change over time in the tropical cyclone activity and climate drivers (Li *et al*., 2013; Vecchi *et al*., 2013; Bhatia *et al*., 2019) Firstly, scatter plots and line/bar graphs were created with regression best fit lines (Mavume *et al*., 2009; Kuleshov *et al*., 2010). Then regression analysis and an analysis of variance (ANOVA) was run for the time series data relating to each climate variable at the point of genesis and for tropical cyclone metrics, to assess the statistical relationship of change over time for each climate variable and metric of tropical cyclone activity (Foltz *et al*., 2018). The trend analysis was required to demonstrate the statistical changes over time (Li *et al*., 2013; Foltz *et al*., 2018). Additionally, the rate of change was computed using the gradient of the regression line, while decades within the study period (1980-2016) were compared to each other to assess the percentage increase or decrease relative to each decade for each climate variable and metric of tropical cyclone activity (Elsner *et al*., 2008; Kuleshov *et al*., 2010).

4.3.3.5 Multivariate Regression Analysis

Multivariate multiple regression analysis was chosen as the preferred regression method to determine the collective influence that the chosen climate variables had on different metrics of tropical cyclone activity (Ziegel, 2004; Menkes *et al*., 2012; Fitchett & Grab, 2014; Clem *et al*., 2016; Young & Wessnitzer, 2016). Specifically, the latitude, longitude, duration (tropical cyclone and peak intensity), wind speed and pressure at peak intensity (Astier *et al*., 2015; Diamond *et al*., 2015a, b; Wing *et al*., 2015). The tropical cyclone activity and the climate drivers from the point of genesis were also regressed against the following modes of variability ENSO, IOD, SAM, MJO, PDO and volcanic activity (Girishkumar *et al*., 2015; Song *et al*., 2018; Vishnu *et al*., 2018). Since the climate variables are by nature inter-related and have overlapping impacts on more than one metric of tropical cyclone activity, it is best to model them simultaneously with multivariate regression to prevent collinearity (Chang-seng & Jury, 2010; Jobson, 2012; Saha & Wasimi, 2013). The multivariate regression tests the dependent variables (metrics of tropical cyclone activity) against the collective influence of the independent variables which are the recorded climate drivers at the point of genesis and modes of variability in this case (Jobson, 2012; Zhao & Wang, 2018). The output was used to construct the multivariate multiple regression equations for each scenario. Another reason for using multivariate regression was to prevent redundancy and multicollinearity, which is inherent in the data, since climate variables used in this study are mechanistically related e.g. higher sea surface temperature and air temperature promote higher relative humidity (Jobson, 2012).

Firstly, a Multivariate Analysis of Variance (MANOVA) was run to examine which continuous variables, if any demonstrated a strong correlation to any of the tropical cyclone activity metrics (Ziegel, 2004; Jobson, 2012). MANOVA was used instead of ANOVA, due to its ability to test all the independent variables against multiple dependent variables simultaneously (Ziegel, 2004). Then this information was used to run a multivariate regression.

The form of the regression model in matrix form is:

$$\begin{pmatrix} y_{11} & \cdots & y_{1m} \\ y_{21} & \dots & y_{2m} \\ \vdots & \ddots & \vdots \\ y_n & \cdots & y_{nm} \end{pmatrix} = \begin{pmatrix} 1 & x_{11} & \cdots & x_{1p} \\ 1 & x_{21} & \dots & x_{2p} \\ \vdots & \vdots & \ddots & \vdots \\ 1 & x_{n1} & \cdots & x_{np} \end{pmatrix} \begin{pmatrix} b_{01} & \cdots & b_{0m} \\ b_{11} & \dots & b_{1m} \\ \vdots & \ddots & \vdots \\ b_{p1} & \cdots & b_{pm} \end{pmatrix} + \begin{pmatrix} e_{11} & \cdots & e_{1m} \\ e_{21} & \dots & e_{2m} \\ \vdots & \ddots & \vdots \\ e_{n1} & \cdots & e_{nm} \end{pmatrix}$$

(Ziegel, 2004; Jobson, 2012)

The model writes all values up to *nm* at the same time. The standard multiple regression equation form can be written as:

$$Y = b_0 + b_1x_1 + b_2x_2 + \cdots + b_px_p + \varepsilon_i \qquad \text{If } i \in \{1 \dots n\}$$

(Ziegel, 2004; Jobson, 2012)

Where, Y is the predicted value of the tropical cyclone metric of activity in question (frequency, latitude, longitude, duration, peak intensity). X_1 to X_n are the actual observed values of the climate variable (independent variable). B_0 is the constant and represents the y-intercept (i.e. this is the number of tropical cyclones occurring regardless of the size of the independent variables. While the b_1-b_n values are the coefficients (regression slope) provided from the multivariate regression tests for each independent variable. ε refers to the random error term. The results from the regression provide the co-efficient, the standard error and the constant. These are then input into the regression models matrix equation.

4.4 Conclusion

This study has adapted and applied methods from tropical cyclone studies, which examined aspects of tropical cyclone activity at a basin-wide and regional scale (Ash & Matyas, 2012; Diamond *et al*., 2012) and investigated variability related to tropical cyclone activity (Chang-seng & Jury, 2010; Fitchett & Grab, 2014; Diamond *et al*., 2015a, b; Young & Wessnitzer, 2016). Additional research methods were adapted from investigative frameworks used to determine how tropical cyclone trends changed over time and the nature and extent that climate and environmental variables influence tropical cyclone activity (Li *et al*., 2013; Foltz *et al*., 2018; Bhatia *et al*., 2019). Generally, modes of variability, including but not limited to ENSO are examined in relation to their effects on tropical cyclone activity (Saha & Wasimi, 2013; Wing *et al*., 2015; Clem *et al*., 2016; Vishnu *et al*., 2018; Zhao & Wang, 2018). While investigations based on tropical cyclone activity generally follow an approach that attempts to reconcile tropical cyclone activity with environmental variables in order to discern the drivers of the tropical cyclone behaviour (Kang & Elsner, 2016; Scoccimarro *et al*., 2017). In order to apply these methods within a hemispheric based framework, descriptive analysis was performed on the metrics of tropical cyclone activity and the climate variables associated with these metrics of activity in order to examine the overall, mean, minimum, maximum and ranges of tropical cyclone activity and the climate variables (Huangfu *et al*., 2018). Following this, the tropical cyclone activity and the climate variables at the point of genesis were examined across time to discern any change over time. By adopting the approaches usually applied at a basin or regional scale, this study examined tropical cyclone activity at a basin-wide scale (only focused on Southern Hemisphere basins), with an additional layer of analysis focused on the hemispheric scale (where all the relevant Southern Hemisphere storm and climate data were integrated), which provided an overall state of the hemispheric tropical cyclone activity and trends in the climate variables during genesis. However, these approaches have also been applied to existing hemispheric studies (cf. Kuleshov *et al*., 2009, 2010; Dowdy *et al*., 2012; Defforge & Merlis, 2017a; Yoshida *et al*., 2017). In order to integrate the climate variables and tropical cyclone activity metrics during the genesis and intensification phases, the use of factor analysis allowed the study to narrow down and associate the relevant climate variables that influence tropical cyclone genesis and intensification within the Southern Hemisphere (Frank & Young, 2007). Multivariate regression and correlation were performed to provide the statistical significance regarding the trends of change in tropical cyclone activity, the climate variables at the point of genesis and the modulation of multiple modes of variability, which allowed the study to place an emphasis on the aspects which have clear relationships to the changes in tropical cyclone activity (Jobson, 2012).

5. Results

5. Results: Mean Conditions, Time Trends and Variability

5.1 Mean Conditions of the Southern Hemisphere Tropical Cyclones

Describing the mean conditions and states of tropical cyclone activity is an important aspect when constructing a climatology for Southern Hemisphere tropical cyclones. This will also assist in comparing tropical cyclone activity in the Southern Hemisphere to the Northern Hemisphere. The ocean basins of the Southern Hemisphere examined here have been divided into four sub-regions; the South Indian Ocean (SIO), West and East Australian regions (WA and EA) and the South Pacific (SP). The mean conditions explored relate to the metrics of tropical cyclone activity, which includes; a) frequency of occurrence, b) season of occurrence, c-d) location of genesis (latitude and longitude), e) the time taken to attain lifetime maximum intensity, and f) the lifespan of the tropical cyclones. Each aspect of tropical cyclone activity will be approached in two manners. First, this section will evaluate and compare tropical cyclone activity between each Southern Hemisphere basin (SIO, WA, EA and SP), to explore the similarities or difference in mean tropical cyclone activity across these basins. The descriptive statistics: maximum and minimum values will then assist in assessing the extremes across each basin. Overall averages are examined to demonstrate the general nature of tropical cyclone activity in the Southern Hemisphere, while the variability from mean conditions is explored using standard deviations from the mean.

5.1.1 Total Number of Tropical Cyclones per Basin

The total count of tropical cyclones was attained for each year based on storm season from November to April, across the period 1980-2016 (Table 5.1). The frequency for individual Southern Hemisphere basins was also calculated over this period. The basin with the greatest frequency of storm formation is the SIO, which accounts for 45% (n=493) of the total Southern Hemisphere storm occurrences, which is expected as it is the largest basin. This represents 20-30% more storms per year compared to the other basins. The SP follows this, accounting for 21% (n=493) of the storms, while the EA and WA regions account for 19% and 15% (n=493) of the storms respectively. In addition to the large number of storm occurrences, the SIO has the greatest mean occurrence of storms, with a rate of 5.9 storms per season. This is similarly followed by the SP and the EA regions, with mean rates of 2.8 and 2.6 storms per season respectively. The WA region has the lowest storm occurrences with a mean rate of 1.9 storms per season. Compared to the other three regions, the SIO storm occurrence falls above the inter-basin average of 5.3 storms per season (Figure 5.1). Once the storm counts were normalised by the basin area (in km2), the SIO still indicates the highest percentage (29%) of storm occurrence. However, the EA basin has a larger percentage of storm counts (28%), followed by the WA basin (21%) after normalisation. The SP, however, indicates a lower percentage (21.5%) of storm counts compared to the WA and EA basins after normalization.

A similar trend of occurrence exists regarding the maximum number of storms observed for each basin within a season over the 1980-2016 period. A maximum of 12 storms were recorded in the SIO over 1997, followed by the SP and EA regions, with 9 (1983) and 6 (1996) storms respectively. A maximum of 4 storms per season which occurred in 5 separate years over 1980-2016 was recorded for the WA region (Table 5.1). Examining the minimum activity per year, the SIO was the only basin that did not experience a zero-storm count over any of the seasons during the study period. The lowest annual minimum storm count recorded for the SIO was 2 storms in 2011. For the Southern Hemisphere, the maximum number of storms recorded was 22 storms in 1997, while the minimum number of storms recorded was eight during 2009 and 2016. During these seasons, the SIO storms accounted for the higher than average frequency observed in the Southern Hemisphere.

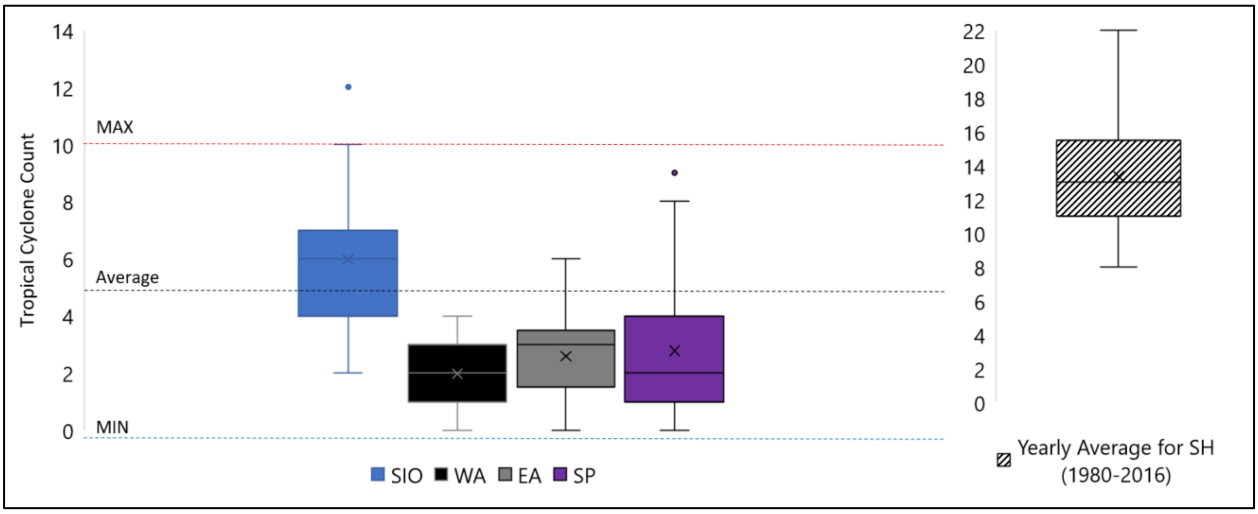

Figure 5.1 Distribution of annual average storm counts across individual Southern Hemisphere basins (SIO, WA, EA and SP) with maximum, minimum and average storm counts for the hemisphere indicated by the dotted lines and by the whiskers (maximums and minimums) for the individual basins. The upper and lower ends of the boxes indicate the upper and lower quartiles, while the center line in each box indicates the median. The x indicates the mean (left). Total annual average box-plot distribution of storms from all Southern Hemisphere basins (right).

The SD demonstrates the variability of storm occurrence around the mean, over the study period. For the Southern Hemisphere, the mean represented by $\bar{X}$ storm frequency per year was 13.3 storms (SD=3.3 storms). At the basin-scale, the SP has the greatest variability ($\bar{X}$=2.8, SD=2.16). A similar variability ($\bar{X}$=6, SD=2.11) was recorded for the SIO. A lower variability in storm frequency is observed for the EA region ($\bar{X}$=2.6, SD=1.36) and the WA region ($\bar{X}$=2, SD=1.21). For the Southern Hemisphere as a whole, ($\bar{X}$=13, SD=3.3) the first SD from the mean indicates a variability of approximately 10-16 storms per year. In terms of their contribution, the SIO and SP regions have storm occurrences which deviate the most from mean conditions in the Southern Hemisphere. The EA and WA regions, have similar standard deviations from their mean, however, the EA region has a comparatively larger mean storm occurrence and distribution than the WA region (Figure 5.1).

Table 5.1 Tropical Cyclone Frequency (1980-2016): Descriptive statistics of tropical cyclone occurrence within individual basins compared to total number per year for all Southern Hemisphere basins combined. Starred values indicate the basin with the highest value. The standard deviation along with one standard deviation from the mean indicates the variability around the mean per basin and for the Southern Hemisphere tropical cyclones.

Summary Statistics	SIO	WA	EA	SP	All Basins
SUM	221*	73	96	103	493
Mean	5.97*	1.97	2.59	2.78	13.32
SD	2.11	1.21	1.36	2.16*	3.30
+- 1 SD	4-8	1-3	2-4	1-5	10-16
MAX	12 (1997)	4 (multiple)	6 (1996)	9 (1983)	22 (1997)
MIN	2	0	0	0	8

5.1.2 Mean Tropical Cyclone Seasonality of the Southern Hemisphere

The tropical cyclone season of occurrence across the calendar year for the Southern Hemisphere (Table 5.2) indicates that storms occur seasonally, with the majority of events taking place over the Southern Hemisphere summer months (NDJFM). The main observation is that during the JFM season there is no instance when no storms occur, and this applies to all the Southern Hemisphere basins. Therefore, tropical cyclone activity is persistent throughout this JFM season (peak season), with the majority of storm occurrences taking place during these three months. The NDJ-FMA denotes the full Southern Hemisphere tropical cyclone season across 1980-2016. The zero-storm events (no storm activity) tend to occur during the colder months of the season, in November and April. No storm activity occurred during 16 of the seasons in November and 8 seasons in April. During December only five years are recorded where no storms occur. There is also a general trend of decreasing activity over time. The maximum storm activity in the Southern Hemisphere took place in the earlier years (1980-1997) of the study period, with decreased storm counts occurring closer to the present (2000-2016).

The longest seasons occurred in 1997 and 2003, where tropical cyclone activity initiated in October, with the last storm recorded in June of those seasons (Table 5.2). The shortest seasons occurred in 1988, 2011 and 2012 (excluding 2016 due to missing data: See Section 4.2.2) and were caused by zero storm events in April and November. The earliest that a tropical cyclone season initiated was in 1993, with a storm occurrence taking place in September. The latest a season initiated, occurred in 1988, when the first storm of the season occurred in January. Apart from the seasonal occurrence now established, several outlier storms occur in the colder months. A total of eight tropical cyclones have been recorded for May. Three storm events occurred within the Austral winter months of June, with one storm occurring in September. The JAS season (winter months of the Southern Hemisphere) displays no storm activity across the study period. Therefore, during these months there is very little potential for storm formation recorded over 1980-2016. This coincides with the norward shift in tropical precipitation bands and the ITCZ observed over 1980-2016 (Figure 3.3). For the Southern Hemisphere, the overall season which tropical cyclone occurrences are observed, extends from the earliest in September, to the latest in June for the majority of tropical cyclone events (excluding outliers in the winter months).

Table 5.2 Total storm frequency per month over study period (1980-2016). The darker hues indicate years and months with higher frequency, while the white blocks indicate 0-storm months and years. All Southern Hemisphere basins (SIO, WA, EA and SP) are represented by this yearly and monthly breakdown of storm counts.

Year	Jan	Feb	Mar	Apr	May	Jun	Jul	Aug	Sep	Oct	Nov	Dec
1980	5	4	3	0	0	0	0	0	0	0	0	0
1981	3	2	3	1	0	0	0	0	0	0	2	2
1982	2	1	2	3	0	0	0	0	0	1	1	0
1983	3	3	3	2	0	0	0	0	0	0	1	2
1984	2	4	2	1	0	0	0	0	0	1	1	2
1985	6	2	3	2	0	0	0	0	0	0	0	2
1986	2	3	3	3	1	0	0	0	0	0	0	1
1987	2	2	3	2	0	0	0	0	0	0	0	2
1988	3	4	1	1	0	0	0	0	0	0	0	0
1989	3	7	3	3	0	0	0	0	0	0	2	1
1990	2	3	6	0	0	0	0	0	0	0	1	1
1991	2	1	1	1	1	0	0	0	0	0	1	2
1992	1	6	1	3	0	0	0	0	0	0	1	3
1993	2	5	1	1	1	0	0	0	1	0	0	3
1994	5	3	6	3	0	0	0	0	0	0	0	2
1995	2	3	2	2	0	0	0	0	0	0	1	1
1996	4	4	2	3	0	0	0	0	0	0	1	2
1997	7	3	3	0	2	1	0	0	0	1	2	3
1998	4	5	4	1	0	0	0	0	0	0	3	2
1999	3	1	4	1	0	0	0	0	0	0	1	3
2000	5	3	4	2	0	0	0	0	0	0	0	2
2001	3	1	1	4	0	1	0	0	0	0	0	1
2002	2	4	2	1	1	0	0	0	0	0	0	2
2003	3	5	3	1	1	1	0	0	0	0	1	2
2004	2	3	4	0	1	0	0	0	0	0	1	3
2005	2	4	3	1	0	0	0	0	0	0	2	1
2006	1	3	4	1	0	0	0	0	0	0	1	0
2007	3	3	7	0	0	0	0	0	0	1	1	1
2008	4	3	3	0	0	0	0	0	0	0	2	1
2009	1	2	3	1	0	0	0	0	0	0	0	1
2010	3	4	4	1	0	0	0	0	0	0	1	3
2011	3	4	1	0	0	0	0	0	0	0	0	1
2012	4	2	2	0	0	0	0	0	0	0	0	2
2013	4	3	1	3	0	0	0	0	0	1	0	3
2014	2	1	3	2	0	0	0	0	0	0	0	4
2015	3	2	3	3	0	0	0	0	0	0	1	1
2016	2	2	1	3	0	0	0	0	0	0	0	0

The tropical cyclone activity within each season indicates slight differences between each basin. The tropical cyclone season for the SIO and SP regions both start during the months of October to November and end by the months of May to June, with the major season (defined by occurrence larger or equal to the basin means) occurring across the months of

DJFMA. The same overall tropical cyclone season, which spans the NDJFMA months is observed for the WA and EA regions, with the major season spanning DJFMA. Tropical cyclones do not occur in July or August in the Southern Hemisphere. For each basin, the maximum tropical cyclone activity occurs during the months of JFM, across the 1980-2016 period. Examining the highest number of storm occurrences per month and per basin, a total of 54 storms occurred in the SIO during January from 1980-2016, while a total of 28 storms occurred in the SP during February (Table 5.4). The largest total number of storms that occurred in the WA (17 storms) and the EA (28 storms) basins from 1980-2016, are recorded during March. These months of highest total storm activity can be taken as the periods when tropical cyclone activity peaked across the study period. While storms did occur during June and October in the SIO and SP, no storms occur during these months in the WA and EA regions. The SIO appears to be the only basin which has a large number of storm occurrences during the month of November (Table 5.3).

Table 5.3 Total storm counts summarising the activity of Southern Hemisphere tropical cyclones for each basin across the study period from 1980-2016.

	Jan	Feb	Mar	Apr	May	Jun	Jul	Aug	Sep	Oct	Nov	Dec
SIO	54	51	42	21	5	1	0	0	1	4	17	25
WA	13	14	17	13	1	0	0	0	0	0	3	12
EA	16	22	28	14	1	0	0	0	0	0	3	12
SP	27	28	18	8	1	2	0	0	0	1	5	13

The greatest variability from 1980-2016 is observed for the SIO storms ($\bar{X}$=18.4, SD=20.4), though this may be primarily due to the relatively larger frequency of storms that occur during the SIO peak storm season (Table 5.4). The lowest variability from the mean is observed for WA storms ($\bar{X}$=6.1, SD=7), while a similar magnitude of variability from the mean is calculated for the EA storms ($\bar{X}$=8, SD=10,) and SP storms ($\bar{X}$=8.5, SD=10.5,). During

February between 1980-2016, there was an average of 29 tropical cyclone occurrences across the four Southern Hemisphere basins.

Table 5.4 Summary of total storm activity from 1980-2016. Mean, standard deviation, maximum and minimum statistics for the four Southern Hemisphere basins computed for all months (Jan-Dec) and years (1980-2016).

Basin	SIO	WA	EA	SP
Mean	18.42	6.08	8.00	8.58
SD	20.47	6.96	10.03	10.52
MAX	54.00	17.00	28.00	28.00
MIN	0.00	0.00	0.00	0.00

5.1.3 Latitude of Genesis

The mean latitude at which tropical storms attained tropical cyclone intensity (point of genesis where wind speeds were greater than 119 $km.h^{-1}$) is consistently found over the latitudinal band of 15-16°S from the equator (Table 5.5, Figure 5.2). This mean latitudinal uniformity in tropical cyclone genesis location across the southern hemisphere is indicative of a preferential formation zone. Regarding the extremes of tropical cyclone genesis location, the SIO storms demonstrate a relatively equatorward maximum genesis latitude of 18.86°S, followed by the WA region with a maximum genesis latitude of 19.92°S. The EA and SP indicate the latitudinal values, 24.44°S and 23.33°S respectively. This places the EA and SP genesis locations closest to the southern poles (Table 5.5). The SIO and WA regions are, therefore, the basins which have genesis locations closest to the equator, but by a small margin.

Table 5.5 Latitude of genesis for Southern Hemisphere tropical cyclones.

Basin	SIO	WA	EA	SP
Mean	15.39	15.60	15.74	15.81
SD	1.75	2.70	2.34	2.88
+- 1SD	13.63-17.14	12.90-18.31	13.40-18.09	12.93-18.69

In terms of the non-averaged distribution of genesis location (Figure 5.2) the maximum latitude of storm genesis observed was 31.3°S (2013), while the minimum was 6.37°S (1988). Both these extremes were observed in the SIO, which is notable, as it has the comparatively smallest mean maximum value of latitude. Examining the first SD, all basins have an approximate mean latitude of genesis of 15°S and a SD=2, indicating a range of 13-18°S at which their storms underwent genesis.

5.1.3.1 Generalised Tropical Cyclone Formation Zones

The location at which individual storms undergo genesis and subsequent intensification (the point that they reach LMI) is spread across the Southern Hemisphere basins (Figure 3.1), however, density analysis using a kernel method indicates that there are specific hotspot regions in each basin, where storms have a greater tendency to form and reach LMI, compared to other regions. These regions can be considered as the optimal zones of tropical cyclone genesis and intensification.

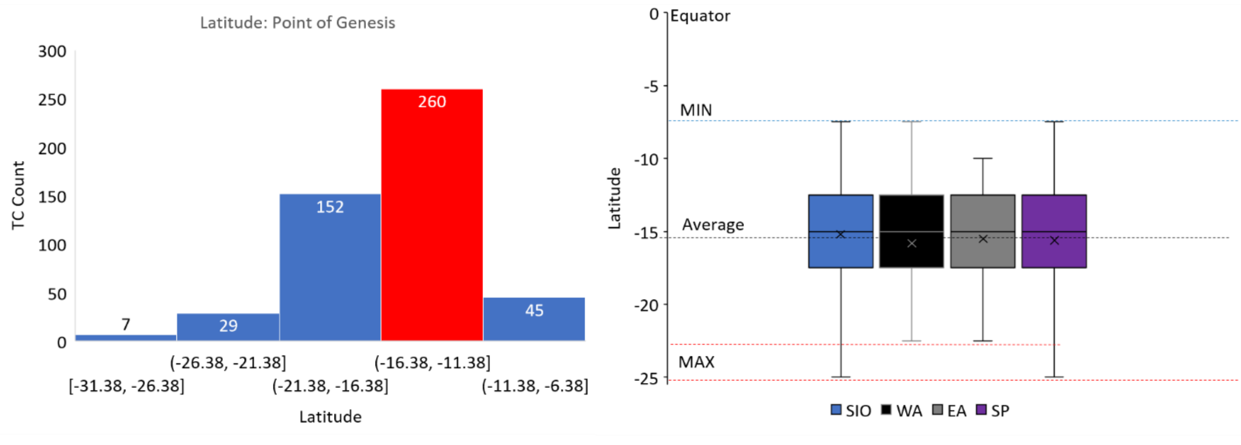

Figure 5.2 Distribution of latitudes tropical cyclone genesis occurred from 1980-2016, with red bar indicating the interval/bin where the largest number of storms occurred (left). Distribution and five number summaries of latitude indicate the minimum, maximum and mean latitudes at the point of genesis across Southern Hemisphere basins from 1980-2016. The basin means are indicated by the x and median by the lines inside the box. 50% of the latitudinal values fall between the lower and upper quartiles of each box (right).

The ‘highest’ kernel density (Figure 5.3) of 7.7-6.2 indicates the regions of high storm formation activity within a small area, while the lowest density score of 1.4-0 indicates the regions with little to no storm activity across an area. There are three main development regions regarding the approximate locations of storm genesis, with one in the SIO (Figure 5.3) located at 17°S 60°E, the second around the WA coastline zone at 17°S 120°E and in the SP at 17°S 190°E. There is a minor zone in the SIO at 15°S 85°E. In addition, there is a small zone in the SIO at 15°S 85°E. The main zones where LMI is attained a majority of the time, have centers at approximately 1°S of the above mentioned genesis zones (see Figure 5.3).

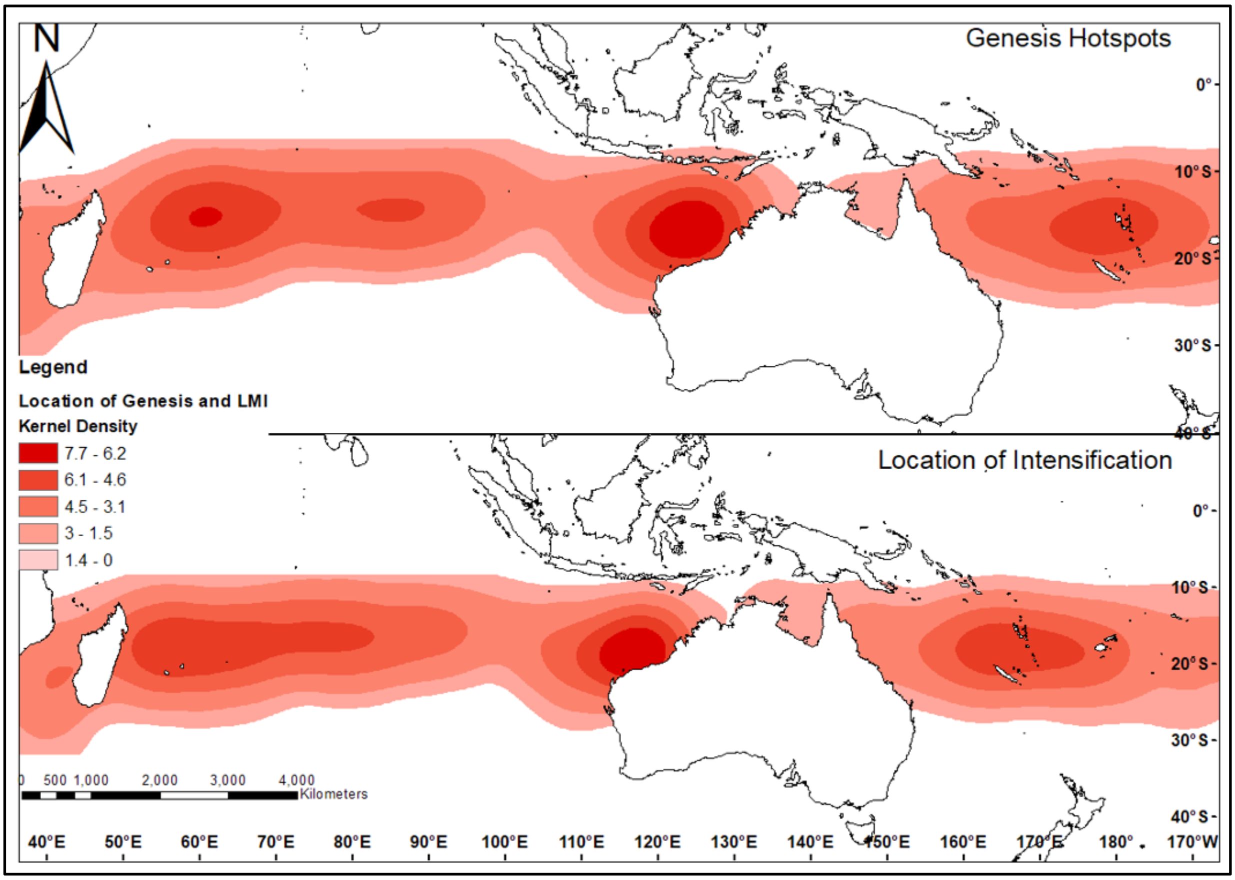

Figure 5.3 Density maps indicating regions where (1) Southern Hemisphere tropical cyclones experience the highest and lowest storm genesis and (2) attain their highest intensity i.e. their LMI zones. Density is represented by kernel density (area squared divided by the number of tropical cyclone genesis events from 1980-2016).

The latitudes of formation, where the majority of storms underwent genesis, range from 11-21°S of the equator (Figure 5.2). Based on the quartile-distribution used to provide a range of the longitudinal zones of storm genesis, the majority of storms were observed to form within the ranges of; 60-80°E in the SIO, 107-117°E for WA, 133-160°E for EA and 170-195°W for the SP basin. In addition, when referring back to the position of the ITCZ (Section 2.2.2, Figure 3.3), the regions the ITCZ shifts over during the tropical cyclone season coincide with the genesis and intensification hotspots to an extent. Pertaining to this, the diagonal convergence zones (Outlined in Section 3.2.3.1) over the SP basin also coincides with the genesis and intensification hotspots.

5.1.4 Tropical Cyclone Lifetime Maximum Intensity

LMI does not demonstrate a high degree of variation across each of the four basins or for the Southern Hemisphere as a whole (Table 5.6). The mean LMI for all Southern Hemisphere tropical cyclones (1980-2016) is recorded as 50.16 $m.s^{-1}$. A relatively large mean LMI of 50.51 $m.s^{-1}$ is recorded for SIO storms, while EA storms have the lowest mean LMI of 49.68 $m.s^{-1}$. The greatest LMI of 72.02 $m.s^{-1}$ is observed in the WA region, and is larger than the LMI observed in the other basins by 3-9 $m.s^{-1}$. This pattern is also observed in the distribution of LMI across the basins (Figure 5.4). The maximum LMI recorded for the SIO storms was 63 $m.s^{-1}$, however, this is the lowest LMI value, compared to the maximum values observed for the other basins. The mean LMI recorded for the Southern Hemisphere tropical cyclones over the study period, is approximately 50 $m.s^{-1}$. The general locations where LMI is attained (Figure 5.3), as mentioned, is similar to the genesis locations. As the distance from the equator increases, then the incidence of lower intensity tropical cyclones (category 1-3) appears to increase.

Table 5.6 Mean LMI in $m.s^{-1}$ reached for Southern Hemisphere tropical cyclones. Values computed from 1980-2016 LMI data for each basin (SIO, WA, EA and SP) and the Hemisphere (combined averages of each basin).

Basin	SIO	WA	EA	SP	Southern Hemisphere
Mean	50.51	49.43	49.22	49.68	50.16
SD	5.6	9.9	8.6	8.9	4.37
+- 1SD	45-56	39-59	41-58	41-59	46-55
MAX	63.02	72.02	64.31	68.81	58.73
MIN	33.44	33.44	33.44	33.44	38.12

The greatest variability of LMI (Table 5.6) is observed for the WA storms ($\bar{X}$=49, SD=10). This is a variation of 20 units between the upper and lower bounds of the first SD, compared to the smaller variation of 11 units calculated for SIO storms. The SIO storms have the lowest variability from the mean LMI ($\bar{X}$=50.5, SD=5.6). The EA ($\bar{X}$=49, SD=8.6) and SP ($\bar{X}$=49.6, SD=9) storms have a relatively high but similar variability from the mean (17 and 18 units of difference respectively). Overall, the mean storm LMI is similar between the basins, but the SD, min and max values vary, specifically for the SIO, which has the lowest SD, min and max values among the regions. This provides an indication that the LMI recorded for Southern Hemisphere tropical cyclones demonstrates greater variability within the WA, EA and SP basins, pointing to a larger spread of storm intensities from the mean for storms occurring in basins east of the SIO (Figure 5.4).

5.1.4.1 Time Required to Attain Lifetime Maximum Intensity

The time taken by storms to reach LMI was calculated by counting the days from the point of genesis to the time that the highest storm intensity was attained per storm (Table 5.7). There are five categories, based on the time a storm will take to intensify to the point of attaining its LMI. Zero days was used as the category which represents all storms which took under 24 hours to reach LMI. All other storms were allocated a category from one, two and three days to reach LMI, with the maximum category being 4-12 days to reach LMI. Since a small number of storms took an excess of four days to attain their maximum intensity, the grouping of 4-12 days was used to combine these events into a single category.

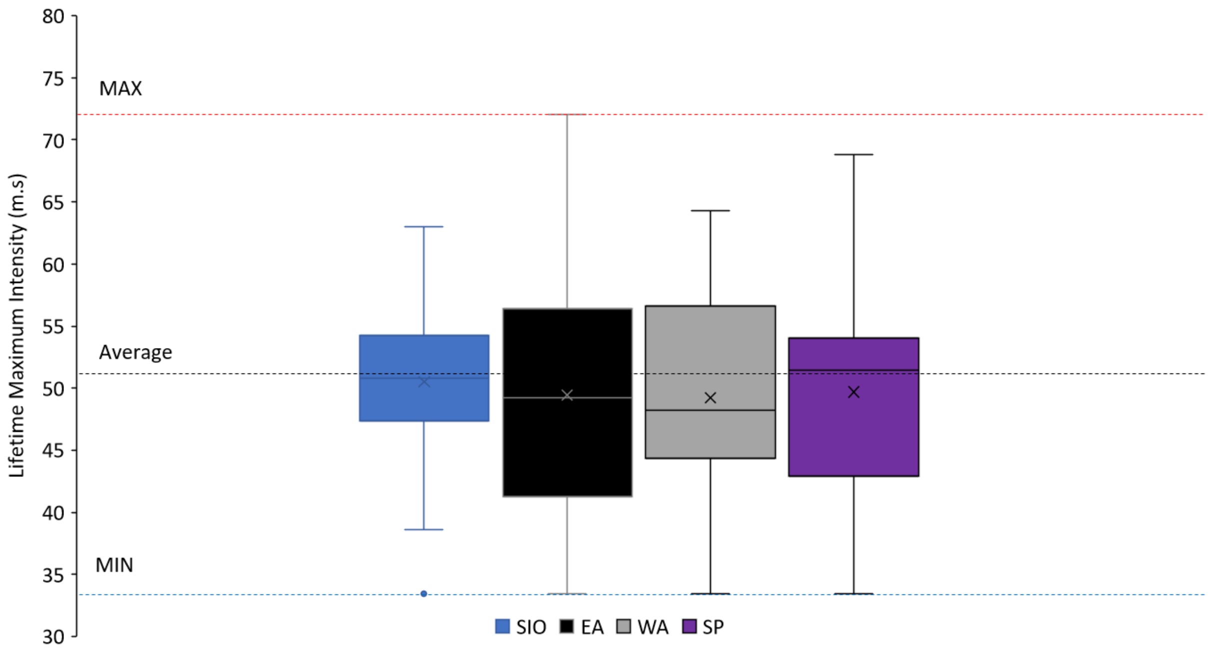

Figure 5.4 Tropical cyclone windspeed recorded at the point of LMI. Five number summary indicating the spread of the mean, max and min values of LMI for Southern Hemisphere storms in the four basins from 1980-2016. Red, blue and black dotted lines indicate the max, min and mean computed for all basins.

The magnitude of LMI increases with the time taken for a storm to attain its LMI, as the mean LMI for Southern Hemisphere tropical cyclones is the lowest for the zero-day category, compared to the three, and 4-12 day categories, which have comparatively larger LMIs. As the time taken for a storm to reach LMI increases, the duration that the tropical cyclones spend at their respective LMI also demonstrates an increase. For example, the storms that take the shortest time to reach LMI (0-2 days) are recorded to spend the least days at LMI with a range of 1.4-1.8 days. The storms which take 3-12 days to reach their

LMI, spend comparatively more time at that LMI, with a duration of 2-2.5 days. The maximum values indicate that storms taking less than 24-hours (zero days) and 4-12 days to attain LMI can persist at their LMI for an average of six days. The minimum values indicate that all categories of intensity (category 1-5) have storms which persist at their LMI for at least one day.

The majority of storm events are composed of storms which take the shortest time to achieve their LMI, while the storms which take a longer time to attain LMI account for a smaller number of storms. Regarding the maximum LMI values recorded, only the storms in the zero-day interval were observed with an LMI of less than 135 knots, while the rest of the intervals contain maximum LMI values of over 150 knots. This indicates that storms which took less than 24 hours to intensify, may be unable to intensify into an extreme category 5 storm, however, a borderline category 5 storm is possible. In addition to this observation, the highest wind speeds tend to be found for the storms which take the longest (3 and 4-12 days) to attain LMI.

Table 5.7 Lifetime maximum intensity metrics for tropical cyclones (Latitude, longitude, LMI, LMI wind speed, Days at LMI and Pressure at LMI) categorised by the time taken to attain the LMI of the tropical cyclone. 0-days, 1,2,3 and 4-12 day categories denote the time taken to achieve maximum intensity. 0 days indicates storms which took less than 24-hours to attain LMI.

0 Days to LMI	*Latitude of LMI*	*Longitude of LMI*	*LMI*	*Average LMI Wind speed*	*Days at LMI*	*Pressure LMI*
			Count = 128 Storms			
Mean	17.49	113.21	73.48	37.80	1.44	970
Minimum	9.35	34.67	65	33.44	1	924
Maximum	31.60	222.51	135	69.45	6	1000
Sum			9405	4838.35	184	119288
P-value (95.0%)	0.75	8.70	2.54	1.31	0.13	2
			Count = 197 Storms			
1 Day to LMI	*Location LMI*	*Longitude*	*LMI*	*LMI Wind speed*	*Days at LMI/Highest Category*	*Pressure LMI*
Mean	17.41	117.93	99.56	51.22	1.59	950
Minimum	8.54	37.80	70	36.01	1	890
Maximum	29.13	221.55	155	79.74	5	988
Sum			19613	10089.79	314	177649
P-value (95.0%)	0.47	6.90	2.68	1.38	0.11	3
			Count = 108 Storms			
2 Days to LMI	*Location LMI*	*Longitude*	*LMI*	*LMI Wind speed*	*Days at LMI/Highest Category*	*Pressure LMI*
Mean	17.23	112.78	110.63	56.91	1.84	939
Minimum	10.51	15.15	70	36.01	1	900
Maximum	29.42	207.13	150	77.17	4	980
Sum			11948	6146.32	199	99581
P-value (95.0%)	0.65	10.03	3.52	1.81	0.16	3
			Count = 30 Storms			
3 Days to LMI	*Location LMI*	*Longitude*	*LMI*	*LMI Wind speed*	*Days at LMI/Highest Category*	*Pressure LMI*
Mean	16.55	100.88	119.25	61.35	2.03	930
Minimum	11.03	38.44	85	43.73	1	895
Maximum	20.70	193.65	150	77.17	4	967
Sum			3578	1840.42	61	26957
P-value (95.0%)	0.88	17.74	6.44	3.31	0.37	8
			Count = 30 Storms			
4-12 Days to LMI	*Location LMI*	*Longitude*	*LMI*	*LMI Wind speed*	*Days at LMI/Highest Category*	*Pressure LMI*
Mean	17.01	94.35	118.33	60.88	2.50	930
Minimum	9.50	34.98	73	37.30	1	884
Maximum	22	194.75	155	79.74	6	976
Sum			3550	1826.28	75	27896
P-value (95.0%)	1.10	18.71	7.18	3.69	0.40	8

5.1.4.2 Location and Duration of Lifetime Maximum Intensity

The mean latitude at which the Southern Hemisphere tropical cyclones reach LMI is recorded at approximately 17-18°S of the equator. The trend in the longitudinal location at which LMI is attained, indicates a decrease in the location that LMI is attained as the time to reach LMI increases. This establishes that storms which take the longest to attain their LMI are found in the relatively eastern regions of the Southern Hemisphere basins, while storms that take the shortest time to reach LMI are found towards the western regions of the Southern Hemisphere basins. The location of LMI is additionally represented in a density and distribution map (Figure 5.5), which indicates a tendency for high intensity tropical cyclones (category 4-5) to form closest to the equator. However, there are zones where category 4-5 storms have occurred excessively poleward over latitudes of approximately 20°S. Apart from this, the category 5 storms do not extend poleward of 20°S. An increased area is affected by higher intensity storms during the 2000-2016 period, as demonstrated by the increased coverage of regions with LMI magnitudes above 100 knots. The incidence of activity further poleward is also demonstrated by the increased density of high intensity storms over the regions of 5-10°S during 2000-2016, compared to the 1980-1999 period.

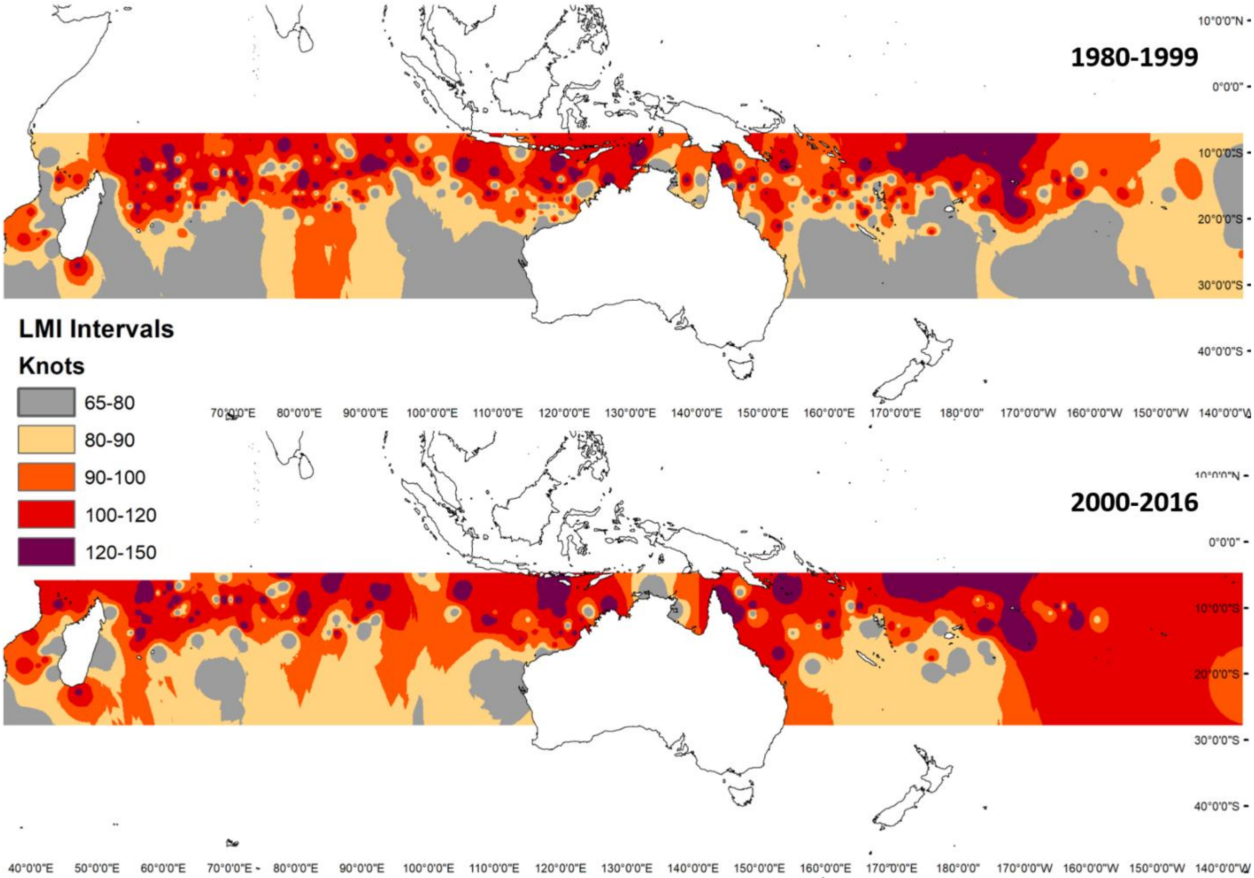

Figure 5.5 Interpolated spatial distribution and change over time between 1980-1999 and 2000-2016 for tropical cyclone maximum intensity.

The duration that storms spent at LMI across the basins (Table 5.8), indicates that the SIO and WA storms have a mean duration above that of the hemisphere. While the duration at LMI for the EA and SP storms falls below the mean duration of LMI (1.7 days) calculated for all the storms in the Southern Hemisphere. The distribution of the time which tropical cyclones spent at their LMI across the basins, indicates that the SIO tropical cyclone duration at LMI is distinctly different to the other three basins, with a high mean duration spent at LMI, while the EA region has a outlier whereby a tropical cyclone duration at LMI was recorded as four days, which is much higher than the maximum recorded duration at LMI of three days (also in the EA region).

Table 5.8 Duration (average number of days) spent at LMI for tropical cyclones across the four Southern Hemisphere basins (1980-2016).

Basin	SIO	WA	EA	SP	Southern Hemisphere
Mean	1.74	1.68	1.47	1.52	1.67
SD	0.35	0.72	0.41	0.43	0.22
MAX	2.44	4.00	2.00	2.50	2.15
MIN	1.00	1.00	1.00	1.00	1.27

The mean duration of LMI across the Southern Hemisphere indicates the amount of time that a tropical cyclone managed to sustain its maximum intensity (Figure 5.6). The mean duration which tropical cyclones spent at LMI per basin indicates little variation, with a range of 1.4-1.7 days. The longest mean duration spent at LMI was observed as 1.7 days, for SIO storms. The WA storms have the largest SD, and therefore a large variability (0.9-2.4 days) about the mean for duration at LMI. Similarly, the maximum duration, spent at LMI was 4 days and was observed for storms in the WA region. This is 50% greater than the duration storms spent at their LMI in the EA region. A similar maximum duration spent at LMI of around 2.5 days is recorded for SIO and SP storms.

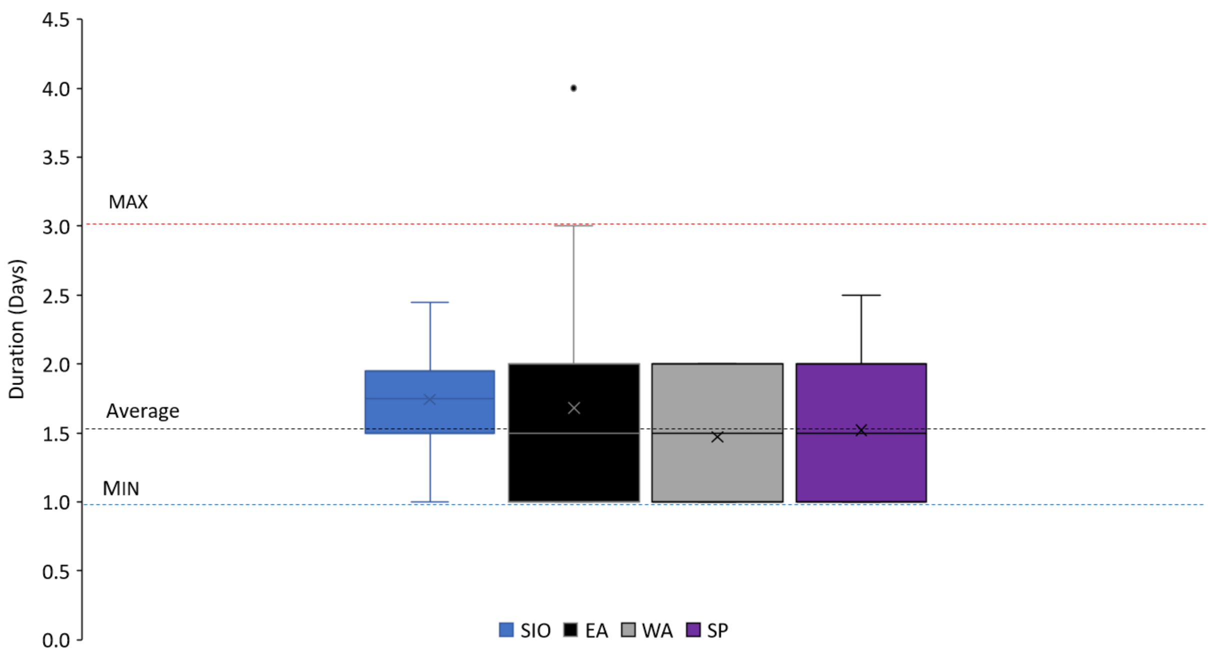

Figure 5.6 Average duration which storms spent at their LMI windspeed across the four Southern Hemisphere basins. Box plots indicating Minimum, maximum and mean lifetimes. Whiskers indicate extreme upper and lower values and the point indicates outlier values.

5.1.4.3 Lifetimes of Tropical Cyclones

The mean duration of the SIO and EA storms from genesis to dissipation (Table 5.9), is approximately 12 days, which is relatively long compared to the WA and SP storm lifetimes. The lowest mean duration of 9 days is observed for the WA storms, with a mean duration of 10 days observed for the SP storms. The largest variability in storm lifetime is observed within the EA ($\bar{X}$=12, SD=3.64). The lowest variability from the mean regarding storm lifetime is observed for the SIO storms ($\bar{X}$=12.5, SD= 1.65). The minimum duration observed for the SIO storms was 9.6 days, which is still longer than the minimum storm lifetime of 5 days observed within the WA, EA and SP basins. The maximum duration recorded for the WA and EA storms was 20 and 22 days respectively. The SIO and EA storms have the top

10% of values for storm duration, which is reflected in the basin means (Table 5.9). The WA and SP regions contain the bottom 10% of values for duration at LMI, which is also reflected in their basin means.

Table 5.9 Descriptive statistics: Duration (days) of Southern Hemisphere tropical cyclones from the date of genesis to dissipation.

Basin	SIO	WA	EA	SP
Mean	12.49	8.73	12.04	10.02
Std.	1.65	2.77	3.64	2.38
+- 1SD	10.84-14.13	5.96-11.49	8.40-15.68	7.64-12.41
MAX	16.33	20.00	22.00	14.00
MIN	9.67	5.00	5.00	5.00

In terms of the percentage distribution of tropical cyclone intensity (

Figure 5.7), the SIO accounts for the majority of tropical cyclone counts at each category of intensity, which is an expected result, as the largest number of tropical cyclone occurrences are recorded within this basin. However, once normalised, only the majority of category 4 storms are recorded to occur in the SIO. The category 5 storms occur mostly in the SP basin, which accounts for almost 50% more category 5 storms compared to the other three basins. All the basins indicate a similar distribution of occurrence regarding category 2 storms, while an anomalously high percentage of category 1 storms are recorded for the EA basin. The majority of Southern Hemisphere tropical cyclones consist of category 1 storms, followed by category 3 and 4 storms. This infers that more storms have a tendency to exceed category 2 wind speeds and intensify into a category 3 or 4 tropical cyclone.

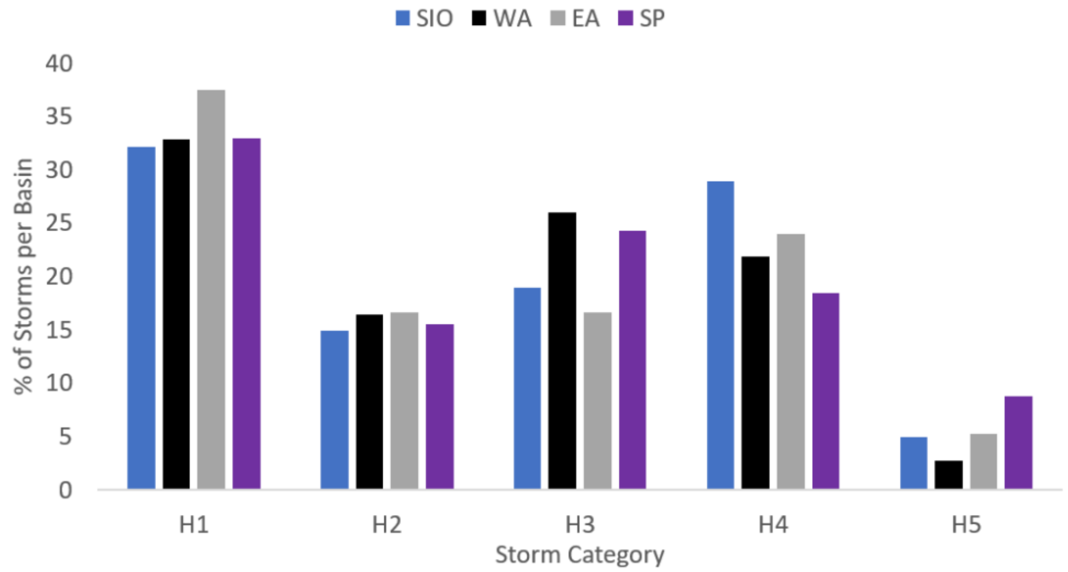

Figure 5.7 Distribution of storm category per basin based on the percentage per category calculated by finding the percentage of each category relative to the basin total.

5.2 Climate Drivers of Tropical Cyclone Activity

5.2.1 Nature of Variables at the Point of Genesis

The ocean-atmospheric climate variables that are examine here include a) sea surface temperature, b) air temperature, c) omega, d) relative humidity, e) vertical wind shear (including v and u wind components) and f) geopotential height. Apart from sea surface temperature and wind shear, the above variables will be discussed with reference to the 1,000mb and 850mb heights at which they were recorded. Sea surface temperature data provides the surface layer of the ocean heat content, while shear is calculated using 1,000mb and 850mb v and u wind values, to create the shear exponential power (α) and the vertical shear metric in m.s^{-1} (Section 4.3.1). These variables are assigned as the drivers of tropical cyclone genesis and this section will explore the nature of these climate drivers. The mean states, and the peak/optimal and minimum magnitudes of each climate variable are examined at the point of storm genesis. The optimal/peak intervals are the magnitudes of each climate variable at which the greatest number of storm occurrences take place. This is determined using the histograms of each climate variable, to extract the values of each driver which promotes the most storm occurrences in the Southern Hemisphere. Providing an interval for more than one peak column allowed for a more accurate and statistical representation of the climate drivers (up to 1 SD), as some interval bins (magnitude ranges) were so close together, that excluding them could have resulted in discarding magnitudes which fell within the range of natural variability (Section 4.3.3.2).The descriptive statistics, five number summaries and the notable standard deviations are also presented for each climate variable. The x-axis for the histograms indicates the intervals of magnitude for each climate driver.

5.2.1.1 Sea Surface Temperature at the Point of Genesis

At the point of genesis, the average sea surface temperature recorded for all Southern Hemisphere storms was 28.1°C (SD=0.7°C). The mean sea surface temperature recorded (Table 5.10) for SIO storms was 27.7°C. The remaining three basins had similar means of approximately 28.4°C recorded at the point of genesis. Regarding the variability of sea surface temperatures, the SIO storms have the lowest variability from the mean ($\bar{x}$=27.74°C, SD=0.52°C), while the WA storms ($\bar{x}$=28.4°C, SD=0.80°C) and EA storms ($\bar{x}$=28.5°C SD=0.79°C) exhibit similar variability with the first SD of 28°C-29°C. Similarly, the SP storms have a relatively high variability from the mean ($\bar{x}$=28.4, SD=0.73°C). Based on the standard deviation, the storms in the SIO have the lowest distribution of sea surface temperatures from the mean at the point of genesis, in comparison to the other three basins. Regarding the maximum sea surface temperatures recorded at the point of genesis, the highest sea surface temperatures observed for the SIO and the WA storms was 28.9°C and 29.2°C respectively. The maximum sea surface temperatures of 30.5°C was observed for the EA storms and 30°C for SP storms; indicating a pattern of higher sea surface temperatures present during storm genesis over the eastern basins. Similar minimum sea surface temperatures are observed over the SIO (26.38°C, 1987), EA (26.33°C, 2008) and SP (26.90°C, 1995) during the period of 1980-2016. The lowest sea surface temperature of 24.9°C (1988) was recorded at the point of genesis in the WA region. This minimum sea surface temperature falls below the 26.5°C threshold by a magnitude of 1.6°C. The notable finding is that at some point, the minimum sea surface temperatures observed during genesis occurred below the 26.5°C threshold, for all the Southern Hemisphere basins . Regarding the distribution of sea surface temperatures (Figure 5.8), 46 storms (9.33%, n=493) underwent genesis at a sea surface temperature interval below 26.5°C.

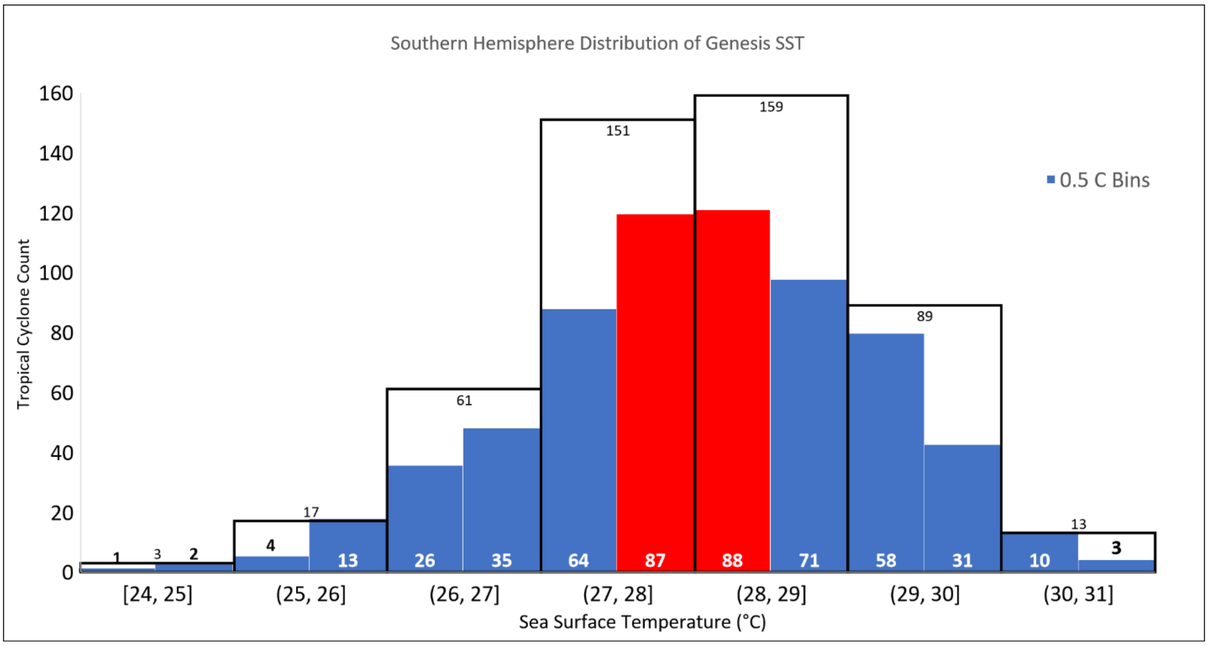

Figure 5.8 Sea surface temperature distribution for storms at genesis. The distribution of sea surface temperature at the point of genesis, for all the Southern Hemisphere tropical cyclones has been arranged by 0.5°C and 1°C bins. The peak bars (red) indicate the bin intervals of sea surface temperature at which the majority of storms reached genesis.

Examining the distribution of sea surface temperature, 175 storms (35.5%, n=493) underwent genesis at a sea surface temperature of 27.5-28.5°C. Since this temperature interval has the largest number of tropical cyclones occurring at these magnitudes, the corresponding sea surface temperatures are taken as the optimal magnitude for storm formation; i.e. Southern Hemisphere storms demonstrate a preference for formation at these optimal magnitudes. The first SD for sea surface temperature recorded for the SIO storms was lower compared to the other Southern Hemisphere basins (See Table 5.10; Figure 5.9). Incidentally, 305 storm genesis events (62%, n=493) are recorded to have taken place at a sea surface temperature between 27-29°C. This indicates that the optimal magnitude of sea surface temperature at the point of genesis, occurs within the first SD from the mean. The minimum sea surface temperatures at which storms genesis has occurred, ranges from 24-26°C, which incidentally falls below the 26.5°C threshold.

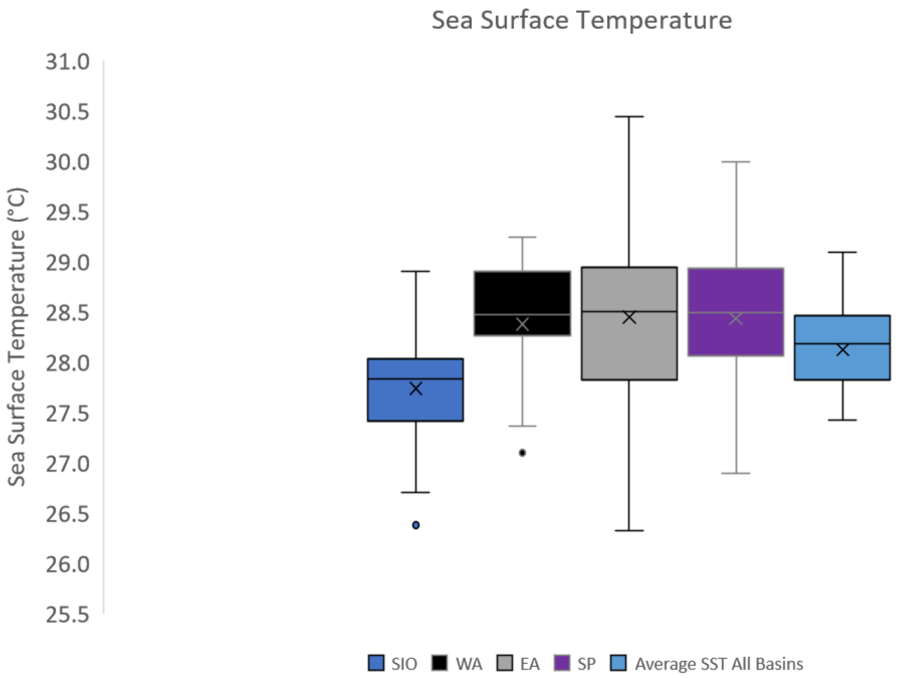

Figure 5.9 Sea surface temperature five number summary for tropical cyclones across the Southern Hemisphere at the point of genesis.

The distribution of the sea surface temperatures at the point of genesis for Southern Hemisphere storms (Figure 5.9), indicates that the SIO storms have a distinctly lower range and mean regarding sea surface temperatures. In comparison, the other Southern Hemisphere basins demonstrate a larger range and mean. This indicates that overall the sea surface temperature at the point of genesis in the SIO is essentially lower compared to the other basins. Regarding the other basins, the EA region displays the largest variation and range of sea surface temperatures with relatively high minimum and maximum values.

Table 5.10 Descriptive statistics: Sea surface temperature averages for Southern Hemisphere tropical cyclones at the point of genesis.

	SIO	WA	EA	SP
Mean	27.74	28.38	28.45	28.43
SD	0.52	0.80	0.79	0.73
+- 1SD	27-28	28-29	28-29	28-29
MAX	28.90	29.24	30.45	29.99
MIN	26.38	24.91	26.33	26.90

5.2.1.2 Air Temperature at the Point of Genesis

The mean air temperature at the point of genesis, for the Southern Hemisphere storms is 27.5°C at the 1,000mb level and 18.7°C at the 850mb level (Figure 5.10, Figure 5.11). At the basin-scale, the lowest mean air temperature of 27.3°C was observed for the SIO storms, while the highest mean air temperature of 27.8°C was recorded for the SP storms. At the 850mb level, a similar pattern is observed, with the lowest mean temperature of 18.5°C recorded for the SIO storms and the highest mean temperature of 18.9°C recorded in the SP (Table 5.11).

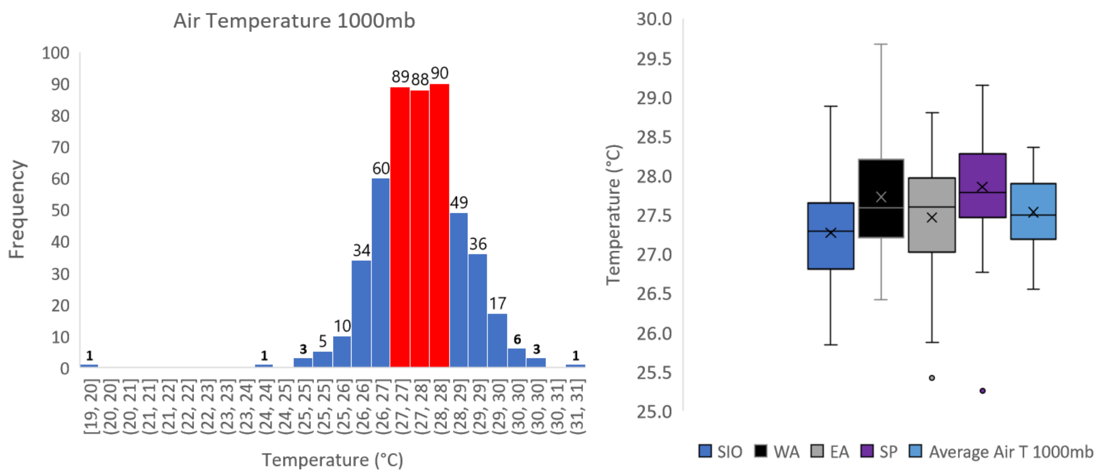

Figure 5.10 Air temperature at the 1,000mb level: distribution at the point of genesis (left) and the inter-basin comparison of air temperature for the Southern Hemisphere tropical cyclones (right).

The numerical distribution of air temperature at the 1,000mb level (Figure 5.10, Table 5.11), indicates that 267 storms (54%, n=493) occurred when the air temperature was within a magnitude of 27°C-28°C. At the 850mb level (Figure 5.11), 264 storms (53.5%, n=493) occurred when the air temperature was within a magnitude of 18-19°C. Therefore, the majority of Southern Hemisphere storms indicate a preference for air temperatures of 27°C-28°C (1000mb) and 18-19°C (850mb), making these the optimal magnitudes of air temperature at which storms underwent genesis. The histogram distribution for the 1,000mb and 850mb levels, indicates that a majority of storms form within a small range of air temperatures, but the minimum magnitudes at which some storms occur, such as 19°C (1,000mb) and 9°C (850mb) infers that the optimal intervals of formation are not exclusive and that storm formation is possible at lower and higher air temperatures. However, from both 1,000mb and 850mb levels it is observed that no storms have formed at air temperatures between 20-24°C and 10-14°C.

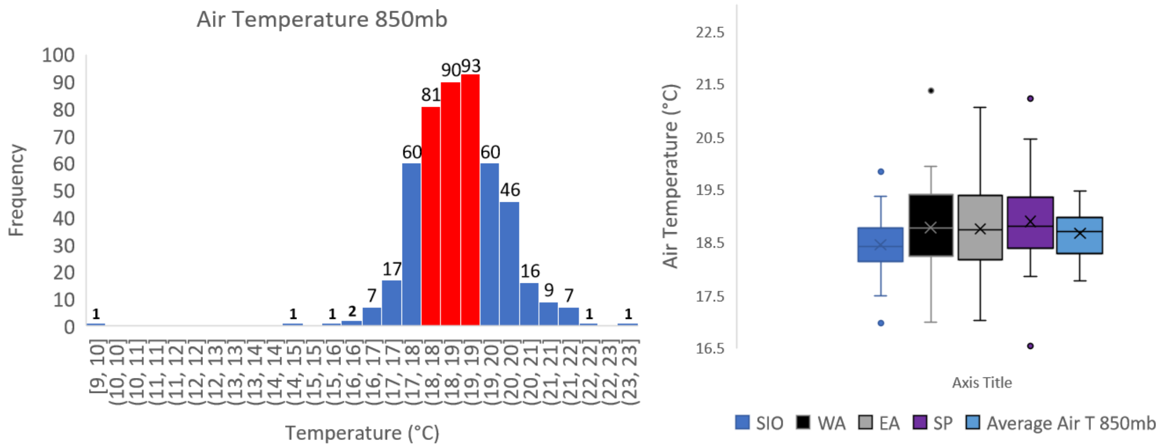

Figure 5.11 Air temperature at the 850mb level: distribution at the point of genesis (left) and the inter-basin comparison of air temperature for the Southern Hemisphere tropical cyclones (right).

The SIO storms demonstrate the lowest variability (Table 5.11) of air temperatures during the point of genesis, recorded at 1,000mb (SD=0.62°C, $\bar{X}$= 27.3°C) and 850mb (SD=0.54°C, $\bar{X}$=18.5°C) respectively. The greatest variability of air temperatures at the 1,000mb level is recorded for WA storms (SD=0.85°C, $\bar{X}$=27.9°C) and for EA storms (SD=0.87°C, $\bar{X}$=18.8°C) at the 850mb level. At the 1000mb level, the SIO and EA storms have comparatively low maximum air temperatures of approximately 28°C, while the WA and SP storms have maximum air temperatures within 29°C. At the 850mb level, a maximum temperature of 19.8°C is observed for the SIO storms, while the WA, EA and SP maximum air temperatures fall within the 21°C range.

Table 5.11 Air temperature descriptive statistics at 1,000mb and 850mb across Southern Hemisphere basins.

Air T 1,000mb					Air T 850mb			
Basin	SIO	WA	EA	SP	SIO	WA	EA	SP
Mean	27.27	27.73	27.46	27.85	18.45	18.78	18.76	18.90
SD	0.62	0.85	0.76	0.77	0.54	0.87	0.87	0.84
+- 1SD	27-28	27-29	27-28	27-29	18-19	18-20	18-20	18-20
MAX	28.88	29.67	28.80	29.15	19.83	21.37	21.05	21.22
MIN	25.84	26.42	25.42	25.26	16.97	16.99	17.02	16.54

5.2.1.3 Omega/Vertical Velocity at the Point of Genesis

Vertical motion (Figure 5.12, Figure 5.13) within the atmosphere from the surface to the tropopause, is described by omega. Using omega is necessary to measure the vertical motion/velocity present during and over the point of storm genesis (Section 4.2.4). For the Southern Hemisphere storms , the mean value of omega was -0.01pascal.s^{-1} at 1,000mb and -0.15pascal.s^{-1} at 850mb. At the 1,000mb level, the mean omega at the point of genesis is the same for all basins, with a magnitude of approximately -0.01pascal.s^{-1}. However, a comparatively weaker vertical velocity is observed for the WA storms, where a mean of -0.004pascal.s^{-1} was recorded. During the point of genesis, at 850mb, the SIO and WA regions displayed the lowest mean omega values of -0.14 and -0.13pascal.s^{-1} respectively. The highest mean value of -0.19pascal.s^{-1} was observed for genesis events in both the EA and SP regions. For all Southern Hemisphere genesis events, the omega values have a larger negative magnitude at an increased height (i.e. the 850mb level), compared to the surface, which indicates greater upward motion. However, the eastern (SIO and WA) and western (EA and SP) regions of the hemisphere, display a pattern of weaker and stronger mean values of omega respectively (Table 5.12); demonstrating the presence of larger buoyancy and horizontal convergence during the point of genesis over the western basins. The maximum omega is similar across the basins, however, the WA region has a positive value of 0.04pascal.s^{-1} at both levels. The minimum values mirror the east-west pattern of difference observed in air temperature, with the highest omega values recorded over the SIO and WA regions at the 1,000mb level (-0.04pascal.s^{-1} each) and 850mb level (-0.25 and -0.33pascal.s^{-1} respectively). The smallest omega values are observed for the EA and SP storms at 1,000mb (-0.06pascal.s^{-1} each) and 850mb (-0.53 and -0.58pascal.s^{-1} respectively).

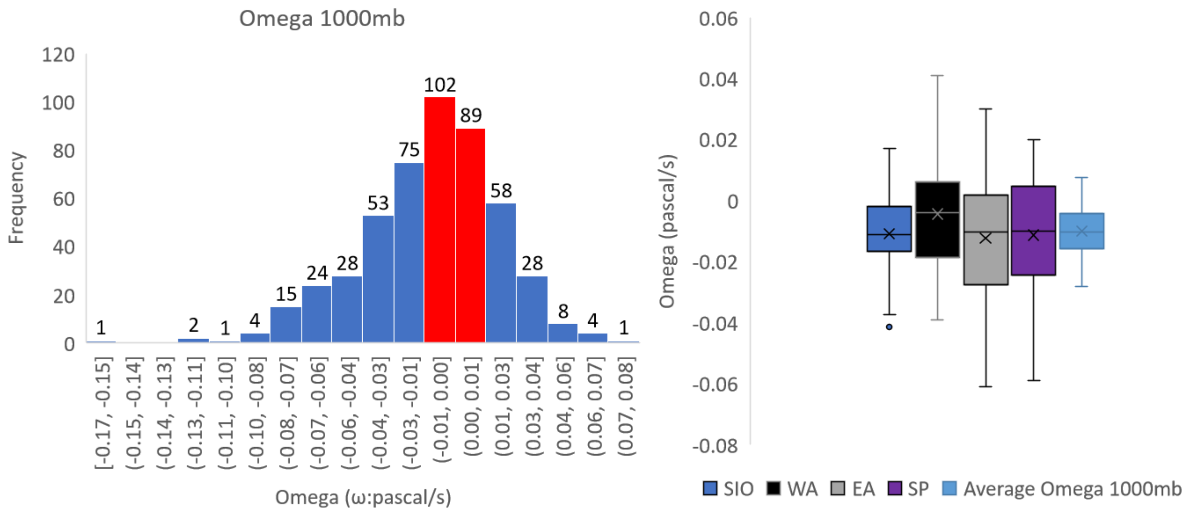

Figure 5.12 Omega/vertical velocity at the 1,000mb level: The distribution of omega at the point of genesis (left) and the inter-basin comparison of omega with five-number summary for the Southern Hemisphere tropical cyclones (right).

Based on the distribution of Omega at 1,000mb, 197 storms (38.7%, n=493) occur at a magnitude of -0.01-0.01pascal.s^{-1}. At the 850mb level, 183 storms (37%, n=493) occur at a magnitude of -0.18- -0.07pascal.s^{-1}. Therefore, the optimal magnitudes of omega at which the largest number of storms undergo genesis are -0.01-0.01pascal.s^{-1} (1000mb) and -0.18- -0.07pascal.s^{-1} (850mb). The difference between the magnitudes of omega at the 1000mb and 850mb levels, indicates that omega demonstrates a stronger magnitude at a greater height (850mb), compared to omega at the near surface (1,000mb) during storm genesis, across the Southern Hemisphere.

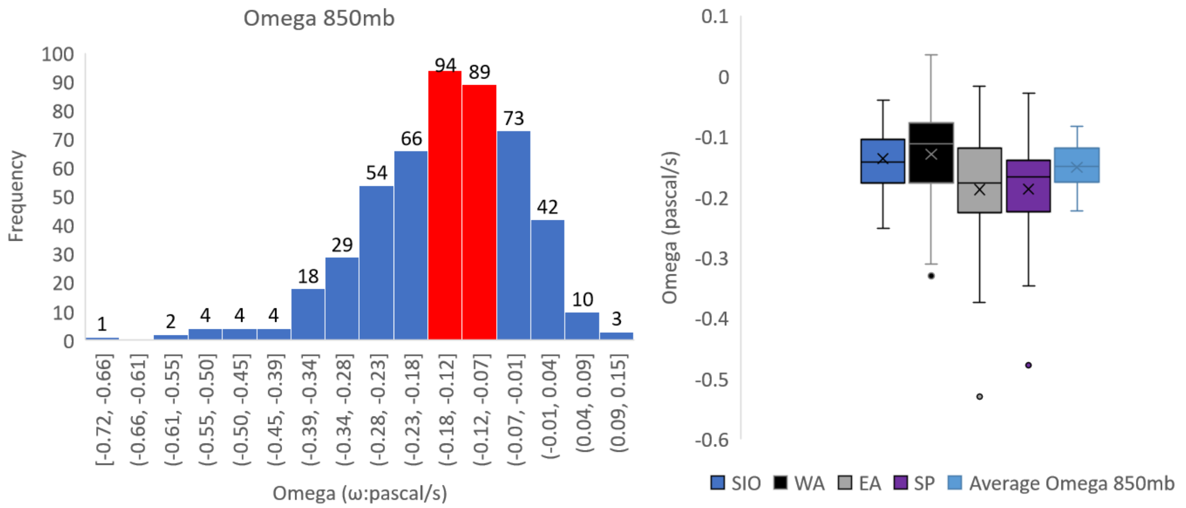

Figure 5.13 Omega/vertical velocity at the 850mb level: The distribution of omega at the point of genesis (left) and the inter-basin comparison of omega with five-number summary for the Southern Hemisphere tropical cyclones (right).

Based on the similar mean omega ($\bar{X}$=-0.01pascal.s^{-1}) observed during storm genesis across all basins (except the WA region) and the small SD, the variability from the mean omega is negligible at the 1000mb level (Table 5.12). At the 850mb level, the greatest variability from the mean omega was observed for the EA region ($\bar{X}$=-0.19, SD=0.10pascal.s^{-1}), while the lowest variability was observed in the SIO ($\bar{X}$=-0.14, SD=0.05). Negative magnitudes of omega are observed for the majority of the basin means (except WA at the 1000mb level), which infers that a negative magnitude of omega is commonly present during storm genesis events across the Southern Hemisphere. However, the distribution of omega (Figure 5.12, Figure 5.13) indicates that a large proportion of storms also occurred when omega was positive.

Table 5.12 Omega: Descriptive statistics at 1,000mb and 850mb across Southern Hemisphere basins.

Omega 1,000mb					Omega 850mb			
Basin	SIO	WA	EA	SP	SIO	WA	EA	SP
Mean	-0.01	0.00	-0.01	-0.01	-0.14	-0.13	-0.19	-0.19
SD	0.01	0.02	0.02	0.02	0.05	0.08	0.10	0.09
+- 1SD	-0.02- 0.002	-0.02- 0.01	-0.03- 0.01	-0.03- 0.008	-0.18-- 0.08	-0.21-- 0.04	-0.28-- 0.08	-0.27-- 0.09
MAX	0.02	0.04	0.03	0.02	-0.04	0.04	-0.02	-0.03
MIN	-0.04	-0.04	-0.06	-0.06	-0.25	-0.33	-0.53	-0.48

5.2.1.4 Relative Humidity at the Point of Genesis

High relative humidity is required during the point of genesis, as it allows deep moist convection and the formation of thunderstorm cloud bands (Section 2.2.1.1). For the Southern Hemisphere storms, the mean relative humidity observed was 81.9% at 1,000mb and 81.1% at 850mb. Individually, a mean relative humidity of approximately 81% was observed at the 1000mb level for the SIO, WA, and SP storms, however, the highest mean relative humidity of 84.6% was observed for the EA storms (Figure 5.14). Once again, the pattern of difference observed for air temperature and omega is visible for relative humidity between the east and western regions of the Southern Hemisphere. At the 850mb level, the mean relative humidity for the SIO storms (79.5%) and WA storms (80.6) are relatively high, however, they fall below the magnitudes observed for the EA and SP storms, where a mean relative humidity of 84.94% and 83.34% is observed respectively (Figure 5.15).

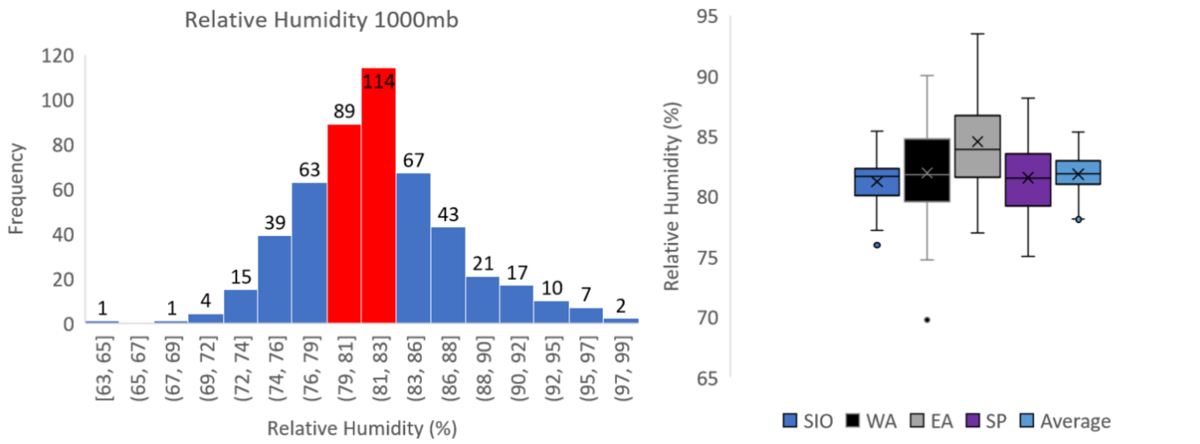

Figure 5.14 Relative Humidity at the 1,000mb level: distribution at the point of genesis (left) and inter-basin comparison of relative humidity with five-number summary for the Southern Hemisphere tropical cyclones (right).

With a mean relative humidity of 81% (SD=2.1%), the lowest variability at 1,000mb was observed for the SIO storms. At the 1,000mb level, the relative humidity demonstrates the greatest variability for the WA storms ($\bar{X}$=81.9%, SD=4.3%) and EA storms ($\bar{X}$=84.6%, SD=4.56%). For relative humidity recorded at the 850mb level, the lowest variability was observed for the SIO storms ($\bar{X}$=79.5%, SD=3.9%) and WA storms ($\bar{X}$=80.6%, SD= 6.3%). While the highest variability from the mean relative humidity at the 850mb level (Table 5.13) was recorded for the EA storms ($\bar{X}$=84.9, SD= 6.9%) and SP storms ($\bar{X}$=83.3%, SD=6.7%). The larger deviations from the mean indicates that a greater range of relative humidity values are present at the point of genesis in the western region of the Southern Hemisphere, compared to the eastern region. This pattern is visible in the distribution of the 850mb box-plot (Figure 5.15), where a smaller mean and range of relative humidity values are observed for the SIO and WA storms, compared to the higher mean and range of relative humidity values observed for EA and SP storms (Figure 5.14, Figure 5.15).

The maximum relative humidity values at the point of genesis are above 85% across all basins at both the 1,000mb and 850mb levels. Notably the highest maximum relative humidity of 93.5% was observed for the EA storms, at the 1,000mb level and 99.8% at the 850mb level. The maximum magnitude of relative humidity observed for the SIO storms was 85.4% and 86.2% at the 1,000mb and 850mb levels respectively. The maximum relative humidity observed for the remaining basins was over 90% at both levels, except for the SP storms. The minimum relative humidity of 68.2% was recorded for the SP storms, at the 850mb level. While the minimum relative humidity observed for WA storms had a magnitude of 69.8% and 68.9% at the 1,000mb and 850mb levels respectively.

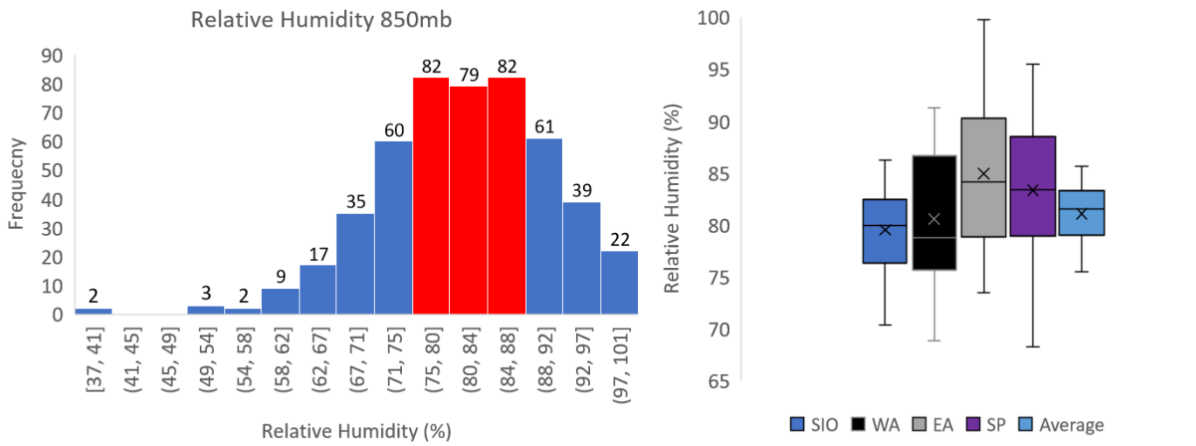

Figure 5.15 Relative Humidity at 850mb level: distribution at the point of genesis (left) and inter-basin comparison of relative humidity with five-number summary for the Southern Hemisphere tropical cyclones (right).

The histogram distribution of relative humidity (Figure 5.14,Figure 5.15) indicates that the peak number of storms underwent genesis when the magnitudes of relative humidity at 1,000mb was 79-83%. In this case 203 storms (41%, n=493) formed at these optimal magnitudes. At the 850mb level, a relative humidity of 75-88% was observed as the optimal magnitude at which the largest number of storms underwent genesis. Specifically, 183 storms (37%, n=493) underwent genesis at this optimal magnitude. Storm genesis events for the Southern Hemisphere have not been observed to occur below a relative humidity of 63% at the 1,000mb level or below 37% at the 850mb level. This infers that high moisture levels at the surface are required for successful storm genesis. This is also demonstrated by the higher optimal magnitude of relative humidity observed at the 1000mb level.

Table 5.13 Relative Humidity descriptive statistics at 1,000mb and 850mb for tropical cyclones occurring in Southern Hemisphere basins.

Relative Humidity 1,000mb					Relative Humidity 850mb			
Basin	SIO	WA	EA	SP	SIO	WA	EA	SP
Mean	81.25	81.97	84.55	81.57	79.54	80.58	84.94	83.34
SD	2.09	4.31	4.56	3.22	3.93	6.30	6.88	6.75
+- 1SD	79-83	78-86	80-89	78-85	76-83	74-87	78-92	77-90
MAX	85.41	90.00	93.50	88.16	86.24	91.25	99.75	95.50
MIN	76.00	69.75	76.99	75.01	70.38	68.83	73.50	68.24

5.2.1.5 Wind Shear (v-wind, u-wind and Vertical Shear Components) at the Point of Genesis

The wind shear exponent (Section 4.1.3) varies with terrain. Over water it is approximately 0.1α. The larger the exponent (α), the larger the wind speed gradient or shear. Mean v-wind shear observed at the point of genesis for all the Southern Hemisphere storms was 0.02α, while the mean u-wind shear observed was 0.06α. The lowest mean v-wind shear of 0.01α was recorded for the SIO storms, with the highest mean v-wind shear of 0.05α recorded for the WA storms. At the point of genesis, the largest variability from the mean conditions of v-wind shear was observed for the EA storms ($\bar{x}$=0.04, SD=0.24α), while the smallest variability was recorded for the SP storms ($\bar{x}$=0.04, SD=0.17α). The average v-wind shear at the point of genesis does not vary between basins by a large magnitude, however, the SD and extreme magnitudes of v-wind shear (max and min) do (Table 5.14,Figure 5.16).

Table 5.14 Vwind shear (left) and Uwind shear (middle) and vertical shear (right) descriptive statistics across Southern Hemisphere basins

Vwind shear (α)					Uwind Shear (α)				Vertical Shear (m.s^{-1})			
Basin	SIO	WA	EA	SP	SIO	WA	EA	SP	SIO	WA	EA	SP
Mean	0.01	0.05	0.04	0.04	0.06	0.01	0.12	0.03	2.89	3.18	3.29	3.24
SD	0.19	0.22	0.24	0.17	0.14	0.37	0.27	0.25	0.64	1.10	1.19	1.37
+-	-0.18-	-0.17-	-0.20-	-0.12-	-0.08-	-0.36-	-0.15-	-0.22-	2.24-	2.09-	2.10-	1.87-
1SD	0.20	0.27	0.27	0.21	0.20	0.37	0.38	0.28	3.53	4.28	4.49	4.61
MAX	0.59	0.68	0.37	0.53	0.32	1.01	0.99	0.56	5.14	5.20	5.48	7.49
MIN	-0.36	-0.37	-1.02	-0.42	-0.39	-1.12	-0.33	-0.88	1.28	0.83	1.34	1.48

In this case, the minimum values do not represent the smallest wind shear, but the maximum shear in the opposite wind direction. The maximum or positive values of shear indicate a northward wind direction. The negative values therefore indicate a southward wind shear direction. The smallest negative v-wind shear of -0.37α and -0.36α was observed for the WA storms and the SIO storms respectively. The largest negative v-wind shear exponent of -1.02α was observed for the EA storms. The maximum positive v-wind shear of 0.68α was observed for the WA storms, followed by the SIO and SP storms, which demonstrated a maximum positive shear of 0.59α and 0.53α respectively.

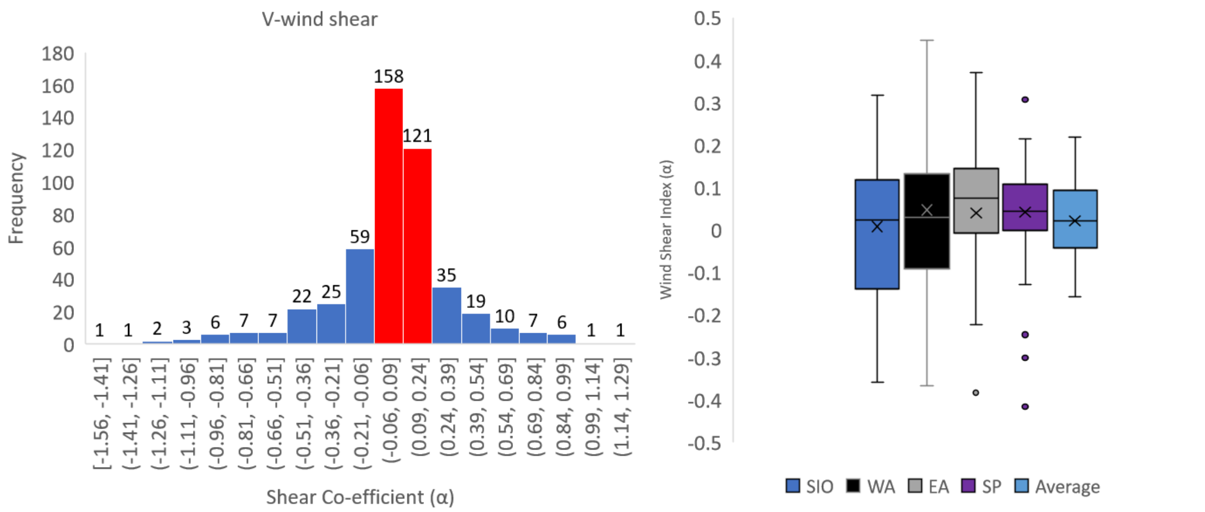

Figure 5.16 V-wind shear distribution at the point of genesis (left) and inter-basin comparison of v-wind shear with five-number summaries for the Southern Hemisphere tropical cyclones (right).

Regarding u-wind shear, the highest mean value of 0.12α was observed for the EA storms, while the lowest mean value of 0.01α was observed for the WA storms. However, the EA storms have multiple positive outlier values of u-wind shear, which could be skewing the distribution (Figure 5.17). The lowest variability from the mean u-wind shear was observed for the SIO storms ($\bar{x}$=0.06α, SD=0.14α), while the greatest variability from the mean was observed for the WA storms ($\bar{x}$=0.01α, SD of 0.37α). The maximum u-wind shear of 1.01α was observed for the WA storms and 0.99α for EA storms, while the comparatively lower maximum values of u-wind shear were observed for the SIO storms (0.32α) and SP storms (0.56α). Similar to v-wind shear, the positive and negative u-wind shear denote eastward and westward wind shear directionality respectively. The highest magnitudes for u-wind shear of -1.12α were observed for the WA storms and -0.88α for SP storms, while the lowest magnitudes of shear were observed for the SIO storms (-0.39α) and SP storms (-0.33α). The overall distribution of the data between the basins and hemisphere are similar (Figure 5.17), however, there were many outliers which skew the representation of the maximum and minimum u-wind shear values. The u-wind shear demonstrates a lower range and distribution in comparison to the v-wind shear, as indicated by the five number summaries (Figure 5.16, Figure 5.17).

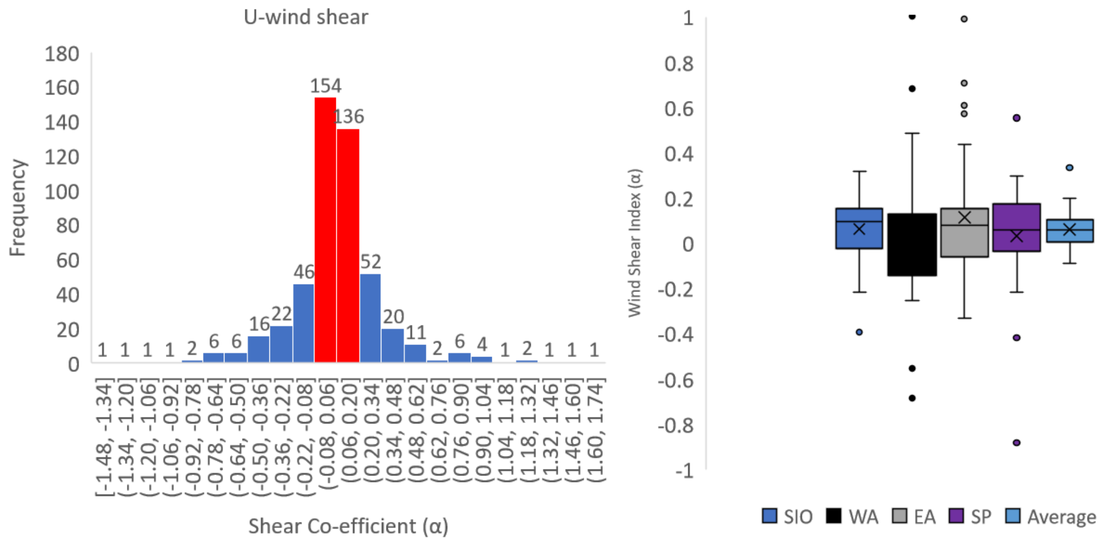

Figure 5.17 U-wind shear distribution at the point of genesis (left) and inter-basin comparison of u-wind shear with five number summaries for the Southern Hemisphere tropical cyclones (right).

The histogram distributions of v-wind and u-wind (Figure 5.16, Figure 5.17) shear indicates that the peak number of storms underwent genesis when the magnitude of v-wind shear was -0.06-0.24α, at which 306 storms (62%, n=493) occurred. When the magnitude of u-wind shear was -0.08-0.20α, 290 storms (58.8%, n=493) occurred. These are the optimal magnitudes at which the majority of storms underwent genesis in the Southern Hemisphere. Both the histogram distributions indicate similarities in terms of the frequency counts per interval. Regarding v-wind and u-wind shear, storms can occur at both positive and negative shear magnitudes, but with a minor skewing towards negative shear values for v-wind and positive shear values for u-wind. The optimal intervals (red) are responsible for a large proportion of storm genesis events for both v-wind and u-wind shear, compared to the other climate variables.

Vertical shear is described as the difference in windspeed with height (Figure 5.18). When the vertical shear at the point of genesis was 1-4 $m.s^{-1}$, 307 storms (62%, n=493) were observed to occur.

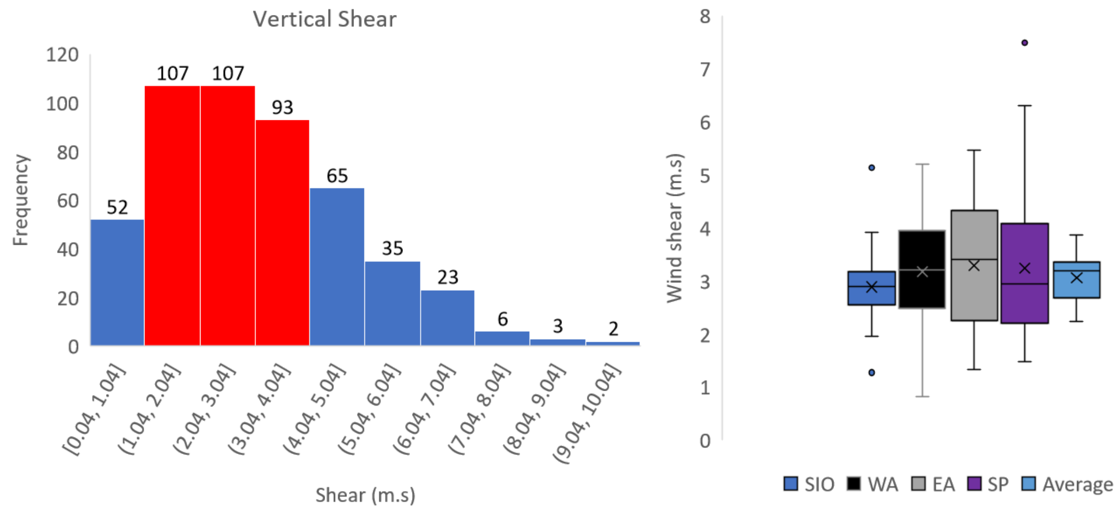

Figure 5.18 Vertical shear distribution at the point of genesis (left) and inter-basin comparison of vertical shear with five-number summaries for the Southern Hemisphere tropical cyclones (right).

The distribution indicates that as shear increases, the storm frequency decreases. The vertical shear recorded for Southern Hemisphere storms demonstrates a range of 2-4 m.s^{-1}. The basin distribution indicates that climatologically, vertical shear is higher for the EA region, but lower for the SIO and SP regions. The range of vertical shear observed for the SIO storms approximately matches the hemispheric range. Larger ranges of vertical shear were observed for the remaining basins, however, the magnitudes recorded still fell within the 1-4 m.s^{-1} shear interval (Figure 5.18). The overall mean vertical shear at which storms form is approximately 3 m.s^{-1} for the entire Southern Hemisphere. It is also observed that relatively few storms underwent genesis at very low magnitudes of vertical shear, as only a few storms formed when vertical shear was below 0-1 m.s^{-1}. The maximum vertical shear of 7.5 m.s^{-1} was observed for the SP storms, while the minimum vertical shear of 0.83 m.s^{-1} was observed for the WA storms. Based on the magnitudes of vertical shear, the SP region demonstrates a greater genesis potential, as the largest variability and maximum shear occurred within this basin. The SP storms, therefore, demonstrate a larger range of vertical shear magnitudes at which genesis can be initiated. The lowest variability from the mean vertical shear was observed for the SIO storms ($\bar{x}$=2.89 $m.s^{-1}$, SD=0.64), while the remaining basins demonstrate a greater variability from their respective means ($\bar{x} \approx 3.2$ $m.s^{-1}$ for all three basins, SD >1.1 $m.s^{-1}$).

5.2.1.6 Geopotential Height at the Point of Genesis

Geopotential height is used as a proxy for estimating the environmental stability and to estimate height of the pressure surfaces. High geopotential values infer the presence of warmer air and therefore, unstable atmospheric conditions (Section 4.2.4). The average geopotential height at the point of genesis within the Southern Hemisphere is 43m at the 1,000mb level and 1463m at the 850mb level. The mean values observed for the SIO storms at the 1,000mb level was 56m and 1475m at the 850mb level. The mean geopotential heights observed for the SP storms at the 1,000mb level was 32m and 1540m at the 850mb level, while the mean values observed for the EA storms was 38m at the 1,000mb level and 1450m at the 850mb level (Table 5.15). The lowest variability in geopotential height was observed for the SIO storms at the 1,000mb level ($\bar{x}$=56m, SD=12.9) and at the 850mb level ($\bar{x}$=1475m, SD=12.7m). The geopotential heights observed for the WA storms have the greatest variability at 1,000mb ($\bar{x}$=41m, SD=21m) and at 850mb ($\bar{x}$=1457m, SD=27m).

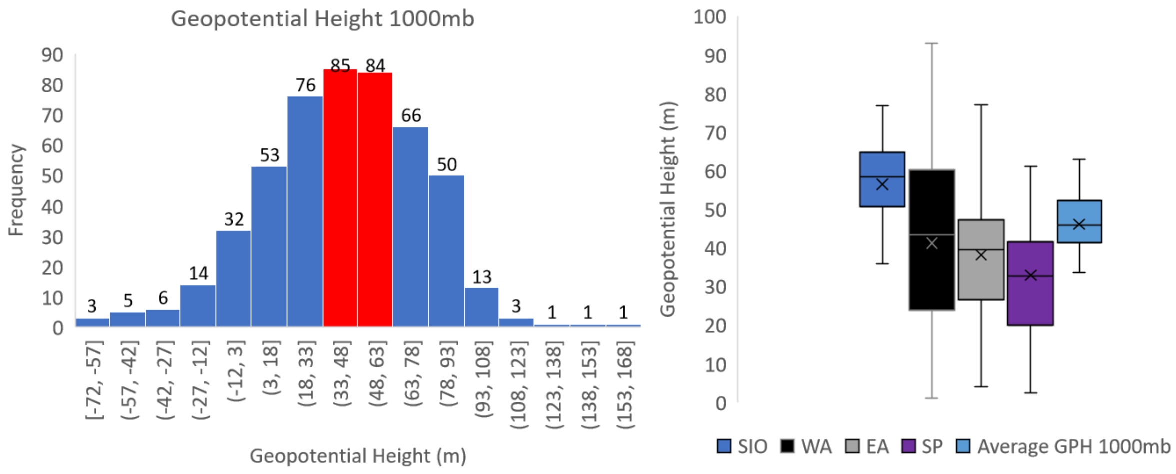

Figure 5.19 1,000mb Geopotential Height: distribution at the point of genesis (left) and inter-basin comparison of geopotential height with five-number summaries for the Southern Hemisphere tropical cyclones (right).

The largest geopotential heights observed at the point of genesis for the SP storms was 97m at the 1,000mb level and 1506m at the 850mb level. Although, a slightly larger maximum geopotential height of 1507m at the 850mb level was observed in the WA region. A relatively high minimum geopotential height of 13.50m at 1,000mb is observed for SIO storms. The same pattern exists for the minimum geopotential heights at 850mb, with the lowest values of 1396m, 1360m and 1400m observed for the EA, WA and SP storms respectively, while the highest geopotential height of 1433m was observed for the SIO storms. At both levels the distribution of the geopotential heights exhibits a progressive decrease in mean magnitudes from the west to east, with storms from the western basins demonstrating larger mean heights than the storms in the eastern basins.

Table 5.15 Geopotential Height descriptive statistics at 1,000mb and 850mb across Southern Hemisphere basins

Geopotential Height 1,000mb					Geopotential Height 850mb			
Basin	SIO	WA	EA	SP	SIO	WA	EA	SP
Mean	56.49	41.23	38.15	32.89	1475.20	1457.31	1450.25	1450.99
SD	12.85	21.27	17.95	18.43	12.69	27.66	26.15	18.76
+-SD	44-69	20-63	20-56	14-51	1463-1488	1430-1485	1424-1476	1432-1470
MAX	76.80	93.00	79.00	97.00	1496.60	1507.00	1500.60	1506.33
MIN	13.50	1.00	4.00	2.33	1433.00	1396.00	1360.00	1400.50

The distribution (Figure 5.19,Figure 5.20) of geopotential height indicates that 173 (35%, n=495) storms formed when the magnitude of geopotential height was 33-63m at the 1,000mb level and 1457-1485m at the 850mb level. There are no storm formation events observed below -72m at the 1,000mb level and below 1345m at the 850mb level. Storm formation also tends to decrease once geopotential height increases above 168m at the 1,000mb level and above 1555m at the 850mb level. Based on the boxplots, larger magnitudes of geopotential height are recorded for the SIO storms, compared to the other basins (Figure 5.19). The largest range of geopotential height about the mean, however, is observed for the WA region (Figure 5.19, Figure 5.20). Additionally, the distribution and means of the 850mb geopotential heights observed in the eastern region (EA and SP) are much smaller than the means and distribution of geopotential height observed for the western basins (SIO and WA).

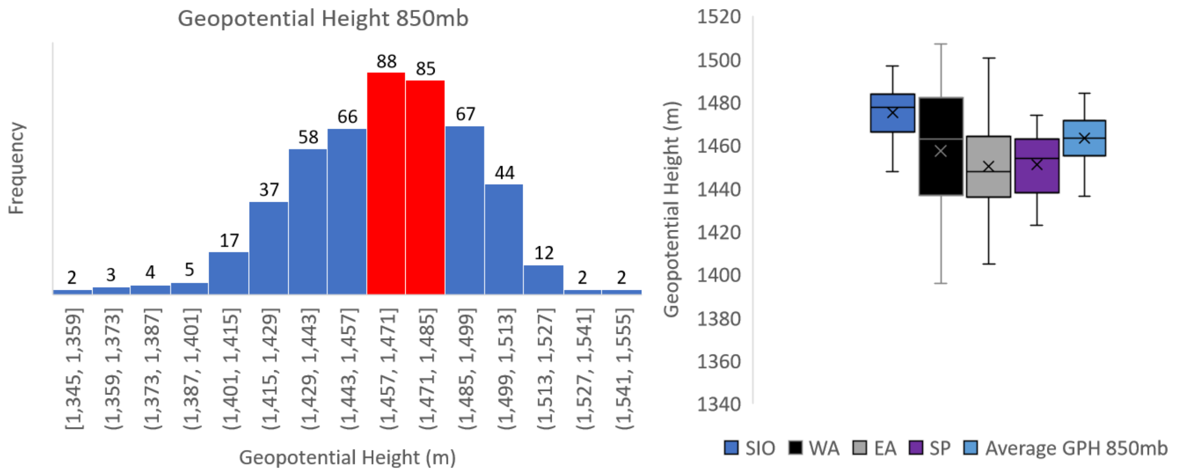

Figure 5.20 850mb Geopotential Height: distribution at the point of genesis (left) and inter-basin comparison of geopotential height with five-number summaries for the Southern Hemisphere tropical cyclones (right).

5.2.1.7 Solar Flux at the Point of Genesis

The mean solar flux observed at the point of storm genesis for the Southern Hemisphere was 185W.m^{-2}. The highest mean solar flux of 197W.m^{-2} was observed for SIO storms, while the lowest mean solar flux of 168W.m^{-2} was observed for the EA storms (Table 5.16,Figure 5.21). The highest mean values are observed in the eastern basins (SIO and WA), while the lowest mean values are observed in the western basins (EA and SP), again indicating an east-west disparity in the Southern Hemisphere. The lowest variability from the mean, for solar flux at the point of genesis was observed for EA storms (SD=27.5W.m^{-2}) and for SIO storms (SD=29.4W.m^{-2}), while the highest variability was observed for the WA storms (SD=39.6W.m^{-2}) and SP storms (SD=39.9W.m^{-2}). A similar maximum solar flux of 280W.m^{-2} was observed at the point of genesis for storms in the WA and SP basins. The lowest maximum solar flux of 243W.m^{-2} was observed for storms in the EA region. The minimum solar flux of 95W.m^{-2} was recorded for the SP storms, while a relatively higher minimum solar flux of 140W.m^{-2} was observed for storms in the SIO.

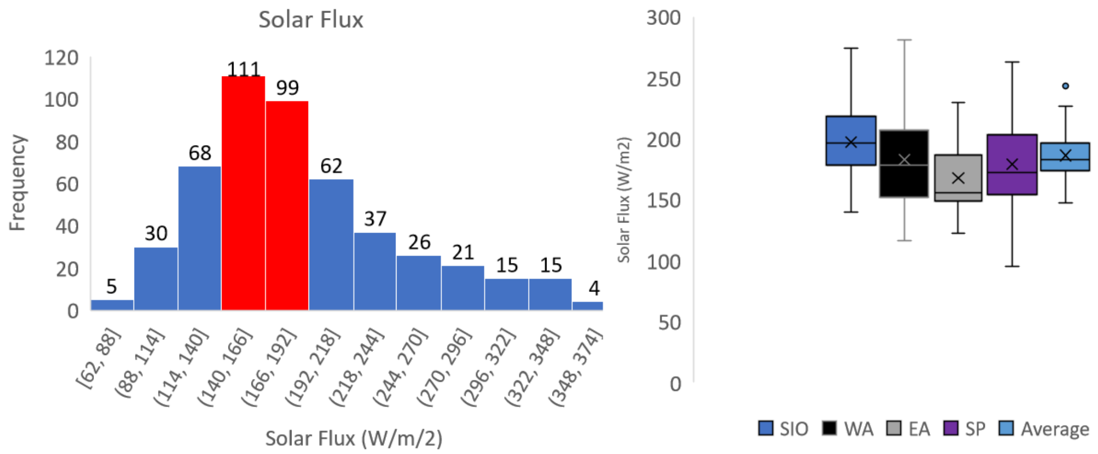

Figure 5.21 Solar flux distribution at genesis (left) and inter-basin distribution (right).

Regarding the distribution of solar flux at the point of genesis (Figure 5.21), 210 (43%, n=493) tropical cyclones occurred when the solar flux was at a magnitude of 140-218W.m^{-2}, making this interval the optimal magnitude for solar flux, at which the largest number of tropical cyclones are observed to undergo genesis in the Southern Hemisphere. The distribution is skewed towards the lower end, indicating that higher magnitudes of solar flux are associated with a lower occurrence of storm formation. This is true for the lower magnitude intervals of solar flux, that are <62W/m^{-2}, at which fewer storms occur.

Table 5.16 Solar flux descriptive statistics across Southern Hemisphere basins

Solar Flux				
Basin	SIO	WA	EA	SP
Mean	197.56	183.05	167.95	179.20
SD	29.42	39.60	27.45	37.97
+- 1 SD	168-227	143-223	140-195	141-217
MAX	274.52	280.90	243.40	279.70
MIN	140.03	116.85	122.90	95.25

5.2.2 Summary of Optimal Ranges at the Point of Genesis

The optimal, maximum and minimum magnitudes of each climate variable, observed during the point of genesis at the 1,000mb and 850mb levels is summarised below (Table 5.17).

These optimal intervals are a core part of the results, as they provide the intervals (magnitudes) at which the largest number of formation events take place. This informs on the specific range of magnitudes at which Southern Hemisphere tropical cyclones tend to form, but by using histogram distributions and the min/max statistics, the extremes at which tropical cyclones can undergo genesis is also captured. Both the minimum and maximum values observed at the point of genesis fall to the extremes of the optimal conditions, and this applies to all the values between the optimal, minimum and maximum values. An important note is that the histograms for the climate variables at the point of storm genesis, from which the optimal intervals are based and captured (Table 5.17), do not indicate a threshold of any kind, but display a preferred magnitude at which most storms tend to occur in the Southern Hemisphere. Furthermore, the observation that storms undergo genesis outside of the optimal intervals (which are themselves ranges), indicates that a threshold may not exist for any of the climate variables examined at the point of genesis.

Table 5.17 Summary of Drivers: Peak Optimal interval and MIN and MAX of drivers at the point of genesis.

Variable	Optimal Intervals at the point of Genesis	MIN at the point of Genesis	MAX at the point of Genesis
Sea Temperature (°C)	27.5-28.5	24.06	31.39
Solar Flux (W.m^2)	140-192	62	374
Pressure (mb)	1002-1007	973	1023
Air T 1000(°C)	27-28	19	31
Air T 850(°C)	18-19	9	23
Omega 1000(pascal.s^{-1})	-0.01-0.01	-0.17	0.08
Omega 850(pascal.s^{-1})	-0.18-0.07	-0.72	0.15
RH 1000(%)	79-83	63	99
RH 850(%)	75-88	37	100
v-wind shear (α)	-0.06-0.24	-1.56	1.29
u-wind shear (α)	-0.08-0.20	-1.48	1.74
GPH 1000(m)	33-63	-72	168
GPH 850(m)	1457-1485	1345	1555

5.3 Genesis Requirements: Minimum, Majority and Category 5 Scenarios

To determine and evaluate the genesis requirements for tropical cyclones in the Southern Hemisphere, the climate variables at the point of genesis for each storm (with an emphasis on sea surface temperature) were examined in three scenarios. Sea surface temperature was chosen as a primary factor for storm genesis as it scored highly in the factor analysis and multivariate regression (see Section 5.5). Factor analysis was performed to determine the general contribution each driver had towards explaining the variability at the point of genesis and their role in providing conducive conditions for storm genesis. The first genesis scenario (Figure 5.22) outlines the magnitude of each climate driver at the point of genesis required for a Southern Hemisphere tropical cyclone to undergo genesis at the lowest observed sea surface temperatures. This was computed by attaining the average magnitude of each driver for the storms which were initiated at the lowest observed sea surface temperatures (<26.5°C). The second scenario (Figure 5.23) examined and summarised the conditions that promote the majority of the Southern Hemisphere storms to undergo genesis. Specifically, the optimal/peak interval bins (magnitudes) determined from the climate variable histograms were used (e.g. the sea surface temperature interval at which the largest number of storms had occurred) which was 27.5-28.5°C in this case. This was applied for the rest of the climate variables, by using their optimal/peak intervals associated with the majority of storm occurrences (Table 5.17). This second scenario provides the most common conditions required for the majority of storm genesis events in the Southern Hemisphere. The third scenario (Figure 5.24) examined the minimum sea surface temperature and the subsequent driver values required for a storm to attain a category 5 intensity in the Southern Hemisphere. This was done using the category 5 storms, which had sea surface temperatures within the minimum histogram interval (27-28°C) at the point of genesis. The driver magnitudes associated with these category 5 storms were then averaged and presented in the third scenario.

The factor analysis (Table 5.18) for all climate variables at the point of genesis, indicates that the first two factors account for 58.9% of the variability. For the first factor, a negative correlation to relative humidity at the 1,000mb level (r=-0.48), a high positive correlation to air temperature at the 1,000mb level (r=0.95) and the 850mb level (r=0.78) and sea surface temperature (r=0.76), indicate that these variables have a large positive and negative (for relative humidity) loadings on factor one. Therefore, factor one appears to describe the thermodynamic climate variables at the point of genesis. The second factor is loaded on positive correlations to solar flux and omega (850mb), with a high negative correlation to relative humidity (850mb) and v-wind shear. The loadings of omega (r=0.79) and v-wind shear (r=-0.35) demonstrate that factor two describes the dynamic climate variables at the point of genesis. However, the large loadings of upper level relative humidity (r=-0.87) and solar flux (r=0.55) indicate that factor two may also describes the upper atmospheric thermal environment during genesis. The factor weightings apply to genesis scenarios one and three. Only pressure and geopotential height were excluded from the factor analysis, as they are majorly diagnostic variables of the large-scale environment (Section 4.2.4).

Table 5.18 Factor Analysis Results: Factor loadings and correlations to minima climatic drivers at genesis. Values in bold have the highest squared cosine relation in regard to explaining the variability of the respective factors.

	Factor 1 (31.0%)	Factor 2 (27.9%)
Sea surface temperature	**0.7554**	0.1521
Solar Flux	0.2171	**0.5439**
Air Temp. 1000	**0.9532**	0.0905
Air Temp 850	**0.7806**	-0.0412
Omega 1000	-0.0848	**0.3886**
Omega 850	-0.2506	**0.7941**
RH 1000	**-0.4848**	-0.4365
RH 850	-0.3759	**-0.8702**
v-wind shear	0.3004	**-0.3519**
u-wind shear	-0.2383	0.2310

5.3.1 Summary of Genesis Scenarios/Flow charts

5.3.1.1 Genesis Under Minimum Sea Surface Temperatures

The climate drivers related to the storm genesis events with the lowest minimum sea surface temperatures at the point of genesis are visible in the first genesis flow diagram (Figure 5.22). The genesis flow diagram indicates that storms which underwent genesis under these extremely low sea surface temperatures, also tend to have relatively low values observed for the other thermodynamic variables, including air temperature at both 1,000mb and 850mb levels, relative humidity and solar flux. Regarding the dynamic variables observed for genesis events occurring at minimum sea surface temperatures, the magnitude of omega is similarly very small, while meridional and zonal wind shear demonstrates large positive magnitudes. These low magnitudes of the thermodynamic variables are usually non-conducive to storm genesis in terms of the accepted model of genesis conditions (Section 2.3.2). Consequently, the observed storm intensities attained under these conditions were not very high. The LMI was low with a high central pressure and the storms only lasted an average of one day. Based on these observations, the storms undergoing genesis at the minimum sea surface temperatures, are observed to only intensify to the point of a category 1 tropical cyclone, with no higher intensity category observed for storm genesis events with these minimum thermodynamic magnitudes. Therefore, while it is possible for storms to undergo genesis at low sea surface temperatures and a low energy environment, they do not indicate an ability to intensify or persist effectively.

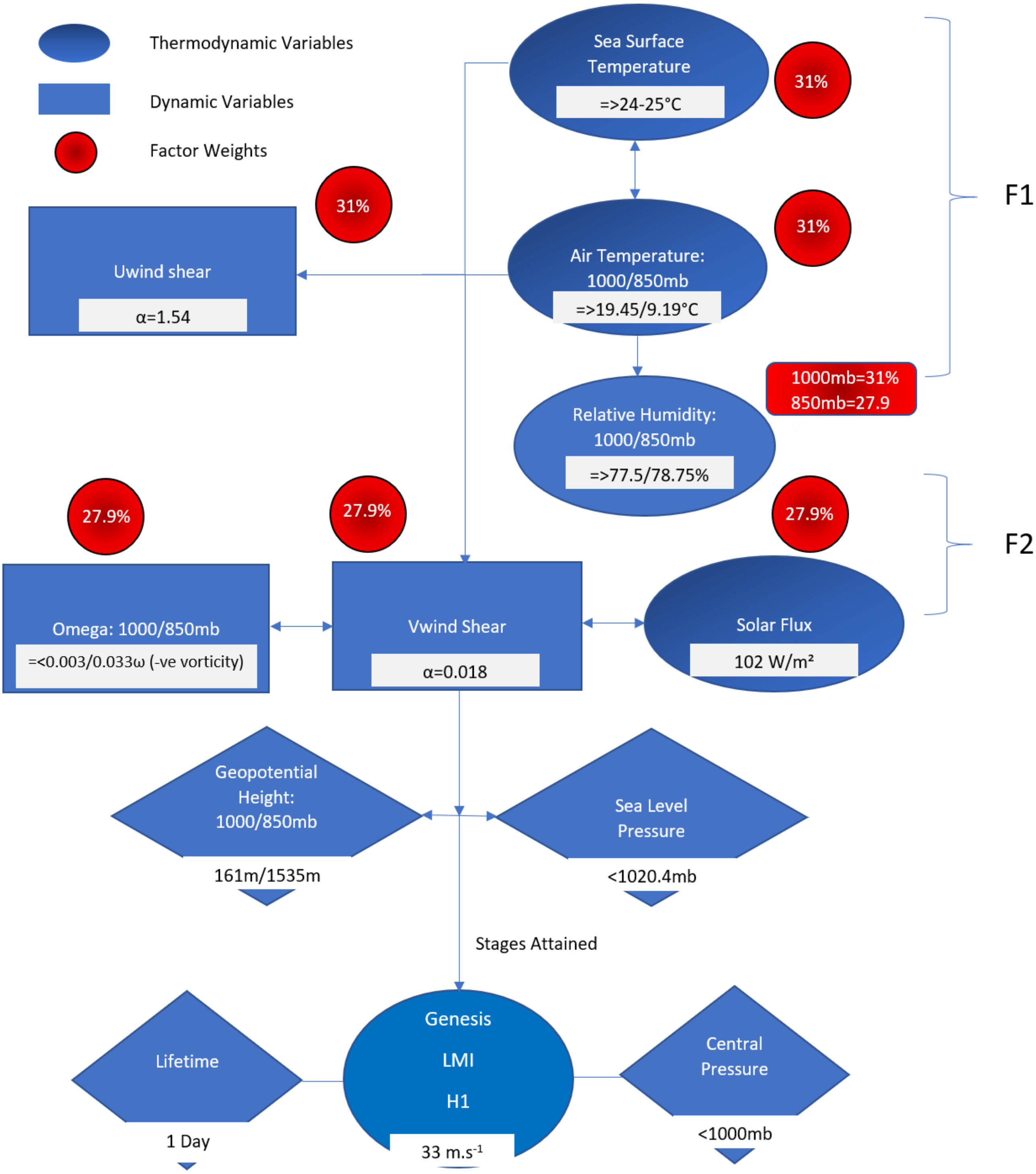

Figure 5.22 Minimum sea surface temperature for a tropical cyclone at genesis, along with the magnitudes of the other drivers and the weightings assigned with factor analysis to the two factors (F1 and F2). All variables weighted on F1 and F2 factors are grouped together respectively.

5.3.1.2 Optimal Scenario Observed for Majority of Genesis Events

The second factor analysis (Table 5.19) applies only to the second genesis scenario, as this scenario examined the optimal intervals (magnitudes) of the climate drivers at the point of genesis which promoted the maximum occurrence of storms in the Southern Hemisphere (Figure 5.23). The first two factors from the factor analysis performed on these optimal climate variables, explains 41.4% of the variability. Sea surface temperature does not indicate a major loading on factor one in this scenario; when climate variable magnitudes outside of the optimal intervals are excluded. Omega (850mb) and solar flux indicate positive loadings ($r>0.60$) for factor one, while relative humidity indicates the highest negative loadings for factor one at the 850mb level ($r=-0.91$) and the 1000mb level ($r=0.85$), indicating that this factor mostly describes the moisture and thermodynamic influences on storm genesis. Regarding factor two, which accounts for 16.3% of the variability; air temperature demonstrates the highest loading at 1000mb (0.95) and 850mb (0.70), followed by sea surface temperature ($r=0.56$). Factor two has high positive loadings for the thermodynamic variables, so it partly describes the thermal influence at the point of genesis. Compared to the minimum genesis scenario (Figure 5.22), this optimal scenario (Figure 5.23), indicates that the thermodynamic variables (sea and air temperature, solar flux and relative humidity) have an increased influence on the variability at the point of genesis. Omega (850mb) has a much larger loading within this optimal scenario, indicating a high influence of upward motion on the variability for the majority of genesis events.

Table 5.19 Factor analysis of variables for the magnitude of climate drivers at peak storm occurrences.

	Factor 1 (25.06%)	Factor 2 (16.34%)
AirT. 1000	0.1661	**0.9515**
AirT 850	0.0279	**0.7048**
Omega 1000	0.3947	0.0477
Omega 850	**0.8467**	-0.1205
RH 1000	**-0.6628**	-0.1908
RH 850	**-0.9128**	-0.2356
Pressure SLP	0.0567	-0.0957
New SST Genesis	-0.1365	**0.5561**
Solar W/m	**0.6739**	0.0377
v-wind shear	-0.1116	0.1108
u-wind shear	0.0201	-0.0941

Larger magnitudes of the thermodynamic and dynamic variables are observed for the optimal genesis scenario (Figure 5.23), compared to the minimum genesis scenario. For the thermodynamic variables, sea surface and air temperature, relative humidity and solar flux indicate larger magnitudes at the point of genesis, with air temperatures closely following the optimal sea surface temperatures. While a large negative range of omega is observed, indicating high buoyancy and horizontal convergence. V-wind shear also has a much larger magnitude for this optimal genesis scenario, while the u-wind shear is smaller. These changes in magnitude for the climate drivers allows for increased conducive conditions. This offers an explanation for the larger number of storm genesis events taking place at these magnitudes. The optimal magnitudes observed in this scenario also indicate an influence on the tropical cyclone intensity, which is observed to have a higher mean range of intensity for a larger number of storms. Additionally, a longer lifetime is observed for storms occurring at the optimal magnitudes, compared to the minimum genesis scenario.

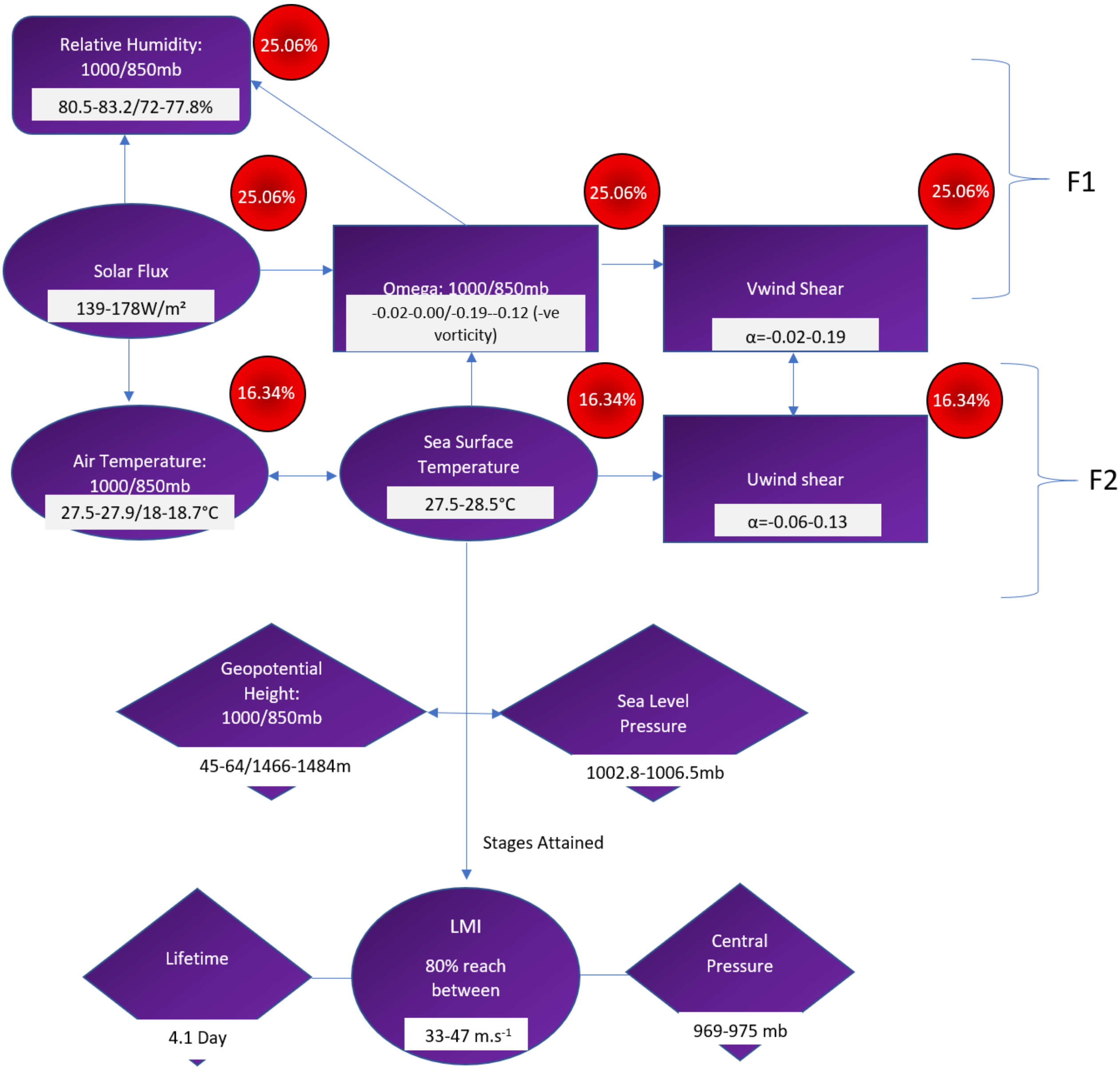

Figure 5.23 Peak tropical cyclone occurrence and conditions of climate drivers within this peak interval which led to the largest number of storm genesis events. All variable weighted on the F1 and F2 factors are grouped together respectively.

5.3.1.3 Minimum requirements for a Category 5 Tropical Cyclone

The genesis flowchart capturing the minimum sea surface temperature at which a category 5 tropical cyclone can develop (Figure 5.24), indicates that the sea surface temperature can be as low as 27°C. Within the subset of these minimum sea surface temperatures at the point of genesis, the mean magnitudes of the climate drivers are presented. The significant difference compared to the optimal genesis scenario, is that mean relative humidity is required to be extremely high at over 92%. The mean solar flux and air temperature (850mb) falls within similar magnitudes as those observed for the optimal/peak genesis scenario. Air temperature at the surface is lower however, with an observed mean magnitude of 26°C (compared to 27°C at the optimal/peak scenario). Omega at 850mb is higher (-0.22pascal.s^{-1}) while v-wind shear falls into the upper end of the majority peak interval (-0.20α). These conditions as illustrated (Figure 5.24) allow for a category 5 tropical cyclone to form and attain an LMI of approximately 84 m.s^{-1}, with an extremely low central pressure (930mb). Under these genesis conditions, the category 5 storm demonstrates a lifespan of six days. The three scenarios offer tentative evidence that the climate variables at the point of genesis, have an influence on the intensity/LMI attained by a tropical cyclone in the Southern Hemisphere. From these scenarios, a higher range of sea surface and air temperatures are accompanied by larger magnitudes of relative humidity and omega.

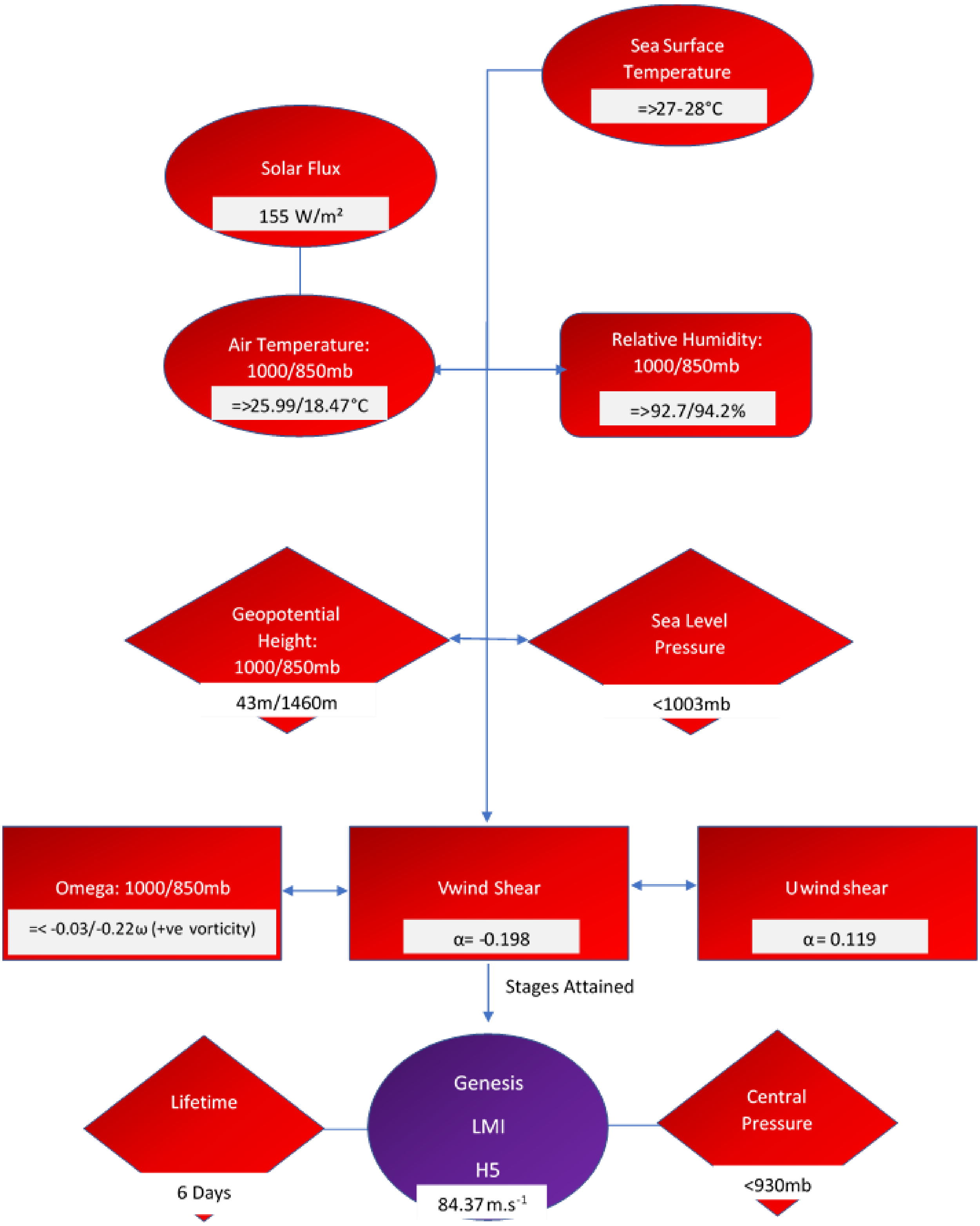

Figure 5.24 Minimum sea surface temperature for a category 5 tropical cyclone at genesis, along with the magnitudes of the other drivers.

5.3.2 Dynamics of Sea Surface Temperature at the Point of Genesis

Tropical cyclone intensity and sea surface temperature are examined in relation to each other in this section. The observation of minimum sea surface temperatures at the point of genesis (Table 5.20) indicates that as tropical cyclone intensity increases (from H1-H5 or category 1-5), so does the absolute minimum sea surface temperature. The lowest sea surface temperature observed was 24.06°C for a category 1 storm, but 27.26°C for a category 5 storm.

Table 5.20 Minimum sea surface temperature at each SST interval from 24-31°C.

SST Interval	24-25	25-26	26-27	27-28	28-29	29-30	30-31
Basin	SIO	SP	SIO	EA	SP	WA	EA
Category (Saffir Simpson Scale)	1	2	1	1	1	1	1
Lifetime	5	8	20	15	8	13	10
Date Genesis	6/21/01	2/24/89	12/3/82	5/9/91	4/19/83	2/20/85	2/11/87
Latitude Genesis	-26	-27	-15	-13	-15	-15	-12
Longitude Genesis	34	220	50	154	222	112	135
TC: Start Windspeed	65	65	65	65	65	65	65
Pressure Genesis	1000	970	991	983	975	950	992
AirT 1000	19	24	26	27	29	27	27
AirT 850	9	15	18	19	19	18	18
Omega 1000	0.00	0.02	-0.04	-0.02	-0.01	-0.02	0.00
Omega 850	0.03	0.00	-0.14	-0.16	-0.15	-0.16	-0.18
RH 1000	78	83	81	84	83	81	90
RH 850	79	78	78	80	83	86	94
GPH 1000	161	145	73	59	29	-14	33
GPH 850	1535	1546	1487	1480	1455	1405	1455
Sea Level Pressure	1020	1016	981	1006	1002	998	998
New SST Genesis	24	25	26	27	28	29	30
Solar W/m	102	214	172	132	110	172	113
Vwind Shear	-0.02	-0.03	-0.01	0.36	0.04	0.48	-0.09
Uwind Shear	1.54	-0.04	0.38	-0.07	0.20	0.01	0.07

Maximum sea surface temperatures are similar for all tropical cyclone intensity categories, inferring that the maximum sea surface temperatures are not the main driver of intensification (i.e. a category 1 tropical cyclone has a higher max temperature than a category 5 tropical cyclone). This is also observed for category 1 and category 2 storms (Table 5.21), which were observed to undergo genesis at lower and higher sea surface temperatures, matching that of higher intensity storms, yet they did not intensify past a category 1 tropical cyclone.

Table 5.21 Statistical summary for the sea surface temperatures at the point of genesis and the storm categories of intensity. The categories H1 to H5 are representative of the category 1-5 scale from the Saffir-Simpson scale of intensity.

SST for each Category of Intensity	**Category 1**	**Category 2**	**Category 3**	**Category 4**	**Category 5**	**Population Value**
MIN	24.06	25.29	25.79	26.07	27.26	24.06
MAX	30.91	30.49	30.27	30.66	30.39	30.91
Q1	25.76	26.99	26.98	27.17	27.53	27.36
Q3	27.1	28.27	28.34	28.04	29.41	28.9
Median	26.33	27.89	27.32	27.57	28.25	28.15
Std. Dev	0.97	1.03	0.90	0.65	1.01	1.11

The minimum sea surface temperature at storm genesis is arranged to display the sea surface temperature distribution per storm category (Saffir-Simpson scale). The first aspect to note is that the minimum sea surface temperatures for all categories except category 5 storms, fall below 26.5°C (Table 5.21). The category 1 storms have the lowest mean sea surface temperature at genesis. The category 5 storms have the highest mean sea surface temperature. This indicates that in the Southern Hemisphere, higher sea surface temperatures will result in higher intensity storms. The category 2 storms, however, have a comparatively higher mean sea surface temperature than the category 3 and 4 storms (Figure 5.25). The sea surface temperature range indicated by the Q1 and Q2 values for category 5 storms are much higher, than the other storm categories. Examining (Figure 5.25) it is observed that the minimum temperature required for genesis of a storm increases with the category. Sea surface temperature has a statistically significant forcing on Southern Hemisphere storm category ($r=0.29$; $p= <0.001$). The minimum sea surface temperature at each degree interval from 24 to 31 (Table 5.20) was also examined per storm to determine any trends in tropical cyclone activity and the climatic drivers during storm genesis at these lowest sea surface temperatures. At the minimum end of each sea surface temperature interval (even 30-31°C), only low intensity category storms (H1 and H2) are observed to form. The location of genesis indicates that the storms undergoing genesis at higher sea surface temperatures are found closer to the equator. The storm which formed at 24-26°C is located at a mean of 26.5°S, while the storm formed at 26-31°C indicates a lower latitude of 14°S. Air temperature and relative humidity increase with sea surface temperature, while omega values, sea level pressure and 850mb geopotential height decreases with increased sea surface temperatures in reference to these minimum sea surface temperatures at the point of genesis.

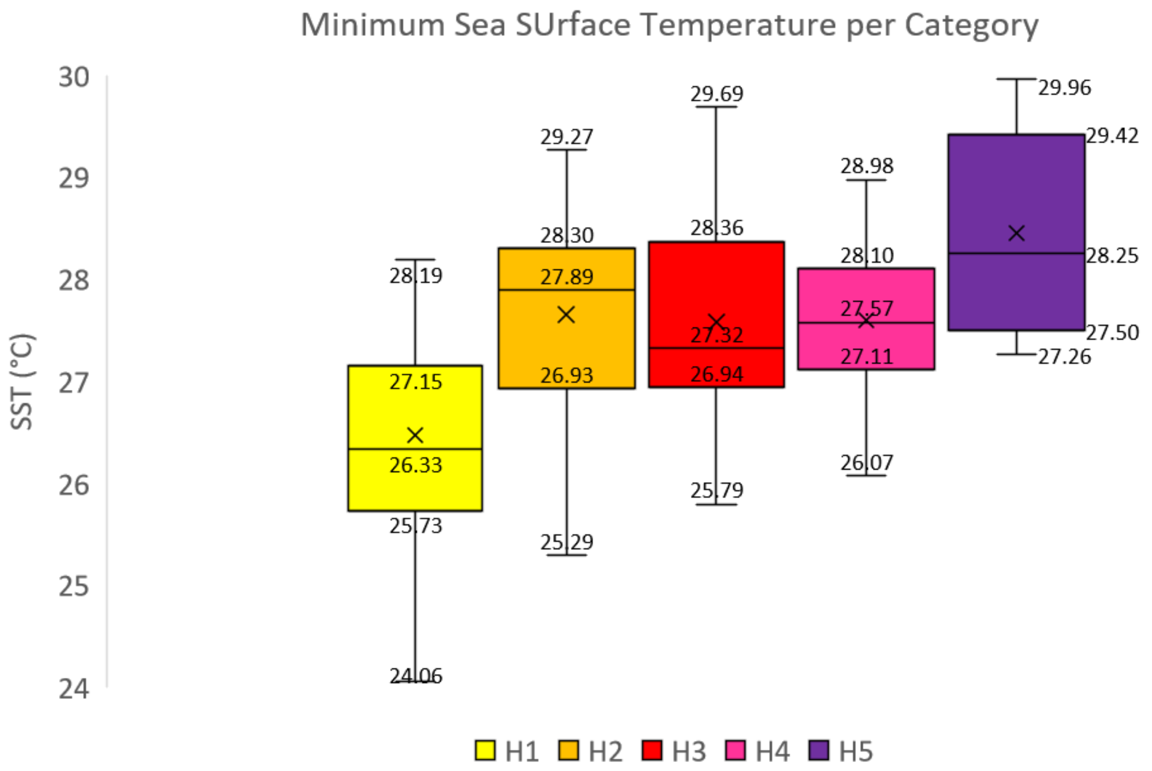

Figure 5.25 Minimum sea surface temperature per storm category.

5.4 Time Trends in Tropical Cyclone Activity and Climate Drivers at the Point of Genesis

This section of the results will examine the changes over the study period from 1980-2016 related to the tropical cyclone activity (frequency, latitude, longitude, lifetime duration, LMI, and category of intensity) and the drivers during the point of storm genesis (sea surface temperature, air temperature, omega, relative humidity, wind shear and geopotential height). Having established the nature (states and magnitude) of the drivers at the point of genesis, the change over time regarding these drivers will be determined. This will highlight the impacts and resultant shifts and variability of tropical cyclone activity and the climate variables at the point of genesis over time. The statistical significance and rate of change for the time trends will also be examined.

5.4.1 Time Trends of Tropical Cyclones (1980-2016)

5.4.1.1 Change in Tropical Cyclone Frequency

The tropical cyclone frequency does not demonstrate any statistically significant changes over time (Figure 5.26). Individually, the only basin with an increase in tropical cyclone frequency is the SIO basin (r=0.11, p=0.5293, R2=0.01). However, this is attributed to the increased storm activity from 1990-1997. The number of tropical cyclones in the WA region is decreasing at a rate of $0.02.yr^{-1}$ (r=-0.17, p=0.3045, R2=0.03), while there is a decreasing rate observed in the EA region of $0.03.yr^{-1}$ (r=-0.20, p=0.2365, R2=0.04). The SP has the smallest decrease in storm number at a rate of $0.01.yr^{-1}$ (r=-0.06, p=0.7115, R2=0.00). The frequency of tropical cyclone occurrence for the entire Southern Hemisphere (Figure 5.26) is decreasing at a rate of $0.04.yr^{-1}$ (r=0.11, p=0.4831, R2=0.01). In the decade from 1991-2000, there were an average of 15 storms occurring per year, which was above the overall average of 13.3 storms per year compared to the recent decade of 2001-2016 for which an average of 12 storm occurrences are recorded.

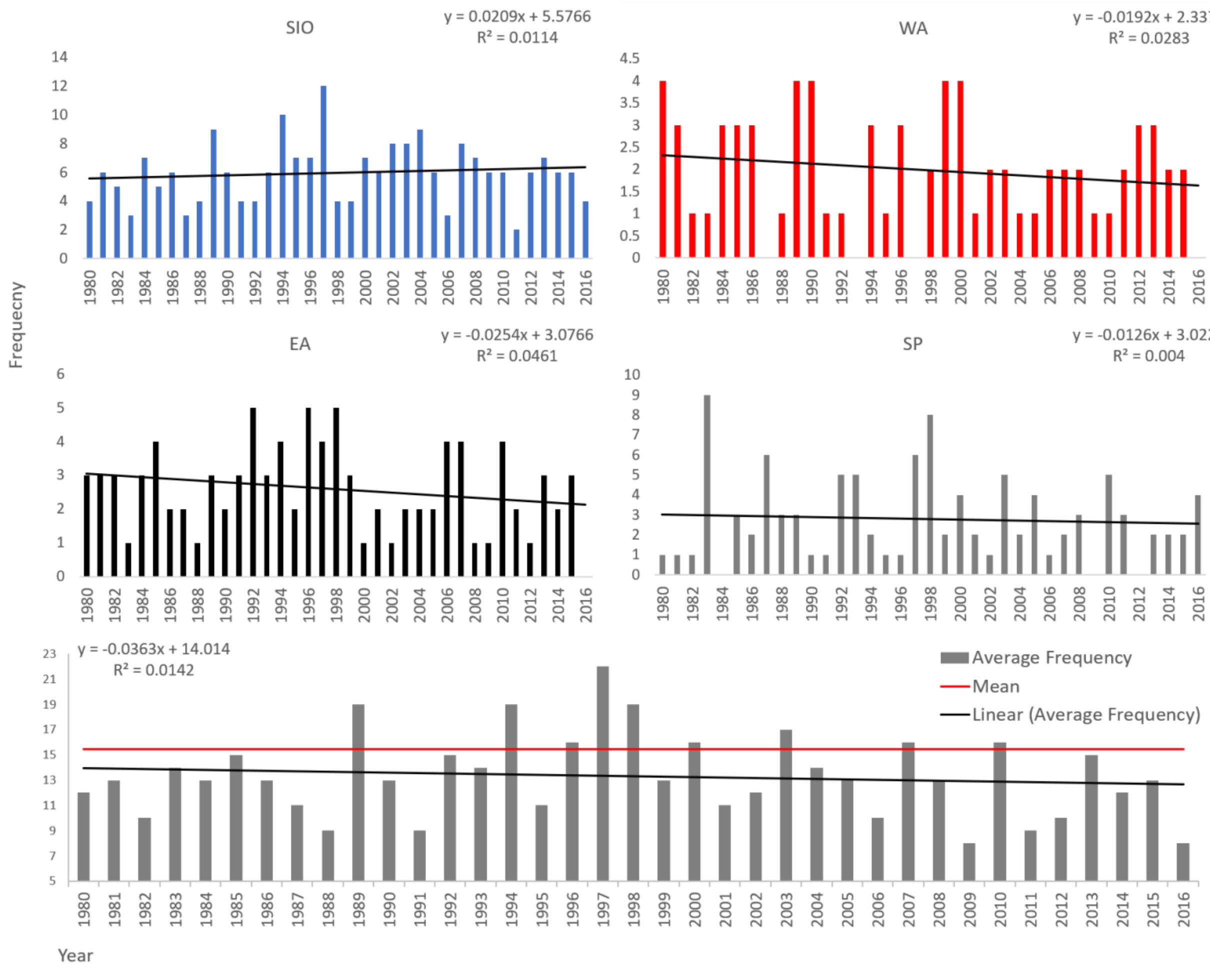

Figure 5.26 Time trends: Frequency of tropical cyclone occurrence from 1980-2016 (Nov-Apr) for individual basins and the combined hemisphere counts. Regression lines (black) and linear regression equation for each basin and the Southern Hemisphere. Mean (red line) indicates the average frequency for the Southern Hemisphere.

As for the change in geographical distribution of tropical cyclone occurrence (Figure 5.27), the poleward extents of activity have shifted further south. This is observed by examining the 2000-2016 mean boundary, which indicates the greatest extent of tropical cyclone occurrence, i.e. no storm was observed below the boundary. During this period more storms have formed further south compared to the 1980-1999 period, where the boundary of activity was located at a more equatorward latitude than present. This indicates that recent storms have been undergoing genesis further south of the usual formation bands. This shift has consequently exposed more regions to tropical cyclone landfall. With newly impacted areas further south of the 1980-1990 boundary of activity, observed over the east and west Australian coasts and the southern African coastline at approximately 20°, 21° and 30°S of the equator respectively.

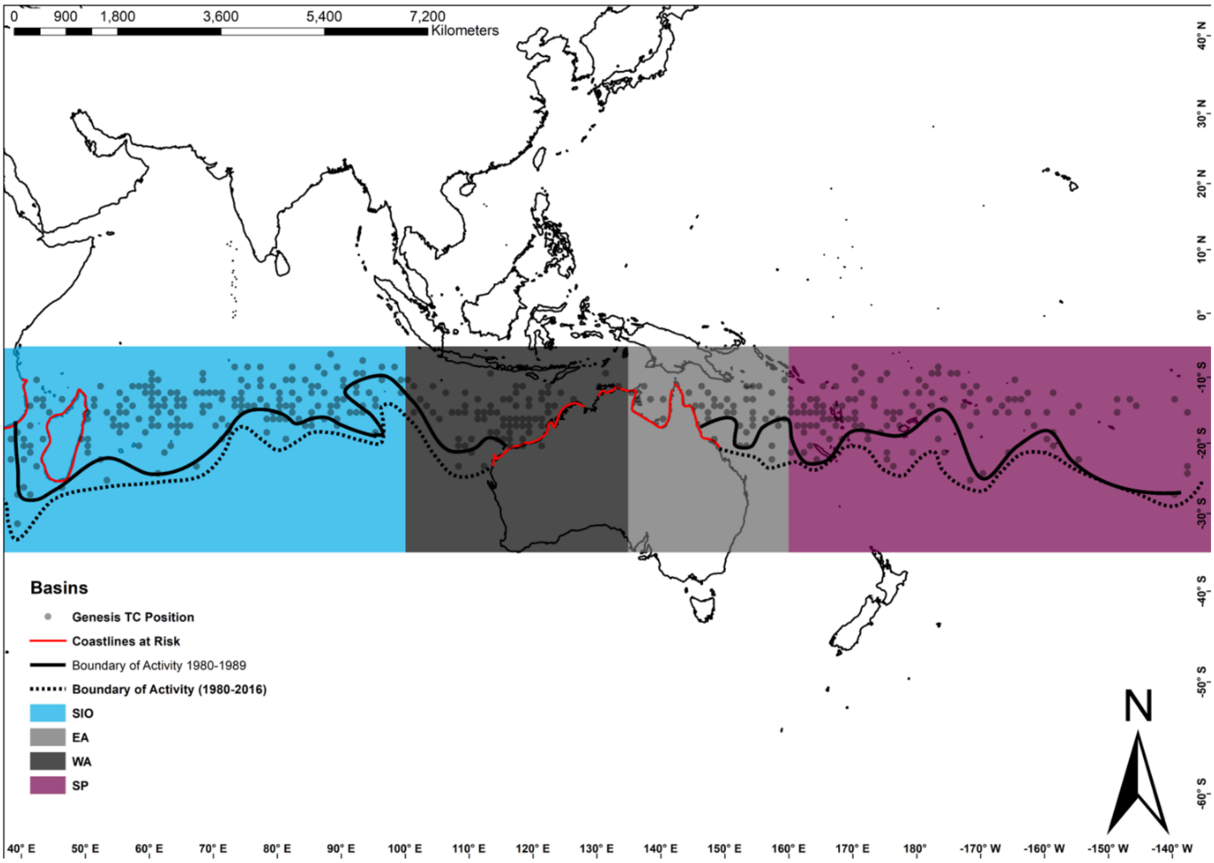

Figure 5.27 Map of study regions and the change in tropical cyclone activity extent from 1980-1999 to 2000-2016. Red regions are regions at risk of landfall activity, dotted line indicates the present (2000-2016) extent of tropical cyclone activity.

5.4.1.2 Lifetime Maximum Intensity

An increasing trend is observed for LMI, across all the basins. For the SIO storms, the increase in maximum intensity is statistically significant, with a rate of 0.23 $m.s^{-1}.yr^{-1}$ (r=0.43, p=0.017, $R^2$0.19). A statistically significant increase for the SP storms was also observed, with a rate of 0.36 $m.s^{-1}.yr^{-1}$ (r=0.41, p=0.023,R^2=0.17). The EA and WA regions do not demonstrate any statistically significant trends, with the rate of increase in LMI for the WA storms observed as 0.39 $m.s^{-1}.yr^{-1}$ (r=0.18,p=0.3293, R^2=0.04) and 0.15 $m.s^{-1}.yr^{-1}$ (r=0.30, p=0.1073,R^2=0.09) for the EA storms. The EA and WA regions have weak correlations and R^2 values, indicating that the increasing trends are not statistically significant, and the regression model does not explain the trend effectively. The SIO and SP regions, however, indicate a statistically significant positive correlation between time and LMI. The hemisphere average is also statistically significant with an increase in LMI observed at a rate of 0.24 $m.s^{-1}.yr^{-1}$ (r=0.62, p=<0.01, R^2= 0.39). This indicates that the maximum intensity attained by tropical cyclones is increasing in magnitude over time for the Southern Hemisphere as a whole. The correlation is strong, and the p-value is at the 1% confidence interval. Compared to the average of the Southern Hemisphere, the SIO maximum intensity falls just below the rate of increase, while the SP exhibits a rate of increase which is 0.12 $m.s^{-1}.yr^{-1}$ larger than the hemisphere's average. Furthermore, each successive year displays an average maximum intensity above the mean intensity observed for the hemisphere. Even when the average maximum intensity for a year decreases below the mean (Figure 5.28), the subsequent mean LMI remains higher than the previous yearly magnitudes of LMI. This indicates a compounding increase in LMI over time. From 1980-1989, the mean maximum intensity attained by Southern Hemisphere tropical cyclones was 46 $m.s^{-1}$, however, from 2000-2009, the mean maximum intensity attained was 52 $m.s^{-1}$. The evidence supports an increase in the maximum intensity attained by tropical cyclones across the Southern Hemisphere.

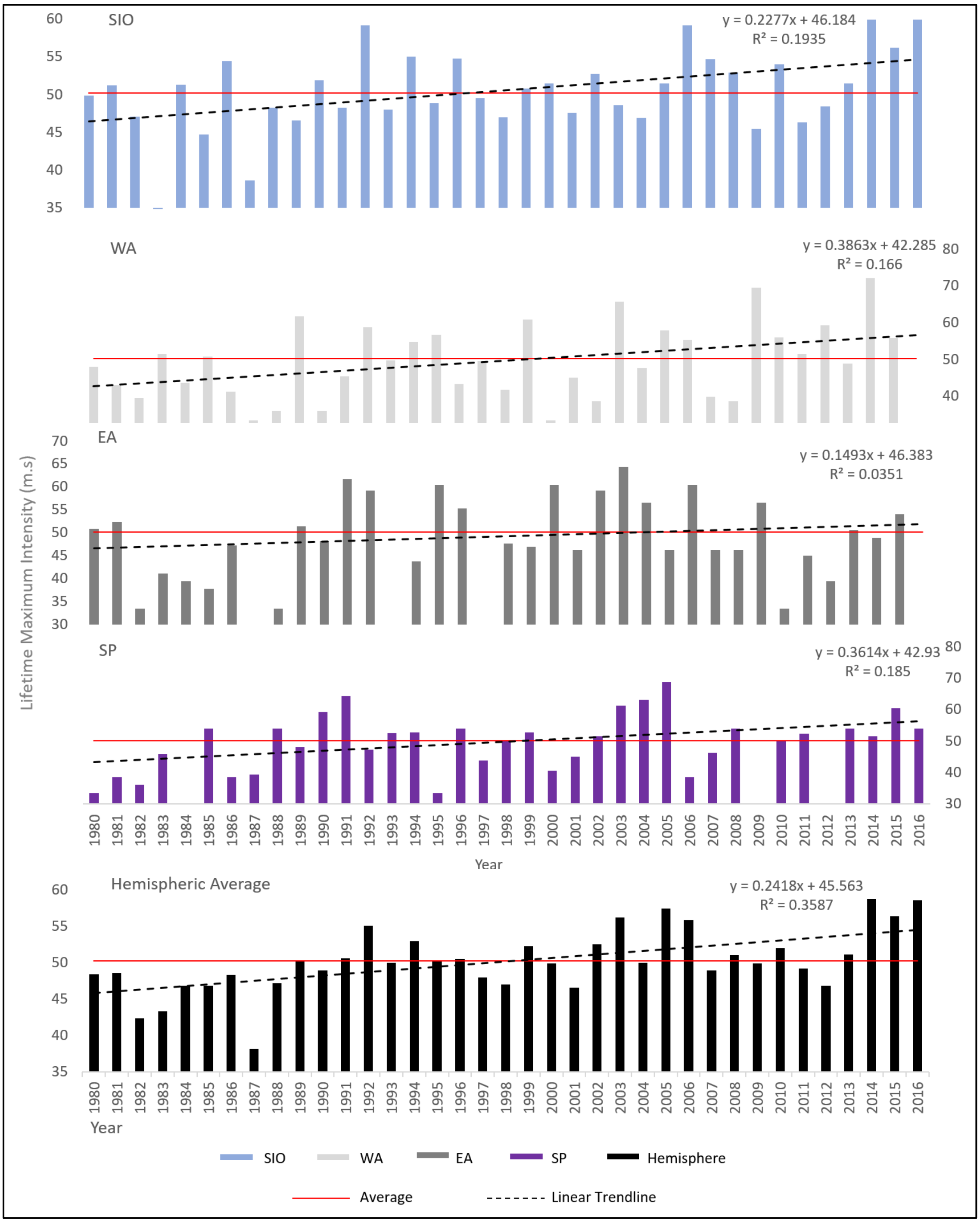

Figure 5.28 Time trends: LMI of tropical cyclones from 1980-2016 (Nov-Apr) for individual basins and the combined average for the hemisphere.

5.4.1.3 Change in Latitude at the Point of Genesis

There are no statistically significant trends related to the rate of change in latitude at the point of genesis (Figure 5.29). Positive rates of change are observed for the SIO and WA storms. In the SIO, the latitude of genesis is increasing by 0.02°.yr^{-1} (r=0.07, p=0.7301) and 0.04°.yr^{-1} (r=0.11, p=0.5789) in the WA region. A similar negative rate of change is observed for the EA and SP storms, with an average decrease in the latitude of genesis by 0.04°.yr^{-1} in the EA region (r=-0.23, p=0.2182) and the SP region (r=-0.14, p=0.4500). None of the R^2 values for the above statistics are over 0.03. The results denote a poleward shift in latitude of genesis for the SIO and WA regions, while genesis latitude appears to be shifting equatorward in the EA and SP regions. The average rate of increase in genesis for the Southern Hemisphere storms is 0.02°S.yr^{-1} (r=0.04, p=0.8532). This indicates a poleward trend in genesis latitude.

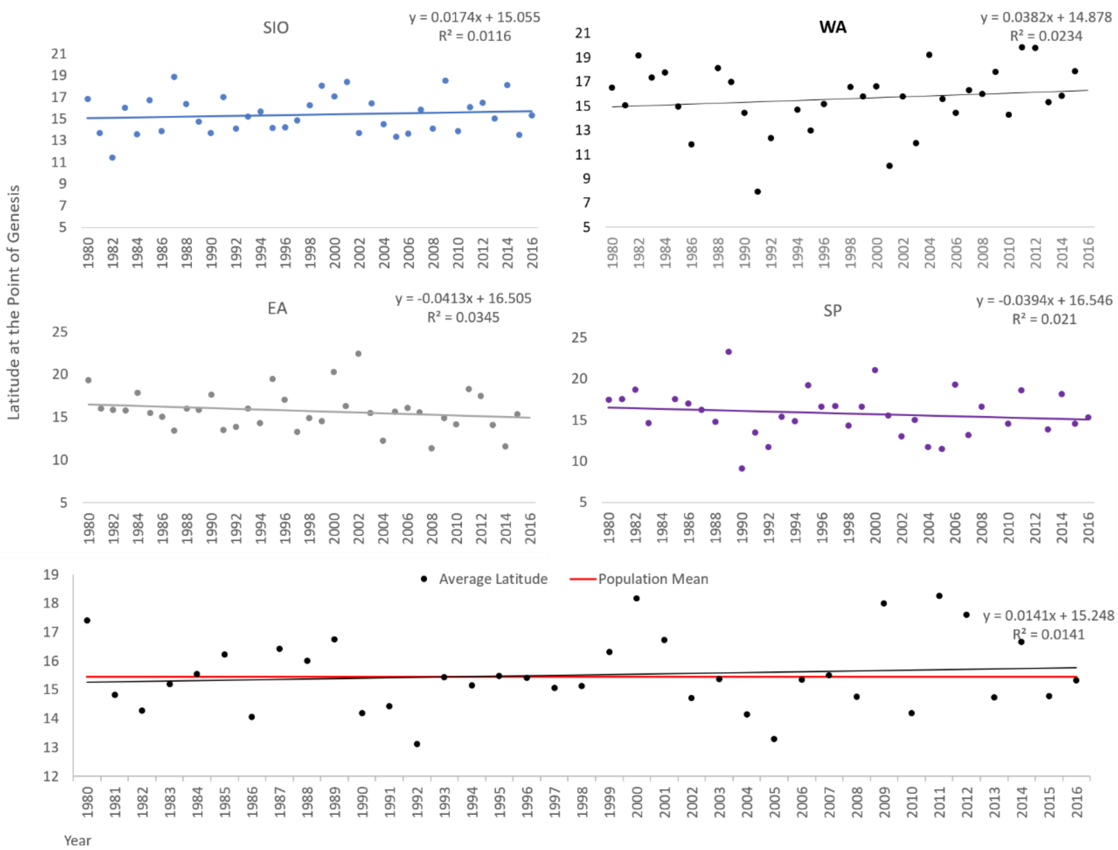

Figure 5.29 Time trends: Latitude of genesis for tropical cyclones from 1980-2016 (Nov-Apr) for individual basins and the combined hemisphere averages.

The locations of storm formation and the distribution over time is indicated by the storm density per decade from 1980-2016 (Figure 5.30). The first element to note is that the mean storm genesis location shifts with time in a latitudinal and longitudinal direction. From 1980-1999, there is a westward shift of the highest formation zone toward the Madagascan coastline. This is accompanied by a slight poleward shift and increase in storm density over this region. The genesis hotspot of the WA coast becomes slightly more diffuse but remains in its approximate position. The SP genesis hotspot of formation has become less intense and migrated westward. The zone over the EA bay area has disappeared. Regarding the 2000-2016 period (Figure 5.30), the SIO zones of formation have migrated further west, with the development of a southwestward component extending further down into the Mozambique Channel of the coast of Southern Africa. The formation zone of the WA coastline is still stationary compared to the 1999 period. The SP formation zone has become increasingly diffuse and has migrated eastwards relative to its eastward position. The 2010-2016 period is not a full decade, however, at the equatorward extent of the formation zone, there is more storm activity observed below the 10°S region, indicating an overall migration of activity away from the equator. During the 1999-2016 period there appears to be more storm events in the Mozambique channel. These density maps (Figure 5.30) along with the boundary of activity (Figure 5.27) reflect the poleward migration of storm formation zones to an extent, and provides a visual reference for the modest rates of change observed in the time trend graphs on latitude of storm genesis in the Southern Hemisphere (Figure 5.29).

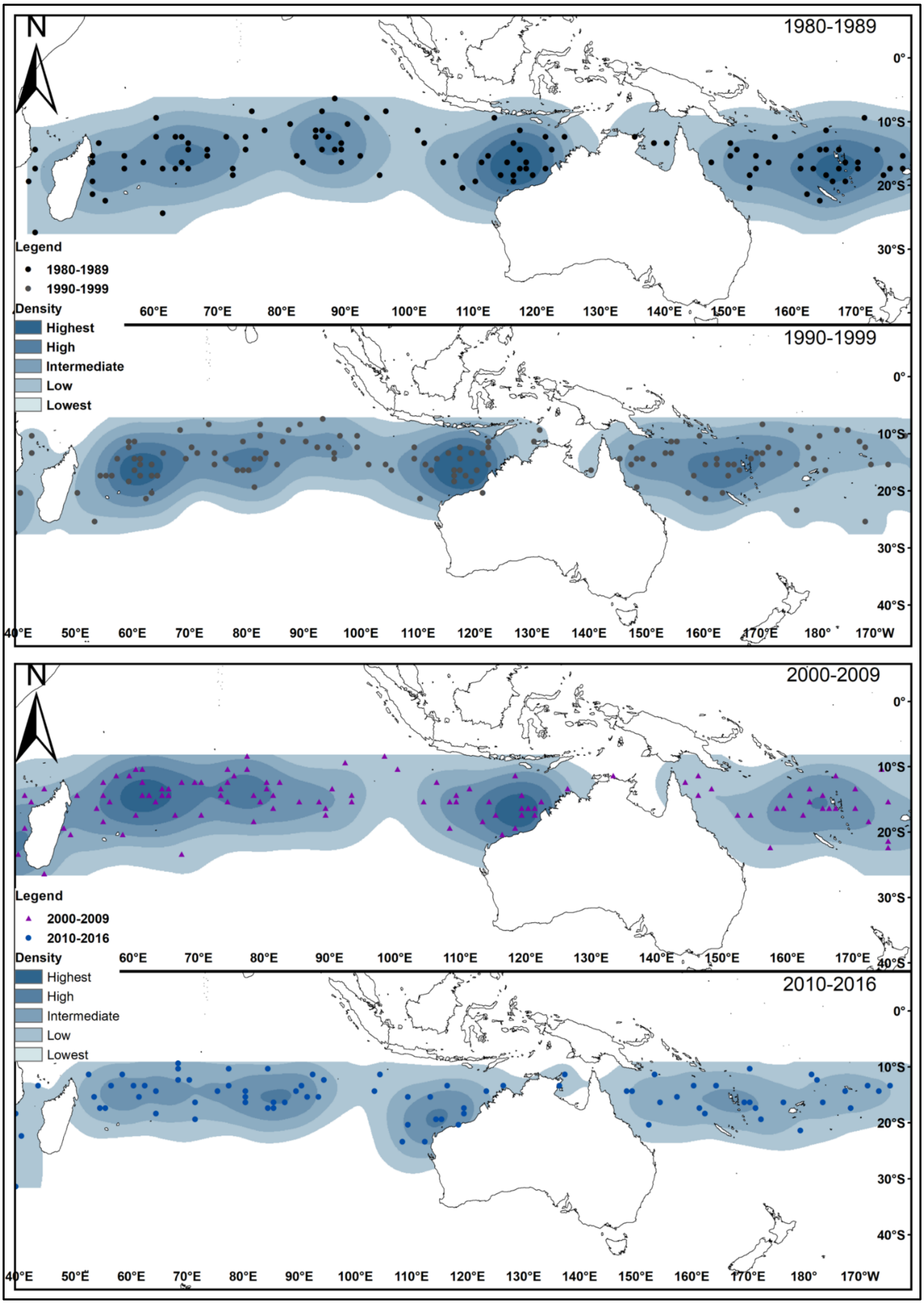

Figure 5.30 Density maps indicating regions of highest and lowest storm genesis from a) 1980-1999 and b) 2000-2016.

5.4.1.4 Change in Longitude of Tropical Cyclone Genesis

The longitude for Southern Hemisphere tropical cyclones at the point of genesis (Figure 5.31) does not provide substantial information on storm activity, however, the proximity to coastlines and whether storms are forming closer to them can be described. No significant trends were found for longitude at the point of genesis. The longitudinal shift for the location of SIO storm genesis is decreasing at a rate of 0.06°E.yr^{-1} (r=-0.14, p=0.4629), while an increasing shift of 0.05°W.yr^{-1} (r=0.07, p=0.7117) was observed for the WA storm genesis locations. The longitudinal shift recorded for the EA genesis locations is decreasing by a rate of 0.15°E.yr^{-1} (r= -0.23, p=0.2168), while for the SP storm genesis locations, a shift of 0.05°W.yr^{-1} (r=0.07, p=0.7287) was observed. The overall shift observed for the Southern Hemisphere genesis locations was 0.25°E.yr^{-1} (r=-0.13, p=0.4783). The highest rate of change regarding longitude was observed for the EA region, with an eastward shift toward the Indian Ocean. The EA and SP storms indicate a shift in longitude away from the Australian landmass and over the SP Ocean. The mean longitude of genesis for all Southern Hemisphere tropical cyclones from 1980-1999 was 114°E, however, over the 2000-2016 period, the mean genesis has shifted eastward to 107°E, which is large change considering the mean longitude of genesis is 110°E.

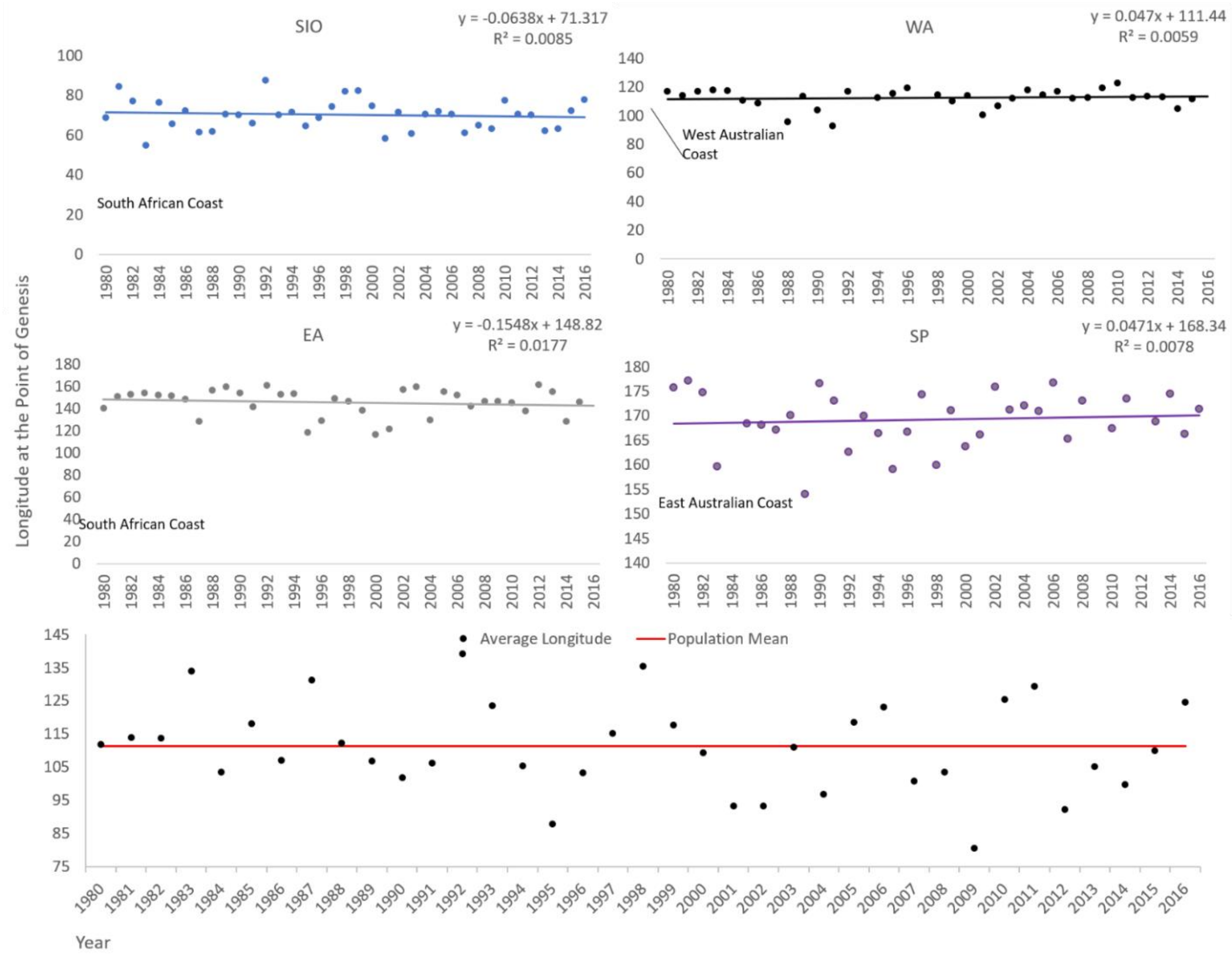

Figure 5.31 Time trends: Longitude of genesis for tropical cyclones from 1980-2016 (Nov-Apr) for individual basins and the combined hemisphere averages.

5.4.1.5 Duration of Tropical Cyclones

There are no statistically significant results related to the changing trends in tropical cyclone duration. For reference, the mean duration of tropical cyclones in the Southern Hemisphere is four days. The SIO especially has no meaningful change recorded for the duration of tropical cyclones (r=-0.0006, p=0.9976). The remaining three regions have extremely small magnitudes of change regarding the duration of their tropical cyclones with an increase of 0.008 days.yr^{-1} recorded for the WA region (r=0.13, p=0.4996), and 0.02 days.yr^{-1} recorded for the EA region (r=-0.16 p=0.4043). The decrease in tropical cyclone lifetime of 0.04

days.yr^{-1} (r=0.25 p=0.1846) was observed for the SP region. The rate of decrease observed in tropical cyclone duration for the hemisphere was 0.02 days.yr^{-1} (r=0.09, p=0.6491). In the WA, EA and SP regions, the trends indicate that the lifetime or duration at which a tropical cyclone persists is decreasing by a small and insignificant rate over time. For all storms in the hemisphere, storm lifetime indicates an increase, with more years experiencing above average days at tropical cyclone intensity (Figure 5.32). However, none of these trends can be interpreted meaningfully, due to the low correlations and p-values.

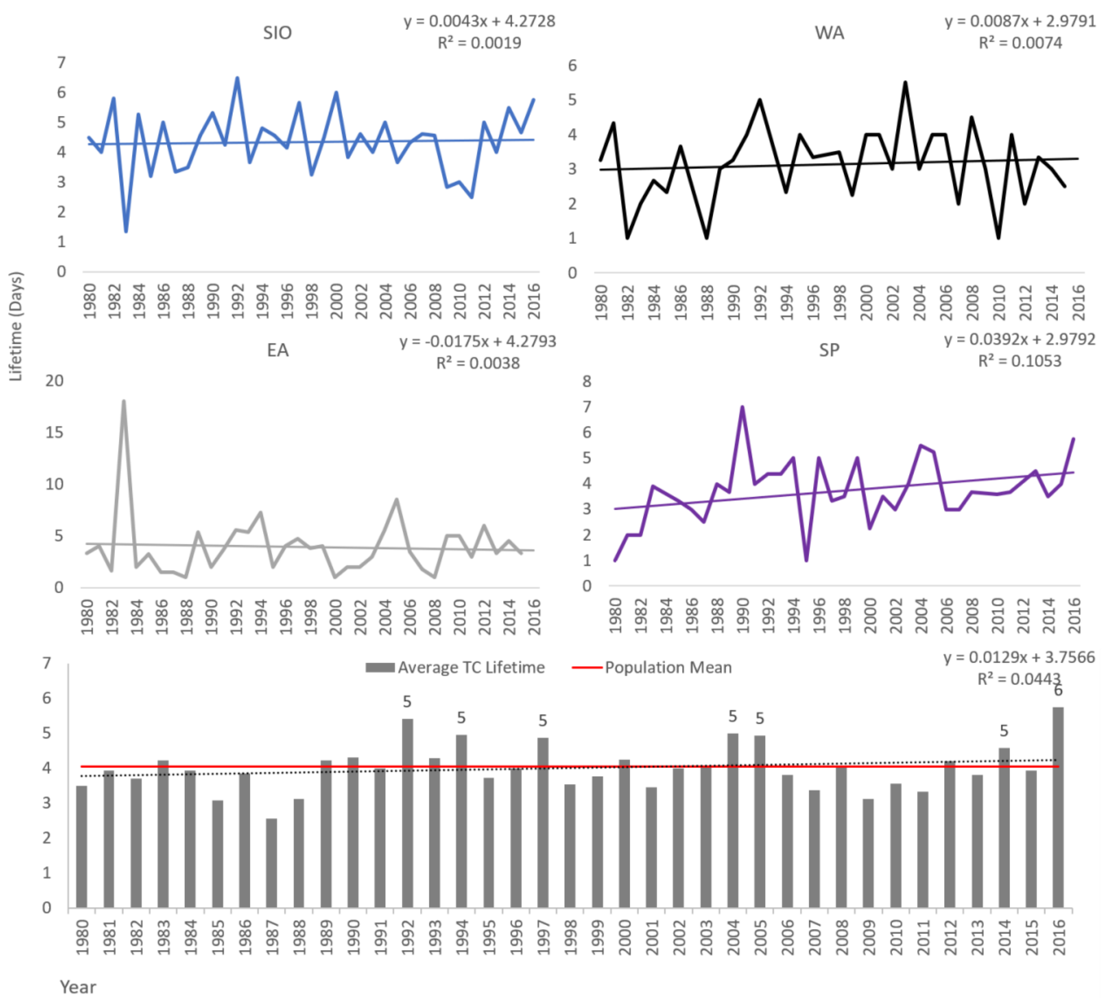

Figure 5.32 Time trends: Duration from genesis for tropical cyclones from 1980-2016 (Nov-Apr) for individual basins and the combined hemisphere averages.

These results supply a reference point for the state of change in the Southern Hemisphere storm metrics. However, the trend of change over time is masked by the high variability found in the tropical cyclone duration data, especially in the EA basin, which has storms with durations ranging from 9-15days ($\bar{X}$=12 days, SD=3.6) about the mean (Table 5.9). From 1980-1999 the mean lifetime of tropical cyclones was 3.9 days, which increased to 4.7 days over the 2000-2016 period.

5.4.1.6 Category of Intensity for Tropical Cyclones

The trends over time related to storm category according to the Saffir-Simpson scale, are examined for the combined number of Southern Hemisphere storms from 1980-2016. The number of category 1 storms display a statistically significant decreasing trend of 0.1.yr^{-1} (r=-0.5018, p=0.0016). Category 2 storms indicate a decrease in storm number of 0.01.yr^{-1} (r=-0.0382, p=0.8225). A moderate decreasing trend of 0.05.yr^{-1} (r=-0.3138, p=0.0586) is observed for category 3 storms. Category 4 storms indicate a strong and statistically significant increase of 0.08.yr^{-1} (r=0.4381, p=0.0067). Finally, category 5 storms indicate a strong statistically significant increase in storm number by a rate of 0.04.yr^{-1} (r=0.4406, p=0.0064). From these results, low intensity storms (category 1-3) are decreasing over time, while the high intensity storms (category 4-5) are increasing in number over time in the Southern Hemisphere. Within the last 16 years (2000-2016) an increased number of category 4 and 5 storms have successively exceeded their yearly mean counts (Figure 5.33), indicating that even within the increasing categories, there are extreme increases in the occurrence of high intensity tropical cyclones.

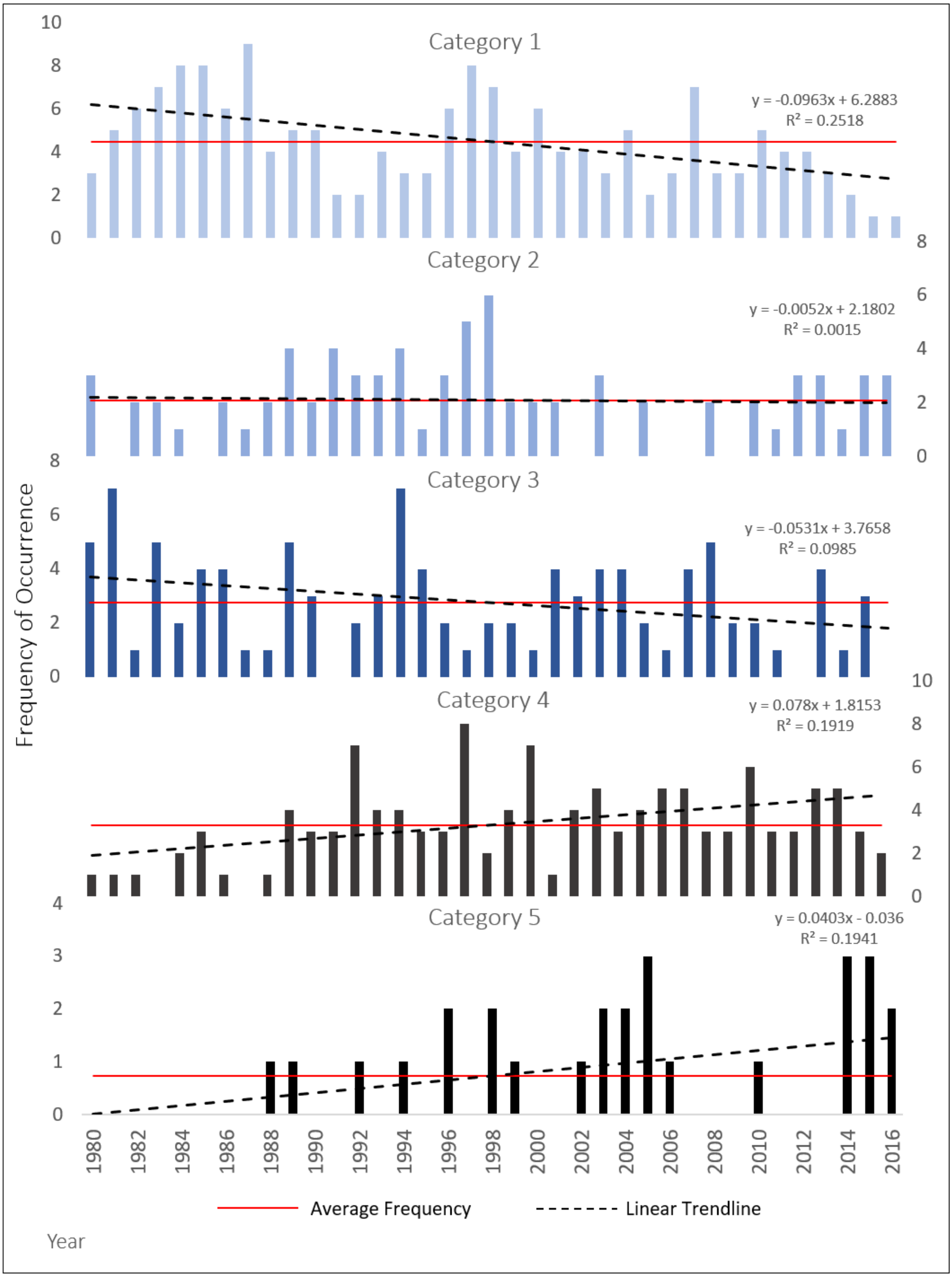

Figure 5.33 Tropical cyclone frequency per intensity category (category 1-5) according to the Saffir-Simpson scale.

5.4.2 Time Trends of Drivers at the Point of Genesis (1980-2016)

The time trends for the drivers (Table 5.22) examined here will include the thermodynamic variables of sea surface temperature, air temperature, and relative humidity at the 1,000mb and 850mb levels, and the dynamic variables which will include, omega, v-wind and u-wind shear and vertical wind shear during the time of storm genesis for all Southern Hemisphere tropical cyclones within the study period. Specifically, the change of magnitude for each variable will be examined for individual basins (SIO, WA, EA, SP) and then the Southern Hemisphere, which is denoted by the combined storm events from all four basins. The regression and statistical p-values for the relation of geopotential height and time are provided, however, geopotential height is not included as a driver, as it mainly provides information related to the height of pressure surfaces, and pressure is a metric representing tropical cyclone intensity, not a driver. These changes of magnitude over time for the climate drivers are specifically captured at the location and date of genesis. The increase is therefore specific to the tropical cyclone environment. These time trends of each climate driver at the point of genesis is calculated, with emphasis placed on how the magnitudes of these drivers at the point of genesis are changing and whether these trends of change are statistically significant for the Southern Hemisphere tropical cyclones.

5.4.2.1 Change in Sea Surface Temperature over Time During Genesis

An increasing trend in sea surface temperatures is observed at the point of genesis across all the basins and the Southern Hemisphere over the study period (Table 5.22). The increase in sea surface temperature is recorded as statistically significant for the SIO and SP basins. For the SIO storms, the rate of increase in sea surface temperature at the point of genesis is

0.02°C.yr^{-1} (r=0.45, p=0.0056). The change in sea surface temperature at the point of genesis in the SP region has increased by a rate of 0.03°C.yr^{-1} (r=0.46, p=0.0046).

Table 5.22 Time trends for drivers during storm genesis. r, p and R^2 values.

Driver	SIO	WA	EA	SP	Hemisphere Average
Sea surface temperature					
R^2	0.1993	0.0570	0.0048	0.2078	0.2650
r	0.4465	0.2388	0.0690	0.4559	0.5148
p	0.0056	0.1546	0.6850	0.0046	0.0011
Air Temperature 1,000mb					
R^2	0.3484	0.0546	0.0796	0.0072	0.3456
r	0.5902	0.2336	0.2822	0.0847	0.5879
p	0.0001	0.1640	0.0906	0.6180	0.0001
Air Temperature 850mb					
R^2	0.2071	0.0142	0.0065	0.0100	0.1363
r	0.4550	0.1193	0.0807	-0.0998	0.3692
p	0.0047	0.4819	0.6348	0.5566	0.0245
Omega 1,000mb					
R^2	0.0004	0.0113	0.0810	0.0446	0.1013
r	0.0205	-0.1061	-0.2845	-0.2112	0.3183
p	0.9042	0.5318	0.0879	0.2095	0.0549
Omega 850mb					
R^2	0.1475	0.0304	0.0290	0.1467	0.1927
r	-0.3841	-0.1744	-0.1703	-0.3830	0.4390
p	0.0189	0.3020	0.3137	0.0193	0.0066
Relative Humidity 1,000mb					
R^2	0.0607	0.0143	0.0419	0.0142	0.1531
r	-0.2463	-0.1194	-0.2047	0.1192	0.3913
p	0.1417	0.4814	0.2243	0.4823	0.0166
Relative Humidity 850mb					
R^2	0.0081	0.0161	0.0004	0.0775	0.0004
r	-0.0901	0.1267	-0.0204	0.2783	0.0205
p	0.5959	0.4548	0.9045	0.0953	0.9040
Vertical Shear					
R^2	0.0936	0.1599	0.0009	0.0178	0.0743
r	0.3060	0.3999	-0.0305	0.1332	0.2727
p	0.0655	0.0142	0.8579	0.4318	0.1025
Vwind shear (Meridional)					
R^2	0.1275	0.0778	0.0056	0.0831	0.0521
r	0.3571	0.2789	-0.0745	-0.2883	0.2282
p	0.0300	0.0946	0.6611	0.0835	0.1744
Uwind shear (Zonal)					
R^2	0.0726	0.0936	0.0143	0.0136	0.0018
r	-0.2695	0.3059	-0.1196	0.1167	0.0421
p	0.1068	0.0656	0.4809	0.4916	0.8046
Geopotential height 1,000mb					
R^2	0.3938	0.0193	0.0000	0.0013	0.0864
r	0.1068	-0.1735	-0.1995	-0.0629	0.2940
p	0.0002	0.4636	0.9948	0.8479	0.0774
Geopotential height 850mb					
R^2	0.2747	0.0024	0.0054	0.1082	0.0452
r	-0.6276	-0.1391	-0.0012	-0.0366	0.2126
p	0.0030	0.7971	0.6991	0.0759	0.2065

The WA and EA regions display no statistically significant trends in sea surface temperature during genesis. However, for the WA and EA storms, the rate of increase observed for sea surface temperature at the point of genesis for the WA storms is 0.02°C.yr^{-1} (r=0.24, p=0.1546) and 0.008°C.yr^{-1} (r=0.07, p=0.6850) for the EA storms. For all storms in the Southern Hemisphere, a statistically significant increase in sea surface temperature is observed at the point of genesis, with a rate of 0.02°C.yr^{-1} (r=0.51, p=0.0011). The results indicate that Southern Hemisphere storms are experiencing statistically significant increases in sea surface temperature during the phase of formation. Notably, the highest rate of sea surface temperature increase per year is observed for the SP storms. The first two decades from 1980-1999, indicate a mean sea surface temperature at the point of genesis of 27.42°C.yr^{-1}, with an increase of 0.03°C per decade (27.93 to 27.97°C) observed over the 1980-1999 period. However, from 2000-2016 the mean sea surface temperature at the point of genesis increased to 28.33°C. This reflects an increase of 0.91°C over the past 16 years, which is an increase of 0.6°C per decade from 2000-2016. This indicates that there was a low magnitude increase in Southern Hemisphere sea surface temperatures at the point of genesis from 1980-1999, which then indicates a greater rate of increase from 2000-2016. Examining the minimum and maximum sea surface temperatures at the point of genesis; both indicate an increase in magnitude over time (Figure 5.34). The minimum sea surface temperature indicates a statistically significant and larger magnitude of increase over time of 0.02°C.yr^{-1} (r=0.37, p=0.024) while maximum temperatures are increasing by 0.01°C.yr^{-1} (r=0.31, r=0.058). Therefore, the increasing trends of mean, minimum and maximum sea surface temperatures, indicates that Southern Hemisphere storms are forming at higher temperatures than previously observed.

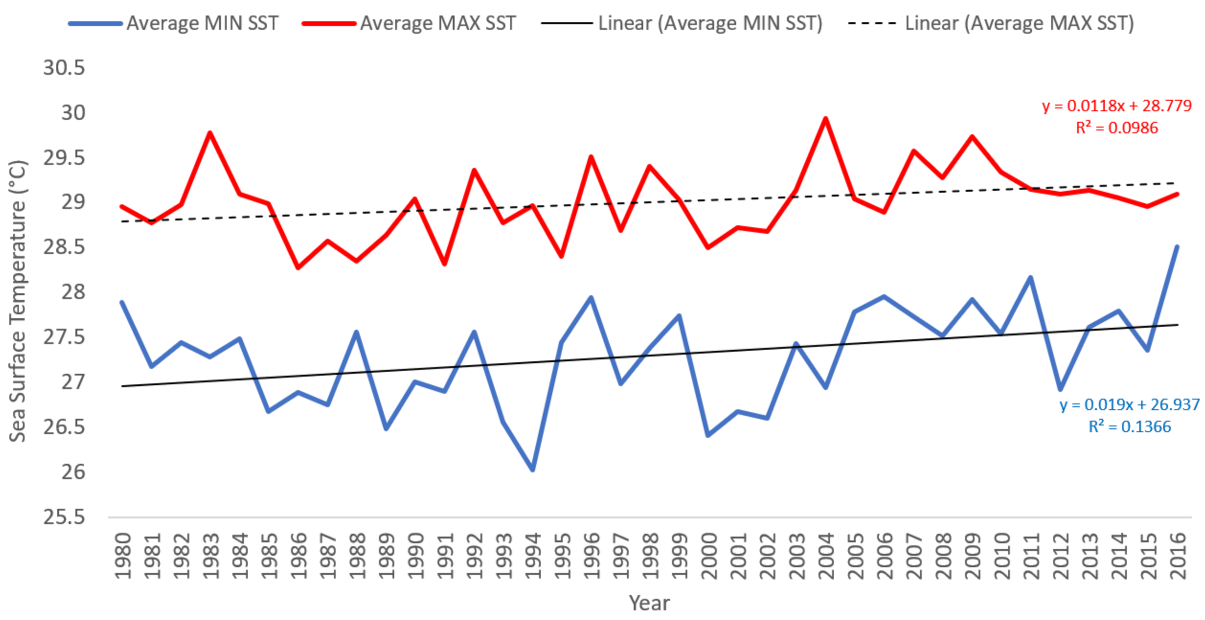

Figure 5.34 Minimum and maximum sea surface temperatures at the point of storm genesis. Change and rate of change over time, with linear regression best fit line and equation for both min and max metrics.

5.4.2.2 Change in Air Temperature over Time During Genesis

During the point of genesis, an increasing trend across all basins and the Southern Hemisphere is recorded for air temperature at the near surface level of 1,000mb (Table 5.22). The only statistically significant increase in air temperature at the 1,000mb level was recorded for the SIO storms, with an observed rate of 0.04°C.yr^{-1} (r=0.5902, p=0.0001). For the remaining basins, an increasing rate of 0.02°C.yr^{-1} (r=0.2336, p=0.1640) for the WA storms, 0.02°C.yr^{-1} (r=0.2822, p=0.0906) for the EA storms and 0.006°C.yr^{-1} (r=0.0847, p=0.6180) for the SP storms was observed. For all the storms in the Southern Hemisphere, a statistically significant increase of 0.02°C.yr^{-1} (r=0.52, p=0.0011) is observed in air temperature at the 1,000mb level.

During the point of genesis, an increasing trend across all basins and the Southern Hemisphere is recorded for air temperature at the 850mb level (Table 5.22). Similar to the trend for the 1,000mb level, at the 850mb level the only statistically significant trend in air temperature was found for the SIO storms, with an observed increase of 0.03°C.yr^{-1} (r=0.4550, p=0.0047). The change in air temperatures observed for the remaining basins during the point of genesis demonstrate an increasing rate of 0.007°C.yr^{-1} (r=0.1193, p=0.4819) for the WA storms, 0.02°C.yr^{-1} (r=0.0807, p=0.6348) for the EA storms and 0.006°C.yr^{-1} (r=-0.0998, p=0.5566) for the SP storms. For all the storms in the Southern Hemisphere, a statistically significant increase of 0.02°C.yr^{-1} (r=0.3692, p=0.0245) is observed in air temperature at the 850mb level.

The increasing trends for air temperature, are similar across the 1,000mb and 850mb levels. The SIO is the only basin which demonstrates a statistically significant increase in air temperature at both levels, with the 1,000mb level indicating a greater rate of increase in air temperature (+0.01°C) compared to the 850mb level during the point of genesis. The increasing trend observed for the Southern Hemisphere is also statistically significant across both the 1,000mb and 850mb levels, indicating that increasingly higher air temperatures are present during the time and over the locations at which storms are undergoing genesis. From 1980-1999 the mean air temperature at the 1,000mb level during genesis was 27.29°C and from 2000-2016 the mean air temperature was 27.83°C. This reflects a change of 0.56°C over 16 years with a rate of 0.4°C per decade from 2000-2016. At the 850mb level, a mean air temperature of 18.52°C was recorded from 1980-1999, and 18.85°C from 2000-2016. This reflects an increase of 0.33°C, at a rate of 0.2°C per decade from 2000-2016. Therefore, the increase in air temperature at the point of genesis is slower at the 850mb level compared to the 1,000mb level.

5.4.2.3 Change in Omega (Vertical Motion) over Time During Genesis

During the point of genesis, a decreasing trend across all basins and the Southern Hemisphere is recorded for omega/vertical velocity at the near surface level of 1,000mb (Table 5.22). There are no statistically significant trends observed for omega at this 1,000mb level. The rate of change observed in omega at the point of genesis is decreasing for SIO storms by a negligible degree. The trends in omega observed for the WA and EA storms, indicate a decrease of 0.0001pascal.s^{-1}.yr^{-1} (r=-0.1061, p=0.5318) and 0.0005pascal.s^{-1}.yr^{-1} (r=-0.2845, p=0.0879) respectively. A decreasing trend of 0.005pascal.s^{-1}.yr^{-1} (r=-0.2112, p=0.2095) was observed for the SP storms. For all storms in the Southern Hemisphere, a decrease of 0.018pascal.s^{-1}.yr^{-1} (r=0.3183, p=0.0549) is observed in omega at the 1,000mb level but falls short of statistical significance.

During the point of genesis, a decreasing trend across all basins and the Southern Hemisphere is recorded for omega/vertical motion at the 850mb level. A statistically significant decrease in omega at the 850mb level is observed for the SIO storms, with a rate of -0.002pascal.s^{-1}.yr^{-1} (r=-0.3841, p=0.0189). The trends observed for omega at the 850mb level for the WA and EA storms indicate a decreasing rate of 0.0009pascal.s^{-1}.yr^{-1} (r=-0.1744, p=0.3020) and 0.0005pascal.s^{-1}.yr^{-1} (r=-0.1703, p=0.3137) respectively. A statistically significant decrease of 0.005pascal.s^{-1}.yr^{-1}(r=-0.3830, p=0.0193) was observed for the SP storms. A statistically significant decrease of 0.018pascal.s^{-1}.yr^{-1} (r=0.4390, p=0.0066) in omega at the 850mb level, is observed for all the storms in Southern Hemisphere.

The overall trend in omega at the point of genesis, at both the 1,000mb and 850mb levels demonstrates a decrease. At the 1,000mb level the mean omega changes from -0.007pascal.s^{-1} during 1980-1999 to -0.013 during 2000-2016. As noted, this change is not statistically significant. At the 850mb level the magnitude of omega decreased from a mean of -0.16pascal.s^{-1} from 1980-1999 to -0.22pascal.s^{-1} during the 2000-2016 period. This is a decrease of 0.06pascal.s^{-1} at a rate of 0.004pascal.s^{-1}.yr^{-1}. Due to the nature of the omega value, it may appear that the changes are small in magnitude, however, the mean omega for the study period is -0.15pascal.s^{-1} and even changes of a small magnitude can influence this variable, as observed above. The statistically significant decrease in omega, observed during genesis for the individual regions (SIO and SP) and the Southern Hemisphere, indicates that omega values related to the 850mb levels of the storm genesis environment are changing over time. The overall decrease in omega indicates an increase in upward vertical velocity, which infers that at the point of genesis, increased buoyancy and horizontal convergence is present.

5.4.2.4 Change in Relative Humidity over Time During Genesis

During the point of genesis, a decreasing trend (Table 5.22) for relative humidity at the near surface level of 1,000mb is recorded across all basins except the SP, with a decreasing trend also recorded for all the storms in the Southern Hemisphere. A decreasing trend of relative humidity at the 1,000mb level is observed for the SIO storms, with a rate of 0.05%.yr^{-1} (r=-0.2463, p=0.1417). Decreasing trends of relative humidity at the point of genesis are observed for the WA and EA storms, with a rate of 0.04%.yr^{-1} (r=-0.1194, p=0.4814) and 0.09%.yr^{-1} (r=-0.2047, p=0.2243) respectively. An increasing trend in relative humidity is observed for the SP storms, with a rate of 0.01%.yr^{-1} (r=0.1192, p=0.4823). For all storms in the Southern Hemisphere, a statistically significant decrease of 0.02%.yr^{-1} (r=0.3913, p=0.0166) is observed in relative humidity at the 1,000mb level.

There are no statistically significant trends related to relative humidity at the 850mb level. During the point of genesis, an increasing trend in relative humidity at the 850mb level is recorded across all basins except the SIO, with a decreasing trend recorded for the all the storms in the Southern Hemisphere. A decreasing trend in relative humidity at the 850mb level is observed for the SIO storms, with a rate of 0.03%.yr^{-1} (r=-0.0901, p=0.5959). Decreasing rates of relative humidity for the WA and EA storms are observed, with a rate of 0.04%.yr^{-1} (r=0.1267, p=0.4548) and 0.02%.yr^{-1} (r=-0.0204, p=0.9045) respectively. An increasing rate of relative humidity is observed for the SP storms, with a rate of 0.22%.yr^{-1} (r=0.2783, p=0.0953). For all storms in the Southern Hemisphere, no statistical significance is observed for the decreasing trend of 0.02%.yr^{-1} (r=0.0205, p=0.9040) in relative humidity at the 850mb level during genesis.

Only relative humidity at the 1,000mb level for all the Southern Hemisphere storm occurrences, demonstrates a statistically significant rate of decrease over time. The SIO and SP are the only basins to demonstrate a consistent trend at both 1,000mb and 850mb levels. The relative humidity is decreasing at both levels in the SIO, while it is increasing at both levels in the SP. There is a decrease in relative humidity at the 1,000mb level during genesis for the other two basins (WA and EA), but an increase in relative humidity at the 850mb level. The mean relative humidity at the 1,000mb level was 82.3% from 1980-1999 and 81.25% from 2000-2016. This indicates an overall decrease, which as indicated is statistically significant. At the 850mb level, the mean relative humidity was 81.02% from 1980-1999 and 81.15% from 2000-2016. This is a negligible change in relative humidity.

5.4.2.5 Change in v-wind (Meridional) and u-wind (Zonal) Shear During Genesis

Statistically significant trends in v-wind shear (Table 5.22) are only observed for the SIO. In the SIO, v-wind shear observed at the point of genesis has been increasing at a rate of 0.006α.yr^{-1} (r=0.3571, p=0.0300). The v-wind shear for WA storms is increasing at a rate of 0.005α.yr^{-1} (r=0.2789, p=0.0946) and for the EA storms is decreasing at a rate of 0.001α.yr^{-1} (r=-0.0745, p=0.6611). The v-wind shear for the SP storms is decreasing at a rate of 0.005α.yr^{-1} (r=-0.2883, p=0.0835). For the Southern Hemisphere, the v-wind shear is increasing at a rate of 0.019α.yr^{-1} (r=0.2282, p=0.1744). The mean v-wind shear exponent from 1980-1999 was 0.007α and 0.038α from 2000-2016. The mean meridional shear exponent has therefore increased by a large magnitude and indicates an increase of v-wind shear over time of 0.031α at a mean rate of 0.01α per decade.

No statistically significant trends are observed for the u-wind component of shear (Table 5.21). In the SIO, u-wind shear observed at the point of genesis is decreasing at a rate of 0.003α.yr^{-1} (r=-0.2695, p=0.1068). The u-wind shear for the WA storms has been increasing at a rate of 0.009α.yr^{-1} (r=0.3059, p=0.0656) and decreasing for the EA region at a rate of 0.002α.yr^{-1} (r=-0.1196, p=0.4809). For the SP storms, u-wind shear at the point of genesis has been increasing at a rate of 0.001α.yr^{-1} (r=0.1167, p=0.4916). For the Southern Hemisphere, the magnitude of u-wind shear is increasing by 0.02α.yr^{-1} (r=0.1167, p=0.4916). The mean u-wind shear at the point of genesis from 1980-1999 was 0.052α and 0.072α from 2000-2016. This indicates an increasing trend of u-wind shear over time of 0.020α, with a mean rate of 0.01α per decade.

5.5 Multivariate Multiple Regression of Tropical Cyclone Activity, Drivers and Modes of Variability

Multivariate multiple regressions (Figure 5.35, Figure 5.36, Figure 5.37) were done following MANOVA tests. First the climate drivers (predictors) at the point of genesis and tropical cyclone metrics of activity (responses) at the point of genesis were run through multivariate regression. The response or dependent variables included storm and tropical cyclone lifetime (TC lifetime), latitude, longitude and TC season (frequency). Then the tropical cyclone metrics of activity (responses) were regressed against modes of variability (Niño 3.4, SOI, MEI, DMI, SAM, PDO and MJO). The tropical cyclone activity at the point which tropical cyclones attained their LMI was then run through multivariate regression against the modes of variability. The models for each metric of tropical cyclone activity are provided. These models are based on the co-efficients from the multivariate regression and compiled using a standard multiple regression equation in matrix format.

5.5.1 Climate Drivers/Variables at the Point of Genesis

From the multivariate multiple regression for the metrics of 493 tropical cyclones and their drivers (Figure 5.35), only air temperature (1,000mb), omega (850mb), relative humidity (1,000mb), relative humidity (850mb), sea level pressure and sea surface temperature demonstrate in so specific order, an influence over tropical cyclone lifetime, storm lifetime, category, latitude, longitude and seasonal occurrence (frequency) at a 0.05 significance level. The following are the specific metrics of Southern Hemisphere tropical cyclone activity and the climate drivers they demonstrate a statistically significant relationship with:

Storm lifetime is positively related to solar flux (p=0.029), indicating that as solar flux increases, storm lifetime increases. Tropical cyclone lifetime (the time the storm persists at category 1 or above), is related to sea surface temperature (p=<0.001). This infers that the higher the sea surface heat content, the longer the tropical cyclone will remain at category 1 or above. This agrees with the above results (Figure 5.6,Figure 5.28) which indicate storm category and lifetime are increasing along with the significantly increasing trend in sea surface temperature at the point of genesis. Therefore, the sea surface temperature (Table 5.22) at the point of genesis demonstrates a modulation on the duration and intensification of the Southern Hemisphere tropical cyclones. Related to this, the category of storm (1-5) is related to omega at 850mb (p=0.003:-) and v-wind shear (p=0.008) and to sea surface temperature (p=<0.001) and solar flux (p=0.025). This further indicates that the climate variables and their magnitudes at the point of genesis demonstrate a possible influence over tropical cyclone intensification. As omega and wind shear decrease and sea surface temperature and solar flux increase, then storm intensity increases. The latitude of genesis is related to omega at 1,000mb (p=0.022) and 850mb (p=<0.001:-) and relative humidity at 1,000mb (p=0.008) and 850mb (p= 0.006:+), sea surface temperature (p=<0.001) and u-wind shear (p=0.033). Therefore, as omega (1,000mb), relative humidity (850mb) and sea surface temperature increase, the latitude of genesis increases, which infers that the Southern Hemisphere tropical cyclones are favouring poleward formation as a result of the climate variables modulations at the point of storm formation. This also implies that if omega (850mb), relative humidity (1,000mb) and u-wind shear decrease or present negatively at the point of genesis, then the latitude of storm genesis could take place equatorward instead of poleward.

$$\begin{pmatrix} Total\ Lifetime \\ Tropical\ Cyclone\ Lifetime \\ Category\ (1-5) \\ \text{Latitude (Genesis)} \\ \text{Longitude (Genesis)} \\ \text{Number of TCs (Season)} \end{pmatrix} = \begin{pmatrix} -8.18 \\ 55.71 \\ -93.10 \\ -355.45 \\ -4199.85 \\ 2184.88 \end{pmatrix} + \begin{pmatrix} -0.49 \\ 0.56 \\ 0.06 \\ -0.31 \\ -10.25 \\ 3.32 \end{pmatrix}(AirT1) + \begin{pmatrix} 0.57 \\ 0.38 \\ -0.17 \\ -0.27 \\ -1.42 \\ 0.44 \end{pmatrix}(AirT2) + \begin{pmatrix} -3.39 \\ -0.13 \\ -0.03 \\ 13.42 \\ -47.14 \\ -6.56 \end{pmatrix}(Omega1)$$

$$+ \begin{pmatrix} -0.40 \\ -2.20 \\ -2.30 \\ -7.87 \\ 65.56 \\ -21.27 \end{pmatrix}(Omega2) + \begin{pmatrix} -0.09 \\ -0.05 \\ -2.30 \\ -0.15 \\ -1.06 \\ -0.27 \end{pmatrix}(RH1) + \begin{pmatrix} 0.07 \\ 0.04 \\ 0.00 \\ 0.08 \\ 1.32 \\ 0.12 \end{pmatrix}(RH2) + \begin{pmatrix} -0.01 \\ 0.15 \\ -0.03 \\ -0.13 \\ -2.82 \\ 0.22 \end{pmatrix}(GPH1)$$

$$+ \begin{pmatrix} 0.01 \\ -0.15 \\ 0.03 \\ 0.15 \\ 2.37 \\ -0.19 \end{pmatrix}(GPH2) + \begin{pmatrix} 0.003 \\ 0.12 \\ 0.05 \\ 0.11 \\ 1.03 \\ 0.00 \end{pmatrix}(Pressure) + \begin{pmatrix} 0.11 \\ 0.51 \\ 0.30 \\ 1.04 \\ 8.19 \\ -0.29 \end{pmatrix}(SST) + \begin{pmatrix} 0.01 \\ 0.004 \\ 0.00 \\ 0.00 \\ -0.03 \\ 0.01 \end{pmatrix}(Solar)$$

$$+ \begin{pmatrix} -0.83 \\ -0.61 \\ -0.46 \\ -0.79 \\ 2.89 \\ 0.38 \end{pmatrix}(Vshear) \begin{pmatrix} -0.10 \\ -0.04 \\ -0.33 \\ -1.03 \\ -11.00 \\ 1.20 \end{pmatrix}(Ushear)$$

Figure 5.35 Multivariate multiple regression model for southern hemisphere tropical cyclone metrics of activity (responses) demonstrating significant relationships to the climate variables/drivers (predictors) at the point of genesis.

The longitudinal dimension of genesis position is also related to omega (p=0.022) and relative humidity at the 850mb level (p=0.002) and sea surface temperature (p= 0.001). As these three factors increase in magnitude, then the longitude will of genesis will shift towards the east. Coincidentally, sea surface temperature is demonstrating an increase along with relative humidity at the 850mb level (Table 5.22), and longitude does demonstrate an eastward shift over time (Figure 5.31), thereby supporting the results of this regression. The tropical cyclone seasonal occurrence, which indicates frequency per year, is related to air temperature at 1,000mb (p=0.026) and omega at 850mb (p=0.001). As these factors increase, then the probability for increased storms per season increases.

$$\begin{pmatrix} Frequency \\ Latitude\ (Genesis) \\ Longitude\ (Genesis) \\ Total\ Lifetime\ (Genesis - Dissipation) \\ Tropical\ Cyclone\ Lifetime \end{pmatrix} = \begin{pmatrix} 2.75 \\ 17.92 \\ 100.35 \\ 8.45 \\ 4.11 \end{pmatrix} + \begin{pmatrix} 0.05 \\ -0.17 \\ 2.21 \\ -0.01 \\ 0.05 \end{pmatrix} (Volcano) + \begin{pmatrix} 1.29 \\ -0.21 \\ -23.62 \\ -0.95 \\ 0.39 \end{pmatrix} (Nino34) + \begin{pmatrix} 0.17 \\ 1.49 \\ 14.42 \\ -1.20 \\ -1.02 \end{pmatrix} (SOI)$$
$$+ \begin{pmatrix} 1.11 \\ 0.90 \\ 43.13 \\ 0.39 \\ -1.28 \end{pmatrix} (MEI) + \begin{pmatrix} 1.36 \\ 0.73 \\ -11.21 \\ 3.55 \\ -0.45 \end{pmatrix} (DMI) + \begin{pmatrix} 0.09 \\ -0.25 \\ 1.67 \\ -0.18 \\ 0.13 \end{pmatrix} (SAM) + \begin{pmatrix} 0.07 \\ -0.09 \\ 1.82 \\ -0.58 \\ -0.58 \end{pmatrix} (PDO)$$
$$+ \begin{pmatrix} 0.19 \\ -1.29 \\ -3.28 \\ 1.65 \\ 1.65 \end{pmatrix} (MJO)$$

Figure 5.36 Multivariate multiple regression model of southern hemisphere tropical cyclone metrics (responses) at the point of lifetime maximum intensity and the modes of variability (predictors). The models included are those with tropical cyclone metrics that demonstrated a statistically significant relationship with one or more of the modes of variability.

5.5.2 Modes of Variability

Modes of variability were run through multivariate multiple regression against tropical cyclone activity at the point of genesis (Figure 5.36). The following modes were related at a significance level of 0.05 to tropical cyclone activity at the point of genesis; longitude of genesis was related to volcanic activity (p=0.022), the Niño 3.4 index (p=0.017) and the multivariate ENSO index (p=0.002). This indicates that under increased volcanic activity and a positive ENSO, longitude of genesis is likely to shift eastward, while a negative ENSO event which manifests in the Niño 3.4 zone will influence storm location but favour a westward shift. Storm lifetime is related to the DMI (p=0.012), therefore in a positive Indian Ocean dipole stage, storms may have longer durations. Tropical cyclone lifetime is related to the SOI (p=0.016), and this suggests that tropical cyclone lifetime will increase when SIO is negative or ENSO is in a warm phase. The multivariate multiple regression suggests that the ENSO mechanism has the prevalent influence over Southern Hemisphere tropical cyclone activity, as the three indices used to measure an ENSO event are correlated to different aspects of tropical cyclone activity. Storm frequency and the latitude of genesis were not statistically related to any of the modes of variability. Of note is that the large-scale modulators such as PDO and SAM/AAO fail to demonstrate a modulative effect on tropical cyclone activity in the Southern Hemisphere.

$$\begin{pmatrix} Latitude\ (LMI) \\ Longitude\ (LMI) \\ Lifetime\ Maximum\ Intensity\ (m.s) \\ Duration\ at\ LMI \end{pmatrix} = \begin{pmatrix} 20.10 \\ 107.02 \\ 55.82 \\ 1.96 \end{pmatrix} + \begin{pmatrix} -0.09 \\ 2.42 \\ 0.21 \\ -0.01 \end{pmatrix}(Volcano) + \begin{pmatrix} 0.76 \\ -29.84 \\ 8.61 \\ -0.08 \end{pmatrix}(Nino34) + \begin{pmatrix} 0.75 \\ 17.38 \\ -0.77 \\ -0.27 \end{pmatrix}(SOI) + \begin{pmatrix} -0.93 \\ 56.21 \\ -9.94 \\ -0.18 \end{pmatrix}(MEI) + \begin{pmatrix} 0.28 \\ -23.66 \\ -8.89 \\ -0.24 \end{pmatrix}(DMI) + \begin{pmatrix} -0.10 \\ 3.91 \\ 2.26 \\ -0.02 \end{pmatrix}(SAM) + \begin{pmatrix} 0.16 \\ 0.83 \\ 0.84 \\ -0.09 \end{pmatrix}(PDO) + \begin{pmatrix} -1.57 \\ -9.08 \\ -3.19 \\ -0.15 \end{pmatrix}(MJO)$$

Figure 5.37 Multivariate multiple regression of southern hemisphere tropical cyclone activity and metrics (responses) at the point of genesis. The metrics included demonstrated a statistically significant relationship with one or more of the modes of variability (predictors) within each model.

Modes of variability were run through multivariate multiple regression against tropical cyclone activity during and related to the intensification stage (Figure 5.37). The following modes were related at a significance level of 0.05 to storm activity during the LMI phase; the longitude at which a tropical cyclones LMI was attained, demonstrated multiple relationships, starting with volcanic activity (p=0.022), the Niño 3.4 (p=0.007), SOI (p=0.033:+) and MEI (p=<0.001). These values indicate that when all the modes of variability are in a positive state, except for the Niño 3.4, then the longitude at which LMI takes place will increase, most likely in an eastward direction, therefore following the longitudinal pattern recorded at the point of genesis. The actual intensity a tropical cyclone attains in terms of wind speed is related to the Niño 3.4 ($p=0.026$) and the SAM ($p=0.046$). This indicates that a positive ENSO and SAM mode will favour the incidence of higher intensity in tropical cyclones. Once again, as with tropical cyclone activity at genesis, the ENSO variable scores highest in terms of demonstrating a relationship to the genesis and LMI phases of Southern Hemisphere tropical cyclone activity.

5.6 Results: Conclusion

5.6.1 Mean Conditions

The highest number of tropical cyclones are observed in the SIO, followed by the SP. The lowest occurrence of storms is observed in WA. The variability observed in each basin is similar for the SIO and SP, with high variability from the mean number of occurrences recorded for both these basins. A lower variability of storm occurrences is observed in the WA and EA regions, but with the smallest variability of storm occurrence recorded in the WA region. The tropical cyclone season for the Southern Hemisphere basins follow similar patterns, with a commencement in the summer months from November, a peak of activity in the February and March and a decline of activity over the April months. No tropical cyclone activity has been recorded for the June and July months. When the tropical cyclones form in the Southern Hemisphere basins, the locations of genesis are relatively constant. Uniformity is especially observed for the latitude of formation, with a majority of genesis events taking place from 11-21°S of the equator. The longitude of genesis is based on the basin, with a preferred region of formation recorded for each basin. For the SIO (60-80°E), the WA (107-117°E) the EA (133-160°E) and the SP (170-195°W). The tropical cyclones are additionally recorded to attain maximum intensity within these regions of formation. The intensity reached by the Southern Hemisphere tropical cyclones follows a pattern of decrease in numbers over time for the lower intensity storms (Category 1 to 3), but an increase in occurrence of high intensity storms (Category 4 to 5).

5.6.2 Drivers at the Point of Genesis

The climate drivers reflect the magnitudes of each driver during the genesis stage and were only examined for storms which reached tropical cyclone intensity (category 1). The magnitudes reflected at this time are therefore taken as the magnitudes which played an influential role in allowing the storm to form and attain tropical cyclone intensity, and also influenced the duration, lifetime and intensity of the tropical cyclone. By applying histograms which provide a distribution (bins/intervals) of the magnitude for each driver and the number of storms which fall within each magnitude interval, the magnitudes at which the majority of storms were determined. The magnitude at which the greatest number of storms form, indicates that these are therefore optimal or preferential magnitudes which are more likely to promote successful storm genesis. The use of the histograms also indicated that no threshold exists for any driver, and that even while more storms tended to form at specific optimal intervals, there were instances where storms formed outside of these preferential magnitudes. While these drivers indicate that they play an influential role in the storm genesis stage, it does not discount or rule out the existence or influence of other potential drivers or factors for tropical cyclone genesis. This is supported by the factor analysis, as the drivers examined in this study only account for approximately 50% of the variability at the point of genesis, which implies that other factors not examined in this study account for the other 50%. From these optimal and minimum magnitudes, which were based on the distribution data for climate drivers, genesis flow charts were also created. These genesis flow charts offer the optimal scenarios at which the greatest number of storms have undergone genesis. The minimum conditions required for a storm genesis event i.e. the observed minimum, as storms may have formed under smaller magnitudes, but were not captured in our study data or regions. The minimum magnitudes required for a Southern Hemisphere category 5 tropical cyclone are also captured in the flow charts, which is an attempt to link the genesis drivers to the intensification process.

5.6.3 Change over Time in Tropical Cyclone Activity

The changes in tropical cyclone activity were used to examine the metrics which are changing significantly over the 1980-2016 period and expose the implications this would have on the zones of formation and intensification, frequency and intensity as they relate to tropical cyclones. Tropical cyclone frequency for all Southern Hemisphere basins is decreasing, while LMI or the highest intensity attained by tropical cyclones across their lifetime is increasing across the Southern Hemisphere by 2.4 $m.s^{-1}$ per decade as recorded from 1980-2016. This is synchronous with the increased occurrence of in high intensity tropical cyclones in the Southern Hemisphere over this time period. The western basin (SIO and WA) tropical cyclones are undergoing genesis at increasingly poleward latitudes, while the eastern basin (EA and SP) tropical cyclones are forming at latitudes closer to the equator. Both these rates of change are not significant. However, it highlights a disparity between conditions over the east and west regions of the Southern Hemisphere. The density distribution of tropical cyclone formation indicates an overall poleward shift in tropical cyclone genesis locations, and an eastward migration of these zones for the SIO and SP tropical cyclones.

5.6.4 Change over Time in the Magnitude of Drivers at the Point of Genesis

The drivers or the climate variables which have known and potential influences over tropical cyclone formation were examined over time, to observe how these formation factors were changing over time and whether these changes are linked to above alterations of tropical cyclone activity. Importantly, since these variable were extracted for the location and time of each tropical cyclone genesis event from 1980-2016, if any changes were taking place for them, it would infer that the alterations of these drivers are a product of climate change, which would infer an impact of climate change on the genesis environment of tropical cyclones of the Southern Hemisphere. The drivers examined include the thermodynamic (sea surface and air temperature, relative humidity and solar flux) and the dynamic (wind shear and vertical motion) variables at the 1,000mb and 850mb levels, which provides a vertical section of the environment at the point of genesis. From the variables examined omega, v-wind and u-wind shear and solar flux are new variable being examined at the point of genesis. All variables except omega at the 1,000mb level and u-wind shear do not demonstrate a statistically significant change over time. At the point of genesis for the combined basins, sea surface temperature, air temperature (both levels), relative humidity (850mb), vertical shear and v-wind and u-wind shear demonstrate an increase in magnitude over 1980-2016. Omega (both levels) and relative humidity (1,000mb) demonstrate a decrease in magnitude over 1980-2016. However, regarding v-wind shear, an increasing trend is observed in the western basins (SIO and WA), while a decreasing trend is observed in the eastern basins (EA and especially the SP).

5.6.5 Response to Genesis Drivers and Modes of Variability

The use of multivariate regression was applied in examining the modes of variability and how they relate and influence tropical cyclone activity and the climate drivers at the point of genesis. The major results indicate that it is primarily the ENSO indices (Niño 3.4, SOI and MEI) which are statistically related to tropical cyclone activity and the climate drivers at the point of genesis. The remaining major modes such as the SAM and PDO, which drive large changes of the ocean and atmosphere and which were expected to indicate some forcing on tropical cyclone activity and the climate drivers at the point of genesis did not demonstrate such relationships. The regression equations constructed from the multivariate regression offer models which can be used as a predictor. Based on the different magnitude inputs for the drivers and modes of variability, these models can provide an output of the possible tropical cyclone activity for the Southern Hemisphere as a whole.

The results of this study demonstrate new information and provides an update to existing work (Table 2.1, Table 2.2) regarding trends and change in tropical cyclone activity, in addition to new genesis parameters which influence storm formation such as omega and v-wind shear. The genesis flow diagrams created here provide a simplified tool to use as a benchmark to compare tropical cyclone activity. The optimal magnitudes for each large-scale environmental/climate variable at the point of genesis provide information on the preferred or most influential magnitudes of the known and new influencers of tropical cyclone genesis. The multivariate regression allowed for the modelled response of the metrics of tropical cyclone activity to a set of independent variables or predictors in place of the usual linear regression and therefore models considers the complex interactions between the predictors and the resultant effect on the response variable such as tropical cyclone duration and frequency. Importantly, there is also indication that the climate variables at the point of genesis have an influence over the intensification phase and duration of the Southern Hemisphere tropical cyclones.

6. Discussion

6. Introduction: Discussion

6.1. New Southern Hemispheric Conditions of Formation

One of the earliest studies examining the formation of tropical cyclones was carried out by Palmen (1948), which provided a qualitative formation theory and put forward the 26.5°C sea surface temperature as the threshold required for tropical cyclone formation. The environmental conditions and mechanisms which influence tropical cyclone formation, as established by Gray (1968, 1979), were some of the earliest quantitative investigations. These studies by Gray (1968, 1975, 1977, 1979, 1998) provided an understanding of tropical cyclone formation and a seasonal genesis index, which detailed the influencing variables driving tropical cyclone genesis. Gray's research has since been applied in both observational and model-based tropical cyclone studies (Menkes *et al*., 2012; Murakami *et al*., 2012a; Camargo, 2013; Li *et al*., 2013; Yu *et al*., 2016; Klotzbach *et al*., 2017). However, since the establishment of these conditions for formation, there has been limited re-examinations or revisions regarding tropical cyclone genesis climatology (Defforge & Merlis, 2017a; Bhatia *et al*., 2019).

The studies that did investigate drivers of tropical cyclone genesis, explored one aspect such as sea surface temperature (Dare & McBride, 2011; Defforge & Merlis, 2017a), relative humidity (Li *et al*., 2013) and pressure (Kuleshov *et al*., 2008). This is indeed seen as a deficiency in the research, as the indices by Gray (1968, 1979) were created at a time when the tropical cyclone data for the Southern Hemisphere were scarce and heterogeneous, as they were derived from multiple sources at differing resolutions, with relatively low-quality and quantity of data for the Southern Hemisphere existing prior to 1980 (Watterson *et al*, 1995; Landsea *et al*., 2006).

This first section of the discussion will present the new formation parameters for tropical cyclones in the Southern Hemisphere, with a focus on the minimum magnitudes of the climate variables and the most frequent or optimal magnitudes observed at the point of genesis (i.e. the climatological magnitudes) from 1980-2016. Then these new conditions will be evaluated in relation to the existing conditions of genesis. The comparison between the southern and Northern Hemisphere conditions and the possible reasons behind any divergence will be presented, followed by the implications of the findings with a focus on the implications for the genesis sea surface temperature thresholds. The changes over time in tropical cyclone activity and the climate drivers/variables at the point of genesis will then be discussed, with the implications of these changes also examined. Modes of variability, climate drivers and their influence on tropical cyclone activity will also be included.

6.1.1. New Mean Conditions of Formation for Southern Hemisphere Storms

In this study, the climate variables were examined at the point of tropical cyclone genesis for 493 storm events in the Southern Hemisphere, to determine the most frequent (optimal) and minimum climatological conditions present at the time of tropical cyclone formation. The genesis flow charts (Figure 5.22,Figure 5.23,Figure 5.24) present the minimum and optimal magnitudes of each climate variable at the point of genesis, the greatest storm intensity these magnitudes are observed to support, and the factor weighting outlining the influence which each climate variable had on storm formation.

6.1.1.1 Mean Thermodynamic Factors

The average sea surface temperature at the point of genesis for the Southern Hemisphere, was approximately 28°C. Regarding the sea surface temperatures at the point of genesis, a difference is present between the western regions (SIO and WA) and eastern regions (EA and SP). The western regions have mean sea surface temperatures of 28°C, while the eastern regions have a mean sea surface temperature of +28.4°C recorded at the time of genesis (Table 5.10). The maximum sea surface temperatures over the eastern regions was 29°C, and 30°C over the western regions. There are similar findings, where the eastern regions of the South Indian Ocean (80-100°E) indicated lower mean sea surface temperatures of 28.3-29.8°C during tropical cyclone genesis, while higher sea surface temperatures of 29.3-30.3°C were reported for the western (50-80°E) regions (Mavume *et al*., 2009). Similarly, Defforge and Merlis (2017a, b) reported that the Southern Hemisphere basins display higher sea surface temperatures at the point of tropical cyclone genesis, compared to the North Atlantic region, which has a lower mean sea surface temperature of 25.7°C observed during genesis. In the South Pacific, the lowest genesis sea surface temperature observed was 27°C (Defforge & Merlis, 2017a). It is specifically when the Northern Hemisphere basin sea surface temperatures are factored in, that the overall mean magnitude decreases to 26.5°C, due to the climatologically cooler genesis sea surface temperatures observed for the northern basin storms (Defforge & Merlis, 2017a). Since it is only the average which reflects the 26.5°C threshold, it does not perform as an accurate or realistic value, and its application over the Southern Hemisphere may not be viable as a benchmark or threshold for storm genesis (Defforge & Merlis, 2017a).

Mean air temperature at the near surface, closely follows the sea surface temperature with an average of 27.5°C for the Southern Hemisphere. This observation (Figure 5.10) for the Southern Hemisphere air temperature, may reflect the thermodynamic air-sea interaction (heat exchange) observed between the ocean surface and lower atmosphere (Evans &

Waters, 2012; Evans & Webster, 2014). At the point of tropical cyclone formation, i.e. the high sea surface temperature also increases the near surface air temperature, which in turn promotes an enhanced buoyant environment that can support deep moist convection (Lin *et al*., 2009; Zhou *et al*., 2017). Additionally, solar flux observed during Southern Hemisphere tropical cyclone genesis, demonstrates a relatively high magnitude of 185 $W.m^{-2}$ (Figure 5.21). The main paper on solar flux by Li *et al*. (2018) indicated that higher solar flux magnitudes, such as those found within this study are not only related to increased tropical cyclone intensity, but also demonstrated a high correlation to changes in global tropical cyclone activity. The mean relative humidity of above 80% at the point of genesis was substantially high for the majority of storms (Figure 5.14, Figure 5.15), which is expected, as it is a core requirement for initiating and sustaining tropical cyclone development and results from the large amount of convection and evaporation taking place during storm genesis (McGauley & Nolan, 2012; Juracic & Raymond, 2016).

6.1.1.2 Mean Dynamic Factors

The meridional wind shear coefficient (averaged at 0.02α) was found to be relatively low for the Southern Hemisphere storms (Figure 5.17). The mean vertical shear of 3 $m.s^{-1}$ (Figure 5.18) falls well below the value of 15 $m.s^{-1}$ reported in the published requirements for tropical cyclone genesis (Gray, 1977, 1979; Klotzbach *et al*., 2017; Bhaskaran *et al*., 2018). The relatively low mean shear is expected, as storms have a higher likelihood of forming in lower shear environments (Nolan & Rappin, 2008). The mean omega of -0.01$pascal.s^{-1}$ (1,000mb) and -0.15$pascal.s^{-1}$ (850mb) were recorded for Southern Hemisphere tropical cyclones. This indicates an upward motion or large vertical velocity, which appears to increase as height increases, and therefore highlights that the movement of air has less resistance, i.e. more air rises at negative omega values (Song *et al*., 2018). The upward vertical motion represented by omega, also indicates the presence of surface convergence (Figure 4.2), which is usually present at the point of genesis (Gray, 1975; Bhaskaran *et al*., 2018). This infers that omega is a potentially reliable metric for indicating vertical motion in the atmosphere, as it indicates the buoyant conditions present during storm genesis. This assumption is based on the observation that a highly unstable atmosphere and rising air (conditional instability) promotes tropical cyclone genesis (Gray, 1968; McTaggart-Cowan *et al*., 2013; Klotzbach *et al*., 2017; Song *et al*., 2018). Song *et al*. (2018) reported that regions with similarly large (negative) magnitudes of omega at a 500mb height, promote convection and tropical cyclone genesis. Overall, the mean values for each climate variable indicate agreement with existing studies (Gray, 1979; McTaggart-Cowan *et al*., 2013; Klotzbach *et al*., 2017), except for sea surface temperature, which demonstrates higher magnitudes in the Southern Hemisphere than for those reported by global studies (Dare & McBride, 2011; Tory & Dare, 2015; Defforge & Merlis, 2017a). Omega, however, offers a new insight into measuring vertical motion and by extension inferring the presence of surface convergence within the genesis environment.

6.1.2. Observed Minimum Formation Factors

6.1.2.1 Minimum Thermodynamic Factors

The minimum formation factors are derived from the smallest possible magnitude of each climate variable at which a storm underwent genesis. The minimum magnitudes recorded at the point of genesis for sea surface temperature was 24-25°C, and for air temperature was 19-24°C (1,000mb) and 9-16°C (850mb). Once again as with the mean air temperature, the minimum air temperatures at the point of genesis follow the minimum sea surface temperatures (Table 5.10). This indicates that sea surface temperature during genesis interacts with air temperature, mainly by warming the near surface air to a similar degree as the sea surface, as also observed by other studies (Farfan *et al*., 2006; Lin *et al*., 2009; Evans & Webster, 2014). The minimum sea surface temperatures reported by existing tropical cyclone genesis studies, have also observed minimum magnitudes at the point of genesis which fall below 25°C, however, as found within this study (Figure 5.8), only a small proportion of storms formed at these minimum sea surface temperatures (Dare & McBride, 2011; McTaggart-Cowan *et al*., 2015; Tory & Dare, 2015; Defforge & Merlis, 2017a; Bhaskaran *et al*., 2018). It has also been observed that many of the storms resulting from the lower sea surface temperatures (termed non-tropical forming storms) occurred near the end of the basins tropical cyclone season and were characterised as weak shallow tropical cyclones (Mauk & Hobgood, 2012). Similar situations are observed for the storms that formed below 26°C in the Southern Hemisphere, which underwent genesis after April or before November and did not attain an intensity above category 1 (Table 5.4 Table 5.7). Therefore, it appears that while low sea surface temperature genesis events are possible, the storms do not attain high intensities, which appears to be a common observation globally (Evans & Webster, 2014; Tory & Dare,2015; Defforge & Merlis, 2017a).

The lowest intervals of relative humidity range from 63-74% (1,000mb) and 37-67% (850mb). There are no specific magnitudes of moisture content required for formation, only that relative humidity should be above 50-60% to allow deep convection (or cumulonimbus convection) to occur and should extend from the lower to mid troposphere (DeMaria *et al*., 2001; McGauley & Nolan, 2011; Wu *et al*., 2015). Within this study the presence of high relative humidity is observed for a majority of storms (Figure 5.14). In addition, tropical cyclone formation rarely occurs when relative humidity is below 40% (Gray, 1977). Indeed, there are only two cases where relative humidity at the 850mb level was <40% at the time of genesis within this study. The minimum solar flux at the point of genesis ranges from 62-88W.m^{-2}. The observation that fewer storms occur at low solar flux indicates a preference for higher magnitudes of solar flux for tropical cyclone genesis. There is a high correlation to tropical cyclone activity in earlier studies as mentioned, and solar flux is a possible metric of the environmental energy available for storms to utilise, however, there are no studies that have labelled solar flux as a specific driver of tropical cyclone activity (Li *et al*., 2018). It may be that the values are only high at the point of genesis, as a result of tropical cyclones occurring during the summer months, when solar energy input is naturally at a greater magnitude (Camargo *et al*., 2010; Menkes *et al*., 2012; Vecchi *et al*., 2014).

During the point of genesis, the climate variables do not indicate that a preferential threshold value is required for the tropical cyclone formation. The existence of these minimum values observed for each variable during tropical cyclone genesis, indicates that while the Southern Hemisphere tropical cyclones have preferential conditions of formation they are able to undergo genesis at these minimum magnitudes that fall below observed the thresholds, specifically for sea surface temperature and vertical shear (Gray, 1968, 1979; Klotzbach *et al*., 2017).

6.1.2.2 Minimum Dynamic Factors

Vertical wind shear was observed to occur at a minimum interval of 0.4-1.4 m.s^{-1}, however, there were only a few storms which occurred when the vertical shear was this low (Figure 5.18). This is in contradiction with multiple studies on wind shear during tropical cyclone genesis (Gray, 1975; Emanuel, 2010; Tippett *et al*., 2011), which state that a wind shear of 0

$m.s^{-1}$ is the best magnitude for tropical cyclone genesis. However, Nolan and Rappin (2008) reported that Southern Hemisphere tropical cyclone formation and intensification are less likely to occur as efficiently when shear is extremely low (< 1.25 $m.s^{-1}$), which is largely consistent with the results for the Southern Hemisphere storms of this study (Figure 5.18,Table 5.14). Therefore, these northern hemispheric based studies outlining the vertical shear at the point of genesis do not appear to apply within this study, as only a few storms form below 1-2 $m.s^{-1}$ (Figure 5.18). Model-based studies continue to demonstrate that when the climate drivers at the point of tropical cyclone genesis are equalised (using idealised frameworks), lower shear does enhance the frequency of tropical cyclone genesis events (Tory & Frank, 2010; Korty *et al*., 2012a; Yu *et al*., 2016). This again supports the results (Figure 5.18) that more storms tend to prefer lower shear values, however, an absence of shear is just as detrimental to storm genesis and intensification, as tropical cyclones have been observed to intensify and form much more efficiently when some presence of vertical shear was observed over the genesis environment (Nolan & McGauley, 2012; L. Zhang *et al*., 2017).

Regarding wind shear components at the point of genesis, the lowest intervals of v-wind shear (meridional shear) were observed as -1.56 to -0.21α, while u-wind shear (zonal shear) were observed as -1.48 to -0.36α. Essentially, vertical shear is derived from these shear components, therefore larger values of these components indicate a larger vertical shear, and the resultant impacts associated with higher shear should also be observed (Finocchio & Majumdar, 2017). Similar to vertical shear, very few storms form at these high magnitudes of zonal and meridional shear, as these values indicate a large shear co-efficient (Vecchi & Soden, 2007; Osuri *et al*., 2012; Xue *et al*., 2014). The lowest omega intervals that storms formed at were -0.17 to -0.10pascal.s^{-1} (1,000mb) and -0.72 to -0.39pascal.s^{-1} (850mb). This demonstrates that if the negative magnitude of omega is enhanced by a large factor, then there may be a decreased number of storms forming. This holds true in the positive direction (Figure 5.12, Figure 5.13), as comparatively large positive values of omega have been linked to lower occurrences of tropical cyclone genesis (Song *et al*., 2018). More investigation is required regarding the dynamics of omega, a deficit in studies examining omega during tropical cyclone genesis exists (Song *et al*., 2018).

6.1.3. Frequent Formation Factors for Southern Hemisphere Tropical Cyclones

Special attention was given to the optimal intervals at which the majority of storms formed, since they do not represent a threshold, but a preferred range which is observed for the majority of tropical cyclone genesis events in the Southern Hemisphere. The optimal magnitudes for the climate variables are reported at multiple heights and indicates the preferential range of magnitude at which the largest number of storms formed. Apart from these optimal magnitudes, only a few storms form at the extreme minimum or maximum intervals of each climate variable examined. Therefore, these optimal magnitudes can be inferred as the most likely conditions that a tropical cyclone can form under. The following are the optimal conditions of the climate variables which promote the highest number of tropical cyclone formation events in the Southern Hemisphere and are listed as follows:

1) Sea surface temperature: 27.5-28.5°C
2) Air Temperature: 27°C-28°C (1,000mb) and 18-19°C (850mb)
3) Omega: -0.01-0.01pascal.s^{-1} (1,000mb) and -0.18- -0.07pascal.s^{-1} (850mb)
4) Relative Humidity: 79-83% (1,000mb) and 75-88% (850mb)

5) Meridional shear (v-wind component): -0.06-0.24α and Zonal shear (u-wind component): -0.08-0.20α
6) Vertical shear: 1-4 $m.s^{-1}$ (1,000mb-850mb)
7) Solar Flux: 140-218$W.m^{-2}$ (upper atmosphere)

The sea surface temperatures at the point of genesis found within this study are significantly greater than the 26.5°C threshold established in Gray (1968, 1979) or the 25.5°C threshold presented in recent research (Dare & McBride, 2011; Tory & Dare, 2015; Defforge & Merlis, 2017a). Specifically, when examining the Northern Hemisphere sea surface temperature thresholds (see Table 2.3), the majority of the magnitudes do not exceed 26°C-27°C (Fisher, 1958; Wendland, 1977; Defforge *et al*., 2017). Therefore, the higher distribution of sea surface temperature magnitudes observed at the point of genesis, may be due to the Southern Hemispheres climatologically warmer sea surface temperatures present during storm genesis (Defforge & Merlis, 2017a, b), or the recent trends of warming observed in the southern basins (Durack *et al*., 2018; Zhang *et al*., 2018). It is projected that under a warming ocean regime, the increased frequency of high intensity tropical cyclones is a result of decreasing vertical shear (L. Zhang *et al*., 2017). However, observations have found that locally, higher sea surface temperatures cannot overcome the dampening effect which vertical shear has on tropical cyclone genesis, but instead, could enhance the negative effects of vertical shear, consequently decreasing the formation potential (Nolan & Rappin, 2008). As for the minimum and mean scenarios, the air temperature at the point of genesis closely follows the magnitude of the sea surface temperature. It is reasonable to state that the optimal air temperature (Figure 5.10, Figure 5.11) is also higher during the majority of tropical cyclone genesis events, as a result of it following the higher sea surface temperatures present during genesis (Evans & Webster, 2014). Some studies have questioned the modulative effect of sea surface temperature on tropical cyclone genesis (Vecchi & Soden, 2007; Tory & Dare, 2015). However, factor analysis weightings reveal that sea surface and air temperature both scored highest in terms of accounting for the variability at the point of genesis (Table 5.18, Table 5.19). This observation can serve as indication that sea surface temperature may have an important modulative effect on tropical cyclone formation.

It should be highlighted that the sea surface temperature and air temperature do not present a large correlation regarding their explanation of variability for the higher intensity storms (Category 5 specifically). Instead, meridional shear, relative humidity and omega (vertical motion) account for the majority of the variability for these major storms at the point of genesis. This indicates that for the majority of storms, the sea and air temperatures are important, but regarding high intensity storms, v-wind shear and omega become more important. This aspect is similarly reflected in the following studies (see: Nolan & McGauley, 2012; Li *et al*., 2013; L. Zhang *et al*., 2017), where vertical shear begins to have a comparatively larger deterministic effect on the intensification of a storm; exceedingly low shear can weaken intensification and exceedingly high shear can cause the storm to dissipate. Similarly, with reference to omega, if vertical motion is low (inferring weak convection), then the storm remains at a low category of intensity, alternatively, with greater convection and upward motion, the environment is reported to promote greater storm intensification (Bracken & Bosart, 2000; Li *et al*., 2013; Song *et al*., 2018). At a larger scale this ocean atmospheric interaction is noted, where changes in the thermohaline circulation (the oceans conveyor of heat energy) instigated the shift of the warmer tropical temperatures poleward, as well as the characteristic regions of low pressure, increased convective activity and vertical shear associated with these tropical environments (Dong & Sutton, 2005). Therefore, the migration of the conditions considered conducive for storm formation are now found poleward of the normal formation zones (Daloz & Camargo, 2018). Within this study, the locations at which storms undergo genesis and intensification have similarly indicated a shift poleward from 1980-2016 (Figure 5.1).

It appears that the majority of tropical cyclone genesis events take place when omega is both in a negative or positive state (-ve or +ve motion) at the near surface level (Figure 5.12). However, it should be noted that omega is a large-scale environmental driver, and its magnitude is derived over a large region, and may not be representative of the vertical motion over a storm's local environment (Hastenrath & Greischar, 2001; Song *et al*., 2018). Additionally, at the near surface level, the majority of storms fall within this positive and negative range (-0.01 to 0.01pascal.s^{-1}), which does not provide a clear picture on the atmospheric motion required for storm genesis, therefore only using surface magnitudes of omega are insufficient to describe upward motion (Bracken & Bosart, 2000; Song *et al*., 2018). However, when factoring in the 850mb level, omega does display a clear negative interval, indicating strong upward motion present during genesis (Figure 5.13).The average equatorial omega, where the highest vertical velocities are present, is approximately -0.05pascal.s^{-1} (Kiranmayi & Maloni, 2011). This is expected, as the overall magnitude of omega should indicate an upward motion, as it coincides with positive vorticity (Franklin *et al*., 1996; Bracken & Bosart, 2000; Song *et al*., 2018). In comparison the 850mb omega at the point of genesis for Southern Hemisphere storms, is much greater in magnitude, which is expected with the strong vertical motion from deep convection inherent within cyclogenesis environments (Bracken & Bosart, 2000; Hastenrath & Greischar, 2001). This indicates that at the 850mb level, omega is much more robust when representing the vertical motion of the environment at the point of genesis. While omega has not been used in tropical cyclone studies regularly, its application as a proxy of vertical motion for the atmosphere at the point of genesis, performs sufficiently as it provides reliable information regarding the large-scale upward motion in the environment within this study and in Song *et al*. (2018). Additionally, factor analysis has indicated that omega accounts for a high percentage of variability in storm genesis (Table 5.18). However, more investigations into this are required, to verify the influence of omega on storm genesis, with specific focus on the eligibility of the reanalysis II datasets representation of omega.

Relative humidity is optimal at any value above 75 % over the 1,000mb and 850mb levels. Since this is above the threshold of 50-60% required for deep moist convection, this interval at which the majority of storms occur makes climatological sense and agrees with the existing literature (Gray, 1977, 1979; McGauley & Nolan, 2011; Wu *et al*., 2015). This study indicates two things regarding relative humidity during the majority of genesis events; firstly, is that the moisture in the atmosphere has to extend to the mid troposphere in the majority of tropical cyclone genesis events, indicating that deep moist convection is present, and secondly, a high moisture content from the surface to the 850mb level is required. The moisture in the atmosphere is required to saturate the air column as a result of convection, which drives warm saturated air upwards (McGauley & Nolan, 2011; Bhaskaran *et al*., 2018). This column must be sustained to allow continual inflow of more moisture and deep convection to take place (McGauley & Nolan, 2011). Consequently, this mechanism is stated as a major requirement in multiple observational (Gray,1968,1979; Farfan *et al*., 2006;

McGauley & Nolan, 2011; Li *et al*., 2013; Bhaskaran *et al*., 2018) and model-based studies (Parodi & Emanuel, 2009; Sahany *et al*., 2012; Wu *et al*., 2015; Yu *et al*., 2016).

With regard to the optimal vertical shear (1-4 $m.s^{-1}$) observed for the Southern Hemisphere storms (Figure 5.18), compared to the optimal shear of 12-15 $m.s^{-1}$ in the Northern Hemisphere, this is a relatively low optimal range (Klotzbach *et al*., 2017). Optimal vertical shear has been reported at larger magnitudes during genesis in the Northern Hemisphere compared to the Southern Hemisphere (Nolan & Rappin, 2008). The required vertical wind shear is usually just below 12-15 $m.s^{-1}$ (25 knots), in the North Atlantic and Pacific regions (DeMaria *et al*., 2001; Nolan & Rappin, 2008). However, lower optimal shear appears to be preferred by storms in the Southern Hemisphere, as it is observed that the majority of tropical cyclone genesis events take place when vertical shear is between 1.25-5 $m.s^{-1}$, which agrees closely with the optimal shear (1-4 $m.s^{-1}$) recorded in this study (Nolan & McGauley, 2012).

The optimal ranges of meridional shear and zonal shear coefficients are comparatively low (Figure 5.16, Figure 5.17), indicating that storms have preference for such magnitudes during genesis, similar to the requirements of vertical shear (Finocchio & Majumdar, 2017). These shear components also indicate an almost equal number of storms occurring within a negative and positive magnitude. This is explained by the different wind shear directions. Positive (negative) shear values indicate westerly (easterly) flows for zonal shear, while positive (negative) shear indicates a northward (southward) flow for meridional shear; however, regardless of shear direction, as long as the wind shear magnitude is optimal, storm genesis is possible (Nolan & Rappin, 2008; Na *et al*., 2018). Relating to directionality of shear, easterly shear has been shown to favour tropical cyclone formation during its genesis phase to a greater extent, compared to westerly shear (Nolan & McGauley, 2012). Indeed, Na *et al*. (2018) reported a relationship between easterly and westerly wind shear, where increased sea surface temperature decreases westerly wind shear and promotes an increase of tropical cyclone intensity. Since the vertical, zonal and meridional shear observed for Southern Hemisphere storms are already comparatively low, the warming of sea surface and air temperatures could further decrease wind shear, and thereby increase tropical cyclone genesis and intensification potential (Nolan & McGauley, 2012; Emanuel, 2013).

Solar flux may similarly play a role in decreasing vertical wind shear as outlined by Li *et al*. (2018), whereby increased solar flux heats the atmosphere, ultimately modulating sea surface and tropospheric temperatures and vertical shear, thereby increasing tropical cyclone activity. This is currently only a plausible mechanism, as the exact modulations of solar flux on the tropical cyclone genesis is not well understood (Li *et al*., 2018). It must be noted that these optimal formation magnitudes for the climate variables (Table 5.17) indicate the values at which tropical cyclone genesis has the highest likelihood of taking place in the Southern Hemisphere. However, the maximum and minimum values indicate that even when these optimal conditions are not met, there is still a possibility of tropical cyclone genesis taking place.

6.1.4 Summary of Findings for the Southern Hemisphere

The values presented for each climate variable during the point of tropical cyclone genesis, serves as the first climatology of tropical cyclone genesis, constructed solely from Southern Hemisphere storms and high-resolution climate data outside of the long-accepted indices by Gray (1968, 1979). The results of this study indicate a lower minimum sea surface temperature at which tropical cyclone genesis is possible for the Southern Hemisphere. The sea surface temperature at which a majority of tropical cyclones undergo genesis in the Southern Hemisphere, however, falls within a higher range than the widely used 26.5°C threshold. Instead, this study agrees more closely to Defforge & Merlis (2017a), who despite agreeing on a threshold at 26.4°C do recognise that the different basins follow sea surface thresholds or magnitudes closer to the basin's climatology. Since the Southern Hemisphere has climatologically warmer genesis sea surface temperatures overall, with the majority of storms from the individual basins (SIO, EA, WA and SP) forming at warmer sea surface temperatures than in the Northern Hemisphere, (Korty *et al*., 2012b; Evans & Webster, 2014; Defforge & Merlis, 2017b; Zhang *et al*., 2018), it can be safely surmised that the Southern Hemisphere tropical cyclones have a significant and substantially different sea surface temperature requirement for tropical cyclone genesis. This highlights that the 26.5°C threshold cannot be applied with confidence for Southern Hemisphere tropical cyclone genesis, or in studies of Southern Hemisphere tropical cyclones. As mentioned, the variables/drivers have magnitudes which indicate preferential genesis conditions, so while there are storms that form at extreme minimum and maximum magnitudes, the majority of Southern Hemisphere tropical cyclones display a tendency to form under the aforementioned optimal peak magnitudes/intervals observed for each climate driver.

While new variables were introduced such as the omega value in place of relative vorticity, the use of the omega value does indicate a pattern in its magnitude during tropical cyclone genesis. Consequently, as omega defines vertical motion, which is highly important in assessing the instability or resistance of upward motion in the atmosphere, it has provided a new parameter with which to apply to genesis indices. Relative humidity and air temperature were in range of the expected values reported by Gray (1968, 1977, 1979). Solar flux demonstrates higher magnitudes during the point of genesis, however, it is a large-scale parameter and its specific modulation is not understood fully. A plausible mechanism describing the influence of solar flux on the climate system is detailed in Li *et al*., 2019), where higher solar flux influences vertical shear (decreases), cloud cover (decreases) and sea surface temperature (increases) indirectly via atmospheric heating and geomagnetic activity, to favour tropical cyclone genesis (Li *et al*., 2018).

6.1.5 Gray's Conditions of Formation and New Examinations

The seasonal genesis index by Gray (1968, 1979, 1998) has been accepted and used widely, as he was the first to quantify the parameters required for tropical cyclone formation. However, the studies while global in their focus were primarily based on the Northern Hemisphere track data (Watterson *et al*., 1995; Ramsay *et al*., 2008). While the Southern Hemisphere and its tropical cyclone occurrences were included, these data were not as reliable or exhaustive as the Northern Hemispheres at the time (Landsea *et al*., 2006; Schreck *et al*., 2014). Regarding the formation parameters, a sea surface isotherm of 26.5°C was found to extend throughout the tropical regions of the ocean basins (Gray, 1968). It was stated that this initiated and sustained high potential buoyancy (ability of air to rise) and therefore the ability for the large cloud formation, which in turn warms the troposphere and creates the initial disturbance, which begins the genesis phase of a tropical cyclone. (Gray, 1979). The increase in surface temperatures and humidity were also found to drive increases in the environment's potential buoyancy (Gray, 1998; Klotzbach *et al*., 2017). Specifically, it was observed to only take a 1°C increase in tropospheric temperatures and a 4mb decrease in pressure to initiate a disturbance intense enough to form a storm (Gray, 1968). As demonstrated in this study (Table 5.7) this general rule is plausible in the Southern Hemisphere, as for each degree of increased sea surface temperatures, more storms occur, with the higher intensity (lowest pressure) storms occurring at relatively higher sea surface temperatures and is also observed by (Kuleshov *et al*., 2010). Gray (1968, 1979) similarly examined the zonal wind shear component, and found that a small or almost zero magnitude of shear was associated with the majority of tropical cyclone genesis events. Meridional shear had no correlation of significance to tropical cyclone genesis (Klotzbach *et al*., 2017). The premise behind vorticity is that it initiates strong surface convergence which enhances the cyclonic upward motion and inflow of moisture into the higher regions of the storm (Gray, 1968; Parodi & Emanuel, 2009).

As it stands the latest factors outlined by Gray's latest contribution in Klotzbach *et al*. (2017) required for tropical cyclone formation and as first stated by Gray (1968, 1975 1979, 1998) are:

1) Warm ocean (26.5°C), well mixed to a 60m depth
2) Conditional instability
3) Low level vorticity
4) Weak vertical wind shear
5) High moisture in the mid troposphere
6) Coriolis force; must occur up to 5°N/S of the equator

[Gray, 1975: pp 30-31; Klotzbach *et al*., 2017: pp. 2321-2322]

These parameters (Section 2.2.1) have not changed much since Gray (1968, 1979) quantified their influence for tropical cyclone genesis. While most of the pioneering works on tropical cyclone genesis climatology and the influencing climate drivers were done by Gray (1968, 1979, 1998), other studies (Watterson *et al*., 1995; Dare & McBride, 2011; Tory *et al*., 2013; Tory & Dare, 2015; Defforge & Merlis, 2017a) have re-examined aspects of this initial framework for tropical cyclone genesis. While the climate drivers of tropical cyclone genesis such as moisture, vorticity, wind shear and a conditionally unstable atmosphere have been confirmed and tested in observational studies (Emanuel, 2005; McPhaden *et al*., 2009; Li *et al*., 2013; Yu *et al*., 2016 et al., 2016 *et al*., 2015) and model-based studies (Evans & Waters, 2012; Ying & Zhang, 2012; Halperin *et al*., 2013; Wu *et al*., 2015; Huangfu *et al*., 2018), sea surface temperature has remained a highly problematic factor to reconcile within models or confirm a threshold for across ocean basins during the point of genesis, due to its variable nature observed across the different basins and hemispheres (Mauk & Hobgood, 2012; Defforge & Merlis, 2017a) The studies that have relevance here, mainly examine the metric of sea surface temperature required for tropical cyclone genesis (Dare & McBride, 2011; Tory & Dare, 2015; Defforge & Merlis, 2017a). In these sea surface threshold studies, Dare and McBride (2011) find that the majority of storms occur at a mean of 25.5°C, which is supported by Tory and Dare (2011), however, lower sea surface temperatures are found only in storms which underwent a gestation (development period) of 18 hours, while it is observed that storms which had a 24-hour gestation period, tend to occur at the 26.5°C threshold. In the study by Defforge & Merlis (2017a) it was stated that the threshold is 26.4°C, but this is only a result of averaging thresholds which were computed from climatologically cooler sea surface temperature formation thresholds in some basins and the warmer thresholds in the others (See Section 6.1.1.1). It is clear that none of these studies have found the sea surface temperature threshold that agrees in totality with this study. This is attributed to their focus on Northern Hemisphere tropical cyclones, or on the global trends, which creates an average that suppresses the Southern Hemispheres relatively high genesis sea surface temperatures at which tropical cyclones form and follow (Mavume *et al*., 2009; Defforge & Merlis, 2017a; Fitchett, 2018).

6.1.6 Variation in Conditions of Formation

This study has demonstrated considerable differences between the existing formation-characteristics of tropical cyclone formation and those observed specifically for the Southern Hemisphere. While sea surface thresholds have been considered important for tropical cyclone genesis and intensification, there are formation events that take place in cold ocean regions and are instead driven by baroclinic influences (see Section 2.3.3.2), which is when temperature gradients exist at a constant pressure (Tory & Dare, 2015; Defforge & Merlis, 2017a). As such sea surface temperature, while important for the majority of formation events, is not all encompassing. This allows for a certain amount of variability in the climate drivers at the point of genesis for each basin and hemisphere (Defforge & Merlis, 2017a; L. Zhang *et al*., 2017). Specifically, Defforge & Merlis (2017a) reported that each basin is climatologically different regarding their average sea surface temperature at the point of genesis. The north Atlantic has the comparatively coldest sea surface temperature thresholds recorded during storm genesis events, while the west Pacific has the warmest thresholds (Defforge & Merlis, 2017a). Within this study, the eastern basins demonstrate greater sea surface temperatures (Section 6.1.1) at the point of genesis compared to the western basins (SIO and WA) and this could be attributed to the greater poleward migration of the 28-29°C isotherm (Figure 3.2) and conducive conditions for storm formation over the EA and SP regions (Tennille & Ellis, 2017) , but could also be attributed to the location of the ITCZ or Diagonal Convergence Zone present over the EA and SP genesis zones (Figure 3.3).

The observation that none of the climate drivers in this study indicate extreme or large changes between the minimum and optimal intervals in the analysis of the histogram distribution, along with relatively smooth transitions between the intervals indicate that the concept of thresholds is not altogether reliable. That is, a storm is not guaranteed to form, even if the thermodynamic climatic conditions are met precisely, and may instead form at an extreme outside of the dedicated thresholds, and in this regard the Southern Hemisphere study agrees with existing studies (McGauley & Nolan, 2011; Defforge & Merlis, 2017a), that a threshold for sea surface temperature may not exist or be plausible, if there are instances observed, where storms have formed outside the threshold.

6.1.6.1 Dynamic Physical Environments

The changing climate and heat-energy structure of the ocean is driving a poleward shift in the mean genesis location of tropical cyclones (Altman *et al*., 2018). However, the rate of the migration differs between the northern and Southern Hemisphere (Kossin *et al*., 2014; Daloz & Camargo, 2018). The Southern Hemisphere demonstrates a larger poleward shift in its sea surface temperature isotherms (Durack *et al*., 2018; Zhang *et al*., 2018; Fitchett, 2018), and in the overall genesis and intensification regions of its tropical cyclones (Kossin *et al*., 2014). This not only shifts favourable and warmer sea surface temperature conditions further poleward, but also the high moisture and convective conditions associated with tropical regions known to be conducive for tropical cyclones (Walsh *et al*., 2016; Daloz & Camargo, 2018). Over the Northern Hemisphere tropics, high sea surface temperatures and low vertical shear are found to increase the occurrence of high intensity storms, while closer to the poles tropical cyclone occurrence is comparatively low, as the oceans are cooler and shear is relatively stronger, (Nolan & McGauley, 2012; L. Zhang *et al*., 2017; Na *et al*., 2018).

Similarly, this study finds that the highest intensity tropical cyclones in the Southern Hemisphere also tend to occur closer to the tropical regions (Figure 5.3, Figure 5.5). Since the poleward migration of tropical conditions is larger for the Southern Hemisphere, the zones of tropical cyclone formation are also migrating poleward faster in the Southern Hemisphere as observed by Kossin *et al*. (2014). This would indicate that the effects of this migration on tropical cyclones will be observed sooner in the poleward regions of the Southern Hemisphere than the north (Daloz & Camargo, 2018). This changes the genesis potential and intensification potential in the Southern Hemisphere in comparison to the Northern Hemisphere, offering another avenue of difference between them, as the mean magnitudes of the climate variables at the point of genesis may also present differently in each hemisphere as a result of the different poleward distribution of heat and tropical conditions (Daloz & Camargo, 2018).

The climatological backgrounds of the northern and Southern Hemisphere and, by extension, each basin is unique (Defforge & Merlis, 2017a). The climatological vertical shear in the North Pacific for one thing, is relatively small (Gray, 1998; Song *et al*., 2018). While the regions that have no tropical cyclone activity or genesis events display climatologically strong magnitudes of vertical shear, which innately inhibits tropical cyclone activity (Nolan & Rappin, 2008). This can account for the higher overall tropical cyclone occurrence in the Southern Hemisphere compared to others, as almost a third of global tropical cyclone events take place here (Diamond *et al*., 2013). Compared to paleo-studies documenting the climate from around 6000 years ago, the Southern Hemisphere receives comparatively more solar radiation than the Northern Hemisphere, during the span of its tropical cyclone season which occurs during the Southern Hemisphere summer (Korty *et al*., 2012a). This may partially account for the higher mean sea surface temperatures observed in the Southern Hemisphere, the larger poleward migration of the sea surface temperature isotherms (Fitchett, 2018; Tennille & Ellis, 2017), the locations of tropical cyclone genesis and intensification (Kossin *et al*., 2014; Daloz & Camargo, 2018) and plausibly explains why the tropical cyclones in the Southern Hemisphere have larger magnitudes of sea surface temperatures during a majority of their tropical cyclone genesis events compared to the Northern Hemisphere.

One of the major drivers responsible for the differences between the south and north hemispheric tropical cyclone activity at an annual scale is the interseasonal variability (Chang-seng & Jury, 2010). During the respective hemispheres summer months, when the sea surface temperatures and moisture are highest and vertical shear is usually at its lowest, the conditions for tropical cyclone genesis are optimal (Nolan & McGauley, 2012; Menkes *et al*., 2012). This is the fundamental difference between the hemispheres, as tropical cyclones follow the warmest seasons (months) in both the north and south (Li *et al*., 2013; Vecchi *et al*., 2014; Camp *et al*., 2019). This seasonality of storm genesis is also observed in the Southern Hemisphere, where the peak storm genesis season occurs from January to March (Table 5.4). Furthermore, while each basin is experiencing an overall increase in mean sea surface temperatures, each basin is experiencing a different rate of increase, specifically in the regions where tropical cyclones form most often (Xue *et al*., 2012). Related to this, in the Southern Hemisphere, there exists more redistribution of ocean heat content between the basins, which have no continental landmass separating them (Lee *et al*., 2015; Gastineau *et al*., 2018). This results from the oceans warming and the subsequent excess heat uptake recorded in the Pacific Ocean, and it has been observed that this excess heat is being channeled into the Indian Ocean via the Indonesian Throughflow (Lee *et al*., 2015). This transfer of heat via the throughflow accounts for the majority of recent ocean heating in the South Indian Ocean up to the depth of 700 m and is responsible for influencing the distribution of heat energy across the Southern Hemisphere to a great extent (Zhang *et al*., 2018). Regarding heat storage, the Northern Hemisphere has a greater ocean mass, which allows more heat to be stored without increasing the mean sea surface temperatures/heat content as greatly as in the Southern Hemisphere (Lee *et al*., 2015). This adds another potential layer of complexity, as to why the Northern Hemisphere tropical cyclones are not as similar to Southern Hemisphere tropical cyclones, as the energy available to them is variable (Halperin *et al*., 2013; Song *et al*., 2018).

6.1.6.2 Variability and Data

Modes of variability must also be included as a possible explanation for the variations observed in storm activity and its drivers between hemispheres, as the ocean basins where tropical cyclone activity occurs each have defining modes of variability (Figure 2.1), which modulate the sea surface temperatures, wind fields and pressure in the region (Kajtar *et al*., 2017). Furthermore, modes of variability are observed to have large influences on tropical cyclone activity (frequency, intensity, size and trajectory), which has been widely documented across the basins with tropical cyclone occurrence (Liu & Chan, 2008; Camargo *et al*., 2010; Gutzler *et al*., 2013; Mao *et al*., 2013; Fitchett & Grab, 2014; Kajtar *et al*., 2017). The inherent variability in each basin should therefore be taken as a contributing factor to explain some of the differences in tropical cyclone activity (Wu & Zhou, 2012). The lack of isolation between the Southern Hemisphere basins, also allows more teleconnections and influence from each basin's modes of variability (Gastineau *et al*., 2018). It is also well known that vertical shear is a major factor in modulating the North Atlantic tropical cyclone occurrence specifically during ENSO events (Kuleshov *et al*., 2009). Meanwhile, in the Southern Hemisphere, ENSO, IOD and the MJO are found to influence changes in the walker circulation over the oceans, which initiates changes in tropical convergence zones and therefore the regions where storms are most likely to undergo genesis (Camargo *et al*., 2009; Ash & Matyas, 2012; Diamond *et al*., 2015).

The SIO basin specifically, has the largest number of tropical cyclone occurrences in the Southern Hemisphere, however, this is not captured by the data used by Gray (1968) and is also not examined in-depth (Ramsay *et al*., 2008). At the time, as mentioned, the data for the SIO was of relatively poor precision and robustness (Landsea *et al*., 2006). Therefore, the threshold used is based on this relatively lower spatial and temporal resolution data and was not highly representative of the Southern Hemisphere tropical cyclones formation zones, frequency, intensity or track motion i.e. translation across the ocean (Watterson *et al*., 1995; Landsea *et al*., 2006; Fitchett & Grab, 2014; Schreck *et al*., 2014).

6.1.7 Implications: Sea Surface Temperature Threshold Debate

The concept of a sea surface temperature threshold for storm genesis, precedes Gray's (1968, 1977, 1979) canonical papers. However, a threshold in this case is defined as the point at which a tropical storm will initiate its genesis phase and develop into a category 1 tropical cyclone (Defforge & Merlis, 2017a). If the 26.5°C, 25.5°C, or 27°C sea surface temperature thresholds which have been proposed by existing studies (summarised in Table 2.3) were valid, then tropical cyclone genesis would be evident in observational and model-based studies at these magnitudes. For example, researchers would have the ability to observe tropical cyclone genesis taking place only at the specified threshold (Korty *et al*., 2012a). However, this is not the case, as storms are able to form well below these thresholds, and the majority of Southern Hemisphere storms generally display a higher preferential sea surface temperature range of 27.5-28.5°C as demonstrated in this study.

The notion that there are no threshold values, is substantiated by studies simulating tropical cyclone activity during pre-industrial and glacial conditions, where storms formed at much lower sea surface temperatures compared to the present (Korty *et al.*, 2012a, b). The thermal and dynamic climate variables discussed within this study, are influenced by the large-scale climate; in the past when large-scale climate varied from the present state it is plausible that climate variables and tropical cyclone genesis climatologies were influenced and manifested differently (Korty *et al.*, 2012b). When sea surface temperatures were lower than pre-industrial periods, the Atlantic and Indian Oceans had lower mean temperatures of 2-3°C but were still able to support storm genesis (Korty *et al.*, 2012a). However, tropical cyclone genesis potential, which is the ability of the environment to support cyclogenesis, displayed a decrease during this time (Korty *et al.*, 2012a; Vecchi *et al.*, 2014). This strengthens the assumption (see Defforge & Merlis, 2017a) that the sea surface temperatures at the point of genesis are a product of their basin climatology, and not of a requisite sea surface temperature threshold. However, since 24°C was the lowest observed temperature at which storm genesis occurred within this study of Southern Hemisphere tropical cyclones (

Figure 5.7), and in existing studies of the pre-industrial (Korty *et al.*, 2012a) and historic periods (Defforge & Merlis, 2017a), it may be plausible to use this minimum value as a threshold. However only a few storms of approximately 1-5% tend to undergo genesis at this low temperature, and it is posited that they only take place due to a baroclinic environment, while the majority of tropical cyclones undergo genesis in the presence of a disturbance (McTaggart-Cowan *et al*., 2013, 2015; Bhaskaran *et al*., 2018; Bhatia *et al*., 2019). Therefore, provided ocean temperatures are >24°C, tropical cyclone genesis can potentially occur, however, there is no method except observation, to determine if this is the lowest temperature at which a tropical cyclone genesis event is possible in the Southern Hemisphere. After all, during the last glacial maximum, the optimal tropical cyclone genesis temperature was modelled to be approximately 24°C, and therefore storms could potentially have developed at lower temperatures in the past, when temperatures (air and sea) were climatologically cooler magnitude (Korty *et al*., 2012a).

6.2 Change over Time

This section will examine the change in both tropical cyclone activity and climate variables (thermodynamic and dynamic) during the point of tropical cyclone genesis, over the period of 1980-2016. The nature and rate of change for tropical cyclone activity and climate variables are required to assess future implications regarding tropical cyclone impacts (Walsh *et al*., 2016; Klotzbach *et al*., 2018). These changes will be discussed in relation to the Northern Hemisphere, to examine the disparities and similarities between the southern and northern basins. Then the implication of these differences and similarities in the climate variables during tropical cyclone genesis will be examined. In addition, existing studies (Sebastian & Behera, 2015; Wu *et al*., 2015; Yu *et al*., 2016; Sun *et al*., 2017; Huangfu *et al*., 2018; Bhaskaran *et al*., 2018; Wehner *et al*., 2018) have examined how tropical cyclone activity and climate drivers related to storm formation have changed over time and how climate change impacts have played out across the ocean basins. A main component of these studies has been tropical cyclone intensity, and how increased temperatures are impacting the severity of storms. This has been an important avenue of climate change research, as increases in the highest intensity (category 3-5) tropical cyclones poses a greater risk and danger to regions which are vulnerable to tropical cyclone landfalls (Fussell *et al*., 2017; Sun *et al*., 2017; Klotzbach *et al*., 2018). Relating to intensity, this study has given specific focus to the geographic nature of southern hemispheric storm intensification, and most importantly to the time it takes storms to attain their maximum intensity in the Southern Hemisphere.

6.2.1 Significant Changes in Tropical Cyclone Activity

6.2.1.1 Lifetime Maximum Intensity

Frequency of occurrence, duration and location of tropical cyclone activity at a basin-wide and hemispheric scale displays no significant change over the study period. However, the maximum intensity attained by a tropical cyclone is the only metric of activity which demonstrated a statistically significant relationship regarding change over time (Figure 5.28). In general, Southern Hemisphere tropical cyclones are experiencing a significant increase in storm intensity of 2.4 $m.s^{-1}$ per decade. Individually, the SIO and SP are the only basins to exhibit statistically significant increases in tropical cyclone intensity of 2.3 $m.s^{-1}$ per decade and 3.6 $m.s^{-1}$ per decade respectively. A similar observation of increasing intensity has also been found in previous studies investigating the SIO (Hassim & Walsh, 2008; Mavume *et al*., 2009; Kuleshov *et al*., 2010; Fitchett, 2018).

The number of storms per category of intensity (category 1-5) displays that category 1 storms (the weakest intensities) are decreasing by 1 storm per decade in the Southern

Hemisphere, while category 4 and 5 storms (the strongest intensities), both display significant increasing tends of 0.8 and 0.4 storms per decade. In the west North Pacific (Song *et al*., 2018) and in the other Northern Hemisphere basins (Elsner *et al*., 2008; Ren *et al*., 2014; Wing *et al*., 2015; Gilford *et al*., 2017; Tennille & Ellis, 2017; Zhan & Wang, 2017) the same overall trend is taking place, with the incidence of category 1 and 2 storms decreasing over time, while the category 3 to 5 storms indicate an increased prevalence over time. This study reaches the same conclusion for the Southern Hemisphere storms (Figure 5.33). While there are no significant increases in frequency for all storms, when examining the tropical cyclones per category, a clear trend similar to the above Northern Hemisphere and global scenarios are observed (Kuleshov *et al*., 2010; Klotzbach & Landsea, 2015; L. Zhang *et al*., 2017). In a number of investigations (Ren *et al*., 2014; Xu *et al*., 2017; Foltz *et al*., 2018) and in a projected scenario by Bhatia *et al*. (2018, 2019), intensity and specifically the trend of increasing intensity of tropical cyclones has been linked to increased sea surface temperatures. In addition to this, an increased potential intensity over time across ocean basins (indicating that the oceans will support higher intensities of storms) has also been observed to follow the increased air temperatures in the tropospheric layer (Vecchi *et al*., 2013; Soloviev *et al*., 2014).

6.2.2 Climate Drivers and Change Over Time: Thermal Factors

6.2.2.1 Sea Surface Temperature

For the Southern Hemisphere, sea surface temperature at the point of genesis is increasing significantly at a rate of 0.2°C per decade. The SIO and SP storms have statistically significant increases in sea surface temperature of 0.2 and 0.3° C per decade respectively. The SIO and SP Ocean are both climatologically warm oceans, and an increasing trend of sea surface temperatures is observed across them (Mavume *et al*., 2009; Roxy *et al*., 2014; Zhang *et al*., 2018). In addition, all other oceans of the Southern Hemisphere are experiencing increased sea surface temperatures under the warming regime (Mei *et al*., 2013; Strazzo *et al*., 2015; Burns *et al*., 2016). Since it is recognised that the majority of tropical cyclone genesis events follow the climatological sea surface temperatures of their basins (Defforge & Merlis, 2017b), the increasing trend for the Southern Hemisphere sea surface temperatures during tropical cyclone genesis is expected, i.e. as the oceans warm, the sea surface temperature at the point of genesis will also increase. The significant increasing trends observed in the SIO and SP basins, are explained by the large size of each basin, which allows for a larger signal of warming and explains why the SP basin (the largest basin) has a greater rate of warming sea surface temperatures during tropical cyclone genesis, compared to the hemispheric average (Ren *et al*., 2014; Foltz *et al*., 2018). Since the majority of storms in the Southern Hemisphere and the individual basins demonstrate a tendency to form within warmer sea surface temperature intervals (Figure 5.8; 27.5-28.5°C), more storms can undergo genesis when the sea surface temperature reaches these optimal intervals in a warming climate, provided the other climate factors align to allow a conducive formation environment (Tory & Dare, 2015; Defforge & Merlis, 2017b; Ramsay *et al*., 2017; Scoccimaro *et al*., 2017). It has been challenging to link changes between rising temperatures and tropical cyclone activity, and thereby to find a possible association between climate change and tropical cyclones (Webster *et al*., 2005; Knutson *et al*., 2010; Walsh *et al*., 2016). However, this study can tentatively demonstrate a link between an increasing trend of sea surface temperature and tropical cyclone intensity, and is able to support and replicate findings from model-based studies examining anthropogenic warming and tropical cyclones (Murakami *et al*., 2012a, b; Yoshida *et al*., 2017; Bhatia *et al*., 2018)

6.2.2.2 Air Temperature

The air temperature is increasing at the near surface and the upper regions (850mb level) during tropical cyclones genesis events the Southern Hemisphere. The air temperature at the 1,000mb and 850mb level, both display significant increasing trends of 0.2°C per decade at the point of genesis. The SIO is the only basin displaying a significant increase in air temperature at the 1000 and 850mb levels. Similar to sea surface temperature, the increased air temperature is driven by the warming environment (Evans & Webster, 2014; L. Zhang *et al*., 2017). Indeed, the rate of increase in air temperatures is similar to the sea surface temperature increase observed for the Southern Hemisphere storms. This is substantiated by the increase of temperatures at the lower and mid-level atmospheric heights across the study period (Figure 5.10) and within existing studies, which indicates the large-scale warming currently taking place across the oceans and atmosphere (Vecchi *et al*., 2014; Walsh *et al*., 2016; Bacmeister *et al*., 2018; Wehner *et al*., 2018). The increased sea surface temperature under a changing climate has been unable to account for the full range of variability in tropical cyclone intensity trends (Held & Zhao, 2011). Instead, the surface enthalpy fluxes, involving air temperature, relative humidity and evaporation also play an important role in influencing the genesis potential and intensification process of tropical cyclones (L. Zhang *et al*., 2017). Air temperature changes at the surface are also important boundary conditions that can influence tropical cyclone formation by promoting increased evaporation, moisture capacity of the air and overall convection (Lin *et al*., 2009; L. Zhang *et al*., 2017). Since air temperature at the point of genesis is increasing in the Southern Hemisphere, the possibility that this will promote increased convective activity and provide more energy for tropical cyclone intensification is likely (Lin *et al*., 2009; Soloviev *et al*., 2014). This observation follows model-based simulations run under a warming scenario for the Northern and Southern Hemisphere (Yoshida *et al*., 2017).

6.2.2.3 Relative Humidity

The change in relative humidity is only recorded as statistically significant at the near surface level (1,000mb) with a decreasing rate of 0.2% per decade. Examining the distribution and histograms for relative humidity (Figure 5.14), the majority of storms form when there is high moisture content present. The small decrease in relative humidity, may not be large enough to alter the activity (frequency) of tropical cyclones. The decreasing moisture at the surface levels is difficult to explain, as relative humidity would be expected to increase with the increasing temperature of the air and ocean (Emanuel, 1985; Vecchi *et al*., 2014). In general, warmer environments promote higher moisture storing capacity and this has been observed to promote increased intensification and genesis potential in tropical cyclone systems (Vecchi *et al*., 2014; Wu *et al*., 2015). Specifically, when advected into the genesis region, moist air promotes storm formation, while dry air has been observed to suppress storm formation (Held & Zhao, 2011; Braun *et al*., 2012). The decreasing trend in relative humidity may, therefore, be a contributor to the decreased frequency of tropical cyclones or can pose potential limitations on storm formation in the future.

Moisture content at the 850mb level in particular has been associated with influencing stronger storm intensity (Ying & Zhang, 2012; Wu *et al*., 2015). However, no significant increasing trend is observed (Figure 5.15) for relative humidity at the 850mb level, therefore, increased moisture present during Southern Hemisphere storm genesis may not be contributing to the observed increases in intensity for tropical cyclones in this study. However, it has been stated by Juracic and Raymond (2016) that moisture content has a greater influence on the process of intensification than on storm formation, which may explain the absence of a statistical relationship between relative humidity and tropical cyclone intensity at the 850mb level, since the data were not extracted at the point of intensification in this study (see Section 4.2.2). Therefore, while the significant trend observed at the 1,000mb level during storm genesis in this study is most likely a product of decreased evaporative activity, its influence on changing magnitudes of intensity cannot be verified. However, related to the point of formation, near surface moisture has demonstrated its importance in promoting tropical cyclone genesis (Parodi & Emanuel, 2009). Therefore, based on the lower observed moisture content and the resultant decreased potential for deep moist convection, the significant decreasing trend for relative humidity at the 1,000mb level, may be responsible for contributing to the decreased tropical cyclone genesis in the Southern Hemisphere. Specifically, when high intensity storms form, the genesis flow charts (Figure 5.22, Figure 5.23, Figure 5.24) demonstrate that higher relative humidity is present. While decreasing moisture at the point of genesis may not be impacting the trend of storm intensity at the 850mb level, it may be at the near surface level. Additionally, relative humidity at the surface could potentially be decreasing the frequency of Southern Hemisphere tropical cyclones.

6.2.2.4 Solar Flux

While solar flux indicates no statistically significant trend over time regarding its magnitude during tropical cyclone genesis in the Southern Hemisphere, there are significant correlations between solar flux and tropical cyclone activity. It is observed that a positive correlation (Figure 5.35) exists between solar flux and storm lifetime (the overall duration from tropical storm to dissipation of the tropical cyclone), indicating that if solar flux increases, a possible increase in storm lifetime may occur. Solar flux has been found to influence tropical cyclone activity, specifically, with higher intensity storms occurring when solar flux is high (Li *et al*., 2018). This is indeed notable, as Southern Hemisphere tropical cyclone genesis tends to take place more often at higher magnitudes of solar flux (Figure 5.21). While the change of solar flux during storm genesis is not significant, solar flux is a large-scale variable which is possibly preventing a trend from being detected, as mean solar flux is actually experiencing an increase over time at the global scale (Li *et al*., 2018). However, solar flux mainly influences tropical cyclones via an indirect mechanism detailed in Li *et al*. (2018). This may be another factor which prevents solar flux demonstrating a robust relationship with storm activity. The environmental solar flux still modulates Southern Hemisphere tropical cyclone activity as indicated by the significant relationship observed with storm lifetime and therefore, adds to the literature on the modulating effects of solar flux which have not been examined as much as other metrics of solar activity (Li *et al*., 2018).

6.2.3 Implication of Change in Thermal Factors

The above factors which display a statistically significant change are grouped together due to their thermodynamic properties (cf. Gray, 1968, 1977). These factors have demonstrated an influence on tropical cyclone genesis and the inter-relation between these factors are inferred from the feedback mechanism used to describe the air-sea interaction at the point of genesis, which is well-documented (Emanuel, 1986; Ren *et al*., 2014; Klotzbach *et al*., 2017; L. Zhang *et al*., 2017; Bhaskaran *et al*., 2018). Specifically, the mechanism involves the ocean and air temperature, which provides the warm setting required for the evaporation and increase in relative humidity at the time leading up to and during tropical cyclone genesis and intensification (Gray, 1998; Klotzbach *et al*., 2017; Bhaskaran *et al*., 2018). This allows the air column to attain a state closer to saturation, initiates deep convection and then through the processes of latent heat release and condensation, the cloud bands of the storms are enlarged and more energy from the air and ocean are transferred to the storm circulation (Bhaskaran *et al*., 2018). In addition, it is reported that as tropical cyclones move over colder regions of ocean, they lose energy and decrease in intensity (J.A. Zhang *et al*., 2017; Bhatia *et al*., 2019). At this point the feedback mechanism controlling the heat and moisture flux is weakened, thereby decreasing convective activity and weakening the tropical cyclone (Ren *et al*., 2014; Tory & Dare, 2015; Scoccimaro *et al*., 2017). This further supports the necessity of high heat energy (sea and air temperature) environments for successful and sustainable storm genesis and intensification. Based on these documented mechanisms and processes of the thermodynamic factors during the point of genesis, the increases recently observed in their magnitudes over time, for the Southern Hemisphere (Table 5.22), may serve to intensify the thermal component of genesis, as more energy is available within the environment (Daloz & Camargo, 2018).

The greater amount of energy in the environment that is being observed during tropical cyclone genesis in the Southern Hemisphere has a number of implications on tropical cyclone activity, namely the intensity of the mature storm and the location at which they have the highest probability of forming and intensifying (Bhaskaran *et al*., 2018). The combined effects of these thermal drivers are found to be major contributors to storm intensity, and their role in driving and sustaining intensity of a tropical cyclone is widely accepted (Li *et al*., 2013; Sebastian & Behera, 2015; Wu *et al*., 2015; Juracic & Raymond, 2016; Song *et al*., 2018). The increases therefore observed in these climate variables for the

Southern Hemisphere at the point of genesis are most likely a driver of the increased occurrence of higher intensity storms. Concerning the location of where tropical cyclones intensify or reach their highest intensity, there is a trend of higher intensity storms occurring in the warmer tropical regions at approximately 17°S, with very few category 4-5 storms reaching their highest intensity in colder poleward regions. Category 4 and 5 storms do, however, occur in poleward regions at a maximum of 27°S. These storms, as reported previously, are able to intensify and reach high categories of intensity as they are following the 28° and 29°C sea surface temperature isotherms (Kossin *et al*., 2014; Daloz & Camargo, 2018; Fitchett, 2018). Similarly, the higher intensity storms in this study indicate a minimum sea surface temperature of 27-28°C in order to form, as no category 5 storm has been observed to form below this in the Southern Hemisphere (Figure 5.24). It is, therefore, possible that as the sea surface temperature increases poleward of the usual formation and intensification regions, so will the occurrence of tropical cyclones as projected by Yoshida *et al*. (2017). Indeed, regarding the point of genesis, it has also been observed in this study that compared to 1980, the tropical cyclone genesis positions from 1980-2016 have progressively shifted poleward (Figure 5.3). Tropical cyclone genesis and intensity trends are already being observed in other studies examining the southern, northern and global scales of activity in a warming climate, with regions of maximum intensity shifting poleward along with tropical cyclone genesis locations (Holland & Bruyere, 2014; Kossin *et al*., 2014; Altman *et al*., 2018; Daloz & Camargo, 2018; Fitchett, 2018). Therefore, the changing trends in the thermal climate variables during the point of genesis are mirroring the changes in the large-scale environment, while also instigating changes in tropical cyclone activity similar to the existing changes recently documented for tropical cyclone activity (Kuleshov *et al*., 2010; Kossin *et al*., 2014; Walsh *et al*., 2016).

6.2.4 Change in Drivers: Dynamic Variables

6.2.4.1 Omega

Vertical velocity/omega is an estimate for the large-scale environmental vertical motion and surface divergence, which tends to be small in magnitude, except over a limited horizontal extent where anomalously high convection is present, such as a tropical cyclones or thunderstorm (Wallace & Hobbs, 2006). Omega at the near surface level demonstrates no distinct trend. However, omega at the 850mb level indicates a statistically significant trend of change by -0.18pascal.s^{-1} per decade at the hemispheric scale. Individually, the SIO is the only basin with a significant decreasing trend in omega of -0.02 pascal.s^{-1} per decade. The hemispheric trend of increasing vertical upward motion, indicates that the buoyancy of the atmosphere during the point of genesis is increasing at the 850mb level over time. Omega/vertical motion is better represented at the higher atmospheric levels, compared to the near surface level omega during storm genesis (Song *et al*., 2018). This observation holds true for non-omega metrics of motion in the atmosphere, such as relative vorticity (Yu *et al*., 2016; Klotzbach *et al*., 2017). Omega also indicated patterns of change across time in the study by Kiranmayi and Maloney (2011). This increase in vertical upward motion is an indicator of increased buoyancy, which is driven and influenced in part, by the abovementioned sea surface temperature increases and resultant deep convection taking place during tropical cyclone genesis (Song *et al*., 2018). This is based on the processes reported by Robe and Emanuel (2001), Mauk and Hobgood, (2012) and Bhaskaran et al. (2018), where the convection, driven by surface heating along with moisture fluxes (evaporation) and ocean heat content mixing promotes deep convection, and therefore increases buoyancy during the initial phases of tropical cyclone genesis. More research into the impacts associated with changes in large-scale vertical velocity is required. However, in a warming environment omega will most likely be enhanced (i.e. increased upward motion), as tropical conditions migrate poleward and the high vertical velocity observed over the tropics follows this poleward migration (Sriver, 2013; Tory & Dare, 2015).

6.2.4.2 Vertical Shear

Vertical shear demonstrates a significant change over time, with an increase of 0.3 $m.s^{-1}$ in the WA basin, while v-wind shear (the meridional shear component) indicates an increase of 0.06α per decade in the SIO. Zonal shear (u-wind) demonstrates no statistically significant change over time (Table 5.22). The u-wind shear has not been recorded to impact tropical cyclone genesis, hence no significant change in its magnitude over time is expected to be present (Klotzbach *et al*., 2017). However, both the metrics of shear indicate an increase in the shear environment during the point of genesis in the Southern Hemisphere over time (Table 5.22). With the current mean meridional shear of 0.02α the observed change over time of meridional shear could prevent storm formation and vortex development if the α of shear increases excessively, as observed in existing examinations of wind shear during genesis (Nolan & McGauley, 2012). As discussed for the Southern Hemisphere basins, wind shear $>$ 5 $m.s^{-1}$ tends to limit the genesis potential in a region (Nolan & Rappin, 2008).

The increasing trend of vertical shear observed in the Southern Hemisphere within this study, could impact the formation of tropical cyclones and decrease their occurrence. Such observations of decreased tropical cyclone frequency are already being observed in the Southern and Northern hemisphere, with increased vertical shear being one of the mechanisms proposed as a key contributor (Nolan & Rappin, 2008; Held & Zhao, 2011; Na *et al*., 2018). A possible reason for the increasing vertical shear, is the influence of sea surface temperature, with higher sea surface temperatures found to increase the magnitude of vertical shear (L. Zhang *et al*., 2017; Huangfu *et al*., 2018; Song *et al*., 2018). However, contrary to this sea surface temperatures are also reported to decrease vertical wind shear in the Northern Pacific tropical regions, which potentially brings the mechanisms influencing the change of vertical shear into question (Yu *et al*., 2016). With warmer conditions and sea surface temperatures migrating poleward, the high vertical shear found over the mid-latitudes may decrease, as observed by Yu *et al*. (2016) and Zhang *et al*. (2017b). Based on this study, shear appears to be increasing for the Southern Hemisphere tropical cyclones, even as more storms undergo genesis further poleward and sea surface temperatures increase, indicating that sea surface temperatures may not be responsible for weakening wind shear (see Kossin *et al*., 2014; Tennille & Ellis, 2017). However, this study has not examined vertical shear in relation to geographical distribution. Therefore, future work should investigate the cause of the increasing vertical shear over the oceans and its impact on tropical cyclone genesis.

6.2.4.3 Geopotential Height

While geopotential height is not a driver of tropical cyclone genesis, it is a metric of the large-scale environment, and displays a significant rate of increase over time, though only in the SIO at the 1,000mb and 850mb levels. Geopotential height was used by Li *et al*. (2010) to determine tropical cyclone duration, where high (low) geopotential height coincided in deeper (shallow) convection. Usually, tropical cyclones with deeper convection have higher amounts of moisture and heat energy and are sustained for longer periods of time (Li *et al*., 2010; Sahany *et al*., 2012; Sun *et al*., 2017). From this, the increasing rate of geopotential height with time, points to longer duration tropical cyclones in the SIO, as well as deeper convection taking place (Table 5.22). Incidentally, Kossin (2018) reported that globally tropical cyclones are becoming larger and slower. This agrees with the inferred findings of this study. For the Southern Hemisphere genesis events, geopotential height decreases from the western to eastern regions, with the highest mean geopotential height observed for the SIO, and the lowest mean heights found for the SP (Figure 5.19, Figure 5.20). This infers that the highest convective activity during the point of genesis takes place in the SIO, while the rest of the regions have successively lower convective activity and cooler environmental backgrounds (Li *et al*., 2010; Ying & Zhang, 2012).

Over the South Indian region (within the Mozambique channel) Matyas (2015) found that geopotential height was higher when storm genesis took place, which agrees with the findings of this study. In addition, Kim *et al*. (2017) reported a positive correlation between geopotential height and the initiation of the tropical cyclone season in the Indian Ocean and west Pacific, with tropical cyclone occurrences also increasing in the northern Pacific when increased geopotential height anomalies were present. Under a warming climate regime associated with anthropogenic forcing, the lower atmosphere is undergoing thermal expansion, and the consequence of this is driving an increase in the seasonal mean geopotential height over time (Christidis & Scott, 2015). If Southern Hemisphere tropical cyclones are more likely to initiate their season or to occur when geopotential height is relatively high, then an increase over time of geopotential height could alter the initiation of the season and increase the likelihood of storm genesis events.

6.2.5 Implications of Change in Dynamic Factors

The omega variable displays significant increase for the tropical cyclones of the Southern Hemisphere and at the individual basin-scale in the SIO, which demonstrates that the vertical motion or buoyancy during the point of genesis is increasing. This can potentially support higher rates of deep convection of the moisture and heat energy from the surface, and therefore fuel tropical cyclone genesis and intensification to a greater extent in the SIO and the Southern Hemisphere as a whole (Mauk & Hobgood, 2012; Rai *et al*., 2019). Regarding vertical shear the optimal range is 1-4 $m.s^{-1}$, and the mean shear is 3 $m.s^{-1}$ which is highly favourable for storm and vortex formation (Gray, 1977, 1979; Nolan & Rappin, 2008). In comparison, the increasing trend in vertical shear could potentially increase the mean shear to a point that it is not as conducive to tropical cyclone genesis (Wu *et al*., 2015; Klotzbach *et al*., 2017).

Generally, geopotential height is relatively lower in colder environments, due to increased subsidence and stability of the air masses, and higher in warmer environments due to instability of air masses and the atmosphere (Christidis & Scott, 2015). An increasing trend in geopotential height indicates that the atmosphere and ocean are warming climatologically, with the large-scale instability increasing during tropical cyclone genesis as a result (Pike, 1985; Li *et al*., 2010; Sun *et al*., 2017). Higher values of geopotential height are observed with warmer atmospheric and sea surface temperatures and are additionally implicated in increasing tropical cyclone occurrence (Christidis & Scott, 2015; Kim *et al*., 2017). Consequently, the increasing geopotential height, paired with the increased sea surface and air temperature trends, indicates an increasingly conducive environment being observed at the point of genesis, which could support longer-lived and higher-intensity storms (Vecchi *et al*., 2014; J.A. Zhang *et al*., 2017; L. Zhang *et al*., 2017). Based on the above, the current statistically significant changes observed in the climate drivers (thermodynamic and dynamic, excluding vertical shear), are moving in a direction that favours tropical cyclone genesis and intensification. Consequently, Li *et al*. (2013) reported that vertical shear alone cannot overcome the contributing effects of relative humidity and sea surface temperature relating to the genesis potential of tropical cyclones. Therefore, the increased vertical shear may not be sufficient to impact tropical cyclone activity to the extent of overcoming the favourability promoted by the thermodynamic variables.

6.2.6 Inter-Hemispheric and Basin-Scale Comparisons of Change

Regarding differences between the hemispheres (Walsh *et al*., 2016; Kossin *et al*., 2014; Defforge & Merlis, 2017a; Daloz & Camargo, 2018), the tropical cyclone intensity has indicated a specific pattern of disparity between the basins of the north (Atlantic and Northeast Pacific) and the south (South Indian and Pacific Oceans). This is characterised by the largest increases in tropical cyclone intensity observed for the southern basins, while the smaller increase in intensity is observed for the northern basins (Webster *et al*., 2005; Knutson *et al*., 2010; Klotzbach & Landsea, 2015). This is attributed to the climatologically cooler sea surface temperatures in the Northern Hemisphere, relative to the warmer ocean temperatures observed during storm genesis events in the Southern Hemisphere (Defforge *et al*., 2017b; Xu & Wang, 2018). Additionally, in the Atlantic, the horizontal sea surface temperature gradients are smaller compared to the South Pacific and Indian Oceans (Foltz *et al*., 2018). Atlantic tropical cyclones also display slower movement, which induces cooling of the sea surface, and decreases the available energy for the storm (Foltz *et al*., 2018). Intensity is the only metric which has presented a statistically significant increase within this study of Southern Hemisphere tropical cyclones (Figure 5.28). This paired with the increasing air and sea surface temperatures present during tropical cyclone genesis events for the Southern Hemisphere, suggests that these storms may continue to increase in intensity at a greater magnitude than Northern Hemisphere storms (Bhatia *et al*., 2018). This is a result of the increasing sea surface temperature trends observed during tropical cyclone genesis and the climatological warming of each southern basin (Lynch *et al*., 2014; Sun *et al*., 2017; Durack *et al*., 2018; Rai *et al*., 2019). After all, warmer temperatures, provide more energy for storm development and intensification (Sun *et al*., 2017; Daloz & Camargo, 2018).

The increasing sea surface and air temperatures observed for the Southern Hemisphere tropical cyclones at the point of genesis (Figure 5.34), are similarly observed in the Northern Hemisphere tropical cyclone zones of formation (Held & Zhao, 2011; Ren *et al*., 2014; Vecchi *et al*., 2014; Walsh *et al*., 2016; L. Zhang *et al*., 2017). The warming in both hemispheres is shown to exceed internal variability and can be confidently attributed to anthropogenic warming (Gillett *et al*., 2008; Sun *et al*., 2017; Yamada *et al*., 2017). Similarly, the impacts on tropical cyclone activity, specifically the location at which storms are undergoing genesis and reaching their peak intensity is being influenced by the increases observed in the thermal (moisture, sea and air temperature) climate variables (Emanuel *et al*., 2004; Scoccimaro *et al*., 2017; Sun *et al*., 2017). As Zhan and Wang (2017) reported for the west North Pacific, the poleward expansion of the tropics may be responsible for the increasing trend of sea surface temperatures observed at the point of genesis within in this study (Figure 5.34). As the sea surface temperature isotherms shift poleward, they increase the overall basin temperature, however, the increase in genesis temperatures is more pronounced for the Southern Hemisphere (Burns *et al*., 2016; Ramsay *et al*., 2017). This can be attributed to the different rates of poleward migration/expansion of the temperature gradients regarding the location where tropical cyclones undergo genesis and attain maximum intensity (Kossin *et al*., 2014; Tennille & Ellis, 2017; Zhan & Wang, 2017). It can also be argued that increased tropical cyclone intensity and shifts in genesis location are caused by the larger magnitude of heating in the southern hemisphere, as observed in Daloz & Camargo (2018). In addition, the relatively higher sea surface temperatures observed over the ocean, i.e. the 27, 28 and 29°C isotherms are shifting poleward as observed by Fitchett (2018). These are possible explanations for the increasing trend in temperature parameters observed during the point of genesis within this study (Figure 5.34,Table 5.22). As the isotherms in the Southern Hemisphere migrate poleward (over the 1950-2015 period), the 27 and 28°C isotherms are replacing the usual 25 and 26°C isotherms over the tropical cyclone genesis regions, which start to experience higher than average temperatures related to the higher magnitude isotherms (Fitchett, 2018).

The increase in the sea surface temperatures over the formation zones (Figure 5.3), also explains the higher optimal magnitudes (27.5-28.5°C) observed for the majority of storm genesis events within this study, as opposed to the lower magnitudes of 26.5-27°C at which Northern Hemisphere storms usually undergo genesis (Tory & Dare, 2015; Defforge & Merlis, 2017a). In the Northern Hemisphere the regions of tropical cyclone genesis and intensification are shifting poleward at a much slower rate, which could explain why the Northern Hemisphere does not yet reflect comparatively high temperatures during its tropical cyclone genesis events as observed in the Southern Hemisphere basins (Kossin *et al*., 2014; Walsh *et al*., 2016; Daloz & Camargo, 2018). This does not discount the sea surface temperature forcing on intensity, as Xu *et al*. (2016, 2017, 2018) reported that the maximum potential intensity of north Atlantic tropical cyclones is most likely to be reached when the sea surface temperature is within or higher than the range of 27-28°C, which is similar to the Southern Hemisphere peak optimal sea surface temperature and is still higher than the 26.5°C threshold value that is reported by Gray, (1979) and Klotzbach *et al*. (2017). Lastly, the Indonesian Throughflow demonstrated a warming effect for the Southern Hemisphere basins, as it redistributes heat from the Pacific into the SIO (Zhang *et al*., 2018).

The vertical shear only becomes detrimental past 12-15 $m.s^{-1}$ for the Northern Hemisphere storms (Gray, 1979; Nolan & Rappin, 2008; Nolan & McGauley, 2012; Klotzbach *et al*., 2017), however, for the Southern Hemisphere, fewer tropical cyclones achieve genesis once the vertical shear is larger than 5 $m.s^{-1}$ (Figure 5.18). This is a large difference between the hemispheres, which is further compounded by the increasing trend of vertical shear observed in the Southern Hemisphere. This increase would not threaten tropical cyclone genesis as much in the Northern Hemisphere basins (Vecchi & Soden, 2007; Mauk & Hobgood, 2012; Chen *et al*., 2018; Na *et al*., 2018). However, in the Southern Hemisphere, the optimal shear is 1-4 $m.s^{-1}$, and the increasing rate over time of 0.3 $m.s^{-1}$ is closer to bringing the mean shear of 3 $m.s^{-1}$ over the optimal threshold, which could prompt a potential decrease in tropical cyclone formation for the Southern Hemisphere. This is due to the detrimental effects which vertical shear has on tropical cyclone formation (Nolan & McGauley, 2012). This argument also stands, regarding the meridional shear (α), which also displays an increasing rate that could enhance α to a point where the shear is outside of the optimal range for tropical cyclone genesis in the Southern Hemisphere, and this could become detrimental to storm formation.

The interaction between vertical shear and sea surface temperature has been reported to change with increases in ocean heat content (Nolan & Rappin, 2008; L. Zhang *et al*., 2017). In the Northern Hemisphere, tropical cyclones are found to occur more often and reach their maximum intensity when the sea surface temperatures are high and the vertical wind shear is low (Xu *et al*., 2016; 2018). The increasing sea surface temperatures in the Northern and Southern Hemisphere are instigating lower shear values and therefore promoting intensification (Defforge & Merlis, 2017b). Before 2006, the Atlantic was characterised as having the highest intensity tropical cyclones due to low shear and higher sea surface temperatures than the Indo-Pacific regions (Latif *et al*., 2007). This stronger signal of warming in the Atlantic was responsible for the decreased vertical shear, while over a shorter timescale the increased sea surface temperatures drastically decreased vertical shear over a 24-hour period, which in turn caused an increase in tropical cyclone wind speed and intensity (Xu *et al*., 2017; J.A. Zhang *et al*., 2017; L. Zhang *et al*., 2017).

The long-term finding for the Southern Hemisphere indicates that sea surface temperature is increasing, but an insignificant change in vertical shear is observed for the eastern basins (EA and SP), with a significant increasing trend observed for vertical shear and meridional shear in the SIO and WA regions respectively. According to a model-based projection, the tropical cyclone occurrence in the Northern and Southern Hemisphere will decrease as a result of a 4°C warming scenario, which will instigate large vertical wind shear, making tropical cyclone genesis very difficult (Bell *et al*., 2013). Other modelling studies have previously reported that due to global warming, there will be an increase in vertical shear (Vecchi & Soden, 2007; Halperin *et al*., 2013). Such projections fit better with the trend in the western basins of the Southern Hemisphere, where vertical shear is increasing as sea surface temperatures increase and the frequency of tropical cyclone occurrence decreases (Figure 5.26). A study in the south west Indian Ocean indicates that a warming climate has been projected to impact tropical cyclone frequency only up to 2°C of warming, after which no further decreases in storm activity will take place (Muthige *et al*., 2018).

6.2.7 Implications for Tropical Cyclone Activity

The most noticeable implication from the changes observed in climate drivers at the point of genesis is their possible contribution to the increase in tropical cyclone intensity found within this and existing studies (Li *et al*., 2010; Ren *et al*., 2014; Lin *et al*., 2017). Regarding the relationship between Southern Hemisphere storm activity and climate drivers, the omega, meridional shear, sea surface temperature and solar flux display statistically significant correlations with tropical cyclone intensity (Figure 5.35). The intensity of Southern Hemisphere tropical cyclones is similarly experiencing an increase over time as observed in existing studies (Sobel *et al*., 2016; Daloz & Camargo, 2018; Fitchett, 2018). This increased trend of intensity is related to the climate variables during the point of genesis, specifically, sea surface temperature, air temperature, humidity and vertical shear (Figure 5.35). With the exception of vertical shear, these variables are experiencing an increase over time during the Southern Hemisphere storm events and are responsible for influencing the conditions which favour higher tropical cyclone intensification (Halperin *et al*., 2013; Camargo *et al*., 2014; Bacmeister *et al*., 2018).

Tropical cyclone frequency, which indicated no trend over time, demonstrates a statistically significant correlation to near surface (1,000mb) air temperature and upper air (850mb) omega, indicating that positive magnitudes of these climate variables are related to increased tropical cyclone occurrences. With an increase in vertical wind shear over the western Southern Hemisphere basins (SIO and WA), there may be a larger decrease in tropical cyclone frequency in the future as larger vertical shear significantly suppresses tropical cyclone genesis potential, regardless of the magnitude of the other climate variables at the point of genesis (Nolan & McGauley, 2012; Finocchio & Majumdar, 2017). Once shear is large enough, it prevents the storm from forming by increasing the time required for a vortex (rotating air and moisture column) to develop, up to the point where tropical cyclone genesis fails as the moisture and heat energy are spent or dispersed (Nolan & Rappin, 2008). In addition, tropical cyclone lifetime for storms in the Southern Hemisphere are statistically related (positively) to sea surface temperature (Figure 5.35), which indicates that as sea surface temperature increases, so will the tropical cyclone lifetime. Comparatively, in the western Pacific, tropical cyclone duration has been related to low vertical shear and positive geopotential height anomalies which are commonly instigated by higher sea surface temperatures and together promote larger, slower and longer-lived storms (Schenkel *et al*., 2018; Song *et al*., 2018). Furthermore, the relationship between sea surface temperature and tropical cyclone size (larger storms persist longer over warmer oceans) is another mechanism governing tropical cyclone duration (Sun *et al*., 2017; Chen *et al*., 2018; Rahman *et al*., 2018).

In conclusion, the relationships and change over time of the climate drivers, not only substantiates much previous work (Tory & Frank, 2010; Vecchi *et al*., 2014; Wu *et al*., 2015; Bhaskaran *et al*., 2019), but adds to it, in the manner that new variables such as meridional shear and zonal shear, air temperature and omega demonstrates an optimal range of magnitudes at the point of genesis for Southern Hemisphere tropical cyclones. This indicates that these new climate variables have the ability to influence storms genesis at these specific magnitudes. In addition, these climate variables have displayed statistically significant correlations and changes over time with regard to the tropical cyclone metrics of activity.

6.2.8 Time to Attain LMI

The tropical cyclones included in this study, were separated based on the time it took them to attain their maximum intensity. Firstly, as the time to attain the maximum intensity increases, so does the mean LMI. For storms with zero-day formation times having the lowest LMI and the 3, and 4-12 day formation times displaying the highest LMI. Similar results have been found, where LMI is higher in storms that take longer to form (Sun *et al*., 2017; Schenkel *et al*., 2018; Xu & Wang, 2018). The storms which took the longest to reach their LMI also had the longest duration at that LMI, therefore the longer a storm took to attain its highest intensity, the longer it persisted in the environment (Sun *et al*., 2017). Using cluster analysis, Rahman *et al*. (2018) found that the storms with the highest LMI tend to occur over the warmer ocean regions that have the highest amount of potential energy available. This is opposite to global-based observations by Frank & Young (2007), where, the high intensity storms persist for the shortest duration (1.9-1.2 days for category 4 and 5). A possible reason for the different durations to achieve LMI, points to higher sea surface temperatures and a warm moist environment (Schenkel *et al*., 2018; Rahman *et al*., 2018). This is based on the statistically significant relationships found (in this study; Figure 5.35) between intensity, duration and sea surface temperature, which is well known as a thermodynamic requirement for high intensity tropical cyclones (Emanuel *et al*., 2004; Wing *et al*., 2015; Bhaskaran *et al*., 2018). Storm intensity is also related significantly to omega, shear and solar flux, all of which have the potential to contribute to an environment which is favourable for extreme and sustained storm intensification (Li *et al*., 2013; Wing *et al*., 2015;

Wu *et al*., 2015; Li *et al*., 2018; Song *et al*., 2018). However, as the storm size was not captured for this study, the applicability of the abovementioned size to lifetime relationship, regarding the different periods tropical cyclones took to reach and maintain an intensity (LMI) cannot be resolved here.

6.3 Tropical Cyclones and Modes of Variability

Tropical cyclones are relatively rare events, with only 60-80 tropical cyclones occurring each year globally almost exclusively during the summer months of each hemisphere (Webster *et al*., 2005; Klotzbach *et al*., 2017). This section will discuss the statistically significant relationships observed between modes of variability and their modulation on tropical cyclone activity and the climate drivers related to tropical cyclone genesis. Numerous studies have focused on different modes of variability and their impact or modulation of tropical cyclone activity, including the most common, which is ENSO (Frank & Young, 2007; Kuleshov *et al*., 2009; Menkes *et al*., 2012; Diamond *et al*., 2013; Mao *et al*., 2013), to basin-scale modes such as IOD (Ash & Matyas, 2012; Saha & Wasimi, 2013; Burns *et al*., 2016), MJO (Camargo *et al*., 2009; Diamond & Renwick, 2015) or the modes which have an influence over a large spatial and temporal scale, such as the PDO and SAM (Diamond *et al*., 2013; Allen *et al*., 2014; Wang *et al*., 2015; Clem *et al*., 2016; Gastineau *et al*., 2018). These studies have also determined possible mechanisms by which the modes of variability instigate changes in tropical cyclone activity, such as genesis, intensification, dissipation and motion. Due to the exhaustive literature on this subject, and since the modes of variability were not examined in-depth within this study, only major existing studies and mechanisms will be discussed and outlined in relation to this study's results. Furthermore, while not specifically a mode of variability, volcanic activity was included to demonstrate and capture its forcing capability on the climate variables and tropical cyclone activity. A summary of the statistically significant modulations and the modes of variability involved will be provided, followed by a discussion in relation to the literature.

6.3.1 Significant Modulations

The longitude of tropical cyclone genesis is found to be related to ENSO (-ve phase) and volcanic activity. Storm lifetime is related to DMI (+ve phase), while tropical cyclone lifetime is related to ENSO (-ve phase). The modes of variability related to the intensification metrics of tropical cyclone activity are once again ENSO (all indices: +ve phase) and volcanic activity, which were statistically related to the longitude at which tropical cyclone LMI was attained for the Southern Hemisphere storms. The maximum intensity attained by the tropical cyclones is also related to ENSO, with an additional statistically significant relationship to the SAM (both at +ve phases). From these results, the ENSO mode of variability has the greatest and most common relationship to various metrics of tropical cyclone activity, both during the tropical cyclone genesis and intensification stages, which has also been observed by Mao *et al*. (2013). The unexpected aspect of these results is that none of the other modes of variability such as the MJO or PDO, displayed any significant or strong relationships to tropical cyclone activity, despite being modes that impact major aspects of the Southern Hemisphere and tropical climate system at intraseasonal and decadal timescales (see Allen *et al*., 2014; Tsuboi & Takemi, 2014). Regarding poleward shifts in the location of maximum intensity in the North Pacific, it is observed that the PDO contributes to the environmental increases in sea surface temperatures over the poleward areas of the basin, which allows more storms to form and reach their maximum lifetime intensity, while also increasing intensity magnitudes over the equatorward zones (Zhan & Wang, 2017). This observation was not replicated in this study, at least not under the multivariate regression analysis method used (Section 4.4.3.5).

6.3.1.1 ENSO

Severe tropical cyclones (specifically category 3-5 storms) have demonstrated strong relationships to ENSO (Frank & Young, 2007; Li *et al*., 2013). This is based on a similar principle to the PDO forcing on sea surface temperature, therefore, when positive (warm) ENSO phases occur, the sea surface temperature increase provides a greater potential intensity within the environment for tropical cyclones forming over the Pacific (Zhan *et al*., 2017). This relationship was observed for the Southern Hemisphere within this study (Figure 5.37), whereby intensity displayed higher magnitudes during a positive ENSO. The relation to ENSO and Southern Hemisphere storm intensity is notable, as all the indices representing ENSO (Niño Index, Southern Oscillation Index and the ENSO Multivariate Index) demonstrated a statistically significant relationship with LMI. In the Northern Hemisphere (specifically the Atlantic) the opposite is true, where increased tropical cyclone activity and intensification takes place during the cold phase of ENSO (Dowdy *et al*., 2012).

ENSO has also indicated a link to the location (longitude) at the point of genesis and LMI. Previous Southern Hemisphere examinations of the ENSO mode (Kuleshov *et al*., 2009) indicate that during the cold ENSO events, conducive conditions for tropical cyclone genesis along with the locations of formation, are shifted away from the equator in the SIO through the modulating effect of ENSO on relative humidity and vorticity. While increases in sea surface temperature over the WA region during cold ENSO events promotes increased tropical cyclone genesis within this region (Kuleshov *et al*., 2009; Diamond *et al*., 2015a, b).

Regarding the SP region, as a result of changes in relative humidity, vertical shear, vorticity and sea surface temperature during the cold ENSO events, tropical cyclone genesis was promoted (Kuleshov *et al*., 2009; Diamond *et al*., 2013). However, this reflects a latitudinal element of influence from ENSO, while Zhao & Wang (2018) have also observed a weak but statistically significant correlation with ENSO and the longitudinal aspect of tropical cyclone genesis in the central Pacific region, although such a correlation has only presented as significant after 1998-2015. The existing studies (Kuleshov *et al*., 2009; Diamond *et al*., 2013; Zhao & Wang, 2019) and this study (Figure 5.37) indicate that ENSO influences both storm intensity and the location at which they form. This modulation on tropical cyclone genesis location is thought to be influenced by the changes in sea surface temperature, humidity and wind/pressure anomalies which modulate the environmental conduciveness for tropical cyclone formation, and therefore influence the locations at which tropical cyclone genesis will most likely occur during the different ENSO phases (Kuleshov *et al*., 2009; Ash & Matyas, 2012; Zhao & Wang, 2019).

6.3.1.2 DMI

The IOD index (DMI) has revealed a statistically significant relationship with the storm lifetime of Southern Hemisphere tropical cyclones (Figure 5.36). It is observed in the North Indian Bay of Bengal that during a positive IOD phase, the storms lifetimes are longer than average (Mahala *et al*., 2015). In addition, for the SIO, the positive IOD is observed to increase sea surface temperatures, which increases convection and enhances the ocean barrier layer thickness, thereby initiating and favouring longer lived tropical cyclones, i.e. recorded as higher numbers of tropical cyclone days (Burns *et al*., 2016). This is notable, as the increased sea surface temperatures shared a statistically significant correlation with tropical cyclone lifetime for Southern Hemisphere tropical cyclone events (Figure 5.35). Therefore, the significant relationship now observed between the positive IOD phase and the longer-lived storms appears plausible within this study. The IOD was additionally found to be related to longitude in the west SP region (i.e. affecting mainly western Australian regions) and was observed to instigate an eastward shift in the longitude of storm formation (Magee & Verdon-Kidd, 2018). While this study finds no equivalent relationship, it is noteworthy, as the IOD has long been compared with the ENSO of the Indian Ocean (Ash & Matyas, 2012). This also indicates the ability of the IOD to impact the SP and Australian regions despite their geographical distance from the active IOD zones, therefore supporting the possibility that the IOD could be impacting the majority of storms in the Southern Hemisphere via teleconnections, and thus makes the significant trend observed in this study more tangible.

6.3.1.3 SAM

The SAM in its positive phase was related to Southern Hemisphere tropical cyclone intensity (Figure 5.37). The SAM has been connected to sea surface temperature in specific tropical cyclone genesis zones over the WA region and the Pacific Ocean (Ding *et al*., 2012; Diamond & Renwick, 2015). While in the SIO, the tropical cyclone frequency has demonstrated a statistically significant correlation with the SAM (Mao *et al*., 2013). The increased convective activity and modulation over sea surface temperature and zonal winds is a common feature associated with the SAM and its modulation on tropical cyclone activity (Diamond & Renwick, 2015). In addition, over the Australian region, relative humidity was found to increase during a positive SAM, which contributed to increased tropical cyclone events as reported, however, it was not clear whether intensity was impacted by the SAM, only that higher relative humidity values coincided with higher numbers of storms in the Australian region during a positive SAM (Mao *et al*., 2013). This study can therefore add to the previous work (Mao *et al*., 2013) by demonstrating that the SAM may indicate an influence over the intensity of Southern Hemisphere tropical cyclones at the hemispheric scale. Despite not finding any specific or strong link between SAM and the category of tropical cyclones (low or high categories of intensity) being modulated, the significant relationship between SAM and intensity observed for this study may be a product of the modulation which the SAM has on sea surface temperature, convection and relative humidity, all of which are able to impact intensity (Zhan & Wang, 2017; J.A. Zhang *et al*., 2017).

6.3.1.4 Volcanic Activity

For the Southern Hemisphere, volcanic activity is related to the locations (longitude) pertaining to tropical cyclone genesis and maximum intensification (Figure 5.36, Figure 5.37). These locations are based on the required conditions for tropical cyclones to reach the point of genesis and maximum intensity i.e. where potential intensity is the highest (Evans, 2012). When volcanic eruptions occur (especially large eruptions), they force changes in temperature, solar radiation and the overall heat budget of the planet, via the reflective properties associated with the ash released from the eruptions, which cools the climate (ocean and air heat content) over the affected hemisphere (Evans, 2012; Korty *et al*., 2012a). Volcanic activity has specifically been shown to influence the sea surface temperatures and air temperatures near the surface and upper troposphere, by instigating large and persistent cooling over these regions (Wing *et al*., 2015).

The major influence that volcanic activity has on tropical cyclones is the genesis potential and potential intensity of the environment, which usually decreases in the seasons following large eruptions such as the events of 1982 and 1991 (Evans, 2012; Pausata & Camargo, 2019). Specifically, large eruption events are found to induce a shift of the ITCZ northward (southward) during Southern Hemisphere (Northern Hemisphere) eruptions, which in turn shifts conditions conducive to tropical cyclone genesis north or south respectively (Pausata & Camargo, 2019). Based on the findings in Evans (2012), Wing *et al*. (2015) and Pausata and Camargo, (2019), volcanic eruptions influence environmental factors such as tropical cyclone genesis and intensity potential and therefore, have an influence on the locations where conducive conditions required for storm genesis and intensification can be found. This can be put forward as a possible mechanism for explaining the significant relationship observed between Southern Hemisphere locations of tropical cyclone genesis, intensification, and volcanic eruptions found within this study (Figure 5.36, Figure 5.37). While Pausata & Camargo (2019) reported a latitudinal shift, this study observes a longitudinal shift in tropical cyclone activity. The mechanism involving the ITCZ shifts, may be responsible, as the locations of the ITCZ over the Southern Hemisphere during the storm seasons, overlaps with the longitudinal hotspot locations pertaining to the existing zones of formation (Figure 3.3, Figure 5.3). However, there remains a deficit in the understanding of longitudinal variations in the ITCZ, and more research is required to understand it and the effect it may have on tropical cyclone activity (Byrne *et al*., 2018).

Another mechanism to explain these longitudinal shifts and their relationship to volcanic activity may involve ENSO. In support of this, while no significant patterns related to the ITCZ are found, Khodri *et al*. (2017) revealed a warming pattern of sea surface temperatures across the longitudinal range of the equatorial Pacific following major volcanic eruptions, which tends to promote El Niño events following theses eruptions. Furthermore, as discussed above (Section 6.3.1.1), ENSO events do instigate longitudinal shifts in tropical cyclone activity (Kuleshov *et al*., 2009; Diamond *et al*., 2013). This may point to a relationship between volcanic activity and ENSO, which is responsible for instigating longitudinal shifts in tropical cyclone activity.

6.3.2 Examination of Modes of Variability

There are a multitude of studies which incorporate modes of variability in their investigations, with the aim of explaining the variability observed in tropical cyclones (Kim *et al*., 2012; Menkes *et al*., 2012; Mao *et al*., 2013; Mahala *et al*., 2015; Burns *et al*., 2016; Zhan *et al*., 2017; Patricola & Wehner, 2018; Song *et al*., 2018). While tropical cyclones occur regularly within their respective summer seasons, there are years when occurrences are above average, with increased or decreased intensity storms, or changes in tropical cyclone genesis or tracking locations (Frank & Young, 2007; Li *et al*., 2013). Studies attempt to reconcile these discrepancies from the mean activity, by linking them to physical mechanisms as a way of explaining the cause of the variability in tropical cyclone activity (Chang-seng & Jury, 2010). This section will give a short critical evaluation regarding the accuracy and use of these modes of variability in tropical cyclone studies. This is not to discredit or disprove any existing work, only to provide a different lens in approaching the explanation of variability in line with the results found in this study.

It can be safely assumed that the major climatic modes of variability, including ENSO, PDO and the North Atlantic Oscillation, impose a significant and well-established modulation on tropical cyclone activity, based on the consistent signal and variability they have been observed to account for, which is approximately 70% of the global tropical cyclone occurrences (Frank & Young, 2007). Additionally, the modes of variability such as MJO, IOD and SAM were also observed to account for some of the tropical cyclone variability in the studies which examined them (Frank & Young, 2007; Camargo *et al*., 2009; Chang-seng & Jury, 2010; Werner *et al*., 2012; Clem *et al*., 2016). However, no modes individually or combined, as within this study have been able to explain the variability fully. This has been attributed to random variability (Wing *et al*., 2015), and other physical mechanisms related to the climate and environment, namely barrier layer thickness, solar radiation, volcanoes or changes of temperature within the tropical tropopause layer (Evan, 2012; Malan *et al*., 2013; Wing *et al*., 2015; Burns *et al*., 2016; Li *et al*., 2018). Similarly, the climate and ocean atmospheric dynamics of whole ocean basins are shown to influence the tropical cyclone activity (Wang *et al*., 2009; Mei *et al*., 2015; Ramsay *et al*., 2017) in another basin via teleconnections. Within this study of Southern Hemisphere tropical cyclones (Figure 5.36, Figure 5.37), it is observed that both the major modes of ENSO and SAM along with volcanic activity (a large forcer of the climate system), are the core elements which explain some of the variability of Southern Hemisphere tropical cyclones, however, as in the above existing studies, they do not account for all the variability, and only affect certain aspects of tropical cyclone activity.

6.3.2.1 Spurious Correlations and Problems of Scale

Matters of scale play an important part in the cross-examination of modes of variability (Diamond *et al*., 2012; Mao *et al*., 2013). The modulation of these modes of variability on tropical cyclone activity have been approached differently, with some investigations focused on individual storms, seasons, years and decades of tropical cyclones, but also at different spatial scales ranging from localised (Diamond *et al*., 2012; Werner *et al*., 2012; Diamond & Renwick, 2015a) to basin-wide and global (Frank & Young, 2007; Menkes *et al*., 2012;

Ramsay *et al*., 2012; Wehner *et al*., 2018). While these studies are supported by statistically significant results and produce meaningful trends and patterns, there remains an element of incoherence (Barcikowska *et al*., 2017). This stems from the observation that results and trends or patterns related to the modes of variability are inconsistent across space and time. At a local and regional scale, modes of variability such as the IOD have been shown to impact tropical cyclones differently than observed at a global or basin-wide extent (Ash & Matyas, 2012; Saha & Wasimi, 2013). In addition, over time, there are instances where the impact of the modes on tropical cyclones change, as in the south west Indian Ocean, where the effect of ENSO on track morphology was reversed from the previously observed interactions and impacts (see Ramsay *et al*., 2012; Li & Zhou, 2014). In addition, over the South China Sea prior to 1997, increased tropical cyclone occurrences were observed in La Niña conditions, but post 1997, a decrease in tropical cyclone occurrence was observed (Liu & Chan, 2018). These discrepancies and changes over time do not indicate spurious findings, but instead may be a reflection of the changing climate and environment. An example is the changing activity in the South China Sea, which has been attributed to the northward shift in tropical cyclone tracks and genesis locations along with increased sea surface temperatures which promote increased storm genesis under cooler conditions such as during the La Niña phase of ENSO (Liu & Chan, 2018). There is also the question of whether a percentage of the variability observed in tropical cyclones is not attributed to internal variability, which is masking the true impact of the various modes of variability (Fitchett & Grab, 2014; Mei *et al*., 2015).

The problem of data quality is highlighted regarding the adequacy of data to capture the true nature and patterns of variability in the climate system and its phenomenon such as tropical cyclones (Magee & Verdon-Kidd, 2018). Tropical cyclone track data dates back to the mid 1800's, while much of the climate data such as sea surface temperature, atmospheric and large-scale environmental variables along with the indices for the modes of variability have only been around since the mid 1900's, with high resolution data only available since the 1970's (Landsea *et al*., 2006; Befort *et al*., 2016; Rai *et al*., 2019). This potentially hinders the ability to uncover decadal or even longer-term patterns which may exist. Modes of variability also share a common discontinuity relating to their influence, where, despite statistical significance existing between the mode (ENSO, IOD, MJO, PDO) and metric of tropical cyclone activity (frequency, intensity, track), there are instances (years or seasons) where the observed relationship does not play out consistently (Ash & Matyas, 2012; Mahala *et al*., 2015; Liu & Chan, 2018). This has been explained by non-linearity and the random onset of the modes influence, or other climate forcing which can exacerbate or suppress the mean influence of the mode, such as anomalously high westerly winds or years with increased moisture content as observed in the northern Pacific, where these climatic anomalies intensified storms and increased their lifetimes beyond the usual magnitudes observed during a La Niña phase (Wing *et al*., 2015; Liu, 2019).

There is additional difficulty to reconcile the scale of the modes of variability and the scale of tropical cyclone activity data (Loridan *et al*., 2017). For instance, the modes are presented as indices of monthly averages, which is used and correlated against monthly averages of tropical cyclone data (which itself may have inherent variability between single events). While the indices are now calculated from high resolution data (Rai *et al*., 2019), this still presents questions of whether the effects of the modes should be captured not as an index averaged over time and space, but at a finer resolution, in order to definitively assess the changes the modes have on the environment over a short time, as tropical cyclones by nature only last a short time to begin with. Even when using models with a non-linear setup (to better simulate natural processes), there have been overestimations of the variability compared to observed historical variability (Wu & Zhou, 2012; Koh & Brierley, 2015). Additionally, the modes of variability are found to predominantly modulate the higher intensity storms, providing another reason, the signal may be inconsistent or weak in tropical cyclone variability studies, which include possible impacts on all tropical storms and low intensity tropical cyclones not as strongly affected by the modes of variability (Frank & Young, 2007; Guevara-Murua *et al*., 2015; Wing *et al*., 2015).

6.3.2.2 Tropical cyclones modulating effect on climate

There is increasing interest in the impact that tropical cyclones are having on the climate system (Korty *et al*., 2008; Mei *et al*., 2013; Sriver, 2013). After all, these systems are massive and deal with extremely large quantities of energy, while only having a lifetime of 1-2 weeks at most and 1-5 days at the least (Frank & Young, 2007; Song *et al*., 2018). While the scope of this study does not account for tropical cyclone driven impacts, it is notable to mention this aspect to support the argument, that if a storm is able to impact the climate to a larger extent in a shorter time compared to a mode of variability, then the storm may be capable of causing changes or influencing the presentation of a mode of variability via forcing on the climate system (Mei *et al*., 2013). For instance, tropical cyclones have been shown to cause mixing of the ocean, which impacts temperature equilibriums and stratification to a large degree depending on the storm's intensity (Sriver, 2013). This has been shown to significantly affect global ocean energy budgets, by influencing ocean heat uptake, storage and distribution (Mei *et al*., 2013). Seeing as tropical cyclones rely greatly on heat from the oceans, there has also been debate on whether a feedback between tropical cyclones and climate variability exist (Mei *et al*., 2013). After all modes of variability also impact sea surface heating regimes and energy distribution, and if tropical cyclones decrease these distributions, it could plausibly alter the presentation of the mode itself and its impacts on proceeding tropical cyclones (Xue *et al*., 2012; Malan *et al*., 2013; Kajtar *et al*., 2015; Magee & Verdon-Kidd, 2018).

6.4 Implications of the new knowledge

6.4.1 Applications in climate models

With the increased use of high-resolution (temporal and spatial) climate models, the need for accurate and equally high-resolution observational data is required (Murakami *et al*., 2012a; Camargo & Wing, 2016; Yamada *et al*., 2017; Yoshida *et al*., 2017). This study has used such data to construct an observationally based climatology to describe the optimal conditions at which a tropical cyclone in the Southern Hemisphere will most likely undergo tropical cyclone genesis. Existing models (Korty *et al*., 2012; Camargo *et al*., 2014; Camargo & Wing, 2016) apply the standard conditions set out by Gray (1968, 1979), in the form of genesis potential indices, and this has already been shown to be significantly different from the conditions required in the Southern Hemisphere. It has also been demonstrated that applying the thresholds of climate variables to define the point of occurrence of tropical cyclone genesis is problematic in climate models (Camargo *et al*., 2014, 2016; Wu & Zhou, 2012; Bell *et al*., 2013). This is due to the reliance of threshold values on the present climate, specifically when the sea surface temperature thresholds are involved (Camargo *et* *al*., 2014). For projecting future climates, similar to projecting past climates, threshold values of climate drivers for the genesis of tropical cyclones cannot be used accurately (Korty *et al*., 2012). The results of this study can provide an alternative, and instead of using the existing thresholds, the optimal ranges found in this investigation can be applied to potentially define a tropical cyclone in regional and hemispheric specific models. This will provide a wider possibility of magnitudes for each climate variable investigated at the point of storm genesis, which climate and forecast models can use to base their definitions of a tropical cyclone genesis event, as an alternative to relying on thresholds (Camargo & Wing, 2016).

Indeed, existing models are still limited in accurately projecting tropical cyclone activity or replicating a tropical cyclone that correlates fully with observational datasets (Camargo, 2013). Usually, intensity, sea surface temperature, frequency or geographical shifts in activity are under or over emphasised within these models (Wu & Zhou, 2012; Camargo & Wing, 2016). This is not to say models are unreliable, as short-term, long-term, regional and global climate models have been verified (when compared and correlated to the historical records) to accurately replicate the current observed tropical cyclone intensity and frequency trends (Kim *et al*., 2012; Murakami *et al*., 2012a; Rai *et al*., 2019; Wehner *et al*., 2018). However, the high resolution models that have been able to model tropical cyclone activity with high precision only do so as a result of increased horizontal resolution of the input data and not as a result of better predictions of the large scale environmental factors (Murakami *et al*., 2016; Yamada *et al*., 2017; Camp *et al*., 2019; Rai *et al*., 2019). The problem lies in the accuracy and precision of short-term projections such as tropical cyclone warning systems that deal with predicting the path, intensification and overall activity of a current tropical cyclone threat (Camargo & Wing, 2016). There is also concern regarding the best correlated models (based on their agreement with observation), which have difficulty in projecting high intensity storm landfalls and wind speeds for near-future storm seasons (Murakami *et al*., 2016). This is problematic, as it is these intense storms which are increasing in occurrence (Walsh *et al*., 2016; Bhatia *et al*., 2019). It is therefore important that new models related to early warning systems are developed or updated to allow mitigation or risk management to be planned and initiated (Loridan *et al*., 2017). One of the possibilities to solve this is the developing field of machine learning based models (Loridan *et al*., 2017). The observational data from this study can therefore be useful to newer model approaches for two reasons. One is that the climate data representing the large-scale environment was derived from high-resolution data, while the results offer new potential training data for models to utilise for the Southern Hemisphere (Loridan *et al*., 2017). Secondly, these machine learning based models use quantile-based data and integrate principal components, which will allow them to create projections which can be compared easily to historical data and by using a probabilistic framework also account for the uncertainty usually inherent in approximating the storm wind speeds and by extension the intensity (Loridan *et al*., 2017).

6.4.2 Tropical cyclone risk management

With the latest study (Ramsay *et al*., 2018) for the Southern Hemisphere projecting a significant increase in the intensity of tropical cyclones driven by a warming of the sea surface temperatures by 2°C, coupled with the observations of increased storm intensities (Walsh *et al*., 2016; Daloz & Camargo, 2018; Fitchett, 2018), there is a concern regarding the potential impacts of tropical cyclone activity. The results of this study display an increase in sea surface temperature and intensity, which is in line with the latest model-based results mentioned above. Furthermore, a study by Fitchett (2018) indicates a poleward shift of the most intense storms, which increases the areas at risk from tropical cyclone activity in the future. The results of this study, however, can contribute to the understanding of tropical cyclones, as a new climatology and the optimal tropical cyclone genesis requirements are now available. By integrating this information into forecast models and planning, it will be possible to accurately determine when and where a tropical cyclone will form and whether the environment could influence the tropical cyclones to make landfall or threaten new regions in the Southern Hemisphere (Murakami *et al*., 2012a, b; Ramsay *et al*., 2018). This study has also provided spatial and temporal aspects of mean tropical cyclone activity and the change in this activity over time (Table 5.3, Figure 5.5, Figure 5.27). According to Zhong *et al*. (2018), spatio-temporal mapping and data is highly important to decision makers and researchers (modelers) when attempting to map and decide when and where tropical cyclone activity will pose a risk to a region, and to what extent. Along the coastline of China, assessments based on observational results such as the peak season (months) and locations of tropical cyclone activity and landfall are used to create a hazard assessment and risk-based output to perform as a planning tool for potential tropical cyclone activity (see Zhong *et al*., 2018). With similar results now provided by this study for the Southern Hemisphere basins, such a risk assessment can be constructed for the relevant regions under threat from tropical cyclone activity.

6.5 Limitations

6.5.1 Tropical Cyclone Data Limitations

Firstly, the tropical cyclone data which provided locations, wind speed and date of the tropical cyclone genesis and intensification phases are captured at a 6-hourly interval (Knapp *et al*., 2010). This presents a potential source of inaccuracies regarding the location and the exact time at which a tropical cyclone would have reached genesis or maximum intensity phases, as these important thresholds could have occurred before or after the 6-hour interval (Magee *et al*., 2016). To decrease any of these inaccuracies to the best possible extent, the IBTrACS dataset was used as it is the optimal best track dataset regarding completeness of records (Knapp *et al*., 2010). The IBTrACS dataset was created by integrating multiple sources of data on tropical cyclone tracks, location and wind speed, thereby ensuring spatial coverage of all southern hemispheric tropical cyclone occurrences (Magee *et al*., 2016). Despite, the observation that the limitations mentioned still apply to this dataset, the data is found to be more reliable than using a single source such as the BoM or La Reunion data (Landsea *et al*., 2006; Knapp *et al*., 2010; Diamond *et al*., 2012). Using higher resolution climate data with a maximum of 2.5°x2.5° and a minimum of 0.25°x0.25° spatial resolution, which can account for any variation in location accuracy, as data returned at this scale would cover any discrepancies if they occurred in the IBTrACS which has a 110 km margin of error (i.e. approximately 1°). Since only sea surface temperature is at a minimum of 0.25°x0.25° resolution, the error margin would not have a great effect, as sea surface temperature does not vary greatly in magnitude over a short period of time (Reynolds *et al*., 2007).

The tropical cyclones were all included if all data pertaining to their activity was able to be captured. While this was done to limit bias, which would have been introduced in the process of removing so-called outliers or abnormal storms, there is the possibility despite the IBTrACS superb verification from multiple sources, that some storms that should have been removed due to error in capturing were not (Knapp *et al*., 2010; Ramsay *et al*., 2018). However, this was accounted for by using metrics such as the mean and working with ranges and spread of the data, rather than thresholds and specific values. Therefore, this resulted in foregoing some degree of precision, however, accuracy was maintained. Hence, also why the random error term is included in the multivariate regression equations, to outline the degree of error to be expected (Jobson, 2012). However, the climate variables within the storm environment (the eye, the forward and rear quadrants) vary based on their location (Lin *et al*., 2009; J.A. Zhang *et al*., 2017). For example, air temperature and moisture are usually found to decrease faster at the rear quadrants, hence if sampling of the data is taken from there, it will reflect lower values than the forward quadrants, while temperatures are also usually cooler over the eye region than over the cloud bands (Wu *et al*., 2015; J.A. Zhang *et al*., 2017).

6.5.2 Climate Drivers

Firstly, the reanalysis II dataset has inherent errors, such as human based from data processing (Kanamitsu *et al*., 2002). Assessments of the reanalysis does report that summer long and shortwave flux data does not agree with observational data as well as other analyses, while winter air temperatures do not agree with other analyses (Lindsay *et al*., 2014). However, for the purposes of attaining the most complete and consistent data for multiple different variables across two atmospheric heights, there are no other data sources besides the NCEP-NCAR based reanalyses that are offered. Omega is used to evaluate the vertical motion of the atmosphere and was used as a substitute for relative vorticity (buoyancy relative to the vortex) and the convective strength of the column related to the storm (Yu *et al*., 2016). Omega has only been used in relation to tropical cyclones as a variable of the overall motion in the environment (Song *et al*., 2018). While the angular metric related to vorticity cannot be captured by omega, there are already consensus that vorticity is required for tropical cyclone genesis as it initiates the spin up of the tropical cyclone (Tory *et al*., 2013). Vorticity data was not accessible at the time of data acquisition, and the data size was not practical to extract. While the vorticity metric cannot be used, the omega value still provided the necessary information related to upward motion and buoyancy and inferences on the strength of surface convergence and mass flux, which are main components related to vorticity in tropical cyclone environments, i.e. enhanced convergence, increases upward motion that in turn indicates enhanced vorticity (Tory *et al*., 2013). The trade-off here was that the vorticity element itself was left out, and therefore hemispheric differences in vorticity cannot be determined here, but this has been assessed by Kuleshov *et al*. (2009).

The v-wind shear (meridional) and u-wind shear (zonal) parameters for shear were used to assess their contribution during tropical cyclone genesis and to determine if they influenced the formation process in a different manner to vertical shear. While not usually used on their own as in this study, meridional shear and zonal shear cannot be compared easily to existing shear studies using the α component. This was accounted for by inferring the relative magnitudes of alpha using the mean as a reference, in order to determine high and low shear, which was effective in determining the shear values that supported more genesis events. After all these v-wind and u-wind variables are components used to derive vertical wind shear (Diamond *et al*., 2015), so examining them separately was not arbitrary. However, the canonical vertical wind shear was still calculated for a comparison of the shear environment here and in other studies, as well as to compare the α component from v-wind shear and u-wind shear against it.

7. Conclusion

7. Introduction

The study of tropical cyclones is a diverse and well-researched field, incorporating indices, models and observational data (Murakami *et al*., 2012a, b; Vecchi *et al*., 2014; Song *et al*., 2018). However, an absence of a definitive theory of tropical cyclone genesis persists (Walsh *et al*., 2016). The plethora of studies on tropical cyclones and climate change indicate an increase in the number of intense tropical cyclones accompanied by a decrease in overall storm frequency (Webster *et al*., 2005; Elsner *et al*., 2008; Ren *et al*., 2014; Lin *et al*., 2017; Tennille & Ellis, 2017; Xu *et al*., 2018). A poleward shift in the location of tropical cyclone genesis and the point of LMI has been observed across both the hemispheres (Kossin *et al*., 2014; Daloz & Camargo, 2018). The tropical cyclone intensity trends at a global and hemispheric scale have been subject to changes in observation as a result of data heterogeneity issues inherent in data prior to 1980 (Landsea *et al*., 2006; Kuleshov *et al*., 2010). The increasing trends of intensity demonstrated statistical significance in some instances (e.g. Webster *et al*., 2005), while other studies (Kuleshov *et al*., 2010; Klotzbach *et al*., 2015) re-examined these trends and failed to find a significant trend of increasing intensity.

There has been a larger amount of tropical cyclone research for the Northern Hemisphere compared to research done in the Southern Hemisphere (Figure 2.2). The focus on the impacts of climate change on tropical cyclone activity have also been focused more on the Northern Hemisphere basins (Gleixner *et al*, 2014; Daloz & Camargo, 2018). While research into tropical cyclone genesis requirements and climatology have been well constructed, such as the seasonal genesis indices by Gray (1968, 1979), these studies are predominantly based on Northern Hemisphere tropical cyclone activity and climatology, with poor data quality existing for the Southern Hemisphere at the time (Watterson *et al*, 1995; Landsea *et al*., 2006). Re-examinations of Gray's (1968, 1979) seasonal genesis indices indicate that only observations for the northern hemispheric tropical cyclone activity can be replicated reliably enough to agree with observational data (Watterson *et al*., 1995). Despite this, observational and climate model-based studies still use these genesis indices within the context of the Southern Hemisphere (Emanuel, 2013; Walsh *et al*., 2016). However, investigations indicate that differences in formation factors including sea surface temperature (Mavume *et al*., 2009; Defforge & Merlis, 2017a, b) and vertical wind shear (Nolan & McGauley, 2012) exist for the Southern Hemisphere and Northern Hemisphere tropical cyclone events. In addition, physical differentiations between the ocean basins in the north and south exist, including basin size and resultant heat storage capacity, with the larger oceans having a larger heat capacity (Lee *et al*., 2015; Gastineau *et al*., 2018). While the Northern Hemisphere basins have displayed larger mean temperatures, the Southern Hemisphere has been warming at a rapid rate and also receives more solar energy (Befort *et al*., 2016). The oceans are also not isolated by continental masses, but are instead connected via the Indonesian throughflow, which greatly influences the overall ocean heat and sea surface temperature in the Southern Hemisphere basins (Durack *et al*., 2018; Gastineau *et al*., 2018; Zhang *et al*., 2018)

This section will reflect on the achievements of the study in relation to the aims and provide an outline of the major results generated. The purpose and implications of the study will also be discussed with a conclusion of the chapter focused on the future applications and directions which should be taken within the study of tropical cyclone climatology.

The primary aim of the study was to explore and provide a detailed synoptic climatology of tropical cyclones in the Southern Hemisphere and determine the influences of climate change and synoptic/large-scale environmental variables on tropical cyclone variability and trends. From the examination of metrics of tropical cyclone activity and multiple climate variables at the point of genesis, this study has constructed a general climatology for Southern Hemisphere tropical cyclones. The results from this study additionally contribute to the trends and change over time in tropical cyclone activity and the climate variables at the point of genesis and frame these changes in the context of a warming climate over the last three decades. The study can also contribute to the field of climate modelling, genesis index construction and impact assessments, regarding the projections and mitigation of tropical cyclone impacts.

7.1. Achievement of Study Aims

The study had four main aims with the objective of creating a climatology for the Southern Hemisphere tropical cyclones. Theses aims which were addressed over the 36 year period from 1980-2016. The major findings associated with each aim will be outlined below in the order stated in Section 1.4.

1) Determine the dynamics and climatology of Southern Hemisphere tropical cyclones from 1980- present.

This aim was achieved by extracting the required data on tropical cyclone metrics of activity and climate data from the 1980-2016 storm seasons. The tropical cyclone track data extracted included the annual number of storms in each ocean basin, the latitude and longitude of each tropical cyclone genesis event, density of tropical cyclone genesis and intensification events, the duration of tropical cyclones across their lifetime and the duration, pressure and wind speed related to the tropical cyclones LMI stage. The climate data (sea surface and air temperature, relative humidity, v and u wind shear, omega, sea level pressure, and geopotential height) were extracted for each tropical cyclone at the time and location of storm genesis. The data was then analysed using descriptive statistics to attain the mean and standard deviations for tropical cyclone activity from each year within the Southern Hemisphere basins (SIO, WA, EA and SP) and the combined Southern Hemisphere storm events. The use of five number summaries were used together with the descriptive statistic outputs to determine the seasonality and locations of tropical cyclone occurrence and the nature of the variability and mean states, regarding the metrics of tropical cyclone activity. The linear regression and time trend plots were used to indicate the change within each metric of tropical cyclone activity and the changing magnitude of the climate variables at the point of genesis. This was done for storms from each basin and the hemisphere as a whole.

The mean conditions of tropical cyclone activity indicate a notable separation in the distribution of storm frequency, with an average of 20-30% more storm events occurring in the SIO per year, compared to the other Southern Hemisphere basins. A larger variability regarding frequency is also observed over the SIO. The season of tropical cyclone occurrence is similar for all the basins from December to April, with peak activity in January and February. A majority of tropical cyclone genesis events occur at 11-21°S of the equator, with the distribution being similar for all Southern Hemisphere basins. Of particular importance was the time taken by a tropical cyclone to attain its LMI. It was found that severe tropical cyclones (Category 4-5) took a longer time to reach their intensity than a lower intensity tropical cyclone (Category 1-3). Additional findings regarding the location of genesis and intensification, indicates a poleward shift over the study period, which confirms and updates the existing global findings regarding this poleward migration of storm activity (Kossin *et al*., 2014; Tennille & Ellis, 2017; Daloz & Camargo, 2018).

The major findings regarding the nature of tropical cyclone activity was an increase in tropical cyclone maximum intensity of 2.4 $m.s^{-1}$ per decade during the 1980-2016 period across the Southern Hemisphere. Individually, the tropical cyclones of SIO and SP account for the largest number of tropical cyclone occurrences annually and are experiencing a significant increase in intensity of 2.3 $m.s^{-1}$ and 3.6 $m.s^{-1}$ per decade respectively. The frequency of occurrence, duration and location of tropical cyclone activity at a basin-wide and hemispheric scale displays no significant change over the study period. Regarding the relationship between Southern Hemisphere storm activity and climate drivers, the omega, meridional shear, sea surface temperature and solar flux display statistically significant correlations with tropical cyclone intensity. This indicates that these variables demonstrate a significant influence over tropical cyclone intensity, despite these climate variables being measured at the point of genesis. Existing studies also report that sea surface temperature and an increase in the availability of heat energy in the environment does promote greater potential and observed tropical cyclone intensity (Li *et al*., 2013; Sebastian & Behera, 2015; Song *et al*., 2018). Importantly, this statistically significant increasing trend in tropical cyclone intensity updates and confirms the trend of intensity for the Southern Hemisphere storms which has been absent or weak due to data heterogeneity inherent in the storm data of past studies (Kuleshov *et al*., 2009; Klotzbach *et al*., 2015).

The observed time trends involving the thermodynamic climate variables at the point of genesis were only significant for sea surface temperature, air temperature, relative humidity and solar flux. The dynamic climate variables which demonstrated significant changes included vertical shear, meridional shear and omega, which represents vertical motion at the point of genesis. The importance of the changes in these variables indicates that the climate variables which demonstrate an influence over tropical cyclone genesis and intensification in the Southern Hemisphere are also changing over time, and in turn may be responsible for the observed changes in the tropical cyclone intensity and frequency. Specifically, since the variables of sea surface temperature, air temperature, relative humidity and solar flux indicate a statistically significant relationship to tropical cyclone intensity which demonstrates an increasing trend, it can be inferred that climate warming is responsible for the increased tropical cyclone intensity in the Southern Hemisphere.

Regarding the dynamic variables, vertical shear indicates an increase over time for Southern Hemisphere tropical cyclones. The increase of 0.3 $m.s^{-1}$ in vertical shear and increase of 0.06α per decade in meridional shear observed for the SIO and WA tropical cyclones respectively would not impact Northern Hemisphere tropical cyclones, as they have higher tolerances of up to 12-15 $m.s^{-1}$ (Gray, 1979; Nolan & Rappin, 2008; Klotzbach *et al*., 2017). However, a decrease in storm frequency can be expected or is already playing out since the increase in vertical shear in the Southern Hemisphere basins has the potential to increase above the current optimal values of 1-4 $m.s^{-1}$ observed for southern hemispheric storms in this study and by Nolan & McGauley (2012). The findings of an increasing trend in SIO geopotential height at the point of storm genesis has the potential to increase storm lifetime and size. This inference is based on existing investigations where geopotential height exhibited an increase during tropical cyclone formation (Matyas, 2015; Kim *et al*., 2017) and promoted an increase in tropical cyclone size and duration (Li *et al*., 2010). This also agrees with recent findings by Kossin *et al*. (2018), where a global increase in storm size and slowdown in their translation speed is observed.

2) Assess sea surface temperature, to interrogate the mean, minimum and optimal sea surface temperature required for formation and intensification of tropical cyclones in the Southern Hemisphere.

Aims two and three are similar as they require similar aspects of investigation, however, more attention was allocated to sea surface temperature, as it is noted as a major driver of genesis (Gray, 1968; Klotzbach *et al*., 2017; Bhaskaran *et al*., 2018). Additionally, due to the availability of higher spatial resolution sea surface temperature data compared to the other variables, it was easier to ensure better accuracy in the results (Reynolds *et al*., 2007; Murakami *et al*., 2012a; Rai *et al*., 2019). The climate data (sea surface and air temperature, relative humidity, v and u wind shear, omega, sea level pressure and geopotential height) were analysed using descriptive statistics, five number summaries to extract the mean, maximum and minimum magnitudes along with SD, to determine range and variability for each variable at the point of genesis. The use of histograms facilitated the extraction of optimal magnitudes at which the majority of storm genesis events occurred for each climate variable. Multivariate multiple regression was used with the climate variables as the independent variables and the tropical cyclone metrics of activity as the response/dependent variables to determine any statistically significant influence between the climate variables and tropical cyclone activity.

One of the main aims of this study was to assess the sea surface temperature required for storm genesis to take place. Within this study, the minimum sea surface temperature at which Southern Hemisphere tropical cyclones have formed fell within the 24°C range, which is well below the common formation threshold of 26.5°C (Gray, 1968; Tory & Dare, 2015). Of importance is the optimal magnitude of sea surface temperature at the point of genesis, which was observed as 27.5-28.5°C. This demonstrates the sea surface temperature at which the greatest number of tropical cyclones from 1980-2016 have been observed to undergo genesis. The number of genesis events decreases when the temperature is higher or lower than this range. At a basin-scale a lower mean sea surface temperature at the point of genesis is 29°C in the western basins (SIO and WA) but over one degree greater in the eastern basins (EA and SP). The optimal sea surface temperature for Southern Hemisphere tropical cyclones demonstrates a substantially different magnitude from the Northern Hemisphere temperatures at the point of genesis, and do not follow the canonical 26.5°C threshold (Gray, 1968; Klotzbach *et al.*, 2017). Indeed, the concept of a threshold has been questioned in the past (Dare & McBride, 2011; Tory & Dare, 2015; Defforge & Merlis, 2017a) and it is demonstrated within this study that since storms do have the ability to form outside this threshold, the concept may not stand for Southern Hemisphere tropical cyclones. The difference in sea surface temperatures observed between Southern Hemisphere basins and those required for the Northern Hemisphere storm genesis events (Defforge & Merlis, 2017a) can be attributed to the different climatological background temperatures. For example, higher mean environmental temperatures are able to promote higher mean sea surface temperatures at the point of genesis and conversely so (Defforge & Merlis, 2017a, b).

Based on the factor analysis weightings and multivariate regression, sea surface temperature also accounts for a relatively large amount of variability in the formation process of tropical cyclones, compared to the other climate variables examined at the point of genesis, and it has been found that higher sea surface temperatures above 27°C are required for intense category 4-5 tropical cyclones to form. The implication of the sea surface temperature increase and its influence of storm intensity are already being observed, as the occurrence of more intense tropical cyclones coincide with higher sea surface temperatures (Ren *et al*., 2014; Xu *et al*., 2017; Foltz *et al*., 2018). This is similarly, true for the southern hemisphere storms. Regarding the sea surface temperatures at the point of intensification, the magnitudes follow those observed at the point of genesis closely, with a majority of tropical cyclones undergoing intensification at a sea surface temperature of approximately 27-28°C, indicating that relatively high sea surface temperatures are preferred for the majority of Southern Hemisphere tropical cyclone intensification.

3) Assess mean, minimum and optimal magnitudes of surface pressure, air temperature, relative humidity zonal, meridional and vertical wind shear and the omega associated with each of the genesis events to determine the synoptic requirements and influencers of formation for Southern Hemisphere tropical cyclones.

The mean and minimum magnitudes for each of these climate variables were recorded at the point of genesis for the Southern Hemisphere tropical cyclones. For these variables, the 1,000mb and 850mb levels were examined to determine the difference in the climate variables at the surface and the higher atmospheric heights and the implications they have on the tropical cyclone development. Sea surface temperature and air temperature accounted for the largest amount of variability in tropical cyclone genesis. However, for category 5 storms, omega and meridional shear account for the largest amount of variability at the point of genesis. The optimal air temperature at the near surface 1,000mb level is similar to the sea surface temperature with a magnitude of 27-28°C. This similarity not only indicates that high air temperatures are present during the majority of genesis events but demonstrates the environmental air-sea interaction of the ocean heat transfer into the lower atmosphere. This further enhances convection and moisture, which is favourable for a tropical cyclone genesis environment (L. Zhang *et al.*, 2017; Bhaskaran *et al.*, 2018). Similar magnitudes are observed for relative humidity and vertical shear at the point of genesis compared to existing studies (Nolan & McGauley, 2012; Wu *et al.*, 2015). Optimal vertical shear (1-4 $m.s^{-1}$) is much lower than the 15 $m.s^{-1}$ shear threshold assumed for the Northern Hemisphere (Klotzbach *et al.*, 2017). It has also been stated that tropical cyclone genesis rarely takes place when relative humidity is below 40%, which also falls within the 50-60% range required for deep convection to take place (Gray, 1977; DeMaria *et al.*, 2001; McGauley & Nolan, 2011). This is likely due to the higher sea surface temperatures at the point of genesis, which are known to exacerbate the effect of high shear magnitudes (Nolan & McGauley, 2012). Provided relative humidity is not below 40% and vertical shear falls within 1-4 $m.s^{-1}$, these factors should not prevent tropical cyclone genesis from taking place. The majority of Southern Hemisphere storms had a high magnitude of relative humidity at the point of genesis, indicating a preference for high moisture content during tropical cyclone formation. Higher levels of solar flux have also been present for a majority of tropical cyclone occurrences in the Southern Hemisphere. This is attributed to the coincidence of the tropical cyclone season during summer months when solar flux is naturally higher, but also adds to the existing research by Li *et al*. (2018) which similarly reported increased tropical cyclone occurrences when solar flux is high. Indeed, fewer storms were recorded to form at solar flux magnitudes below 62-88 $W.m^{-2}$ for Southern Hemisphere tropical cyclones in this study.

Omega was used as an estimate of large-scale vertical velocity, to detect upward motion or buoyancy. Not many studies applied omega in the context of tropical cyclones before (Song *et al*., 2018). This study indicates that omega is negative for the majority of genesis events. This is due to negative omega indicating horizontal convergence at the surface and expansion of the atmosphere which results in increased upward motion. Since buoyancy and high rates of upward motion with surface convergence are some of the requirements for tropical cyclone formation (Gray, 1968, 1979; Klotzbach *et al*., 2017; Bhaskaran *et al*., 2018), it appears that omega may be a good estimator of buoyancy and horizontal shear at the point of genesis. However, future studies should incorporate omega and compare it to other metrics of vertical velocity to confirm its role as an influencer over tropical cyclone genesis. The optimal magnitudes for the variables at the point of genesis are below :

1) Air Temperature: 27°C-28°C (1,000mb) and 18-19°C (850mb)
2) Omega: -0.01-0.01pascal.s^{-1} (1,000mb) and -0.18- -0.07pascal.s^{-1} (850mb)
3) Relative Humidity: 79-83% (1,000mb) and 75-88% (850mb)
4) Meridional shear (v-wind component): -0.06-0.24α and Zonal shear (u-wind component): -0.08-0.20α
5) Vertical shear: 1-4 $m.s^{-1}$ (1,000mb-850mb)
6) Solar Flux: 140-218W/m^2 (upper atmosphere)

4) Assess the different roles of ENSO and other mechanisms or modes of variability including but not limited to the IOD, MJO, PDO, AAO (SAM), solar energy flux and volcanic activity regarding tropical cyclone activity across the three major ocean basins regions (SIO, Australian and SP) of the Southern Hemisphere.

To determine the influence which the modes of variability have on tropical cyclone activity, each metric of activity was run through a multivariate regression, with the combined modulators used as the independent variables and the metrics of tropical cyclone activity related to the point of genesis and the point of maximum intensification used as the response/dependent variables. From the modes examined only the ENSO indices, the IOD index, the SAM/AAO index and volcanic eruption events were correlated or indicated a statistically significant relationship to metrics of tropical cyclone activity. Tropical cyclone intensity indicates a positive relationship with warm ENSO phases. All the indices representing ENSO (SOI, Niño 3.4 and the MEI) demonstrated statistically significant relationships to tropical cyclone activity. The longitude of genesis was also related to ENSO, with the direction of the regression indicating that negative phases of ENSO influenced shifts in longitude, while positive phases influenced increased duration in Southern Hemisphere tropical cyclones. The major finding here is that ENSO influences the location and intensification of tropical cyclones, which is similarly recorded by Kuleshov *et al*. (2009) and Diamond *et al*. (2013) for tropical cyclones in the South Indian and Pacific basins. ENSO and IOD both have an influence over tropical cyclone and total storm lifetime. This effect on duration has been linked by existing studies to enhanced sea surface temperatures, convection and moisture content in the environment (Wing *et al*., 2015; Burn *et al*., 2016; Liu *et al*., 2019). The SAM/AAO is found to influence Southern Hemisphere tropical cyclone intensity. SAM has usually been linked to increased storm frequency resulting from its modulation on sea surface temperature and zonal winds, however, the modulation demonstrated by SAM over relative humidity and sea surface temperature is a possible mechanism of influence over intensity (Mao *et al*., 2013; L. Zhang *et al*., 2017).

While not a mode of variability, volcanic activity is observed as an important forcer over tropical cyclone activity. This study finds that volcanic eruptions have a positive direction of influence over the longitudinal location of both tropical cyclone genesis and intensification, indicating that an eastward shift in formation and intensification can be expected after a large eruption event. Recently, similar findings were presented by Pausata & Camargo (2019), whereby volcanic activity is found to shift the locations of the ITCZ away from the hemisphere (north or south) experiencing a large eruption, therefore allowing a greater number of formation events over the hemisphere which the ITCZ has shifted over. The conditions found at the ITCZ are known to promote tropical cyclone genesis and intensification potential, hence the effects on tropical cyclone frequency and intensity (Mavume *et al*., 2009; Evans *et al*., 2012; Wing *et al*., 2015; Pausata & Camargo, 2019). More research is required to reconcile longitudinal variation in the ITCZ and its impact on tropical cyclone activity (Byrne *et al*., 2018).

7.2 Purpose and Implications of the Study

7.3.1 Purpose

This study was undertaken to provide a new viewpoint to a long-accepted theory of tropical cyclone genesis climatology. In reality this climatology was based on older and heterogeneous datasets and low-resolution climate data concerning the large-scale environment of the Southern Hemisphere at the time. By re-examining tropical cyclone activity and the climate variables involved during tropical cyclone genesis, this study has determined new optimal ranges of the climate variables related to the influence of tropical cyclone formation in addition to the patterns and trends of tropical cyclone activity. Therefore, this study has been able to provide a southern hemispheric tropical cyclone climatology, while also outlining the similarities and differences between the southern and Northern Hemispheres.

7.3.2 Implications of the Study

The widely used concept of thresholds for the tropical cyclone genesis climate variables was brought into question by a number of studies (Dare & McBride, 2011; Tory & Dare, 2015; Defforge & Merlis, 2017a), and indicated additional problems when used by models (Camargo & Wing, 2016). Because this study did not remove or filter out storms if they presented as outliers, it was found that not only do the majority of storms have a preferential optimal magnitude for each climate variable, but that they occur across a range of lower and higher magnitudes outside of this optimal range. This indicates that the concept of thresholds does not apply to the genesis of tropical cyclones, as if even one occurrence falls outside the optimal magnitude, it cannot be considered a threshold but a range instead. This will affect how model based studies identify Southern Hemisphere tropical cyclone genesis, as instead of using a threshold of 26°C, the modelers will need to use a probabilistic method based on a range, which makes more sense, as tropical cyclones are natural phenomena and do not operate on the premise of thresholds, but vary greatly regarding their tropical cyclone genesis conditions. Genesis indices, which attempt to determine the conducivity of the environment for tropical cyclone genesis, may also have to start using the new optimal range of sea surface temperature found here, as it is clearly higher than the threshold based off Northern Hemisphere climatology.

This is the first study to examine a selection of the climate variables known to influence tropical cyclone genesis likelihood, using the latest high-resolution datasets. There have been many questions around tropical cyclone intensity, and whether the trends of increase are data artefacts or due to intensity being overestimated in the tropical cyclone datasets. This was only a problem for studies using data prior to 1970/1980 (Landsea *et al*., 2006). This study, however, has used data that has been verified as close to accurate as possible from the 1980s onward, and therefore the intensity trends are relatively more reliable. It is indeed observed that tropical cyclone intensity is experiencing an increasing trend over the Southern Hemisphere. In examining the climate variables, the results regarding the thermodynamic and dynamic variables optimal ranges in relation to the change over time of these variables have different outcomes. The sea surface temperature, air temperature and relative humidity indicate preferences of high magnitudes at the point of genesis and are showing an increasing rate over time (except for relative humidity), inferring that these optimal genesis ranges for the thermodynamic variables are increasing as the climate warms. Intensity is driven by these same variables, which are shown to produce an environment conducive for deep convection and provide larger amounts of heat energy to the storm (Bhatia *et al*., 2019). Therefore, the increasing trends in intensity can be attributed to these variables, as also shown by the correlation between these variables and intensity. The overall outcome is that with a further warming climate and increase in the magnitude of these tropical cyclone genesis climate variables over time the intensity will continue to increase too. The increase in vertical shear, proves detrimental to tropical cyclone genesis and may explain why the frequency of storms is decreasing (L. Zhang *et al*., 2017). Therefore, as vertical shear at the point of genesis increases in the Southern Hemisphere, the storm number may continue decreasing, however, this does not necessarily include a decrease in intensity when storms do form, as the thermodynamic variables supporting greater intensities still indicate growth as observed by this and multiple existing studies (Holland & Bruyere, 2014; Walsh *et al*., 2016; Murakami *et al*., 2016; Defforge *et al*., 2017b; Daloz & Camargo, 2018). While this study has provided new conditions of formation for Southern Hemisphere tropical cyclones, this is not a comprehensive explanation of storm genesis, as the variables examined may not be the only drivers which influence the stage of genesis.

7.4 The implications for future work

It is primarily model based studies and risk management and early warning studies that may be influenced by this study. But it must be noted that a new updated climatology has now been created for the Southern Hemisphere tropical cyclones, which for the first time allows a more definitive separation from Northern Hemisphere tropical cyclones. Future research should examine the tropical cyclone activity and climate drivers which are known to influence tropical cyclone dynamics across larger time periods. Therefore, longer term trends using more robust datasets in the future are required to attain a longer-term climatology (+50 years), to examine decadal trends. This can inform and validate the long-term model-based projections of tropical cyclone activity. However, while this study has provided the observable optimal and minimum magnitudes of climate variables at the point of genesis and has introduced the use of air temperature, v-wind shear, solar flux and omega as potential influencers of tropical cyclone activity, these variables do not account for all of the variability related to tropical cyclogenesis. Therefore, an effort should be made to build upon this work and determine other variables which influence tropical cyclogenesis. In addition, a logical continuation of this research is a focus on Southern Hemisphere tropical cyclone dissipation, to explore the drivers and more intricate dynamics behind the dissipation of tropical cyclones and the areas they are more likely to impact, especially under the poleward shift observed in tropical cyclone activity. One of the factors outlined by this study is the discrepancy which exists between Northern and Southern Hemisphere tropical cyclone studies, resulting from data quality issues inherent in the observational data prior to 1980. Since there now exists a reliable amount of data for the Southern Hemisphere, future tropical cyclone studies can assign greater focus on Southern Hemisphere tropical cyclone activity. What this study also outlines for future research, is that more focus is required regarding the variability of tropical cyclone activity at a hemispheric and global scale.

The mechanisms and effects related to how tropical cyclones are impacting climate over long and short time periods is another avenue which will provide a better understanding regarding the interactions between tropical cyclones and the climate system. While this study has examined some of the conditions required for tropical cyclone formation, the principle mechanisms and physical processes behind the influence of the climate variables was only inferred, therefore an examination of the first principles regarding tropical cyclone genesis may be required, as the exact events around the point of genesis are still unobserved, therefore preventing an encompassing genesis theory for tropical cyclones.

Concerning risk management, the locations and times laid out in this study can be used as a reference to build more detailed probability maps, and plan or undertake risk assessments based high risk regions and return rates of tropical cyclones in the Southern Hemisphere.

References

Allen, R.J., Norris, J.R. and Kovilakam, M. (2014). Influence of anthropogenic aerosols and the Pacific Decadal Oscillation on tropical belt width. *Nature Geoscience*, 7(4): 270-274.

Altman, J., Ukhvatkina, O.N., Omelko, A.M., Macek, M., Plener, T., Pejcha, V., Cerny, T., Petrik, P., Srutek, M., Song, J.S. and Zhmerenetsky, A.A. (2018). Poleward migration of the destructive effects of tropical cyclones during the 20th century. *Proceedings of the National Academy of Sciences*, 115(45): 11543-11548.

Ash, K.D. and Matyas, C.J. (2012). The influences of ENSO and the subtropical Indian Ocean Dipole on tropical cyclone trajectories in the southwestern Indian Ocean. *International Journal of Climatology*, 32(1): 41–56.

Astier, N., Plu, M. and Claud, C. (2015). Associations between tropical cyclone activity in the Southwest Indian Ocean and El Niño Southern Oscillation. *Atmospheric Science Letters*, 16(4): 506-511.

Atkinson, G.D. and Holliday, C.R. (1977). Tropical cyclone minimum sea level pressure/maximum sustained wind relationship for the western North Pacific. *Monthly Weather Review*, 105(4): 421-427.

Bacmeister, J.T., Reed, K.A., Hannay, C., Lawrence, P., Bates, S., Truesdale, J.E., Rosenbloom, N. and Levy, M. (2018). Projected changes in tropical cyclone activity under future warming scenarios using a high-resolution climate model. *Climatic Change*, 146(3-4): 547-560.

Barcikowska, M.J., Knutson, T.R. and Zhang, R. (2017). Observed and simulated fingerprints of multidecadal climate variability and their contributions to periods of global SST stagnation. *Journal of Climate*, *30*(2): 721-737.

Befort, D.J., Wild, S., Kruschke, T., Ulbrich, U. and Leckebusch, G.C. (2016). Different long-term trends of extra-tropical cyclones and windstorms in ERA-20C and NOAA-20CR reanalyses. *Atmospheric Science Letters*, 17(11): 586-595.

Bell, R., Strachan, J., Vidale, P.L., Hodges, K. and Roberts, M. (2013). Response of tropical cyclones to idealized climate change experiments in a global high-resolution coupled general circulation model. *Journal of Climate*, 26(20): 7966-7980.

Bender, M.A., Knutson, T.R., Tuleya, R.E., Sirutis, J.J., Vecchi, G.A., Garner, S.T. and Held, I.M. (2010). Modeled impact of anthropogenic warming on the frequency of intense Atlantic hurricanes. *Science*, 327(5964): 454-458.

Bessafi, M. and Wheeler, M.C. (2006). Modulation of south Indian Ocean tropical cyclones by the Madden–Julian oscillation and convectively coupled equatorial waves. *Monthly Weather Review*, 134(2): 638-656.

Bhaskaran, P.K, Albert, J. and Sahoo, B. (2018). Tropical cyclogenesis for North Indian Ocean Region. In Bhaskaran, P.K, Albert, J. and Sahoo, B. (Eds.) *Climate Change and the Vulnerable Indian Coast,* Ministry of Environment, Forestry and Climate Change, New Delhi: 55-71.

Bhatia, K.T, Vecchi, G.A, Murakami, H., Underwood, S. and Kossin, J. (2018). Projected response of tropical cyclone intensity and intensification in a global climate model. *Journal of Climate*, 31(20): 8281-8303.

Bhatia, K.T., Vecchi, G.A., Knutson, T.R., Murakami, H., Kossin, J., Dixon, K.W. and Whitlock, C.E. (2019). Recent increases in tropical cyclone intensification rates. *Nature Communications*, 10(653): doi:10.1038/s41467-019-08471-z.

Bracken, W.E. and Bosart, L.F. (2000). The role of synoptic-scale flow during tropical cyclogenesis over the North Atlantic Ocean. *Monthly weather review*, 128(2): 353-376.

Bratton, D.C. and Womeldorf, C.A. (2011). The wind shear exponent: comparing measured against simulated values and analyzing the phenomena that affect the wind shear. Proceedings of *ASME 2011 5th International Conference on Energy Sustainability,* Washington DC (7-10 August 2011), 2245-2251.

Braun, S.A., Sippel, J.A. and Nolan, D.S. (2012). The impact of dry midlevel air on hurricane intensity in idealized simulations with no mean flow. *Journal of the Atmospheric Sciences*, 69(1): 236-257.

Bryson, R.A. (1997). The paradigm of climatology: An essay. *Bulletin of the American Meteorological Society*, 78(3), pp.449-456.

Burns, J.M., Subrahmanyam, B., Nyadjro, E.S. and Murty, V.S.N. (2016). Tropical cyclone activity over the Southwest Tropical Indian Ocean. *Journal of Geophysical Research: Oceans*, 121(8): 6389-6402.

Byrne, M.P., Pendergrass, A.G., Rapp, A.D. and Wodzicki, K.R. (2018). Response of the intertropical convergence zone to climate change: Location, width, and strength. *Current Climate Change Reports*, 4(4): 355-370.

Cai, W., Wang, G., Gan, B., Wu, L., Santoso, A., Lin, X., Chen, Z., Jia, F. and Yamagata, T. (2018a). Stabilised frequency of extreme positive Indian Ocean Dipole under 1.5 C warming. *Nature communications*, 9(1419): doi:10.1038/s41467-018-03789-6.

Cai, W., Wang, G., Dewitte, B., Wu, L., Santoso, A., Takahashi, K., Yang, Y., Carréric, A. and McPhaden, M.J. (2018b). Increased variability of eastern Pacific El Niño under greenhouse warming. *Nature*, 564(7735): 201-206.

Callaghan, J. and Power, S.B. (2011). Variability and decline in the number of severe tropical cyclones making land-fall over eastern Australia since the late nineteenth century. *Climate Dynamics*, 37(3-4): 647-662.

Camara, M., Diedhiou, A. and Gaye, A.T. (2010). Spatial and temporal distribution of North Atlantic tropical cyclones. *African Journal of Environmental Science and Technology*, 4(1): 6-12.

Camargo[1], S.J., Barnston, A.G., Klotzbach, P.J. and Landsea, C.W. (2007). Seasonal tropical cyclone forecasts. *WMO Bulletin*, 56(4): 297-309.

Camargo, S.J., Wheeler, M.C. and Sobel, A.H. (2009). Diagnosis of the MJO modulation of tropical cyclogenesis using an empirical index. *Journal of the Atmospheric Sciences*, 66(10): 3061-3074.

Camargo, S.J., Sobel, A.H., Barnston, A.G. and Klotzbach, P.J. (2010). The influence of natural climate variability on tropical cyclones, and seasonal forecasts of tropical cyclone activity. In *Global perspectives on tropical cyclones: From science to mitigation* pp. 325-360.

Camargo, S.J. (2013). Global and regional aspects of tropical cyclone activity in the CMIP5 models. *Journal of Climate*, 26(24), 9880-9902.

Camargo, S.J., Tippett, M.K., Sobel, A.H., Vecchi, G.A. and Zhao, M. (2014). Testing the performance of tropical cyclone genesis indices in future climates using the HiRAM model. *Journal of Climate*, 27(24): 9171-9196.

Camargo, S.J. and Wing, A.A. (2016). Tropical cyclones in climate models. *Wiley Interdisciplinary Reviews: Climate Change*, 7(2): 211-237.

Camp, J., Roberts, M.J., Comer, R.E., Wu, P., MacLachlan, C., Bett, P.E., Golding, N., Toumi, R. and Chan, J.C. (2019). The western Pacific subtropical high and tropical cyclone landfall: Seasonal forecasts using the Met Office GloSea5 system. *Quarterly Journal of the Royal Meteorological Society*, 145(718): 105-116.

Chang, E.K. (2017). Projected significant increase in the number of extreme extratropical cyclones in the Southern Hemisphere. *Journal of Climate*, 30(13): 4915-4935.

Chang-Seng, D.S. and Jury, M.R. (2010). Tropical cyclones in the SW Indian Ocean. Part 1: inter-annual variability and statistical prediction. *Meteorology and Atmospheric Physics*, 106(3-4): 149-162.

Chen, B.F., Davis, C.A. and Kuo, Y.H. (2018). Effects of Low-Level Flow Orientation and Vertical Shear on the Structure and Intensity of Tropical Cyclones. *Monthly Weather Review*, 146(8): 2447-2467.

Chen, H.F., Liu, Y.C., Chiang, C.W., Liu, X., Chou, Y.M. and Pan, H.J. (2019). China's historical record when searching for tropical cyclones corresponding to Intertropical Convergence Zone (ITCZ) shifts over the past 2 kyr. *Climate of the Past*, 15(1): 279-289.

Christidis, N. and Stott, P.A. (2015). Changes in the geopotential height at 500 hPa under the influence of external climatic forcings. *Geophysical Research Letters*, 42(24): 10-798.

Cinco, T.A., de Guzman, R.G., Ortiz, A.M.D., Delfino, R.J.P., Lasco, R.D., Hilario, F.D., Juanillo, E.L., Barba, R. and Ares, E.D. (2016). Observed trends and impacts of tropical cyclones in the Philippines. *International Journal of Climatology*, 36(14): 4638-4650.

Clem, K.R., Renwick, J.A., McGregor, J. and Fogt, R.L. (2016). The relative influence of ENSO and SAM on Antarctic Peninsula climate. *Journal of Geophysical Research: Atmospheres*, 121(16): 9324-9341.

Colbert, A.J., Soden, B.J. and Kirtman, B.P. (2015). The impact of natural and anthropogenic climate change on western North Pacific tropical cyclone tracks. *Journal of Climate*, 28(5): 1806-1823.

Daloz, A.S. and Camargo, S.J. (2018). Is the poleward migration of tropical cyclone maximum intensity associated with a poleward migration of tropical cyclone genesis? *Climate Dynamics*, 50(1-2): 705-715.

Dare, R.A. and Davidson, N.E. (2004). Characteristics of tropical cyclones in the Australian region. *Monthly Weather Review*, 132(12): 3049-3065.

Dare, R.A. and McBride, J.L. (2011). The threshold sea surface temperature condition for tropical cyclogenesis. *Journal of Climate*, 24(17): 4570-4576.

Defforge, C.L. and Merlis, T.M. (2017a). Evaluating the Evidence of a Global Sea Surface Temperature Threshold for Tropical Cyclone Genesis. *Journal of Climate*, 30(22): 9133-9145.

Defforge, C.L. and Merlis, T.M. (2017b). Observed warming trend in sea surface temperature at tropical cyclone genesis. *Geophysical Research Letters*, 44(2): 1034-1040.

DeMaria, M., Knaff, J.A. and Connell, B.H. (2001). A tropical cyclone genesis parameter for the tropical Atlantic. *Weather and Forecasting*, 16(2): 219-233.

Diamond, H.J., Lorrey, A.M., Knapp, K.R. and Levinson, D.H. (2012). Development of an enhanced tropical cyclone tracks database for the southwest Pacific from 1840 to 2010. *International Journal of Climatology*, 32(14): 2240-2250.

Diamond, H.J., Lorrey, A.M. and Renwick, J.A. (2013). A southwest Pacific tropical cyclone climatology and linkages to the El Niño–Southern Oscillation. *Journal of Climate*, 26(1): 3-25.

Diamond, H.J. and Renwick, J.A. (2015). The climatological relationship between tropical cyclones in the southwest Pacific and the southern annular mode. *International Journal of Climatology*, 35(4): 613-623.

Diamond, H.J. and Renwick, J.A. (2015). The climatological relationship between tropical cyclones in the southwest pacific and the Madden–Julian Oscillation. *International Journal of Climatology*, *35*(5), 676-686.

Ding, Q., Steig, E.J., Battisti, D.S. and Wallace, J.M. (2012). Influence of the tropics on the Southern Annular Mode. *Journal of Climate*, 25(18): 6330-6348.

Done, J.M., Holland, G.J., Bruyère, C.L., Leung, L.R. and Suzuki-Parker, A. (2015). Modeling high-impact weather and climate: lessons from a tropical cyclone perspective. *Climatic Change*, 129(3-4): 381-395.

Dong, B. and Sutton, R.T. (2005). Mechanism of interdecadal thermohaline circulation variability in a coupled ocean–atmosphere GCM. *Journal of climate*, 18(8): 1117-1135.

Doocy, S., Daniels, A., Packer, C., Dick, A. and Kirsch, T.D. (2013). The human impact of earthquakes: a historical review of events 1980-2009 and systematic literature review. *PLoS currents*, 5: doi:10.1371%2Fcurrents.dis.67bd14fe457f1db0b5433a8ee20fb833.

Dowdy, A.J., Qi, L., Jones, D., Ramsay, H., Fawcett, R. and Kuleshov, Y. (2012). Tropical cyclone climatology of the South Pacific Ocean and its relationship to El Niño–Southern Oscillation. *Journal of Climate*, 25(18): 6108-6122.

Durack, P.J., Gleckler, P.J., Purkey, S.G., Johnson, G.C., Lyman, J.M. and Boyer, T.P. (2018). Ocean Warming: From the Surface to the Deep in Observations and Models. *Oceanography*, 31(2): 41-51.

Eichler, T.P. and Gottschalck, J., 2013. A comparison of Southern Hemisphere cyclone track climatology and interannual variability in coarse-gridded reanalysis datasets. *Advances in Meteorology*, 2013.

Elsner, J.B., Kossin, J.P. and Jagger, T.H. (2008). The increasing intensity of the strongest tropical cyclones. *Nature*, 455(7209): 92-95.

Emanuel, K.A. (1986). An air-sea interaction theory for tropical cyclones. Part I: Steady-state maintenance. *Journal of the Atmospheric Sciences*, 43(6): 585-605.

Emanuel, K.A. (1988). The maximum intensity of hurricanes. *Journal of the Atmospheric Sciences*, 45(7): 1143-1155.

Emanuel, K. (2000). A statistical analysis of tropical cyclone intensity. *Monthly Weather Review*, 128(4): 1139-1152.

Emanuel, K. (2003). Tropical cyclones. *Annual Review of Earth and Planetary Sciences*, 31(1): 75-104.

Emanuel, K.A., DesAutels, C., Holloway, C. and Korty, R. (2004). Environmental control of tropical cyclone intensity. *Journal of the Atmospheric Sciences*, 61(7): 843-858.

Emanuel, K.A. (2005). Increasing destructiveness of tropical cyclones over the past 30 years. *Nature*, 436(7051): 686-688.

Emanuel, K.A. (2010). Tropical cyclone activity downscaled from NOAA-CIRES reanalysis, 1908–1958. *Journal of Advances in Modeling Earth Systems*, *2*(1): doi: 10.3894/JAMES.2010.2.1.

Emanuel, K.A. (2013). Downscaling CMIP5 climate models shows increased tropical cyclone activity over the 21st century. *Proceedings of the National Academy of Sciences*, 110(30): 12219-12224.

Evan, A.T. (2012). Atlantic hurricane activity following two major volcanic eruptions. *Journal of Geophysical Research: Atmospheres*, 117(D6): doi: 10.1029/2011JD016716.

Evans, J.L. and Waters, J.J. (2012). Simulated relationships between sea surface temperatures and tropical convection in climate models and their implications for tropical cyclone activity. *Journal of Climate*, 25(22): 7884-7895.

Evans, J.L. and Webster, C.C. (2014). A variable sea surface temperature threshold for tropical convection. *Australian Meteorological and Oceanographic Journal*, 64(1): doi: 10.22499/2.6401.007.

Farfán, L.M. and Fogel, I. (2007). Influence of tropical cyclones on humidity patterns over southern Baja California, Mexico. *Monthly Weather Review*, 135(4): 1208-1224.

Finocchio, P.M. and Majumdar, S.J. (2017). A statistical perspective on wind profiles and vertical wind shear in tropical cyclone environments of the Northern Hemisphere. *Monthly Weather Review*, 145(1): 361-378.

Fisher, E.L. (1958). Hurricanes and the sea-surface temperature field. *Journal of Meteorology*, 15(3): 328-333.

Fitchett, J.M. and Grab, S.W. (2014). A 66-year tropical cyclone record for south-east Africa: temporal trends in a global context. *International Journal of Climatology*, 34(13): 3604-3615.

Fitchett, J.M. (2018). Recent emergence of CAT5 tropical cyclones in the South Indian Ocean. *South African Journal of Science*, 114(11-12): 1-6.

Fogt, R.L., Bromwich, D.H. and Hines, K.M. (2011). Understanding the SAM influence on the South Pacific ENSO teleconnection. *Climate Dynamics*, 36(7-8): 1555-1576.

Foltz, G.R., Balaguru, K. and Hagos, S. (2018). Interbasin differences in the relationship between SST and tropical cyclone Intensification. *Monthly Weather Review*, 146(3): 853-870.

Frank, W.M. and Young, G.S. (2007). The interannual variability of tropical cyclones. *Monthly Weather Review*, 135(10): 3587-3598.

Franklin, J.L., Feuer, S.E., Kaplan, J. and Aberson, S.D. (1996). Tropical cyclone motion and surrounding flow relationships: Searching for beta gyres in omega dropwindsonde datasets. *Monthly Weather Review*, 124(1): 64-84.

Fussell, E., Curran, S.R., Dunbar, M.D., Babb, M.A., Thompson, L. and Meijer-Irons, J. (2017). Weather-related hazards and population change: A study of hurricanes and tropical storms in the United States, 1980–2012. *The Annals of the American Academy of Political and Social Science*, 669(1): 146-167.

Gastineau, G., Friedman, A.R., Khodri, M. and Vialard, J. (2018). Global ocean heat content redistribution during the 1998–2012 Interdecadal Pacific Oscillation negative phase. *Climate Dynamics*, doi: 10.1007/s00382-018-4387-9.

Gilford, D.M., Solomon, S. and Emanuel, K.A. (2017). On the seasonal cycles of tropical cyclone potential intensity. *Journal of Climate*, 30(16): 6085-6096.

Gillett, N.P., Stott, P.A. and Santer, B.D. (2008). Attribution of cyclogenesis region sea surface temperature change to anthropogenic influence. *Geophysical Research Letters*, 35(9): doi: 10.1029/2008GL033670.

Girishkumar, M.S., Prakash, V.T. and Ravichandran, M. (2015). Influence of Pacific Decadal Oscillation on the relationship between ENSO and tropical cyclone activity in the Bay of Bengal during October–December, *Climate Dynamics*, 44(11-12): 3469-3479.

Gray, W.M. and Brody, L.R. (1968). Global view of the origin of tropical disturbances and storms. *Monthly Weather Review*, 96(10): 669-700.

Gleixner, S., Keenlyside, N., Hodges, K.I., Tseng, W.L. and Bengtsson, L. (2014). An inter-hemispheric comparison of the tropical storm response to global warming. *Climate Dynamics*, 42(7-8): 2147-2157.

Gray, W.M. (1975). *Tropical Cyclone Genesis*. Fort Collins, Colorado, Colorado State University.

Gray, W.M. (1977). Tropical cyclone genesis in the western North Pacific. *Journal of the Meteorological Society of Japan*, 55(5): 465-482.

Gray, W.M. (1979). Hurricanes: Their Formation, Structure and Likely Role in the Tropical Circulation. In Shaw, D.B. (Ed.) *Meteorology over the Tropical Oceans*, Royal Meteorological Society, James Glaisher House, Grenville Place, Bracknell, 155-218.

Gray, W.M. (1998). The formation of tropical cyclones. *Meteorology and Atmospheric Physics*, 67(1-4): 37-69.

Guevara-Murua, A., Hendy, E.J., Rust, A.C. and Cashman, K.V. (2015). Consistent decrease in North Atlantic Tropical Cyclone frequency following major volcanic eruptions in the last three centuries. *Geophysical Research Letters*, 42(21): 9425-9432.

Gutzler, D.S., Wood, K.M., Ritchie, E.A., Douglas, A.V. and Lewis, M.D. (2013). Interannual variability of tropical cyclone activity along the Pacific coast of North America. *Atmósfera*, 26(2): 149-162.

Haig, J., Nott, J. and Reichart, G.J. (2014). Australian tropical cyclone activity lower than at any time over the past 550–1,500 years. *Nature*, 505(7485): 667-671.

Haikun, Z., Liguang, W. and Weican, Z. (2009). Kernel density estimation applied to tropical cyclones genesis in Northwestern Pacific. Proceedings of *2009 International Conference on Environmental Science and Information Application Technology*, Wuhan (4-5 July 2009), 89-92.

Hall, J.D., Matthews, A.J. and Karoly, D.J. (2001). The modulation of tropical cyclone activity in the Australian region by the Madden–Julian oscillation. *Monthly Weather Review*, 129(12): 2970-2982.

Halliwell Jr, G.R., Gopalakrishnan, S., Marks, F. and Willey, D. (2015). Idealized study of ocean impacts on tropical cyclone intensity forecasts. *Monthly Weather Review*, 143(4): 1142-1165.

Halperin, D.J., Fuelberg, H.E., Hart, R.E., Cossuth, J.H., Sura, P. and Pasch, R.J. (2013). An evaluation of tropical cyclone genesis forecasts from global numerical models. *Weather and Forecasting*, *28*(6): 1423-1445.

Harper, B.A., Stroud, S.A., McCormack, M. and West, S. (2008). A review of historical tropical cyclone intensity in northwestern Australia and implications for climate change trend analysis. *Australian Meteorological Magazine*, 57(2): 121-141.

Hassim, M.E. and Walsh, K.J. (2008). Tropical cyclone trends in the Australian region. *Geochemistry, Geophysics, Geosystems*, 9(7): doi:10.1029/2007GC001804.

Hastenrath, S. and Greischar, L. (2001). The North Atlantic oscillation in the NCEP–NCAR reanalysis. *Journal of Climate*, 14(11): 2404-2413.

Held, I.M. and Zhao, M. (2011). The response of tropical cyclone statistics to an increase in CO2 with fixed sea surface temperatures. *Journal of Climate*, 24(20), 5353-5364.

Henderson-Sellers, A., Zhang, H., Berz, G., Emanuel, K., Gray, W., Landsea, C., Holland, G., Lighthill, J., Shieh, S.L., Webster, P. and McGuffie, K. (1998). Tropical cyclones and global climate change: A post-IPCC assessment. *Bulletin of the American Meteorological Society*, 79(1): 19-38.

Hill, K.A. and Lackmann, G.M. (2009). Influence of environmental humidity on tropical cyclone size. *Monthly Weather Review*, 137(10): 3294-3315.

Ho, R. (2006). *Handbook of univariate and multivariate data analysis and interpretation with SPSS*. Chapman and Hall/CRC.

Holland, G. and Bruyère, C.L. (2014). Recent intense hurricane response to global climate change. *Climate Dynamics*, 42(3-4): 617-627.

Hsu, W.C., Patricola, C.M. and Chang, P. (2018). The impact of climate model sea surface temperature biases on tropical cyclone simulations. *Climate Dynamics*, doi: 10.1007/s00382-018-4577-5.

Huangfu, J., Chen, W., Ma, T. and Huang, R. (2018). Influences of sea surface temperature in the tropical Pacific and Indian Oceans on tropical cyclone genesis over the western North Pacific in May. *Climate Dynamics*, 51(5-6): 1915-1926.

IPCC. (2014). In V. R. Barros, C. B. Field, D. J. Dokken, M. D. Mastrandrea, K. J. Mach, T. E. Bilir, M. Chatterjee, K. L. Ebi, Y. O. Estrada, R. C. Genova, B. Girma, E. S. Kissel, A. N. Levy, S. MacCracken, P. R. Mastrandrea & L. L. White. (Eds.), *Climate change 2014: Impacts, adaptation, and vulnerability. Part B: Regional aspects. Contribution of working group II to the fifth assessment report of the intergovernmental panel on climate change*. Cambridge, United Kingdom and New York, NY, USA: Cambridge University Press, 1670-1696.

Jiang, H. (2012). The relationship between tropical cyclone intensity change and the strength of inner-core convection. *Monthly Weather Review*, 140(4): 1164-1176.

Jobson, J.D. (2012). *Applied multivariate data analysis: volume II: Categorical and Multivariate Methods*. Springer Science & Business Media.

Johnson, N.C. and Xie, S.P. (2010). Changes in the sea surface temperature threshold for tropical convection. *Nature Geoscience*, 3(12): 842-845.

Jourdain, N.C., Marchesiello, P., Menkès, C.E., Lefèvre, J., Vincent, E.M., Lengaigne, M. and Chauvin, F. (2011). Mesoscale simulation of tropical cyclones in the South Pacific: Climatology and interannual variability. *Journal of Climate*, 24(1): 3-25.

Juračić, A. and Raymond, D.J. (2016). The effects of moist entropy and moisture budgets on tropical cyclone development. *Journal of Geophysical Research: Atmospheres*, 121(16): 9458-9473.

Kajtar, J.B., Santoso, A., England, M.H. and Cai, W. (2017). Tropical climate variability: interactions across the Pacific, Indian, and Atlantic Oceans. *Climate Dynamics*, 48(7-8): 2173-2190.

Kanamitsu, M., Ebisuzaki, W., Woollen, J., Yang, S.K., Hnilo, J.J., Fiorino, M. and Potter, G.L. (2002). NCEP–DOE AMIP-II reanalysis (r-2). *Bulletin of the American Meteorological Society*, 83(11): 1631-1644.

Kang, N.Y. and Elsner, J.B. (2015). Trade-off between intensity and frequency of global tropical cyclones. *Nature Climate Change*, 5(7): 661-664.

Khodri, M., Izumo, T., Vialard, J., Janicot, S., Cassou, C., Lengaigne, M., Mignot, J., Gastineau, G., Guilyardi, E., Lebas, N. and Robock, A. (2017). Tropical explosive volcanic eruptions can trigger El Niño by cooling tropical Africa. *Nature Communications*, 8(778): doi: 10.1038/s41467-017-00755-6.

Khouakhi, A., Villarini, G. and Vecchi, G.A. (2017). Contribution of tropical cyclones to rainfall at the global scale. *Journal of Climate*, 30(1): 359-372.

Kim, D., Sobel, A.H., Del Genio, A.D., Chen, Y., Camargo, S.J., Yao, M.S., Kelley, M. and Nazarenko, L. (2012). The tropical subseasonal variability simulated in the NASA GISS general circulation model. *Journal of Climate*, 25(13): 4641-4659.

Kim, D., Kim, H.S., Park, D.S.R. and Park, M.S. (2017). Variation of the tropical cyclone season start in the Western North Pacific. *Journal of Climate*, 30(9): 3297-3302.

Kiranmayi, L. and Maloney, E.D. (2011). Intraseasonal moist static energy budget in reanalysis data. *Journal of Geophysical Research: Atmospheres*, 116(D21): doi: 10.1029/2011JD016031.

Klotzbach, P.J. and Landsea, C.W. (2015). Extremely intense hurricanes: Revisiting Webster et al.(2005) after 10 years. *Journal of Climate*, 28(19): 7621-7629.

Klotzbach, P.J., Chan, J.C., Fitzpatrick, P.J., Frank, W.M., Landsea, C.W. and McBride, J.L. (2017). The science of William M. Gray: His contributions to the knowledge of tropical meteorology and tropical cyclones. *Bulletin of the American Meteorological Society*, 98(11): 2311-2336.

Klotzbach, P.J., Bowen, S.G., Pielke Jr, R. and Bell, M. (2018). Continental US hurricane landfall frequency and associated damage: Observations and future risks. *Bulletin of the American Meteorological Society*, 99(7): 1359-1376.

Knapp, K.R., Kruk, M.C., Levinson, D.H., Diamond, H.J. and Neumann, C.J. (2010). The international best track archive for climate stewardship (IBTrACS) unifying tropical cyclone data. *Bulletin of the American Meteorological Society*, 91(3): 363-376.

Knapp, K.R., Ansari, S., Bain, C.L., Bourassa, M.A., Dickinson, M.J., Funk, C., Helms, C.N., Hennon, C.C., Holmes, C.D., Huffman, G.J. and Kossin, J.P. (2011). Globally gridded satellite observations for climate studies. *Bulletin of the American Meteorological Society*, 92(7): 893-907.

Knutson, T.R., McBride, J.L., Chan, J., Emanuel, K., Holland, G., Landsea, C., Held, I., Kossin, J.P., Srivastava, A.K. and Sugi, M. (2010). Tropical cyclones and climate change. *Nature Geoscience*, 3(3): 157-163.

Koh, J.H. and Brierley, C.M. (2015). Tropical cyclone genesis potential across palaeoclimates. *Climate of the Past*, 11(10): 1433-1451.

Korty, R.L., Camargo, S.J. and Galewsky, J. (2012). Tropical cyclone genesis factors in simulations of the Last Glacial Maximum. *Journal of Climate*, 25(12): 4348-4365.

Korty, R.L., Emanuel, K.A. and Scott, J.R. (2008). Tropical cyclone–induced upper-ocean mixing and climate: Application to equable climates. *Journal of Climate*, 21(4): 638-654.

Korty, R.L., Camargo, S.J. and Galewsky, J. (2012). Variations in tropical cyclone genesis factors in simulations of the Holocene epoch. *Journal of Climate*, 25(23): 8196-8211.

Kossin, J.P., Knapp, K.R., Vimont, D.J., Murnane, R.J. and Harper, B.A. (2007). A globally consistent reanalysis of hurricane variability and trends. *Geophysical Research Letters*, 34(4): doi: 10.1029/2006GL028836.

Kossin, J.P., Olander, T.L. and Knapp, K.R. (2013). Trend analysis with a new global record of tropical cyclone intensity. *Journal of Climate*, 26(24): 9960-9976.

Kossin, J.P., Emanuel, K.A. and Vecchi, G.A. (2014). The poleward migration of the location of tropical cyclone maximum intensity. *Nature*, 509(7500): 349-352.

Kossin, J.P. (2015). Validating atmospheric reanalysis data using tropical cyclones as thermometers. *Bulletin of the American Meteorological Society*, 96(7): 1089-1096.

Kossin, J.P. (2018). A global slowdown of tropical-cyclone translation speed. *Nature*, 558(7708): 104-107.

Kuleshov, Y., Qi, L., Fawcett, R. and Jones, D. (2008). On tropical cyclone activity in the Southern Hemisphere: Trends and the ENSO connection. *Geophysical Research Letters*, 35(14): doi:10.1029/2007GL032983.

Kuleshov, Y., Chane-Ming, F., Qi, L., Chouaibou, I., Hoareau, C. and Roux, F. (2009). Tropical cyclone genesis in the Southern Hemisphere and its relationship with the ENSO. In *Annales Geophysicae,* 27(6): 2523-2538.

Kuleshov, Y., Fawcett, R., Qi, L., Trewin, B., Jones, D., McBride, J. and Ramsay, H. (2010). Trends in tropical cyclones in the South Indian Ocean and the South Pacific Ocean. *Journal of Geophysical Research: Atmospheres*, 115(D1): doi: 10.1029/2009JD012372.

Kunkel, K.E., Karl, T.R., Brooks, H., Kossin, J., Lawrimore, J.H., Arndt, D., Bosart, L., Changnon, D., Cutter, S.L., Doesken, N. and Emanuel, K. (2013). Monitoring and understanding trends in extreme storms: State of knowledge. *Bulletin of the American Meteorological Society*, 94(4): 499-514.

Landsea, C.W., Harper, B.A., Hoarau, K. and Knaff, J.A. (2006) Can we detect trends in extreme tropical cyclones? *Science*, 313(5786): 452-454.

Latif, M., Keenlyside, N. and Bader, J. (2007). Tropical sea surface temperature, vertical wind shear, and hurricane development. *Geophysical Research Letters*, 34(1): 10.1029/2006GL027969.

Lee, S.K., Park, W., Baringer, M.O., Gordon, A.L., Huber, B. and Liu, Y. (2015). Pacific origin of the abrupt increase in Indian Ocean heat content during the warming hiatus. *Nature Geoscience*, 8(6): 445-449.

Leroy, A. and Wheeler, M.C. (2008). Statistical prediction of weekly tropical cyclone activity in the Southern Hemisphere. *Monthly Weather Review*, 136(10): 3637-3654.

Li, W., Du, Q. and Chen, S. (2010). Climatological relationships among the tropical cyclone frequency, duration, intensity and activity regions over the Western Pacific. *Chinese Science Bulletin*, 55(33): 3818-3824.

Li, Z., Yu, W., Li, T., Murty, V.S.N. and Tangang, F. (2013). Bimodal character of cyclone climatology in the Bay of Bengal modulated by monsoon seasonal cycle. *Journal of Climate*, 26(3): 1033-1046.

Li, R.C. and Zhou, W. (2014). Interdecadal change in South China Sea tropical cyclone frequency in association with zonal sea surface temperature gradient. *Journal of Climate*, 27(14): 5468-5480.

Li, Q., Xu, P., Wang, X., Lan, H., Cao, C., Li, G., Zhang, L. and Sun, L. (2016). An Operational Statistical Scheme for Tropical Cyclone Induced Wind Gust Forecasts. *Weather and Forecasting*, 31(6): 1817-1832.

Li, H., Wang, C., He, S., Wang, H., Tu, C., Xu, J., Li, F. and Guo, X. (2017). Modulation of Solar Wind Energy Flux Input on Global Tropical Cyclone Activity. *Journal of Atmospheric and Solar-Terrestrial Physics*, doi: 10.1016/j.jastp.2018.01.018.

Li, H., Wang, C., He, S., Wang, H., Tu, C., Xu, J., Li, F. and Guo, X. (2018). Plausible modulation of solar wind energy flux input on global tropical cyclone activity. *Journal of Atmospheric and Solar-Terrestrial Physics*, doi: 10.1016/j.jastp.2018.01.018.

Lin, I.I., Chen, C.H., Pun, I.F., Liu, W.T. and Wu, C.C. (2009). Warm ocean anomaly, air sea fluxes, and the rapid intensification of tropical cyclone Nargis (2008). *Geophysical Research Letters*, 36(3): doi: 10.1029/2008GL035815.

Lin, N., Jing, R., Wang, Y., Yonekura, E., Fan, J. and Xue, L. (2017). A statistical investigation of the dependence of tropical cyclone intensity change on the surrounding environment. *Monthly Weather Review*, 145(7): 2813-2831.

Lindsay, R., Wensnahan, M., Schweiger, A. and Zhang, J. (2014). Evaluation of seven different atmospheric reanalysis products in the Arctic. *Journal of Climate*, 27(7): 2588-2606.

Linsley, B.K., Wu, H.C., Dassié, E.P. and Schrag, D.P. (2015). Decadal changes in South Pacific sea surface temperatures and the relationship to the Pacific decadal oscillation and upper ocean heat content. *Geophysical Research Letters*, 42(7): 2358-2366.

Liu, K.S. and Chan, J.C. (2008). Interdecadal variability of western North Pacific tropical cyclone tracks. *Journal of Climate*, 21(17): 4464-4476.

Liu, K.S. and Chan, J.C. (2012). Interannual variation of Southern Hemisphere tropical cyclone activity and seasonal forecast of tropical cyclone number in the Australian region. *International Journal of Climatology*, 32(2): 190-202.

Liu, K.S. and Chan, J.C. (2018). Changing relationship between La Niña and tropical cyclone landfalling activity in South China (La Niña and TC landfalling activity in South China). *International Journal of Climatology*, 38(3): 1270-1284.

Liu, L. (2019). Impact of Different Types of ENSO Years on Intensity Changes of Landfalling Tropical Cyclones over China. *Atmosphere*, 10(3): doi:10.3390/atmos10030161.

Loridan, T., Crompton, R.P. and Dubossarsky, E. (2017). A machine learning approach to modeling tropical cyclone wind field uncertainty. *Monthly Weather Review*, 145(8): 3203-3221.

Lucas, C., Timbal, B. and Nguyen, H. (2014). The expanding tropics: a critical assessment of the observational and modeling studies. *Wiley Interdisciplinary Reviews: Climate Change*, 5(1): 89-112.

Luo, J.J., Sasaki, W. and Masumoto, Y. (2012). Indian Ocean warming modulates Pacific climate change. *Proceedings of the National Academy of Sciences*, 109(46): 18701-18706.

Ma, L. and Williams, R. (2017). How Does Intertropical Convergence Zone Variation Impact on Tropical Cyclone in the Northern Hemisphere?. Proceedings of *EGU General Assembly Conference*, Austria (23-28 April 2017), Vol. 19 p. 16196.

Magee, A.D., Verdon-Kidd, D.C. and Kiem, A.S. (2016). An intercomparison of tropical cyclone best-track products for the southwest Pacific. *Natural Hazards and Earth System Sciences*, 16(6): 1431-1447.

Magee, A.D. and Verdon-Kidd, D.C. (2018). On the relationship between Indian Ocean sea surface temperature variability and tropical cyclogenesis in the southwest Pacific. *International Journal of Climatology*, 38(S1): doi:10.1002/joc.5406 .

Mahala, B.K., Nayak, B.K. and Mohanty, P.K. (2015). Impacts of ENSO and IOD on tropical cyclone activity in the Bay of Bengal. *Natural Hazards*, 75(2): 1105-1125.

Malan, N., Reason, C.J.C. and Loveday, B.R. (2013). Variability in tropical cyclone heat potential over the Southwest Indian Ocean. *Journal of Geophysical Research: Oceans*, 118(12): 6734-6746.

Mao, R., Gong, D.Y., Yang, J., Zhang, Z.Y., Kim, S.J. and He, H.Z. (2013). Is there a linkage between the tropical cyclone activity in the southern Indian Ocean and the Antarctic Oscillation?. *Journal of Geophysical Research: Atmospheres*, 118(15): 8519-8535.

Markle, B.R., Steig, E.J., Buizert, C., Schoenemann, S.W., Bitz, C.M., Fudge, T.J., Pedro, J.B., Ding, Q., Jones, T.R., White, J.W.C. and Sowers, T.A. (2015). Atmospheric teleconnections between the tropics and the Southern Hemisphere westerly winds during abrupt climate change. Proceedings of *AGU Fall Meeting,* San Francisco (14-18 December 2015), 36-40.

Marshall, G.J. (2003). Trends in the Southern Annular Mode from observations and reanalyses. *Journal of Climate*, 16(24): 4134-4143.

Matyas, C.J. (2015). Tropical cyclone formation and motion in the Mozambique Channel. *International Journal of Climatology*, 35(3): 375-390.

Maue, R.N. (2009). Northern Hemisphere tropical cyclone activity. *Geophysical Research Letters*, 36(5): doi:10.1029/2008GL035946.

Mauk, R.G. and Hobgood, J.S. (2012). Tropical cyclone formation in environments with cool SST and high wind shear over the northeastern Atlantic Ocean. *Weather and Forecasting*, 27(6): 1433-1448.

Mavume, A.F., Rydberg, L., Rouault, M. and Lutjeharms, J.R. (2009). Climatology and landfall of tropical cyclones in the south-west Indian Ocean. *Western Indian Ocean Journal of Marine Science*, *8*(1): 15-36.

Mawren, D. and Reason, C.J.C. (2017). Variability of upper-ocean characteristics and tropical cyclones in the South West Indian Ocean. *Journal of Geophysical Research: Oceans*, 122(3): 2012-2028.

McBride, J.L. and Keenan, T.D. (1982). Climatology of tropical cyclone genesis in the Australian region. *Journal of Climatology*, 2(1): 13-33.

McBride, J. L., (1995). Tropical cyclone formation. In: Elsberry, R. L. (Ed.), *Global perspectives on tropical cyclones*. World Meteorological Organization, Geneva.

McGauley, M.G. and Nolan, D.S. (2011). Measuring environmental favorability for tropical cyclogenesis by statistical analysis of threshold parameters. *Journal of Climate*, 24(23): 5968-5997.

Mcphaden, M.J., Foltz, G.R., Lee, T., Murty, V.S.N., Ravichandran, M., Vecchi, G.A., Vialard, J., Wiggert, J.D. and Yu, L. (2009). Ocean-atmosphere interactions during cyclone nargis. *Eos, Transactions American Geophysical Union*, 90(7): 53-54.

McTaggart-Cowan, R., Bosart, L.F., Davis, C.A., Atallah, E.H., Gyakum, J.R. and Emanuel, K.A. (2006). Analysis of hurricane Catarina (2004). *Monthly Weather Review*, 134(11): 3029-3053.

McTaggart-Cowan, R., Galarneau Jr, T.J., Bosart, L.F., Moore, R.W. and Martius, O. (2013). A global climatology of baroclinically influenced tropical cyclogenesis. *Monthly Weather Review*, 141(6): 1963-1989.

McTaggart-Cowan, R., Davies, E.L., Fairman Jr, J.G., Galarneau Jr, T.J. and Schultz, D.H. (2015). Revisiting the 26.5 [degrees] C sea surface temperature threshold for tropical cyclone development. *Bulletin of the American Meteorological Society*, 96(11): 1929-1945.

Mei, W., Primeau, F., McWilliams, J.C. and Pasquero, C. (2013). Sea surface height evidence for long-term warming effects of tropical cyclones on the ocean. *Proceedings of the National Academy of Sciences*, 110(38): 15207-15210.

Mei, W., Xie, S.P., Zhao, M. and Wang, Y. (2015). Forced and internal variability of tropical cyclone track density in the western North Pacific. *Journal of Climate*, 28(1): 143-167.

Menkes, C.E., Lengaigne, M., Marchesiello, P., Jourdain, N.C., Vincent, E.M., Lefèvre, J., Chauvin, F. and Royer, J.F. (2012). Comparison of tropical cyclogenesis indices on seasonal to interannual timescales. *Climate Dynamics*, 38(1-2): 301-321.

Michaud, L.M. (2012). On hurricane energy. *Meteorology and Atmospheric Physics*, 118(1-2): 21-29.

Mulyana, E., Prayoga, M.B.R., Yananto, A., Wirahma, S., Aldrian, E., Harsoyo, B., Seto, T.H. and Sunarya, Y. (2018). Tropical cyclones characteristic in southern Indonesia and the impact on extreme rainfall event. *MATEC Web of Conferences*, 229: doi: 10.1051/matecconf/201822902007.

Murakami, H., Mizuta, R. and Shindo, E. (2012a). Future changes in tropical cyclone activity projected by multi-physics and multi-SST ensemble experiments using the 60-km-mesh MRI-AGCM. *Climate Dynamics*, 39(9-10): 2569-2584.

Murakami, H., Wang, Y., Yoshimura, H., Mizuta, R., Sugi, M., Shindo, E., Adachi, Y., Yukimoto, S., Hosaka, M., Kusunoki, S. and Ose, T. (2012b). Future changes in tropical cyclone activity projected by the new high-resolution MRI-AGCM. *Journal of Climate*, 25(9): 3237-3260.

Murakami, H., Vecchi, G.A., Villarini, G., Delworth, T.L., Gudgel, R., Underwood, S., Yang, X., Zhang, W. and Lin, S.J. (2016). Seasonal forecasts of major hurricanes and landfalling tropical cyclones using a high-resolution GFDL coupled climate model. *Journal of Climate*, 29(22): 7977-7989.

Muthige, M.S., Malherbe, J., Englebrecht, F.A., Grab, S., Beraki, A., Maisha, T.R. and Van der Merwe, J. (2018). Projected changes in tropical cyclones over the South West Indian Ocean under different extents of global warming. *Environmental Research Letters*, 13(6): doi: 10.1088/1748-9326/aabc60 .

Na, W., Xinghai, Z., Lianshou, C. and Hao, H. (2018). Comparison of the effect of easterly and westerly vertical wind shear on tropical cyclone intensity change over the western North Pacific. *Environmental Research Letters*, 13(3): doi:10.1088/1748-9326/aaa496.

National Geophysical Data Center/World Data Service (NGDC/WDS). (2018). *NCEI/WDS Global Significant Volcanic Eruptions Database*. NOAA National Centers for Environmental Information. doi:10.7289/V5JW8BSH [Accessed 08 September 2018].

Nguyen, L.T. and Molinari, J. (2015). Simulation of the downshear reformation of a tropical cyclone. *Journal of the Atmospheric Sciences*, 72(12): 4529-4551.

Nolan, D.S. and Rappin, E.D. (2008). Increased sensitivity of tropical cyclogenesis to wind shear in higher SST environments. *Geophysical Research Letters*, 35(14): doi:10.1029/2008GL034147.

Nolan, D.S. and McGauley, M.G. (2012). Tropical cyclogenesis in wind shear: Climatological relationships and physical processes. In Oouchi, K., and Fudeyasu, H. (Eds.) *Cyclones: Formation, triggers, and control*, Nova Science Publishers, New York: 1-36.

Nott, J. (2011). Tropical cyclones, global climate change and the role of Quaternary studies. *Journal of Quaternary Science*, 26(5): 468-473.

Oouchi, K., Yoshimura, J., Yoshimura, H., Mizuta, R., Kusunoki, S. and Noda, A. (2006). Tropical cyclone climatology in a global-warming climate as simulated in a 20 km-mesh global atmospheric model: Frequency and wind intensity analyses. *Journal of the Meteorological Society of Japan. Series. II*, *84*(2): 259-276.

Osuri, K.K., Mohanty, U.C., Routray, A. and Mohapatra, M. (2012). The impact of satellite-derived wind data assimilation on track, intensity and structure of tropical cyclones over the North Indian Ocean. *International Journal of Remote Sensing*, 33(5): 1627-1652.

Palmen, E. (1948). On the formation and structure of tropical hurricanes. *Geophysica*, *3*(1): 26-38.

Parker, C.L., Bruyère, C.L., Mooney, P.A. and Lynch, A.H. (2018). The response of land-falling tropical cyclone characteristics to projected climate change in northeast Australia. *Climate Dynamics*, 51(9-10): 3467-3485.

Parodi, A. and Emanuel, K. (2009). A theory for buoyancy and velocity scales in deep moist convection. *Journal of the Atmospheric Sciences*, 66(11): 3449-3463.

Patricola, C.M. and Wehner, M.F. (2018). Anthropogenic influences on major tropical cyclone events. *Nature*, 563(7731): 339-346.

Pausata, F.S. and Camargo, S.J. (2019). Tropical cyclone activity affected by volcanically induced ITCZ shifts. *Proceedings of the National Academy of Sciences*, 116(16): 7732-7737.

Pezza, A.B. and Simmonds, I. (2005). The first South Atlantic hurricane: Unprecedented blocking, low shear and climate change. *Geophysical Research Letters*, *32*(15).

Pike, A.C. (1985). The use of meteorological data in the prediction of tropical cyclones. *The American Statistician*, 39(4): 335-346.

Pugatch, T. (2019). Tropical storms and mortality under climate change. *World Development*, 117: 172-182.

Quirino, T., and Gopalakrishnan, S.G. (2016). Advanced Diagnostics for the HWRF Hurricane Modelling System. In Mohanty, U.C. and Gopalakrishnan, S.G. (Eds.) *Advanced Numerical Modeling and Data Assimilation Techniques for Tropical Cyclone Predictions,* Capital Publishing Company, Springer Netherlands.

Rahman, M., Yang, R. and Di, L. (2018). Clustering Indian Ocean Tropical Cyclone Tracks by the Standard Deviational Ellipse. *Climate*, 6(2): doi:10.3390/cli6020039.

Rai, D., Pattnaik, S., Rajesh, P.V. and Hazra, V. (2019). Impact of high resolution sea surface temperature on tropical cyclone characteristics over the Bay of Bengal using model simulations. *Meteorological Applications*, 26(1): 130-139.

Ramsay, H.A., Leslie, L.M., Lamb, P.J., Richman, M.B. and Leplastrier, M. (2008). Interannual variability of tropical cyclones in the Australian region: Role of large-scale environment. *Journal of Climate*, 21(5): 1083-1103.

Ramsay, H.A., Camargo, S.J. and Kim, D. (2012). Cluster analysis of tropical cyclone tracks in the Southern Hemisphere. *Climate Dynamics*, 39(3-4): 897-917.

Ramsay, H.A., Richman, M.B. and Leslie, L.M. (2017). The modulating influence of Indian Ocean sea surface temperatures on Australian region seasonal tropical cyclone counts. *Journal of Climate*, 30(13): 4843-4856.

Ramsay, H.A., Chand, S.S. and Camargo, S.J. (2018). A Statistical Assessment of Southern Hemisphere Tropical Cyclone Tracks in Climate Models. *Journal of Climate*, 31(24): 10081-10104.

Rao, S.A., Dhakate, A.R., Saha, S.K., Mahapatra, S., Chaudhari, H.S., Pokhrel, S. and Sahu, S.K. (2012). Why is Indian Ocean warming consistently?. *Climatic Change*, 110(3-4): 709-719.

Ren, D., Lynch, M., Leslie, L.M. and Lemarshall, J. (2014). Sensitivity of tropical cyclone tracks and intensity to ocean surface temperature: four cases in four different basins. *Tellus A: Dynamic Meteorology and Oceanography*, 66(1): 10.3402/tellusa.v66.24212.

Reynolds, R.W., Smith, T.M., Liu, C., Chelton, D.B., Casey, K.S. and Schlax, M.G. (2007). Daily high-resolution-blended analyses for sea surface temperature. *Journal of Climate*, 20(22): 5473-5496.

Ridgway, K.R. and Godfrey, J.S. (2015). The source of the Leeuwin Current seasonality. *Journal of Geophysical Research: Oceans*, 120(10): 6843-6864.

Riehl, H. (1948). On the formation of typhoons. *Journal of Meteorology*, 5(6): 247-265.

Robe, F.R. and Emanuel, K.A. (2001). The effect of vertical wind shear on radiative–convective equilibrium states. *Journal of the Atmospheric Sciences*, 58(11): 1427-1445.

Rodgers, E., Olson, W., Halverson, J., Simpson, J. and Pierce, H. (2000). Environmental forcing of Supertyphoon Paka's (1997) latent heat structure. *Journal of Applied Meteorology*, 39(12): 1983-2006.

Rohith, B., Paul, A., Durand, F., Testut, L., Prerna, S., Afroosa, M., Ramakrishna, S.S.V.S. and Shenoi, S.S.C. (2019). Basin-wide sea level coherency in the tropical Indian Ocean driven by Madden–Julian Oscillation. *Nature Communications*, 10(1257): doi: 10.1038/s41467-019-09243-5.

Roxy, M.K., Ritika, K., Terray, P. and Masson, S. (2014). The curious case of Indian Ocean warming. *Journal of Climate*, 27(22): 8501-8509.

Roxy, M.K., Ritika, K., Terray, P., Murtugudde, R., Ashok, K. and Goswami, B.N. (2015). Drying of Indian subcontinent by rapid Indian Ocean warming and a weakening land-sea thermal gradient. *Nature communications*, 6(7423): doi:10.1038/ncomms8423.

Saha, S., Moorthi, S., Pan, H.L., Wu, X., Wang, J., Nadiga, S., Tripp, P., Kistler, R., Woollen, J., Behringer, D. and Liu, H. (2010). The NCEP climate forecast system reanalysis. *Bulletin of the American Meteorological Society*, 91(8): 1015-1058.

Saha, K.K. and Wasimi, S.A. (2013). Interrelationship between Indian Ocean dipole (IOD) and Australian tropical cyclones. *International Journal of Environmental Science and Development*, 4(6): 647-651.

Sahany, S., Neelin, J.D., Hales, K. and Neale, R.B. (2012). Temperature–moisture dependence of the deep convective transition as a constraint on entrainment in climate models. *Journal of the Atmospheric Sciences*, 69(4): 1340-1358.

Schenkel, B.A., Lin, N., Chavas, D., Vecchi, G.A., Oppenheimer, M. and Brammer, A. (2018). Lifetime Evolution of Outer Tropical Cyclone Size and Structure as Diagnosed from Reanalysis and Climate Model Data. *Journal of Climate*, 31(19): 7985-8004.

Schott, F.A., Xie, S.P. and McCreary, J.P. (2009). Indian Ocean circulation and climate variability. *Reviews of Geophysics*, 47(1): doi: 10.1029/2007RG000245.

Schreck III, C.J., Knapp, K.R. and Kossin, J.P. (2014). The impact of best track discrepancies on global tropical cyclone climatologies using IBTrACS. *Monthly Weather Review*, 142(10): 3881-3899.

Scoccimarro, E., Fogli, P.G., Reed, K.A., Gualdi, S., Masina, S. and Navarra, A. (2017). Tropical cyclone interaction with the ocean: The role of high-frequency (subdaily) coupled processes. *Journal of Climate*, 30(1): 145-162.

Seager, R. and Simpson, I.R. (2016). Western boundary currents and climate change. *Journal of Geophysical Research: Oceans*, 121(9): 7212-7214.

Sebastian, M. and Behera, M.R. (2015). Impact of SST on tropical cyclones in North Indian Ocean. *Procedia Engineering*, *116*: 1072-1077.

Şen, Z., Altunkaynak, A. and Erdik, T. (2012). Wind velocity vertical extrapolation by extended power law. *Advances in Meteorology*, 2012: doi:10.1155/2012/178623.

Shultz, J.M., Shepherd, J.M., Kelman, I., Rechkemmer, A. and Galea, S. (2018). Mitigating tropical cyclone risks and health consequences: urgencies and innovations. *The Lancet Planetary Health*, 2(3): e103-e104, doi:10.1016/S2542-5196(18)30021-4.

Silverman, B.W. (2018). *Density estimation for statistics and data analysis*. Routledge, New York.

Sobel, A.H., Camargo, S.J., Hall, T.M., Lee, C.Y., Tippett, M.K. and Wing, A.A. (2016). Human influence on tropical cyclone intensity. *Science*, 353(6296): 242-246.

Soloviev, A.V., Lukas, R., Donelan, M.A., Haus, B.K. and Ginis, I. (2014). The air-sea interface and surface stress under tropical cyclones. *Scientific Reports*, 4(5306): doi:10.1038/srep05306

Song, J., Klotzbach, P.J., Tang, J. and Wang, Y. (2018). The increasing variability of tropical cyclone lifetime maximum intensity. *Scientific Reports*, 8(16641): doi:10.1038/s41598-018-35131-x.

Song, W., Tang, S. and Wang, X. (2019). Relationship between Pacific Ocean warming and tropical cyclone activity over the western North Pacific. *Stochastic Environmental Research and Risk Assessment*, 33(1): 31-45.

Sriver, R.L. (2013). Observational evidence supports the role of tropical cyclones in regulating climate. *Proceedings of the National Academy of Sciences*, 110(38): 15173-15174.

Strazzo, S.E., Elsner, J.B. and LaRow, T.E. (2015). Quantifying the sensitivity of maximum, limiting, and potential tropical cyclone intensity to SST: Observations versus the FSU/COAPS global climate model. *Journal of Advances in Modeling Earth Systems*, 7(2): 586-599.

Sun, Y., Zhong, Z., Li, T., Yi, L., Hu, Y., Wan, H., Chen, H., Liao, Q., Ma, C. and Li, Q. (2017). Impact of ocean warming on tropical cyclone size and its destructiveness. *Scientific Reports*, 7(8154): doi:10.1038/s41598-017-08533-6.

Swapna, P., Krishnan, R. and Wallace, J.M. (2014). Indian Ocean and monsoon coupled interactions in a warming environment. *Climate dynamics*, 42(9-10): 2439-2454.

Tennille, S. and Ellis, K. (2017). Spatial and temporal trends in the location of the lifetime maximum intensity of tropical cyclones. *Atmosphere*, 8(10): doi:10.3390/atmos8100198.

Terry, J.P. and Gienko, G. (2010). Climatological aspects of South Pacific tropical cyclones, based on analysis of the RSMC-Nadi (Fiji) regional archive. *Climate Research*, 42(3): 223-233.

Temmerman, S., Meire, P., Bouma, T.J., Herman, P.M., Ysebaert, T. and De Vriend, H.J. (2013). Ecosystem-based coastal defence in the face of global change. *Nature*, 504(7478): 79-83.

Timmermann, A., An, S.I., Kug, J.S., Jin, F.F., Cai, W., Capotondi, A., Cobb, K., Lengaigne, M., McPhaden, M.J., Stuecker, M.F. and Stein, K. (2018). El Niño–Southern Oscillation complexity. *Nature*, 559(7715): 535-545.

Tippett, M.K., Camargo, S.J. and Sobel, A.H. (2011). A Poisson regression index for tropical cyclone genesis and the role of large-scale vorticity in genesis. *Journal of Climate*, 24(9): 2335-2357.

Tory, K.J. and Frank, W.M. (2010). Tropical cyclone formation. In Chan, J.C.L., and Kepert, J.D. (Eds.) *Global perspectives on tropical cyclones: From science to mitigation,* World Scientific Publishing, Singapore: 55-91.

Tory, K.J., Dare, R.A., Davidson, N.E., McBride, J.L. and Chand, S.S. (2013). The importance of low-deformation vorticity in tropical cyclone formation. *Atmospheric Chemistry and Physics*, 13(4): 2115-2132.

Tory, K.J. and Dare, R.A. (2015). Sea surface temperature thresholds for tropical cyclone formation. *Journal of Climate*, 28(20): 8171-8183.

Tsuboi, A. and Takemi, T. (2014). The interannual relationship between decreased activity and tropical cyclone genesis in the Indian Ocean. *Geoscience Letters*, 1(9): doi:10.1186/2196-4092-1-9.

Tsuboi, A., Takemi, T. and Yoneyama, K. (2016). Seasonal environmental characteristics for the tropical cyclone genesis in the Indian Ocean during the CINDY2011/DYNAMO field experiment. *Atmosphere*, 7(5): doi:10.3390/atmos7050066.

Tyson, P. D., and R. A. Preston-Whyte. (2000). The Weather and Climate of Southern Africa. Oxford University Press, Cape Town.

Van Der Wiel, K., Matthews, A.J., Joshi, M.M. and Stevens, D.P. (2016). Why the South Pacific convergence zone is diagonal. *Climate dynamics*, 46(5-6): 1683-1698.

Vecchi, G.A. and Soden, B.J. (2007). Increased tropical Atlantic wind shear in model projections of global warming. *Geophysical Research Letters*, 34(8): doi:10.1029/2006GL028905.

Vecchi, G.A., Fueglistaler, S., Held, I.M., Knutson, T.R. and Zhao, M. (2013). Impacts of atmospheric temperature trends on tropical cyclone activity. *Journal of Climate*, 26(11): 3877-3891.

Vecchi, G.A., Delworth, T., Gudgel, R., Kapnick, S., Rosati, A., Wittenberg, A.T., Zeng, F., Anderson, W., Balaji, V., Dixon, K. and Jia, L. (2014). On the seasonal forecasting of regional tropical cyclone activity. *Journal of Climate*, 27(21): 7994-8016.

Velden, C., Harper, B., Wells, F., Beven, J.L., Zehr, R., Olander, T., Mayfield, M., Guard, C.C., Lander, M., Edson, R. and Avila, L. (2006). The Dvorak tropical cyclone intensity estimation technique: A satellite-based method that has endured for over 30 years. *Bulletin of the American Meteorological Society*, 87(9): 1195-1210.

Vishnu, S., Francis, P.A., Shenoi, S.C. and Ramakrishna, S.S.V.S. (2018). On the relationship between the Pacific Decadal Oscillation and monsoon depressions over the Bay of Bengal. *Atmospheric Science Letters*, 19(7): doi:10.1002/asl.825.

Wallace, J.M. and Hobbs, P.V. (2006). Atmospheric Dynamics. In Wallace, J.M. and Hobbs, P.V. (Eds.) *Atmospheric Science: An Introductory Survey*. California, Elsevier: 271-311.

Walsh, K.J, Lavender, S., Scoccimarro, E. and Murakami, H. (2013). Resolution dependence of tropical cyclone formation in CMIP3 and finer resolution models. *Climate Dynamics*, 40(3-4): 585-599.

Walsh, K.J., Camargo, S.J., Vecchi, G.A., Daloz, A.S., Elsner, J., Emanuel, K., Horn, M., Lim, Y.K., Roberts, M., Patricola, C. and Scoccimarro, E. (2015). Hurricanes and climate: the US CLIVAR working group on hurricanes. *Bulletin of the American Meteorological Society*, 96(6): 997-1017.

Walsh, K.J.E., McBride, J.L., Klotzbach, P.J., Balachandran, S., Camargo, S.J., Holland, G., Knutson, T.R., Kossin, J.P., Lee, T., Sobel, A. and Sugi, M. (2016). Tropical cyclones and climate change. *Wiley Interdisciplinary Reviews: Climate Change*, 7(1): 65–89.

Wang, B., Yang, Y., Ding, Q.H., Murakami, H. and Huang, F. (2010). Climate control of the global tropical storm days (1965–2008). *Geophysical Research Letters*, 37(7): doi:10.1029/2010GL042487.

Wang, C., Kucharski, F., Barimalala, R. and Bracco, A. (2009). Teleconnections of the tropical Atlantic to the tropical Indian and Pacific Oceans: A review of recent findings. *Meteorologische Zeitschrift*, 18(4): 445-454.

Wang, X., Wang, C., Zhang, L. and Wang, X. (2015). Multidecadal variability of tropical cyclone rapid intensification in the western North Pacific. *Journal of Climate*, 28(9): 3806-3820.

Wang, B. and Moon, J.Y. (2017). An Anomalous Genesis Potential Index for MJO Modulation of Tropical Cyclones. *Journal of Climate*, 30(11): 4021-4035.

Watterson, I.G., Evans, J.L. and Ryan, B.F. (1995). Seasonal and interannual variability of tropical cyclogenesis: Diagnostics from large-scale fields. *Journal of Climate*, 8(12): 3052-3066.

Webster, P.J., Holland, G.J., Curry, J.A., and Chang, H.R. (2005). Changes in Tropical Cyclone Number, Duration, and Intensity in a Warming Environment. *Science*, 309(5742): 1844–1846.

Wehner, M.F., Reed, K.A., Li, F., Bacmeister, J., Chen, C.T., Paciorek, C., Gleckler, P.J., Sperber, K.R., Collins, W.D., Gettelman, A. and Jablonowski, C. (2014). The effect of horizontal resolution on simulation quality in the Community Atmospheric Model, CAM5. 1. *Journal of Advances in Modeling Earth Systems*, 6(4): 980-997.

Wehner, M.F., Reed, K.A., Loring, B., Stone, D. and Krishnan, H. (2018). Changes in tropical cyclones under stabilized 1.5 and 2.0° C global warming scenarios as simulated by the Community Atmospheric Model under the HAPPI protocols. *Earth System Dynamics*, 9(1): 187-195.

Weinkle, J., Maue, R. and Pielke Jr, R. (2012). Historical global tropical cyclone landfalls. *Journal of Climate*, 25(13): 4729-4735.

Werner, A., Maharaj, A.M. and Holbrook, N.J. (2012). A new method for extracting the ENSO-independent Indian Ocean Dipole: application to Australian region tropical cyclone counts. *Climate dynamics*, 38(11-12): 2503-2511.

Wieners, C.E., de Ruijter, W.P., Ridderinkhof, W., von der Heydt, A.S. and Dijkstra, H.A. (2016). Coherent tropical Indo-Pacific interannual climate variability. *Journal of Climate*, 29(11): 4269-4291.

Wing, A.A., Emanuel, K. and Solomon, S. (2015). On the factors affecting trends and variability in tropical cyclone potential intensity. *Geophysical Research Letters*, 42(20): 8669-8677.

WMO. (2017). WMO Guidelines on the Calculations of Climate Normals. Available at: https://library.wmo.int/doc_num.php?explnum_id=4166 (Accessed 08 March 2019).

Wu, C.C., Zhan, R., Lu, Y. and Wang, Y. (2012). Internal variability of the dynamically downscaled tropical cyclone activity over the western North Pacific by the IPRC regional atmospheric model. *Journal of Climate*, 25(6): 2104-2122.

Wu, L. and Zhao, H. (2012). Dynamically derived tropical cyclone intensity changes over the western North Pacific. *Journal of Climate*, 25(1): 89-98.

Wu, L., Tian, W., Liu, Q., Cao, J. and Knaff, J.A. (2015). Implications of the observed relationship between tropical cyclone size and intensity over the western North Pacific. *Journal of Climate*, 28(24): 9501-9506.

Xu, B., Wu, T. and Li, W. (2014). Screening of calculation methods for wind shear exponent. *Transactions of the Chinese Society of Agricultural Engineering*, 30(16): 188-194.

Xu, J., Wang, Y. and Tan, Z.M. (2016). The relationship between sea surface temperature and maximum intensification rate of tropical cyclones in the North Atlantic. *Journal of the Atmospheric Sciences*, 73(12): 4979-4988.

Xu, W., Rutledge, S.A. and Zhang, W. (2017). Relationships between total lightning, deep convection, and tropical cyclone intensity change. *Journal of Geophysical Research: Atmospheres*, 122(13): 7047-7063.

Xu, J. and Wang, Y. (2018). Dependence of tropical cyclone intensification rate on sea surface temperature, storm intensity, and size in the western North Pacific. *Weather and Forecasting*, 33(2): 523-537.

Xue, Y., Balmaseda, M.A., Boyer, T., Ferry, N., Good, S., Ishikawa, I., Kumar, A., Rienecker, M., Rosati, A.J. and Yin, Y. (2012). A comparative analysis of upper-ocean heat content variability from an ensemble of operational ocean reanalyses. *Journal of Climate*, 25(20): 6905-6929.

Yablonsky, R.M., Ginis, I. and Thomas, B. (2015). Ocean modeling with flexible initialization for improved coupled tropical cyclone-ocean model prediction. *Environmental Modelling & Software*, 67: 26-30, doi:10.1016/j.envsoft.2015.01.003.

Yamada, Y., Satoh, M., Sugi, M., Kodama, C., Noda, A.T., Nakano, M. and Nasuno, T. (2017). Response of tropical cyclone activity and structure to global warming in a high-resolution global nonhydrostatic model. *Journal of Climate*, 30(23): 9703-9724.

Yang, H., Lohmann, G., Wei, W., Dima, M., Ionita, M. and Liu, J. (2016). Intensification and poleward shift of subtropical western boundary currents in a warming climate. *Journal of Geophysical Research: Oceans*, 121(7): 4928-4945.

Ying, Y. and Zhang, Q. (2012). A modeling study on tropical cyclone structural changes in response to ambient moisture variations. *Journal of the Meteorological Society of Japan. Series. II*, 90(5): 755-770.

Yoshida, K., Sugi, M., Mizuta, R., Murakami, H. and Ishii, M. (2017). Future changes in tropical cyclone activity in high-resolution large-ensemble simulations. *Geophysical Research Letters*, 44(19): 9910-9917.

Young, J. and Wessnitzer, J. (2016). Descriptive statistics, graphs, and visualisation. In Robertson, J., and Kaptein, M. (Eds.) *Modern statistical methods for HCI,* Springer, Cham, Switzerland: 37-56.

Yu, J., Li, T., Tan, Z. and Zhu, Z. (2016). Effects of tropical North Atlantic SST on tropical cyclone genesis in the western North Pacific. *Climate dynamics*, 46(3-4): 865-877.

Zhan, R. and Wang, Y. (2017a). Weak tropical cyclones dominate the poleward migration of the annual mean location of lifetime maximum intensity of Northwest Pacific tropical cyclones since 1980. *Journal of Climate*, 30(17): 6873-6882.

Zhan, R., Wang, Y. and Zhao, J. (2017b). Intensified Mega-ENSO Has Increased the Proportion of Intense Tropical Cyclones Over the Western Northwest Pacific Since the Late 1970s. *Geophysical Research Letters*, 44(23): doi:10.1002/2017GL075916.

Zhang, J.A., Cione, J.J., Kalina, E.A., Uhlhorn, E.W., Hock, T. and Smith, J.A. (2017). Observations of infrared sea surface temperature and air–sea interaction in Hurricane Edouard (2014) using GPS dropsondes. *Journal of Atmospheric and Oceanic Technology*, 34(6): 1333-1349.

Zhang, L., Karnauskas, K.B., Donnelly, J.P. and Emanuel, K. (2017). Response of the North Pacific tropical cyclone climatology to global warming: Application of dynamical downscaling to CMIP5 models. *Journal of Climate*, 30(4): 1233-1243.

Zhang, Y., Feng, M., Du, Y., Phillips, H.E., Bindoff, N.L. and McPhaden, M.J. (2018). Strengthened Indonesian throughflow drives decadal warming in the Southern Indian Ocean. *Geophysical Research Letters*, 45(12): 6167-6175.

Zhao, H. and Wang, C. (2018). On the relationship between ENSO and tropical cyclones in the western North Pacific during the boreal summer. *Climate Dynamics*, 52(275): 1-14.

Zhong, S., Wang, C., Yu, Z., Yang, Y. and Huang, Q. (2018). Spatiotemporal Exploration and Hazard Mapping of Tropical Cyclones along the Coastline of China. *Advances in Meteorology*, 2018: doi:10.1155/2018/5479576.

Zhou, W., Held, I.M. and Garner, S.T. (2017). Tropical cyclones in rotating radiative–convective equilibrium with coupled SST. *Journal of the Atmospheric Sciences*, 74(3): 879-892.

Ziegel, E.R. (2004). Computer-aided Multivariate Analysis. *Technometrics*, 46(4), 495-496.

Appendix

Appendix 1A

Tropical Cyclone Frequency for Southern Hemisphere Basins

Frequency	SIO	WA	EA	SP	Mean: SH All Basins	SD: SH All Basins
1980	4	4	3	1	12	1.41
1981	6	3	3	1	13	2.06
1982	5	1	3	1	10	1.91
1983	3	1	1	9	14	3.79
1984	7	3	3	0	13	2.87
1985	5	3	4	3	15	0.96
1986	6	3	2	2	13	1.89
1987	3	0	2	6	11	2.50
1988	4	1	1	3	9	1.50
1989	9	4	3	3	19	2.87
1990	6	4	2	1	13	2.22
1991	4	1	3	1	9	1.50
1992	4	1	5	5	15	1.89
1993	6	0	3	5	14	2.65
1994	10	3	4	2	19	3.59
1995	7	2	1	1	11	2.87
1996	7	2	6	1	16	2.94
1997	12	0	4	6	22	5.00
1998	4	2	5	8	19	2.50
1999	4	4	3	2	13	0.96
2000	7	4	1	4	16	2.45
2001	6	1	2	2	11	2.22
2002	8	2	1	1	12	3.37
2003	8	2	2	5	17	2.87
2004	9	1	2	2	14	3.70
2005	6	1	2	4	13	2.22
2006	3	2	4	1	10	1.29
2007	8	2	4	2	16	2.83
2008	7	2	1	3	13	2.63
2009	6	1	1	0	8	2.71
2010	6	1	4	5	16	2.16
2011	2	2	2	3	9	0.50
2012	6	3	1	0	10	2.65
2013	7	3	3	2	15	2.22
2014	6	2	2	2	12	2.00
2015	6	2	3	2	13	1.89
2016	4	0	0	4	8	2.31

Summary Statistics	SIO	WA	EA	SP	All Basins
SUM	221*	73	96	103	493
Mean	5.97*	1.97	2.59	2.78	13.32
SD	2.11	1.21	1.36	2.16*	3.30
1 SD	4-8	1-3	2-4	1-5	10-16
MAX	12*	4	6	9	22
MIN	2	0	0	0	8

Appendix 2A

Mean Latitude of Genesis for Southern Hemisphere Storms

Year	SIO	WA	EA	SP	Mean	SD
1980	16.83	16.53	19.34	17.50	17.41	2.75
1981	13.68	15.06	16.00	17.53	14.83	4.55
1982	11.43	19.22	15.88	18.72	14.27	4.13
1983	16.01	17.36	15.80	14.60	15.19	1.22
1984	13.60	17.75	17.85		15.54	3.17
1985	16.73	14.96	15.51	17.58	16.22	3.48
1986	13.87	11.85	15.05	16.98	14.06	2.93
1987	18.86		13.43	16.21	16.42	4.67
1988	16.39	18.12	16.01	14.82	16.02	2.88
1989	14.75	17.01	15.87	23.33	16.76	4.63
1990	13.70	14.46	17.63	9.10	14.18	3.88
1991	17.01	7.93	13.50	13.47	14.44	5.09
1992	14.09	12.34	13.91	11.72	13.12	2.16
1993	15.19		15.98	15.40	15.43	4.20
1994	15.67	14.69	14.33	14.88	15.15	2.65
1995	14.16	13.00	19.48	19.25	15.48	3.62
1996	14.24	15.16	17.01	16.60	15.42	2.94
1997	14.86		13.28	16.69	15.07	4.83
1998	16.27	16.58	14.90	14.34	15.13	2.93
1999	18.03	15.79	14.50	16.65	16.31	4.24
2000	17.09	16.64	20.31	21.10	18.18	3.31
2001	18.38	10.08	16.29	15.56	16.73	5.23
2002	13.68	15.82	22.44	13.05	14.72	3.20
2003	16.44	11.93	15.52	15.02	15.38	3.45
2004	14.53	19.27	12.22	11.73	14.14	3.77
2005	13.33	15.61	15.67	11.49	13.30	3.47
2006	13.67	14.42	16.09	19.31	15.35	3.31
2007	15.84	16.33	15.56	13.15	15.49	3.79
2008	14.11	16.03	11.38	16.61	14.77	1.97
2009	18.52	17.85	14.93		17.99	3.38
2010	13.84	14.30	14.15	14.59	14.18	1.78
2011	16.05	19.92	18.33	18.61	18.27	3.19
2012	16.50	19.86	17.51		17.61	2.88
2013	15.01	15.33	14.10	13.88	14.74	2.90
2014	18.11	15.86	11.55	18.18	16.65	7.73
2015	13.53	17.86	15.38	14.55	14.78	3.43
2016	15.34			15.34	15.34	3.11

Basin	SIO	WA	EA	SP
Mean	15.39	15.60	15.74	15.81
SD	1.75	2.70	2.34	2.88
+- 1SD	13.63-17.14	12.90-18.31	13.40-18.09	12.93-18.69
MAX	18.86	19.92	22.44	23.33
MIN	11.43	7.93	11.38	9.10

Appendix 3A

Mean Longitude of Genesis for Southern Hemisphere Storms

LMI	SIO	EA	WA	SP	Mean: LMI	SD: LMI
1980	49.84	48.01	50.80	33.44	48.34	8.80
1981	51.23	42.87	52.30	38.58	48.58	7.86
1982	47.07	39.44	33.44	36.01	42.31	9.24
1983	33.44	51.44	41.16	45.90	43.29	7.76
1984	51.30	43.73	39.44		46.81	11.39
1985	44.71	50.80	37.73	54.02	46.80	12.08
1986	54.45	41.16	47.16	38.58	48.28	9.69
1987	38.58	33.44		39.44	38.12	5.96
1988	48.23	36.01	33.44	54.02	47.16	14.26
1989	46.59	61.73	51.44	48.01	50.23	11.26
1990	51.87	36.01	48.23	59.16	48.87	12.29
1991	48.23	45.44	61.73	64.31	50.59	11.29
1992	59.16	58.65	59.16	47.33	55.05	11.20
1993	48.01	49.73		52.47	49.97	10.95
1994	55.05	54.66	43.73	52.73	52.93	10.01
1995	48.87	56.59	60.45	33.44	50.28	11.41
1996	54.75	43.30	55.30	54.02	50.48	13.15
1997	49.52	49.52		43.73	47.94	12.00
1998	46.94	41.67	47.59	50.16	46.98	12.57
1999	50.80	60.88	46.94	52.73	52.24	13.71
2000	51.44	33.44	60.45	40.51	49.84	13.57
2001	47.59	45.01	46.30	45.01	46.53	9.93
2002	52.73	38.58	59.16	51.44	52.52	12.81
2003	48.55	65.59	64.31	61.22	56.13	13.22
2004	46.87	47.59	56.59	63.02	49.97	14.95
2005	51.44	57.87	46.30	68.81	57.38	14.30
2006	59.16	55.30	60.45	38.58	55.82	12.95
2007	54.66	39.87	46.30	46.30	48.87	12.71
2008	52.91	38.58	46.30	54.02	51.05	10.01
2009	45.44	69.45	56.59		49.84	14.48
2010	54.02	55.95	33.44	49.90	51.93	13.62
2011	46.30	51.44	45.01	52.30	49.16	11.75
2012	48.44	59.16	39.44		46.81	10.63
2013	51.44	48.87	50.59	54.02	51.10	9.67
2014	60.02	72.02	48.87	51.44	58.73	13.82
2015	56.16	55.73	54.02	60.45	56.39	12.62
2016	63.02			54.02	58.52	15.36

Basin	SIO	WA	EA	SP	
Mean	50.51	49.43	49.22	49.68	**50.16**
SD	5.60	9.99	8.62	8.90	4.37
+- 1SD	45-56	39-59	41-58	41-59	46-55
MAX	63.02	72.02	64.31	68.81	58.73
MIN	33.44	33.44	33.44	33.44	38.12

Appendix 4A

Duration of Tropical Cyclones at LMI.

Duration LMI	SIO	EA	WA	SP	Mean: LMI Duration	SD: LMI Duration
1980	2.25	1.33	1.75	1.00	1.75	0.97
1981	1.50	1.00	2.00	1.00	1.46	0.66
1982	1.60	1.33	1.00	1.00	1.40	0.70
1983	1.67	3.00	2.00	1.78	1.86	0.86
1984	2.43	1.67	1.00		1.92	0.95
1985	1.80	1.25	1.33	1.33	1.47	0.64
1986	1.83	1.50	1.67	1.00	1.62	0.51
1987	1.00	1.00		1.50	1.27	0.47
1988	1.75	1.00	1.00	1.00	1.33	0.71
1989	2.44	2.33	1.25	1.33	2.00	1.00
1990	2.00	1.00	2.00	1.00	1.77	0.93
1991	2.25	2.00	2.00	1.00	2.00	1.00
1992	1.75	2.60	1.00	1.80	2.00	0.93
1993	1.50	1.67		2.20	1.79	0.70
1994	1.90	1.75	1.67	2.50	1.89	1.20
1995	1.86	1.00	1.50	1.00	1.64	0.50
1996	1.86	1.50	1.50	2.00	1.69	0.70
1997	1.83	2.25		1.50	1.82	0.91
1998	1.25	1.80	1.50	1.75	1.63	0.83
1999	1.75	3.00	1.50	2.00	2.00	1.35
2000	1.57	1.00	1.75	1.25	1.50	0.63
2001	2.00	1.50	1.00	1.50	1.73	0.65
2002	1.88	1.00	1.00	1.00	1.58	1.00
2003	1.75	2.00	2.00	1.80	1.82	0.88
2004	1.67	2.00	2.00	2.00	1.79	0.80
2005	1.67	4.00	2.00	2.00	2.15	1.21
2006	1.67	1.50	1.50	2.00	1.60	0.84
2007	2.13	1.00	1.00	1.50	1.63	1.02
2008	2.14	1.00	1.00	2.00	1.85	1.07
2009	1.17	3.00	2.00		1.50	0.76
2010	1.33	1.50	1.00	1.40	1.38	0.72
2011	1.00	1.50	2.00	1.00	1.33	0.50
2012	1.83	1.00	1.33		1.60	0.84
2013	1.43	1.67	1.33	1.50	1.47	0.52
2014	2.00	1.50	1.00	2.00	1.75	0.97
2015	1.50	1.33	1.00	1.50	1.38	0.65
2016	1.50			1.50	1.50	0.53

Basin	SIO	WA	EA	SP	
Mean	1.74	1.68	1.47	1.52	1.67
SD	0.35	0.72	0.41	0.43	0.22
MAX	2.44	4.00	2.00	2.50	2.15
MIN	1.00	1.00	1.00	1.00	1.27

Appendix 5A

Average Storm Lifetime from Genesis to Dissipation

Year	SIO	WA	EA	SP	Average Storm Lifetime
1980	11.00	8.50	11.67	5.00	9.83
1981	11.50	9.67	10.00	6.00	10.31
1982	13.60	12.00	13.33	13.00	13.30
1983	13.33	8.00	22.00	9.67	11.21
1984	12.71	6.00	7.33		9.92
1985	14.40	12.33	10.75	7.67	11.67
1986	14.00	10.00	7.50	8.50	11.23
1987	11.00		10.50	9.33	10.00
1988	14.00	5.00	12.00	11.33	11.89
1989	12.33	7.75	10.33	7.67	10.32
1990	15.33	9.75	12.00	13.00	12.92
1991	13.75	11.00	12.67	11.00	12.78
1992	12.50	10.00	13.40	9.20	11.53
1993	9.67		13.67	9.80	10.57
1994	13.60	8.33	13.50	12.50	12.63
1995	11.86	10.00	9.50	6.00	10.73
1996	10.00	9.00	10.40	14.00	10.19
1997	14.83		19.00	12.33	14.91
1998	12.25	11.00	15.60	10.50	12.26
1999	13.00	6.00	12.00	12.50	10.54
2000	13.57	8.50	17.00	7.75	11.06
2001	11.17	7.00	12.50	10.00	10.82
2002	11.75	6.50	5.00	9.00	10.08
2003	11.50	10.00	16.00	8.40	10.94
2004	14.11	7.00	11.50	14.00	13.21
2005	12.83	6.00	14.00	10.25	11.69
2006	16.33	9.00	10.00	13.00	12.00
2007	12.63	8.50	9.00	7.50	10.56
2008	14.57	8.50	6.00	9.00	11.69
2009	9.83	20.00	10.00		11.13
2010	10.50	6.00	10.50	8.20	9.50
2011	12.00	9.00	11.00	10.67	10.67
2012	11.33	7.67	16.00		10.70
2013	11.57	8.00	8.67	14.00	10.60
2014	10.00	7.00	19.00	10.00	11.00
2015	10.50	5.00	10.00	9.50	9.38
2016	13.25			10.50	11.88

Basin	SIO	WA	EA	SP
Mean	12.49	8.73	12.04	10.02
Std.	1.65	2.77	3.64	2.38
+- 1SD	10.84-14.13	5.96-11.49	8.40-15.68	7.64-12.41
MAX	16.33	20.00	22.00	14.00
MIN	9.67	5.00	5.00	5.00

Appendix 6A

Mean Sea Surface Temperatures at the Point of Genesis

SST	SIO	WA	EA	SP	Mean: SST All Basins	SD
1980	28.01	28.93	27.71	28.42	28.28	0.82
1981	27.92	28.40	28.95	28.01	28.27	0.92
1982	27.85	28.67	28.74	27.99	28.21	1.36
1983	27.68	29.21	28.25	28.45	28.32	1.19
1984	27.11	28.48	27.34		27.48	1.36
1985	27.23	28.44	28.52	27.71	27.91	1.12
1986	27.43	28.31	27.70	28.54	27.85	0.96
1987	26.38		29.75	27.17	27.43	1.64
1988	28.16	24.91	27.81	28.64	27.92	1.24
1989	27.38	27.90	28.89	27.03	27.67	1.09
1990	27.66	27.87	27.87	29.23	27.88	1.03
1991	27.40	27.10	27.55	28.25	27.51	0.66
1992	27.86	28.77	29.08	28.88	28.67	0.99
1993	26.93		27.44	28.51	27.60	1.08
1994	26.86	28.38	28.07	28.47	27.52	1.27
1995	28.05	28.24	27.98	26.90	27.98	0.58
1996	28.12	28.29	28.93	29.38	28.52	0.89
1997	27.65		29.34	27.28	27.86	1.38
1998	27.88	28.93	27.76	28.08	28.04	1.06
1999	27.58	27.74	29.21	28.66	28.17	1.18
2000	27.31	28.56	28.92	27.15	27.68	1.23
2001	26.70	28.37	29.34	28.79	27.71	1.59
2002	27.76	27.36	28.49	28.28	27.80	1.00
2003	27.92	29.04	28.85	29.00	28.48	1.02
2004	27.62	28.90	30.45	29.08	28.32	1.30
2005	28.20	28.42	27.88	29.11	28.45	0.81
2006	27.95	28.91	27.98	28.23	28.18	0.63
2007	28.29	28.62	29.07	28.53	28.56	0.73
2008	28.29	29.24	26.33	28.30	28.29	1.05
2009	28.81	28.50	28.38		28.72	1.13
2010	27.73	28.67	29.24	28.74	28.48	0.99
2011	27.86	28.95	28.79	28.47	28.51	0.94
2012	28.25	28.02	28.32		28.19	1.16
2013	27.95	29.13	28.73	29.29	28.52	1.06
2014	27.81	28.73	28.66	28.92	28.29	0.91
2015	27.84	28.47	27.80	29.99	28.26	1.02
2016	28.90			29.28	29.09	0.55

	SIO	WA	EA	SP
Mean	27.74	28.38	28.45	28.43
SD	0.52	0.80	0.79	0.73
+- 1SD	27-28	28-29	28-29	28-29
MAX	28.90	29.24	30.45	29.99
MIN	26.38	24.91	26.33	26.90

Appendix 1B

Time Trends: Change in sea surface temperature over time for individual basins and the hemisphere.

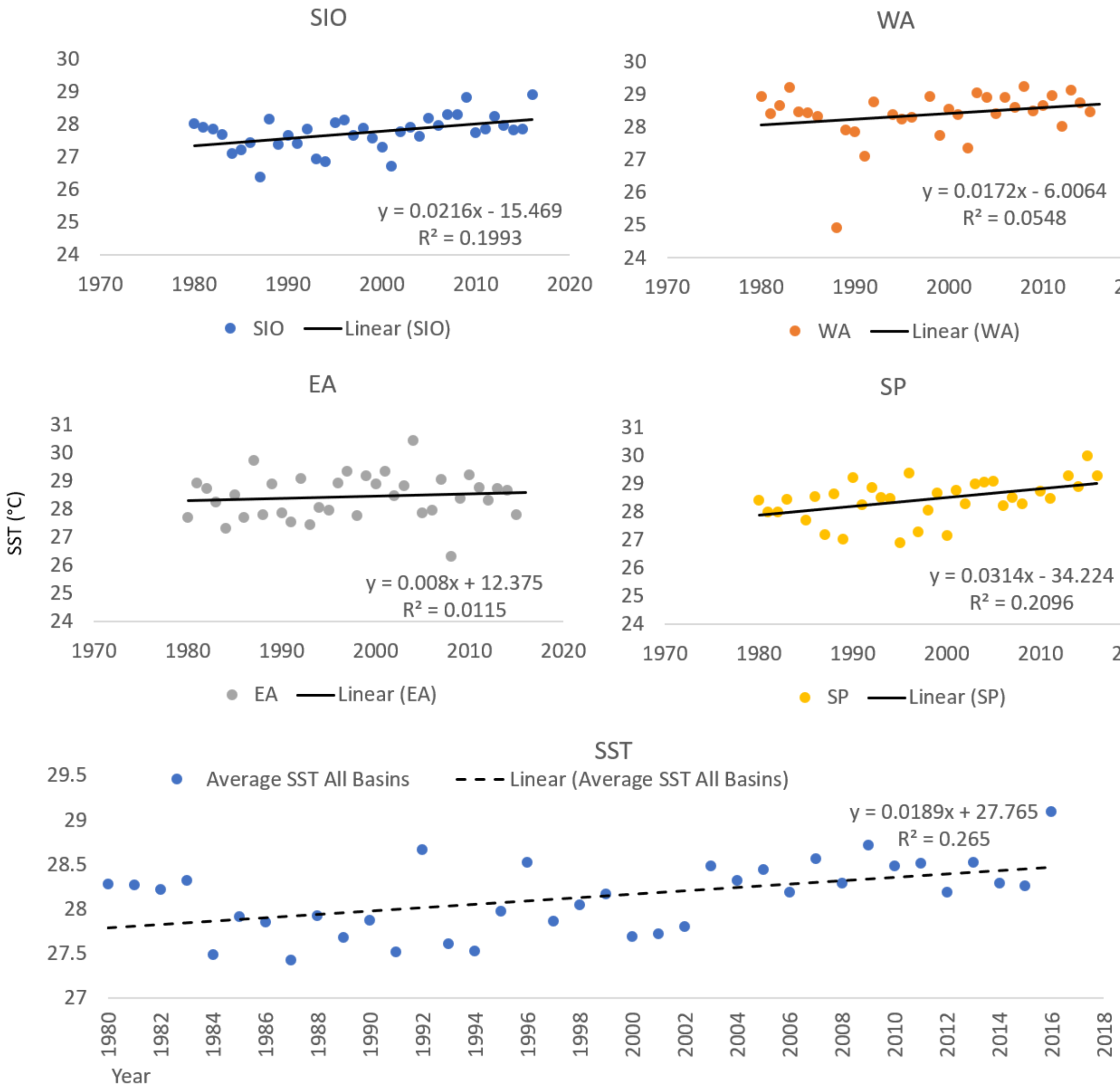

Time Trends: Change in Air temperature (1000mb) over time for individual basins and the hemisphere.

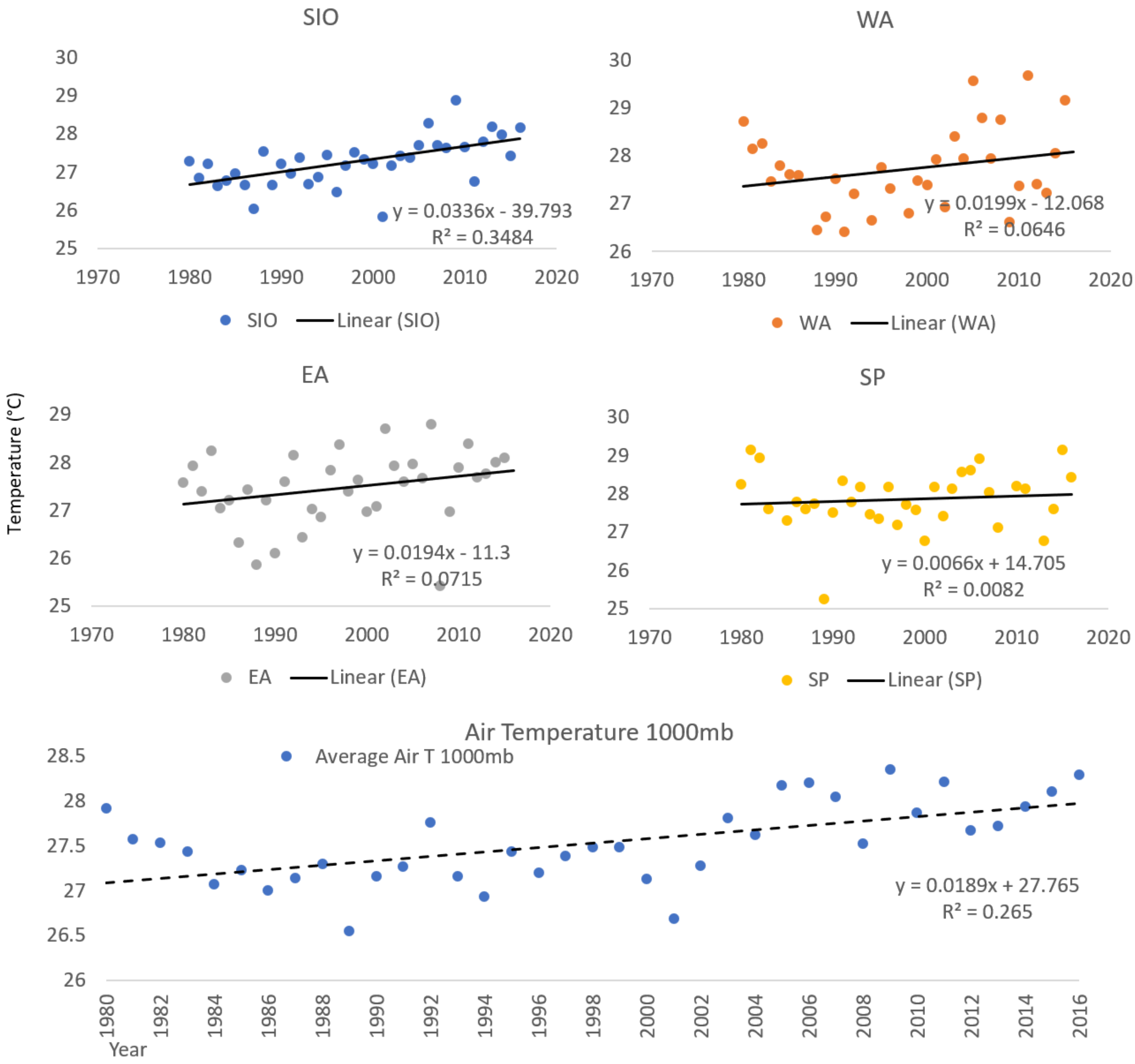

Time Trends: Change in Air temperature (850mb) over time for individual basins and the hemisphere.

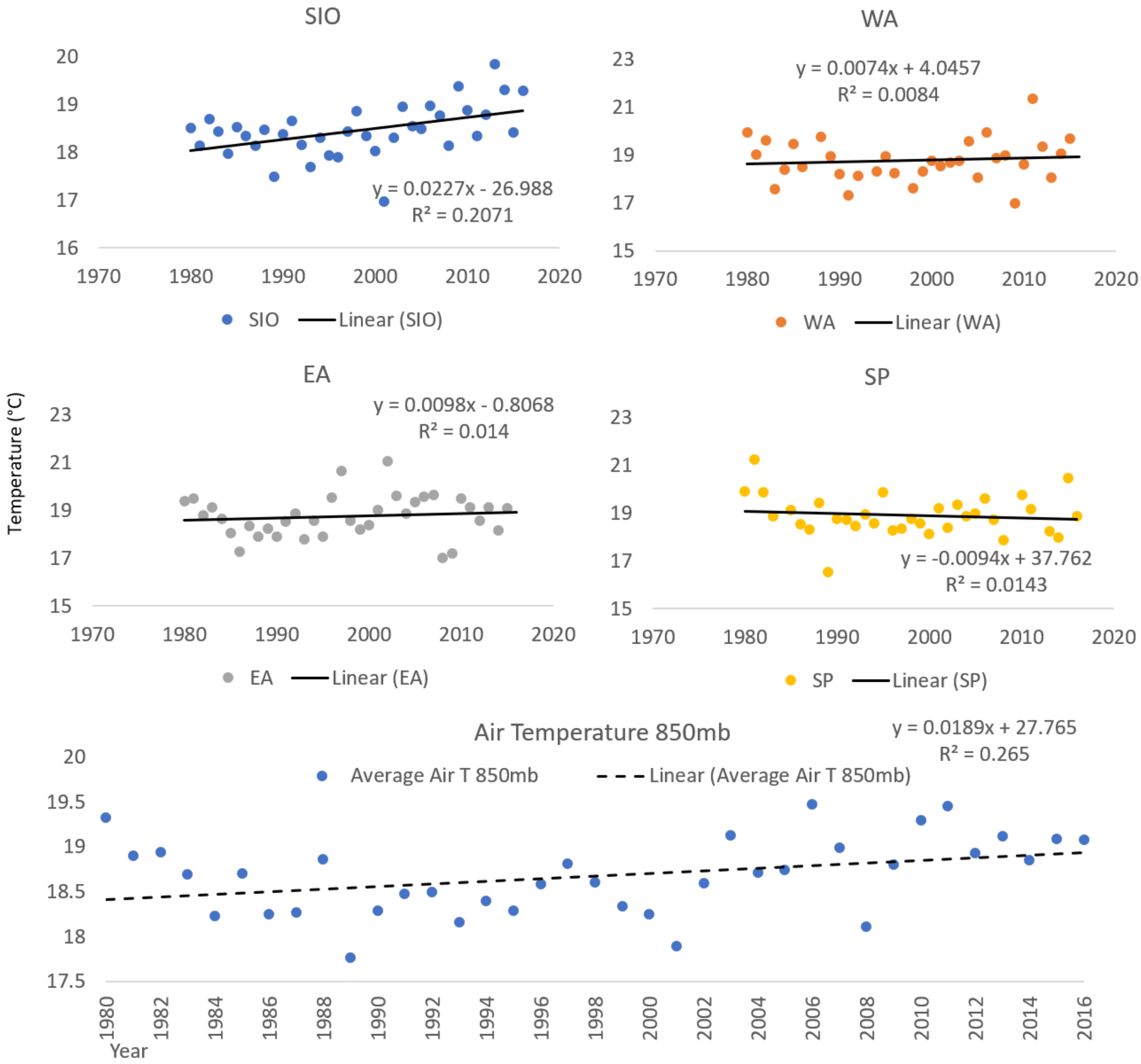

Appendix 4B

Time Trends: Change in Omega (1000mb) over time for individual basins and the hemisphere.

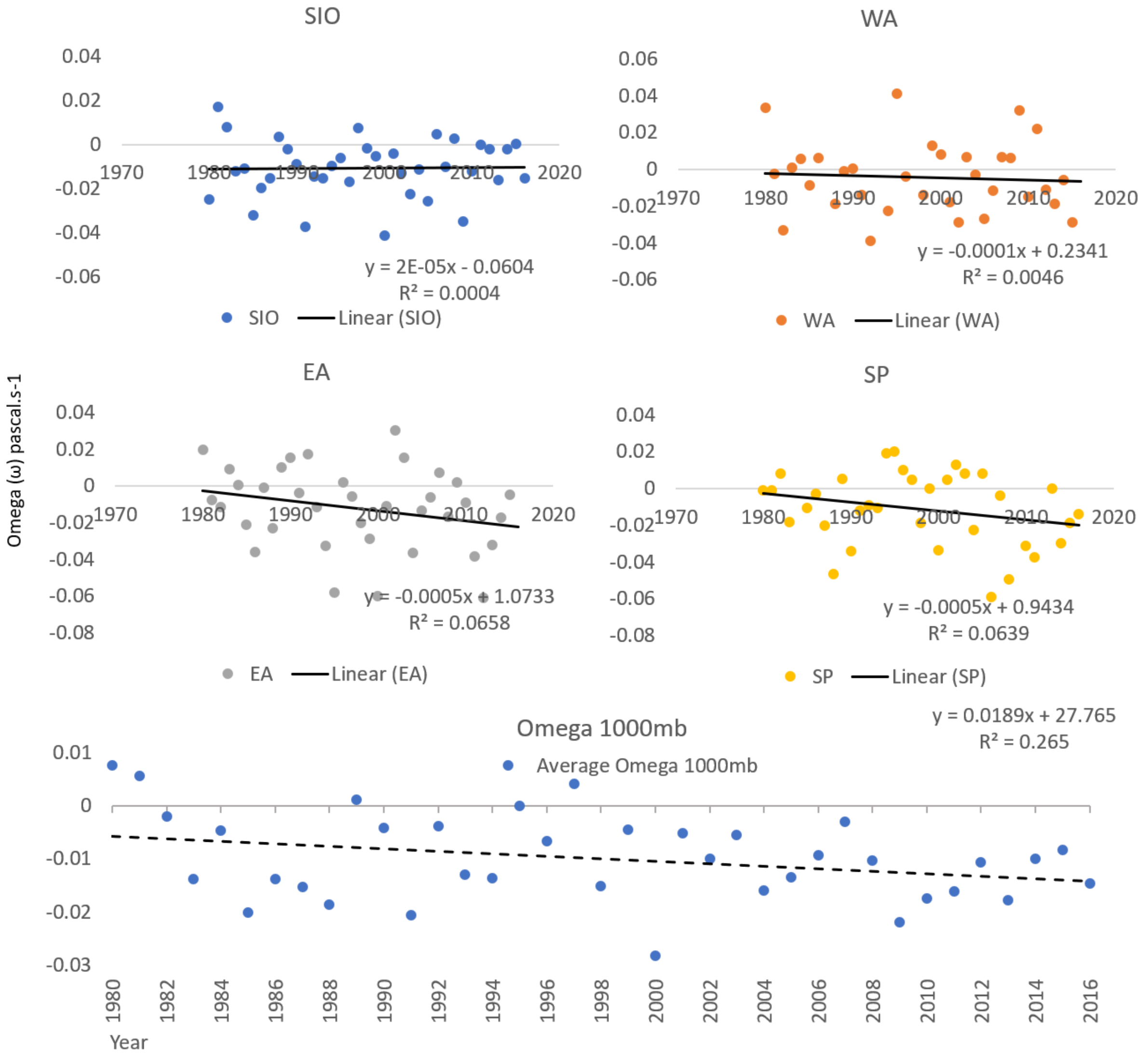

Time Trends: Change in Omega (850mb) over time for individual basins and the hemisphere.

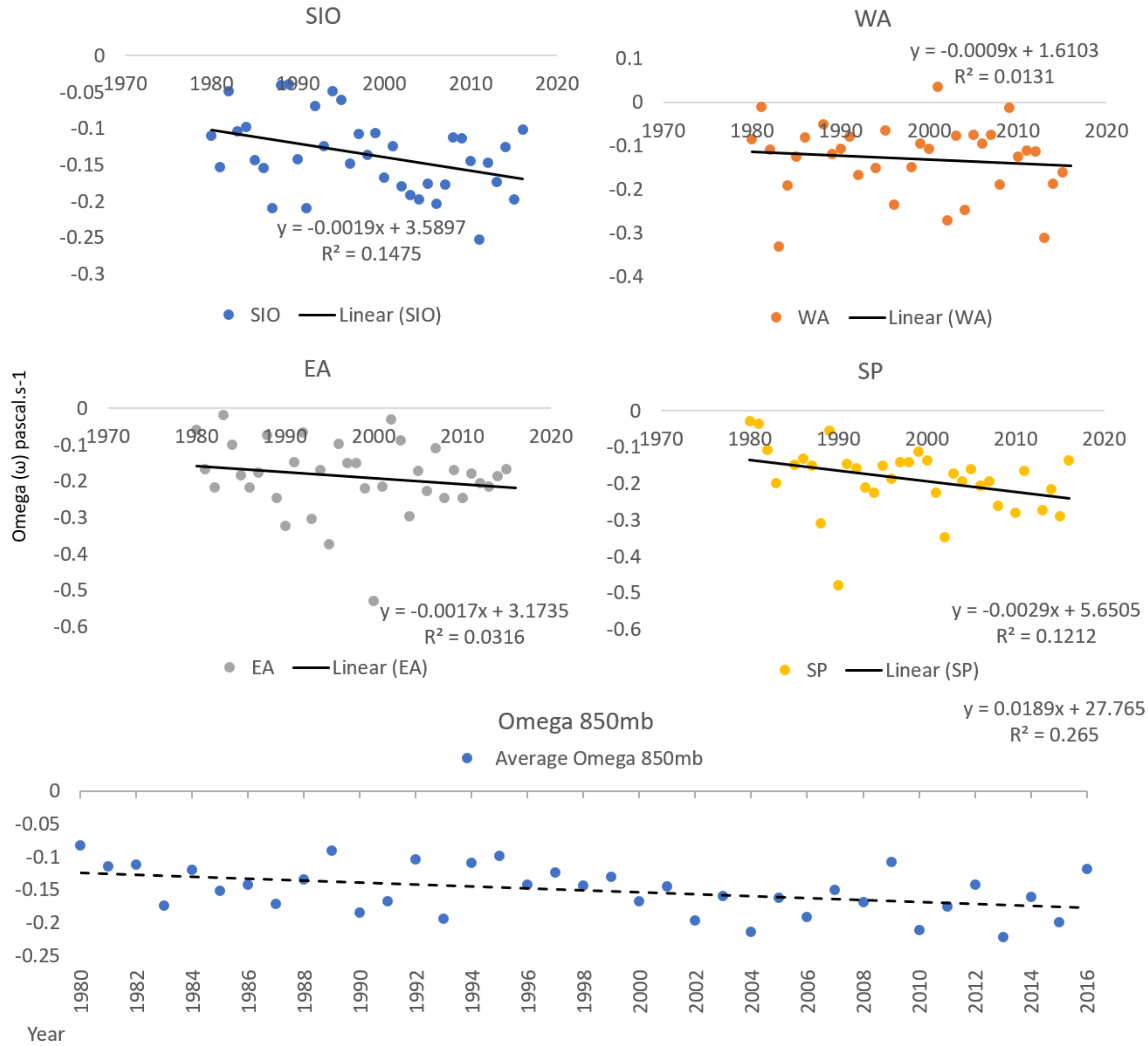

Time Trends: Change in Relative Humidity (1000mb) over time for individual basins and the hemisphere.

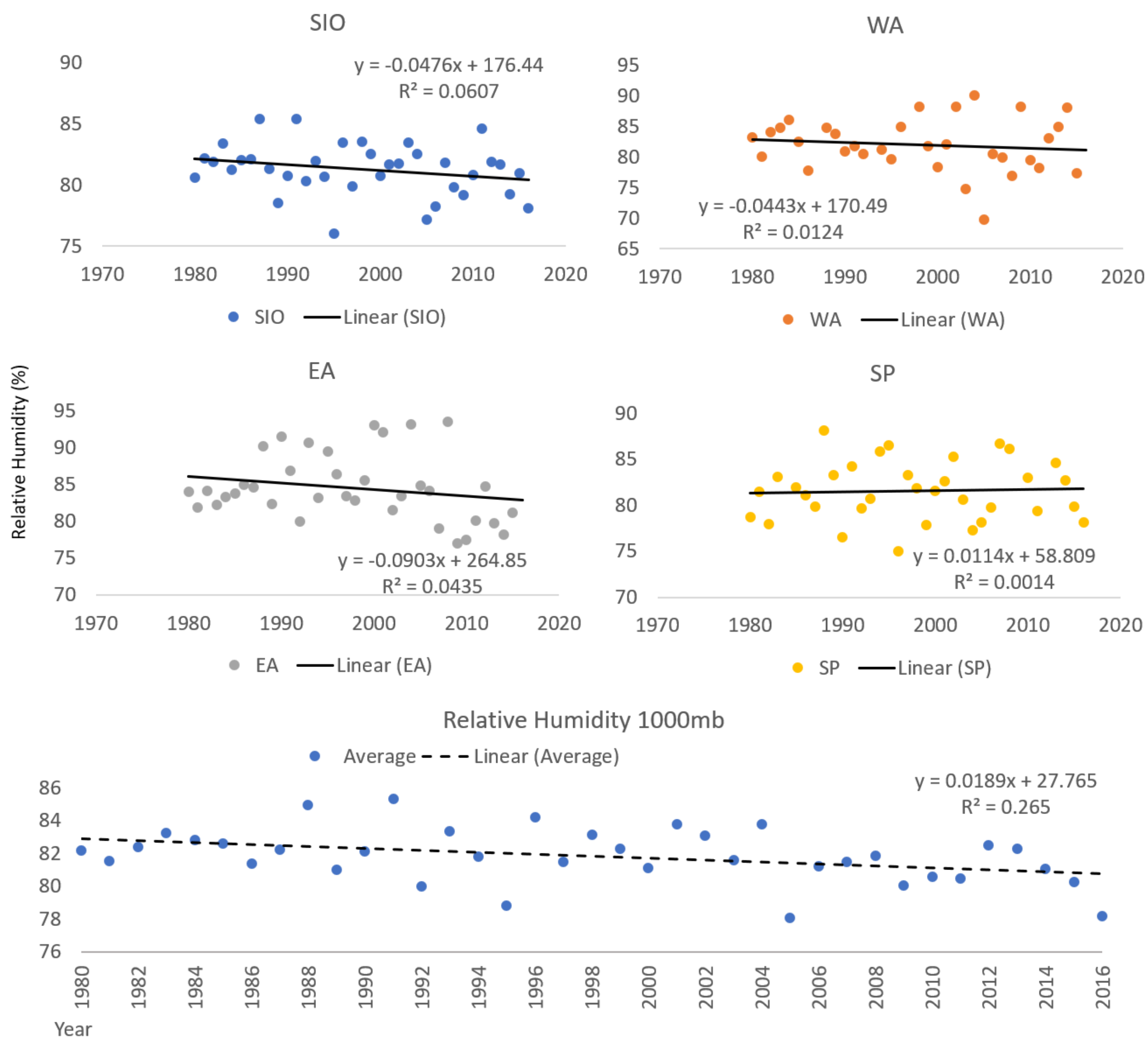

Time Trends: Change in Relative Humidity (850mb) over time for individual basins and the hemisphere.

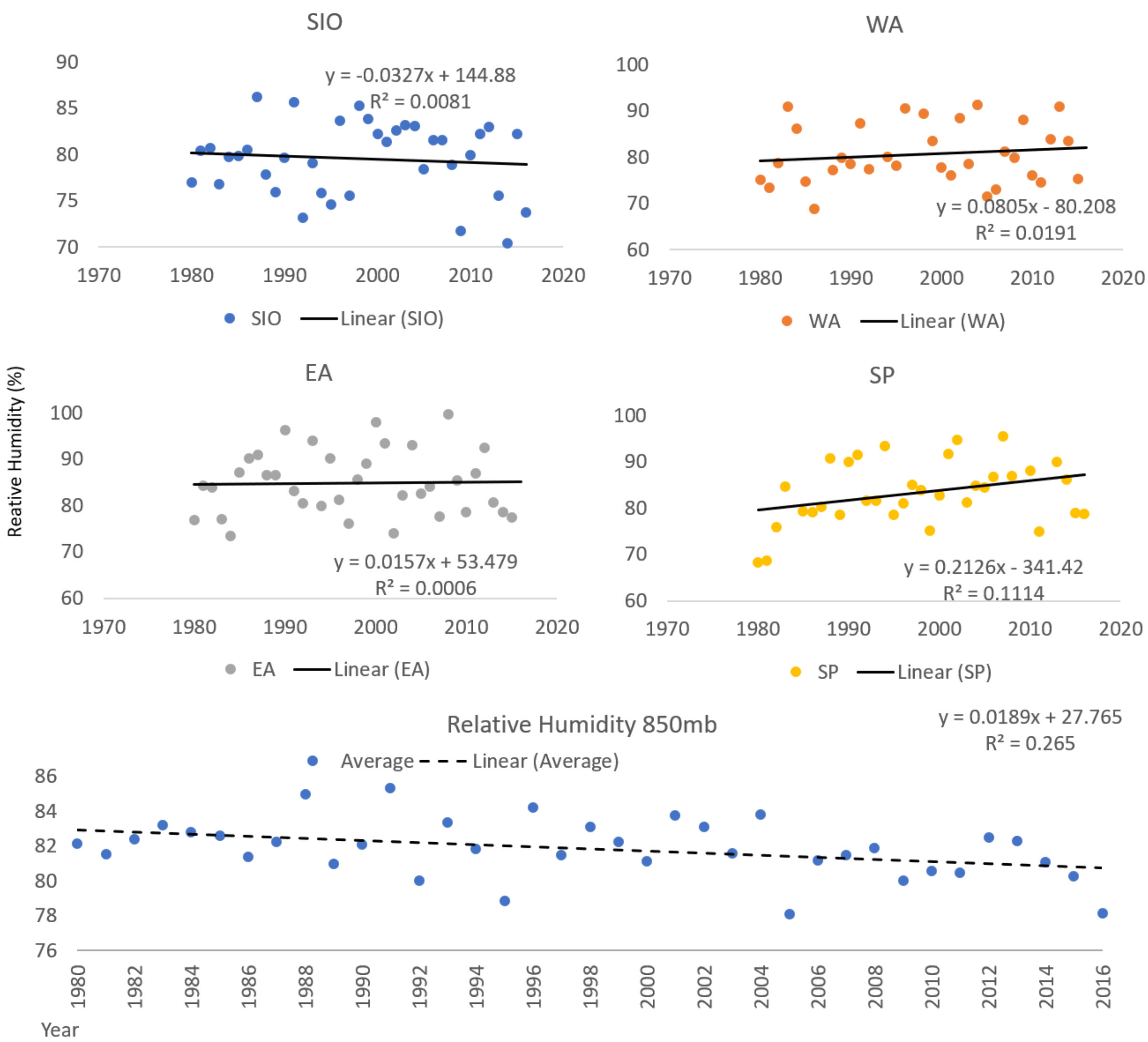

Time Trends: Change in V-wind Shear over time for individual basins and the hemisphere.

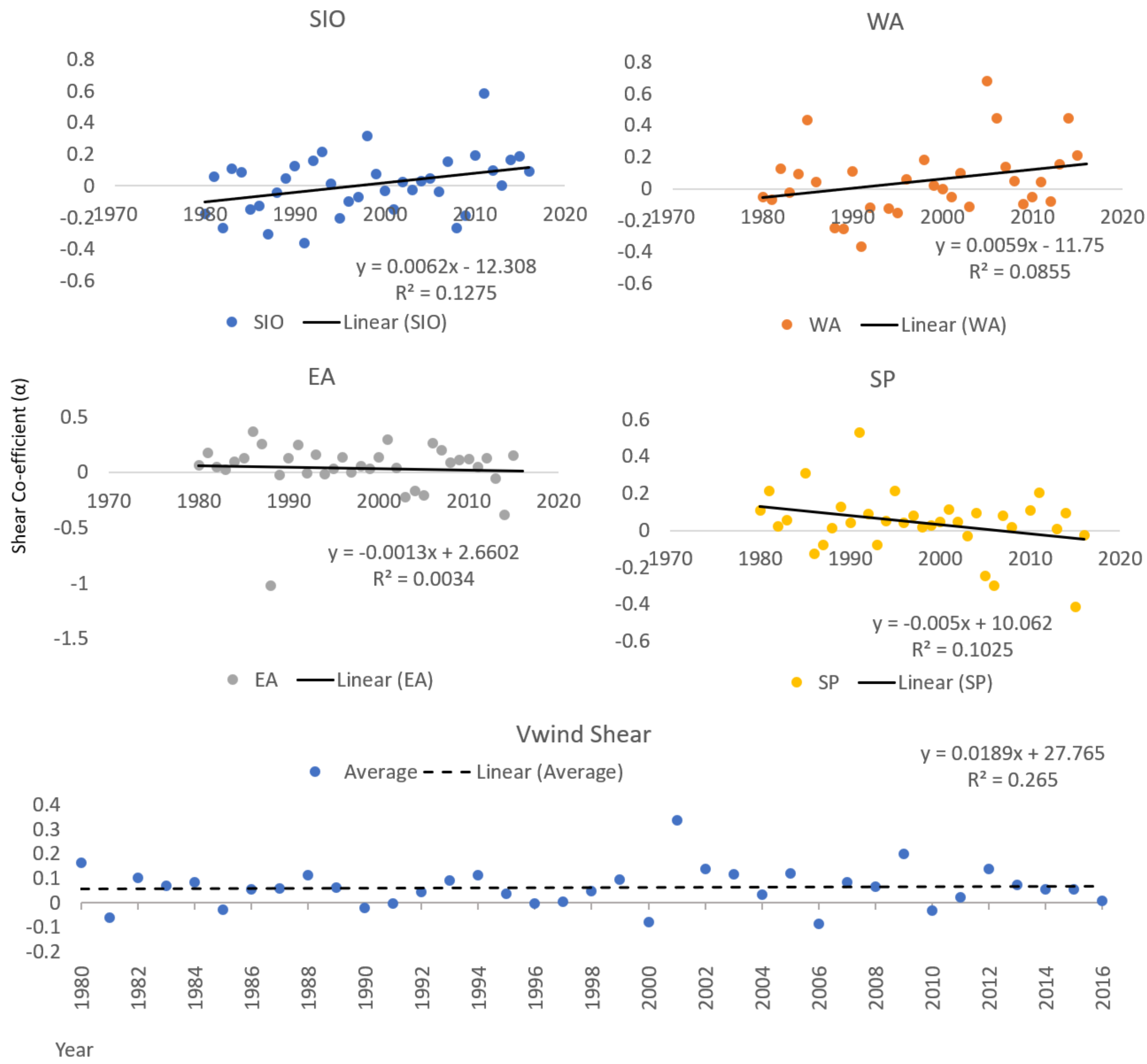

Appendix 9B

Time Trends: Change in U-wind Shear over time for individual basins and the hemisphere.

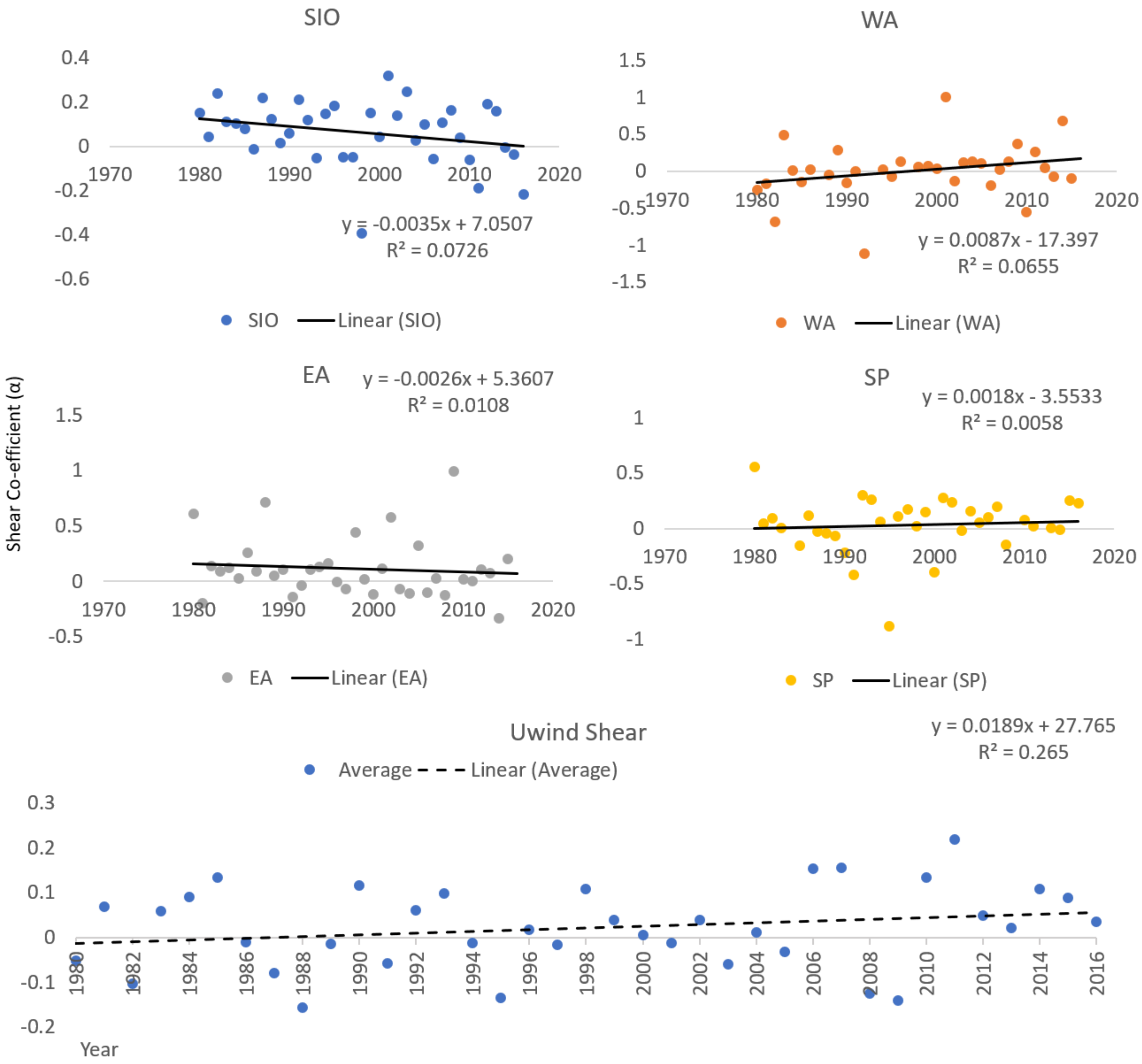

Appendix 1C

Table: MANOVA for climate drivers.

	Source	Statistic	F	Prob>F	
Model	W	0.8914	4.46	0	e
	P	0.1086	4.46	0	e
	L	0.1219	4.46	0	e
	R	0.1219	4.46	0	e
AirT1000	W	0.9896	4.98	0.0261	e
	P	0.0104	4.98	0.0261	e
	L	0.0105	4.98	0.0261	e
	R	0.0105	4.98	0.0261	e
AirT850	W	0.9997	0.15	0.7014	e
	P	0.0003	0.15	0.7014	e
	L	0.0003	0.15	0.7014	e
	R	0.0003	0.15	0.7014	e
Omega1000	W	0.9997	0.14	0.7087	e
	P	0.0003	0.14	0.7087	e
	L	0.0003	0.14	0.7087	e
	R	0.0003	0.14	0.7087	e
Omega850	W	0.9759	11.76	0.0007	e
	P	0.0241	11.76	0.0007	e
	L	0.0247	11.76	0.0007	e
	R	0.0247	11.76	0.0007	e
RH1000	W	0.9945	2.62	0.1062	e
	P	0.0055	2.62	0.1062	e
	L	0.0055	2.62	0.1062	e
	R	0.0055	2.62	0.1062	e
RH850	W	0.9965	1.68	0.1954	e
	P	0.0035	1.68	0.1954	e
	L	0.0035	1.68	0.1954	e
	R	0.0035	1.68	0.1954	e
GPH1000	W	0.9993	0.35	0.5538	e
	P	0.0007	0.35	0.5538	e
	L	0.0007	0.35	0.5538	e
	R	0.0007	0.35	0.5538	e
GPH850	W	0.9994	0.27	0.6011	e
	P	0.0006	0.27	0.6011	e
	L	0.0006	0.27	0.6011	e
	R	0.0006	0.27	0.6011	e
Pressure(SLP)	W	1	0	0.9701	e
	P	0	0	0.9701	e
	L	0	0	0.9701	e
	R	0	0	0.9701	e
SST	W	0.9993	0.32	0.5723	e
	P	0.0007	0.32	0.5723	e
	L	0.0007	0.32	0.5723	e
	R	0.0007	0.32	0.5723	e
SolarWm	W	0.9977	1.09	0.2961	e
	P	0.0023	1.09	0.2961	e
	L	0.0023	1.09	0.2961	e
	R	0.0023	1.09	0.2961	e
V-wind shear	W	0.9998	0.07	0.7851	e
	P	0.0002	0.07	0.7851	e
	L	0.0002	0.07	0.7851	e
	R	0.0002	0.07	0.7851	e
U-wind shear	W	0.9986	0.69	0.4081	e
	P	0.0014	0.69	0.4081	e
	L	0.0014	0.69	0.4081	e
	R	0.0014	0.69	0.4081	e

Appendix 2C

Table: Multivariate regression results for tropical cyclone activity and climate drivers.

Equation	RMSE	"R-sq"	F	P		
Lifetime	4.272111	0.021	0.784984	0.6764		
LifetimeTC	2.452666	0.1232	5.144491	0		
Category	1.216057	0.1796	8.017708	0		
Latitude	3.245463	0.239	11.49635	0		
Longitude	44.93868	0.1661	7.295666	0		
TCSeason	9.766756	0.1086	4.462657	0		
Lifetime	Coef.	Std. Err.	t	P>|t|	[95% Conf.	Interval]
AirT1000	-0.48629	0.649962	-0.75	0.455	-1.76344	0.790859
AirT850	0.56762	0.504272	1.13	0.261	-0.42325	1.558495
Omega1000	-3.39015	7.67381	-0.44	0.659	-18.4689	11.68858
Omega850	-0.39574	2.712645	-0.15	0.884	-5.72598	4.934499
RH1000	-0.09416	0.074241	-1.27	0.205	-0.24004	0.051725
RH850	0.071815	0.040438	1.78	0.076	-0.00764	0.151274
GPH1000	-0.013	0.161298	-0.08	0.936	-0.32994	0.303948
GPH850	0.01125	0.162853	0.07	0.945	-0.30875	0.331249
Pressure	0.003082	0.053327	0.06	0.954	-0.1017	0.107867
SSTGenesis	0.114273	0.223424	0.51	0.609	-0.32474	0.553292
SolarWm	0.010069	0.004598	2.19	**0.029**	0.001034	0.019103
Vshear	-0.83065	0.607671	-1.37	0.172	-2.0247	0.363404
Ushear	-0.10266	0.634094	-0.16	0.871	-1.34863	1.14331
_cons	-8.18432	193.4848	-0.04	0.966	-388.374	372.0056
LifetimeTC						
AirT1000	0.556216	0.37315	1.49	0.137	-0.17701	1.289441
AirT850	0.378043	0.289508	1.31	0.192	-0.19083	0.946916
Omega1000	-0.12912	4.405619	-0.03	0.977	-8.78599	8.527747
Omega850	-2.20294	1.55736	-1.41	0.158	-5.26309	0.857211
RH1000	-0.04723	0.042623	-1.11	0.268	-0.13099	0.036517
RH850	0.037711	0.023216	1.62	0.105	-0.00791	0.08333
GPH1000	0.147229	0.092603	1.59	0.113	-0.03473	0.329191
GPH850	-0.14638	0.093495	-1.57	0.118	-0.3301	0.037333
Pressure	0.119031	0.030616	3.89	**0**	0.058873	0.179189
SSTGenesis	0.505971	0.12827	3.94	**0**	0.253926	0.758016
SolarWm	0.004245	0.00264	1.61	0.108	-0.00094	0.009432
Vshear	-0.60763	0.348871	-1.74	0.082	-1.29314	0.077892
Ushear	-0.0352	0.364041	-0.1	0.923	-0.75052	0.68013
_cons	55.70988	111.0818	0.5	0.616	-162.561	273.9811
Category Saffir						
AirT1000	0.056966	0.185012	0.31	0.758	-0.30658	0.420506
AirT850	-0.1698	0.143541	-1.18	0.237	-0.45186	0.112248
Omega1000	-0.03198	2.18435	-0.01	0.988	-4.32414	4.260182
Omega850	-2.29681	0.772155	-2.97	**0.003**	-3.81406	-0.77956
RH1000	-0.03681	0.021133	-1.74	0.082	-0.07834	0.004714
RH850	0.00466	0.011511	0.4	0.686	-0.01796	0.027278
GPH1000	-0.0322	0.045914	-0.7	0.484	-0.12241	0.058022
GPH850	0.030639	0.046356	0.66	0.509	-0.06045	0.121727
Pressure	0.046793	0.01518	3.08	**0.002**	0.016966	0.07662
SSTGenesis	0.304706	0.063598	4.79	**0**	0.17974	0.429673
SolarWm	0.002943	0.001309	2.25	**0.025**	0.000371	0.005515
Vshear	-0.4595	0.172974	-2.66	**0.008**	-0.79939	-0.11962
Ushear	-0.33156	0.180495	-1.84	0.067	-0.68622	0.023108
_cons	-93.0952	55.07545	-1.69	0.092	-201.316	15.1259
Latitude Genesis						
AirT1000	-0.31128	0.493767	-0.63	0.529	-1.28151	0.658952
AirT850	-0.26554	0.383089	-0.69	0.489	-1.01829	0.487218
Omega1000	13.4177	5.829686	2.3	**0.022**	1.962603	24.8728
Omega850	-7.87223	2.060759	-3.82	**0**	-11.9215	-3.82292
RH1000	-0.15005	0.0564	-2.66	**0.008**	-0.26087	-0.03922

RH850	0.084514	0.03072	2.75	**0.006**	0.02415	0.144878
GPH1000	-0.12784	0.122536	-1.04	0.297	-0.36862	0.112937
GPH850	0.151659	0.123717	1.23	0.221	-0.09144	0.394758
Pressure	0.111601	0.040512	2.75	**0.006**	0.031997	0.191204
SSTGenesis	1.035484	0.169732	6.1	**0**	0.701968	1.369
SolarWm	0.002478	0.003493	0.71	0.478	-0.00439	0.009342
Vshear	-0.78716	0.461639	-1.71	0.089	-1.69426	0.119945
Ushear	-1.02944	0.481712	-2.14	**0.033**	-1.97598	-0.08289
_cons	-355.445	146.9877	-2.42	**0.016**	-644.27	-66.6204
Longitude Genesis						
AirT1000	-10.2472	6.837002	-1.5	0.135	-23.6817	3.1872
AirT850	-1.41519	5.30448	-0.27	0.79	-11.8383	9.007901
Omega1000	-47.1445	80.72142	-0.58	0.559	-205.759	111.4699
Omega850	65.55629	28.53453	2.3	**0.022**	9.487073	121.6255
RH1000	-1.0556	0.78095	-1.35	0.177	-2.59014	0.478931
RH850	1.317074	0.42537	3.1	**0.002**	0.481238	2.15291
GPH1000	-2.81508	1.696708	-1.66	0.098	-6.14904	0.518889
GPH850	2.373176	1.713059	1.39	0.167	-0.99292	5.739268
Pressure	1.031156	0.560949	1.84	0.067	-0.07109	2.133398
SSTGenesis	8.186098	2.350209	3.48	**0.001**	3.568031	12.80417
SolarWm	-0.03444	0.048365	-0.71	0.477	-0.12948	0.06059
Vshear	2.888852	6.392142	0.45	0.652	-9.67145	15.44916
Ushear	-10.9997	6.670086	-1.65	0.1	-24.1062	2.106747
_cons	-4199.85	2035.282	-2.06	**0.04**	-8199.1	-200.606
TC Season						
AirT1000	3.316802	1.485921	2.23	**0.026**	0.397026	6.236578
AirT850	0.442326	1.15285	0.38	0.701	-1.82298	2.707631
Omega1000	-6.55709	17.5436	-0.37	0.709	-41.0296	27.9154
Omega850	-21.2705	6.201558	-3.43	**0.001**	-33.4563	-9.0847
RH1000	-0.27476	0.169728	-1.62	0.106	-0.60826	0.058752
RH850	0.119864	0.092448	1.3	0.195	-0.06179	0.301521
GPH1000	0.218509	0.368754	0.59	0.554	-0.50608	0.943097
GPH850	-0.19477	0.372308	-0.52	0.601	-0.92634	0.536799
PressureSL	0.004566	0.121914	0.04	0.97	-0.23499	0.244122
SSTGenesis	-0.28859	0.510783	-0.57	0.572	-1.29226	0.715074
SolarWm	0.010994	0.010511	1.05	0.296	-0.00966	0.031649
Vshear	0.379049	1.389237	0.27	0.785	-2.35075	3.108845
Ushear	1.200318	1.449645	0.83	0.408	-1.64818	4.048811
_cons	2184.876	442.3384	4.94	**0**	1315.699	3054.053

Appendix 3C

Table: MANOVA for variability and tropical cyclone genesis activity.

	Source	Statistic	F	Prob>F	
Model	W	0.0834	1.98	0.0031	a
	P	1.7516	1.82	0.006	a
	L	3.8469	2.06	0.0018	a
	R	2.0625	6.96	0.0001	u
Volcano Act.	W	0.6369	2.62	0.0512	e
	P	0.3631	2.62	0.0512	e
	L	0.5701	2.62	0.0512	e
	R	0.5701	2.62	0.0512	e
Nino 3.4	W	0.6861	2.1	0.1014	e
	P	0.3139	2.1	0.1014	e
	L	0.4574	2.1	0.1014	e
	R	0.4574	2.1	0.1014	e
SOI	W	0.6146	2.88	0.0365	e
	P	0.3854	2.88	0.0365	e
	L	0.627	2.88	0.0365	e
	R	0.627	2.88	0.0365	e
MEI	W	0.5839	3.28	0.0222	e
	P	0.4161	3.28	0.0222	e
	L	0.7126	3.28	0.0222	e
	R	0.7126	3.28	0.0222	e
DMI	W	0.564	3.56	0.0158	e
	P	0.436	3.56	0.0158	e
	L	0.773	3.56	0.0158	e
	R	0.773	3.56	0.0158	e
SAM	W	0.8948	0.54	0.7434	e
	P	0.1052	0.54	0.7434	e
	L	0.1176	0.54	0.7434	e
	R	0.1176	0.54	0.7434	e
PDO	W	0.8104	1.08	0.3994	e
	P	0.1896	1.08	0.3994	e
	L	0.2339	1.08	0.3994	e
	R	0.2339	1.08	0.3994	e
MJOIndex	W	0.8225	0.99	0.4438	e
	P	0.1775	0.99	0.4438	e
	L	0.2158	0.99	0.4438	e
	R	0.2158	0.99	0.4438	e

Appendix 4C

Table: Multivariate regression results for tropical cyclone activity and modes of variability.

Equation	RMSE	"R-sq"	F	P
Frequency	0.836462	0.1673	0.677946	0.7066
Latitude	1.142669	0.4091	2.336842	0.0473
Longitude	10.42244	0.5562	4.230419	0.0022
Storm Lifetime	1.020148	0.4424	2.677528	0.0263
TC Lifetime	0.585716	0.275	1.280464	0.2945
	t	P>|t|	[95% Conf.	Interval]
Frequency				
Volcano Act.	-0.65	0.519	-0.1976	0.102208
Nino34	-1.72	0.097	-2.82153	0.250889
SOI	-0.3	0.768	-1.33459	0.995656
MEI	1.08	0.288	-0.99539	3.220287
DMI	1.26	0.219	-0.85808	3.586261
SAM	0.4	0.691	-0.36452	0.542019
PDO	0.31	0.759	-0.41255	0.559723
MJOIndex	0.23	0.822	-1.54178	1.926159
_cons	2.31	0.029	0.306884	5.191741
Latitude (Genesis)				
Volcano Act.	-1.75	0.091	-0.37961	0.02995
Nino34	-0.21	0.839	-2.30863	1.888524
SOI	1.92	0.066	-0.10543	3.077855
MEI	0.64	0.526	-1.97766	3.781263
DMI	0.49	0.627	-2.30935	3.761946
SAM	-0.82	0.419	-0.86688	0.371512
PDO	-0.27	0.791	-0.75077	0.577423
MJOIndex	-1.12	0.273	-3.66091	1.076547
_cons	11.02	0	14.58734	21.26042
Longitude (Genesis)				
Volcano Act.	2.43	0.022	0.344997	4.080675
Nino34	-2.53	0.017	-42.7622	-4.47933
SOI	2.04	0.051	-0.09991	28.93525
MEI	3.37	0.002	16.86226	69.39022
DMI	-0.83	0.413	-38.901	16.47622
SAM	0.61	0.55	-3.9797	7.315878
PDO	0.62	0.543	-4.23683	7.877838
MJOIndex	-0.31	0.758	-24.884	18.32704
_cons	6.77	0	69.91931	130.7853
Storm Lifetime				
Volcano Act.	-0.06	0.952	-0.18828	0.177368
Nino34	-1.04	0.31	-2.81923	0.927896
SOI	-1.74	0.093	-2.62591	0.216047
MEI	0.31	0.758	-2.18006	2.961377
DMI	2.69	0.012	0.841789	6.262106
SAM	-0.67	0.509	-0.73323	0.372385
PDO	-2	0.056	-1.17066	0.015125
MJOIndex	1.6	0.121	-0.46664	3.762848
_cons	5.82	0	5.468462	11.42603
Tropical Cyclone Lifetime				
Volcano Act.	1	0.326	-0.05377	0.156169
Nino34	0.75	0.459	-0.68203	1.469374
SOI	-2.57	0.016	-1.83855	-0.20684
MEI	-1.78	0.087	-2.75313	0.198812
DMI	-0.6	0.555	-2.00963	1.102434
SAM	0.85	0.404	-0.18632	0.44847
PDO	-0.45	0.656	-0.41519	0.265627
MJOIndex	-0.26	0.8	-1.36538	1.062978
_cons	4.93	0	2.399986	5.820512

Appendix 5C

Table: MANOVA for modes of variability against tropical cyclone LMI activity.

	Source	Statistic	F	Prob>F	
Model	W	0.043	2.73	0	a
	P	2.0193	2.29	0.0002	a
	L	5.6385	3.02	0	a
	R	2.9164	9.84	0	u
Residual					
Volcanic Activity	W	0.6488	2.49	0.0608	e
	P	0.3512	2.49	0.0608	e
	L	0.5414	2.49	0.0608	e
	R	0.5414	2.49	0.0608	e
Nino 3.4	W	0.5673	3.51	0.0167	e
	P	0.4327	3.51	0.0167	e
	L	0.7629	3.51	0.0167	e
	R	0.7629	3.51	0.0167	e
SOI	W	0.6105	2.93	0.0342	e
	P	0.3895	2.93	0.0342	e
	L	0.638	2.93	0.0342	e
	R	0.638	2.93	0.0342	e
MEI	W	0.5852	3.26	0.0227	e
	P	0.4148	3.26	0.0227	e
	L	0.7089	3.26	0.0227	e
	R	0.7089	3.26	0.0227	e
DMI	W	0.6314	2.69	0.0471	e
	P	0.3686	2.69	0.0471	e
	L	0.5838	2.69	0.0471	e
	R	0.5838	2.69	0.0471	e
SAM	W	0.6185	2.84	0.0388	e
	P	0.3815	2.84	0.0388	e
	L	0.6167	2.84	0.0388	e
	R	0.6167	2.84	0.0388	e
PDO	W	0.7288	1.71	0.1719	e
	P	0.2712	1.71	0.1719	e
	L	0.3722	1.71	0.1719	e
	R	0.3722	1.71	0.1719	e
MJO	W	0.8061	1.11	0.384	e
	P	0.1939	1.11	0.384	e
	L	0.2406	1.11	0.384	e
	R	0.2406	1.11	0.384	e

Appendix 6C

Table: Multivariate regression results for tropical cyclone activity at LMI and modes of variability.

Equation	RMSE	"R-sq"	F	P
Latitude	1.103822	0.384	2.104184	0.071
Longitude	11.42664	0.6619	6.606395	**0.0001**
LMI	4.084965	0.268	1.235407	0.317
LMI Lifetime	0.202949	0.3759	2.033218	0.0804

	Coef.	Std. Err.	t	P>|t|	[95% Conf.	Interval]
Latitude of LMI						
Volcano Act.	-0.08597	0.096411	-0.89	0.38	-0.28379	0.111845
Nino34	0.762408	0.988011	0.77	0.447	-1.26482	2.78964
SOI	0.749598	0.749346	1	0.326	-0.78793	2.287128
MEI	-0.93275	1.355653	-0.69	0.497	-3.71432	1.848819
DMI	0.276518	1.429186	0.19	0.848	-2.65593	3.208966
SAM	-0.10075	0.291519	-0.35	0.732	-0.6989	0.497394
PDO	0.161313	0.312658	0.52	0.61	-0.48021	0.802834
MJOIndex	-1.57244	1.115199	-1.41	0.17	-3.86064	0.715762
_cons	20.09535	1.570844	12.79	0	16.87224	23.31845
Longitude of LMI						
Volcano Act.	2.41876	0.998038	2.42	**0.022**	0.370955	4.466565
Nino34	-29.8384	10.22778	-2.92	**0.007**	-50.824	-8.8527
SOI	17.38455	7.757143	2.24	**0.033**	1.468204	33.30089
MEI	56.20784	14.03357	4.01	**0**	27.41334	85.00234
DMI	-23.6644	14.79478	-1.6	0.121	-54.0208	6.691968
SAM	3.906288	3.01777	1.29	0.206	-2.28567	10.09824
PDO	0.82606	3.236601	0.26	0.8	-5.8149	7.467016
MJOIndex	-9.07951	11.54441	-0.79	0.438	-32.7667	14.60767
_cons	107.0244	16.2612	6.58	0	73.6592	140.3896
LMI						
Volcano Act.	0.208296	0.356794	0.58	0.564	-0.52378	0.940376
Nino34	8.612165	3.65638	2.36	**0.026**	1.109894	16.11444
SOI	-0.7709	2.773139	-0.28	0.783	-6.46091	4.91911
MEI	-9.93954	5.016929	-1.98	**0.058**	-20.2334	0.354345
DMI	-8.89489	5.289057	-1.68	0.104	-19.7471	1.957358
SAM	2.255149	1.078838	2.09	**0.046**	0.041557	4.46874
PDO	0.83949	1.157068	0.73	0.474	-1.53462	3.213598
MJOIndex	-3.19359	4.127068	-0.77	0.446	-11.6616	5.274454
_cons	55.82378	5.813296	9.6	0	43.89588	67.75167
LMIDuration						
Volcano Act.	-0.00948	0.017726	-0.53	0.597	-0.04585	0.026896
Nino34	-0.08339	0.181656	-0.46	0.65	-0.45611	0.289343
SOI	-0.2732	0.137775	-1.98	**0.058**	-0.55589	0.009493
MEI	-0.17787	0.249251	-0.71	0.482	-0.68929	0.333548
DMI	-0.24333	0.262771	-0.93	0.363	-0.78249	0.295833
SAM	-0.01758	0.053599	-0.33	0.745	-0.12756	0.092393
PDO	-0.08848	0.057485	-1.54	0.135	-0.20643	0.029466
MJOIndex	-0.15394	0.205041	-0.75	0.459	-0.57465	0.266767
_cons	1.959123	0.288816	6.78	0	1.366522	2.551725